Institut für Physik und Astronomie
Arbeitsgruppe Prof. Dr. Anders Levermann

Impact, distribution, and adaptation
How weather extremes threaten the economic network

KUMULATIVE DISSERTATION

zur Erlangung des akademischen Grades „doctor rerum naturalium“
(Dr. rer. nat.) in der Wissenschaftsdisziplin „Klimaphysik“

eingereicht an der

Mathematisch-Naturwissenschaftlichen
Fakultät der Universität Potsdam

angefertigt am

Potsdam-Institut für Klimafolgenforschung

vorgelegt von

KILIAN KUHLA

im Januar 2022.

Prof. Dr. Anders Levermann | Hauptbetreuer & 1. Gutachter
Prof. Dr. Ricarda Winkelmann | 2. Gutachterin
Prof. Dr. Klaus Keller | 3. Gutachter

Published online on the
Publication Server of the University of Potsdam:
https://doi.org/10.25932/publishup-55266
https://nbn-resolving.org/urn:nbn:de:kobv:517-opus4-552668

Abstract

Weather extremes pose a persistent threat to society on multiple layers. Besides an average of ~37,000 deaths per year, climate-related disasters cause destroyed properties and impaired economic activities, eroding people's livelihoods and prosperity. While global temperature rises – caused by anthropogenic greenhouse gas emissions – the direct impacts of climatic extreme events increase and will further intensify without proper adaptation measures. Additionally, weather extremes do not only have local direct effects. Resulting economic repercussions can propagate either upstream or downstream along trade chains causing indirect effects. One approach to analyze these indirect effects within the complex global supply network is the agent-based model *Acclimate*. Using and extending this loss-propagation model, I focus in this thesis on three aspects of the relation between weather extremes and economic repercussions.

First, extreme weather events cause direct impacts on local economic performance. I compute daily local direct output loss time series of heat stress, river floods, tropical cyclones, and their consecutive occurrence using (near-future) climate projection ensembles. These regional impacts are estimated based on physical drivers and local productivity distribution. Direct effects of the aforementioned disaster categories are widely heterogeneous concerning regional and temporal distribution. As well, their intensity changes differently under future warming. Focusing on the hurricane-impacted capital, I find that long-term growth losses increase with higher heterogeneity of a shock ensemble.

Second, repercussions are sectorally and regionally distributed via economic ripples within the trading network, causing higher-order effects. I use *Acclimate* to identify three phases of those economic ripples. Furthermore, I compute indirect impacts and analyze overall regional and global production and consumption changes. Regarding heat stress, global consumer losses double while direct output losses increase by a factor 1.5 between 2000–2039. In my research I identify the effect of *economic ripple resonance* and introduce it to climate impact research. This effect occurs if economic ripples of consecutive disasters overlap, which increases economic responses such as an enhancement of consumption losses. These loss enhancements can even be more amplified with increasing direct output losses, e.g. caused by climate crises.

Transport disruptions can cause economic repercussions as well. For this, I extend the model *Acclimate* with a geographical transportation route and expand the decision horizon of economic agents. Using this, I show that policy-induced sudden trade restrictions (e.g. a no-deal Brexit) can significantly reduce the longer-term economic prosperity of affected regions. Analyses of transportation disruptions in typhoon seasons indicate that severely affected regions must reduce production as demand falls during a storm. Substituting suppliers may compensate for fluctuations at the beginning of the storm, which fails for prolonged disruptions.

Third, possible coping mechanisms and adaptation strategies arise from direct and indirect economic responses to weather extremes. Analyzing annual trade changes due to typhoon-induced transport disruptions depict that overall exports rise. This trade resilience increases with higher network node diversification. Further, my research shows that a basic insurance scheme may diminish hurricane-induced long-term growth losses due to faster reconstruction in disasters aftermaths. I find that insurance coverage could be an economically reasonable coping scheme towards higher losses caused by the climate crisis. Indirect effects within the global economic network from weather extremes indicate further adaptation possibilities. For one, diversifying linkages reduce the hazard of sharp price increases. Next to this, close economic interconnections with regions that do not share the same extreme weather season can be economically beneficial in the medium run. Furthermore, economic ripple resonance effects should be considered while computing costs. Overall, an increase in local adaptation measures reduces economic ripples within the trade network and possible losses elsewhere. In conclusion, adaptation measures are necessary and potential present, but it seems rather not possible to avoid all direct or indirect losses.

As I show in this thesis, dynamical modeling gives valuable insights into how direct and indirect economic impacts arise from different categories of weather extremes. Further, it highlights the importance of resolving individual extremes and reflecting amplifying effects caused by incomplete recovery or consecutive disasters.

Zusammenfassung

Wetterextreme stellen für die Gesellschaft eine anhaltende Bedrohung auf mehreren Ebenen dar. Neben durchschnittlich ~37.000 Todesfällen pro Jahr verursachen meteorologische Katastrophen Eigentumsschäden und Wirtschaftsbeeinträchtigungen, wodurch die Lebensgrundlagen und der Wohlstand der Menschen untergraben werden. Während die globale Temperatur – verursacht durch anthropogene Treibhausgasemissionen – ansteigt, nehmen die direkten Auswirkungen klimatischer Extremereignisse zu und werden sich ohne geeignete Anpassungsmaßnahmen weiter verstärken. Hinzu kommt, dass Wetterextreme nicht nur lokal direkte Schäden anrichten, sondern sich wetterbedingte wirtschaftliche Auswirkungen auch entlang der Handelsketten ausbreiten und so indirekte Effekte nach sich ziehen. Ein Ansatz zur Analyse dieser indirekten Auswirkungen innerhalb des komplexen globalen Versorgungsnetzes ist das agentenbasierte Modell *Acclimate*. In meiner Dissertation verwende und erweitere ich dieses Schadenspropagationsmodell, um drei Aspekte der Beziehung zwischen Wetterextremen und wirtschaftlichen Auswirkungen zu untersuchen.

Erstens verursachen extreme Wetterereignisse direkte Schäden in lokaler Wirtschaftsleistung. Die regionalen Auswirkungen werden auf der Grundlage von physikalischen Faktoren und lokalen Produktivitätsverteilungen kalkuliert. Ich berechne tägliche Zeitreihen lokaler Produktionsverluste durch Hitzestress, Überschwemmungen, tropische Wirbelstürme und deren konsekutives Auftreten unter Verwendung von Klimaprojektionsensembles. Die direkten Auswirkungen der oben genannten Katastrophenkategorien sind sehr heterogen in Bezug auf die regionale und zeitliche Verteilung. Ebenso ändert sich ihre Stärke unterschiedlich unter zukünftiger Erwärmung. Meine Forschungsergebnisse zeigen, dass Kapitalstock, welcher von Wirbelstürmen beschädigt ist, langfristige Wachstumsverluste verursacht. Dabei nehmen die Verluste zu, wenn die Heterogenität der Schocks steigt.

Zweitens werden die wetterbedingten Auswirkungen durch wirtschaftliche Wellen innerhalb des Handelsnetzes auf verschiedene Wirtschaftssektoren und Regionen verteilt. In meiner Dissertation, untersuche ich die wirtschaftlichen Wellen mittels *Acclimate* und mache dabei drei Wellenphasen aus. Darüber hinaus berechne ich indirekte Auswirkungen und analysiere die regionalen und globalen Produktionsveränderungen sowie die Auswir-

kungen auf Konsumierende. Für letztere verdoppeln sich zwischen 2000 und 2039 die weltweiten Verluste durch Hitzestress, während im selben Zeitraum die direkten Produktionsverluste nur um den Faktor 1.5 steigen. Im Zuge meiner Forschung identifiziere ich den Effekt der *ökonomischen Wellenresonanz* und führe ihn in die Klimafolgenforschung ein. Dieser Effekt tritt auf, wenn sich die ökonomischen Wellen aufeinanderfolgender Katastrophen überlagern, was wirtschaftliche Reaktionen intensiviert wie beispielsweise eine Steigerung der Konsumverluste. Diese Dynamik der Verluste kann durch zunehmende direkte Produktionsverluste, hervorgerufen etwa durch den Klimawandel, noch verstärkt werden.
Auch Handelsunterbrechungen können wirtschaftliche Auswirkungen haben. Um diese zu berechnen, erweitere ich das Modell *Acclimate* um ein geografisches Transportnetzwerk und weite den Entscheidungshorizont der Wirtschaftsakteure aus. Politisch bedingte plötzliche Handelsbeschränkungen (z. B. ein No-Deal-Brexit) können den längerfristigen wirtschaftlichen Wohlstand der betroffenen Regionen erheblich verringern. Analysen von Transportunterbrechungen in der Taifunsaison zeigen, dass stark betroffene Regionen ihre Produktionen reduzieren müssen, wenn die Nachfrage während eines Sturms sinkt. Zu Beginn eines Sturms können Handelsschwankungen durch alternative Lieferanten ausgeglichen werden, was jedoch bei längeren Unterbrechungen nicht mehr gelingt.

Drittens ergeben sich mögliche Anpassungsmechanismen und -strategien aus direkten und indirekten wirtschaftlichen Reaktionen auf Wetterextreme. Die Analyse der jährlichen Handelsveränderungen in der Taifunsaison zeigt, dass Exporte insgesamt zunehmen. Diese Widerstandsfähigkeit des Handels wächst mit einer höheren Diversifizierung der Handelspartner. Weiterhin zeigt meine Forschung an Wirtschaftswachstumsmodellen, dass ein Versicherungssystem langfristige Wachstumsverluste, verursacht durch Tropenstürme, durch schnelleren Wiederaufbau verringern kann. Ich komme zu dem Schluss, dass ein Versicherungsschutz eine wirtschaftlich sinnvolle Anpassungsstrategie gegenüber höheren Schäden durch die Klimakrise sein kann. Ebenso weisen indirekte Auswirkungen von Wetterextremen innerhalb des globalen Wirtschaftsnetzes auf weitere Anpassungsmöglichkeiten hin. Zunächst vermindert eine diversifizierte Vernetzung die Gefahr eines starken Preisanstiegs. Ebenso kann eine enge wirtschaftliche Verflechtung von Regionen, die nicht dieselbe Unwettersaison haben, mittelfristig wirtschaftlich vorteilhaft sein. Weiterhin sollten bei der Berechnung der Kosten wirtschaftliche Resonanzeffekte berücksichtigt werden. Eine Verstärkung der lokalen Anpassungsmaßnahmen verringert die Amplitude ökonomischer Wellen und damit auch potentielle Verluste in anderen Regionen. Insgesamt sind Anpassungsmaßnahmen notwendig, aber es scheint trotz dieser nicht möglich zu sein, alle direkten oder indirekten Verluste zu vermeiden.

Wie ich in meiner Arbeit darlege, gibt die dynamische Modellierung wertvolle Einblicke in die Art und Weise, wie direkte und indirekte wirtschaftliche Auswirkungen durch

verschiedene Wetterextreme entstehen. Darüber hinaus wird deutlich, wie wichtig es ist, einzelne Extremereignisse aufzulösen und Verstärkungseffekte zu berücksichtigen, die durch unvollständigen Wiederaufbau oder aufeinanderfolgende Katastrophen verursacht werden.

Contents

Introduction

Extreme weather events impair numerous spheres of society and under climate change these threats will intensify. In this thesis, I explore how weather extremes impact regional economic output, analyze the resulting responses of the global trade network, and identify adaptation mechanisms. Before addressing my research questions, I briefly outline the impacts of weather extremes, the current research on climate change and its influence on climate-related extreme events, and how socio-economic models can compute resulting economic repercussions.

1 Extreme weather events

Since the beginning of the century, natural disasters affected on average ~200 million people per year, excluding the COVID-19 pandemic [CRED, 2021]. However, disasters' frequency and impacts are distributed highly heterogeneously between regions and time. On a global scale, the number of climate-related disasters exceeds geophysical disasters by about factor ten [CRED, 2015]. In 2020 the weather extremes with the highest mortality, economic loss, or total number of affected people were heat stress, river flood, and tropical cyclone, respectively [CRED, 2021]. In this thesis, I focus on these three disaster categories and their impacts on society.

Temperature is a key physical factor for the well-being, the functioning, and the preservation of life. As ambient temperatures markedly exceed the normal optimum, animals, plants, and humans usually experience heat stress. The pressure caused by heat affects the welfare of plants [Kotak et al., 2007] as well as animals [Gonzalez-Rivas et al., 2020; Doering et al., 2018]. In daily human life, heat stress increases health problems [Kovats and Hajat, 2008], triggers aggressive behavior [Anderson et al., 2000; Stechemesser et al., 2021] or puts pressure on energy supply [Auffhammer et al., 2017; Wenz et al., 2017]. Furthermore, extreme heat negatively affects economic domains, such as income [Dell et al., 2009], labor productivity [Dunne et al., 2013], or agricultural output [Brás et al., 2021]. These adverse impacts can lead to a reduction of macroeconomic output [Burke et al., 2015], e. g. Australia lost 0.33% to 0.47% of its gross domestic product (GDP) during the heat wave of 2012/13 [Zander et al., 2015]. Despite the economic relevance, research to

date has not yet provided sufficient coverage of production losses correlated to heat stress on a global scale [Auffhammer, 2018].
Next to heat stress, river floods are one of the most frequent extreme events globally [Field et al., 2012]. In this thesis, I expand the term weather extreme by also including river floods, even though a strict definition does not cover these. Two main factors foster river floods. First, flooding occurs more likely during the increased inflow of water masses, which can be due to (often seasonal) snowmelt or heavy rainfall events. Second, natural or artificial catchment characteristics, such as soil properties, bridges, river topography, or lack of washland, also contribute to flood disasters. Globally, about 58 million people per year are exposed to river floods [Dottori et al., 2018]. Merz et al. [2021] estimate the global flood mortality to have been 0.007% between 1977–2019. Further, flood disasters may trigger groundwater contamination [Andrade et al., 2018], outbreak of diseases [Ahern et al., 2005], mental health problems [Tong, 2017], or migration [Dun, 2011]. Besides impacts on human conditions, river floods can cause severe property damage, e.g. the 2002 European flood cost ~USD26 bn [MunichRe, 2021], or overall production losses [Willner et al., 2018b]. Further economic losses can be caused by transportation disruptions [Pregnolato et al., 2017] or declined agricultural production [Chau et al., 2013].
About 150 million people are exposed to tropical cyclones each year [Geiger et al., 2018]. On a global scale, tropical cyclones cause yearly USD~29 bn of direct economic damage on average [Guha-Sapir, 2017]. Due to Earth's wind systems and its topography, trajectories of tropical storms are naturally confined. As a result, many regions do not experience any tropical storms, while some regions are frequently and seasonally exposed to them. For example, in the Northern hemisphere, countries bordering the Western Pacific (e.g. China or the Philippines) are affected by most landfalling tropical storms [Geiger et al., 2018], but Northern Africa – on a similar latitude – remains virtually unaffected. In Western Nations, tropical cyclones are usually referred to as hurricanes and categorized by the Saffir–Simpson hurricane wind scale (SSHWS) depending on their 1-minute maximum sustained wind speed [NHC, 2021]. The scale reaches from category 1 to 5 officially, but for convenience weaker tropical storms below the threshold of category 1 are labeled as category 0. While severe hurricanes (SSHWS categories 4 and 5) account for only 6% of landfalling hurricane events in the United States of America (USA), they contribute almost half of the normalized economic damage from all hurricanes [Pielke et al., 2008]. During a tropical storm, there may be incisions in social life [Morrow and Lazo, 2015], closures of ports [Zhang et al., 2020], disruptions of transportation routes [Yang et al., 2016; Wang et al., 2014], or even destruction of essential facilities [Paxton, 2019]. In the short and medium run, tropical cyclones can disrupt power supply [Mitsova et al., 2018], local fisheries [Thomas et al., 2019], or regular work and production [Vigdor, 2008]. In the longer run, tropical cyclones may cause significant economic growth losses [Krichene et al., 2021], which are particular pronounced in underdeveloped countries due to multiple social aftermaths [Berlemann and Wenzel, 2018].

Extreme events may occur largely isolated, but they can overlap or succeed each other, e.g. consecutive flood and heat wave events in China [Chen et al., 2021]. These events are typically referred to as consecutive disasters and are typologized by de Ruiter et al. [2020], who address the importance of them for future disaster assessments. Consecutive disasters are two or more catastrophes whose occurrences or repercussions overlap in time or space. This includes that extreme events do not have to coincide but their aftermaths do. If a population has not yet recovered from a previous disaster, while the impact of another event affects it, the repercussions of the consecutive disasters overlap. Likewise, extreme events do not necessarily have to occur in the same location for their resulting repercussions to coincide. The subsequent occurrence of one or more disasters may affect health [Fernandez et al., 2005], business structure [Bhaskara and Filimonau, 2021], or risk aversion [Li et al., 2011]. These effects of consecutive disasters are noticeable at the macroeconomic level as well [Gissing et al., 2021]. Despite these studies, the potential impact of consecutive disasters on societies and possible amplification mechanisms are poorly understood and therefore a focus of current research.
Throughout this thesis, an immediate regional impact of a weather extreme is referred to as *direct* effect. However, local extreme weather events do not occur in a void; rather, they are embedded in a complex interconnected world. Hence, correlated impacts in regions outside the disaster locations or feedback mechanisms involving directly affected regions are possible. These are referred to as *indirect* or *higher-order* effects. The state of research to compute indirect and longer-term economic consequences of extreme weather events is outlined in section 3. While weather extremes already cause severe harm in most spheres of society, ongoing anthropogenic climate change will very likely increase the impact of climate-related disasters.

2 Climate change

In the last 100 years, the annual global mean temperature increased by about 1.2 K compared to the pre-industrial era (period 1850-1900) [IPCC, 2021]. Both, temperature and speed of warming, are extraordinary for civilizational scales. The last warmer period was about 125 thousand years ago and the highest rate of warming since the Last Glacial Maximum did not exceed 0.18 K per 100 years [Shakun et al., 2012]. The ongoing rapid climate change results from accelerated greenhouse gas (GHG) emissions, mainly caused by anthropogenic use of fossil fuels. The main GHG emitted is carbon dioxide (CO_2), which is taken up only partially by land and water. Around 41% remains in the atmosphere causing land surface temperature to rise [IPCC, 2021]. Since the pre-industrial era, the global CO_2 concentration has grown by more than 47% and has the highest value for at least 2 million years. Facing rapid climate change, the necessity to comprehend the climate system and simulate future climate has emerged.

Earth's climate can be modeled with different degrees of complexity, and spatial and temporal resolution. Conceptual climate models consist of one or more equations, which reproduce essential nonlinear climate behavior (e.g. Saltzman and Maasch [1988] or Bódai and Tél [2012]). In Earth-system models of intermediate complexity, some physical processes are simplified, and temporal and spatial resolutions are reduced to lower computational time (e.g. Claussen et al. [2002] or Petoukhov et al. [2000]). General circulation models (GCMs) solve the Navier-Stokes-equation in discretized grid cells. GCMs are the most complex climate models (e.g. Jones et al. [2011] or Dufresne et al. [2013]), and the chosen size and order of grid cells may partially lead to regionally different results between them. GCMs are used for climate projections and form the basis for further models (e.g. hydrological models [Leng et al., 2015]) or emulators (e.g. tropical cyclone emulators [Geiger et al., 2021]). Simulations of different Earth-system models are collected in the collaborative framework Coupled Model Intercomparison Project (CMIP) to generate unified simulation ensembles and improve climate models (among others). Phase 5 of CMIP (CMIP5) [Taylor et al., 2012] includes the four GCMs: HadGEM2-ES [Jones et al., 2011], IPSL-CM5A-LR [Dufresne et al., 2013], MIROC5 [Watanabe et al., 2010], and GFDL-ESM2M [Dunne et al., 2012].

The GHG concentration in the atmosphere is an essential driver of Earth's climate. Possible future concentration trajectories are categorized in representative concentration pathways (RCPs). Each pathway[1] corresponds to median warming until the end of the century, e.g. RCP2.6 to +1.6 K or RCP6.0 to +2.8 K [IPCC, 2013]. GCMs driven by an RCP simulate a projection of future warming under that scenario. Due to the inertia of the climate system – a lag between GHG concentration and corresponding global mean temperature – the uncertainty ranges of near-future warming projections (~20 years) exceed variation of different RCPs. That means that results of one GCM driven by different RCPs are barely distinguishable for the next two to three decades. Conversely, near-future warming is mainly already determined by past emissions.

Ongoing climate change will likely change the pattern of extreme weather events. According to the IPCC [2021] extreme heat will increase with a medium to high confidence for every land and coastal region until 2050. Robinson et al. [2021] found that the recorded extreme heat events would have been virtually impossible without global warming over the last years. In about half of the flood-prone regions, the occurrence of river floods increases with a medium to high confidence. Until the 2040s, some regions have to drastically increase adaptation measures towards higher river flood risks to keep current flood protection [Willner et al., 2018a]. Frequency projections of tropical cyclones are still uncertain, and some studies even predict a negative trend [Knutson et al., 2013]. Nevertheless, the frequency of severe tropical storms (SSHWS categories 4 and 5) is projected to increase under global warming. It is estimated that annual exposure to tropical cyclones increases

[1] Recent studies combine RCPs with shared socioeconomic pathways to incorporate alternative socioeconomic development and possible climate policies more strongly in GHG emission scenarios.

by 33 million people (+26% compared to 2015) for +2 K global warming [Geiger et al., 2021].
Beyond the immediate risks of intensifying extreme weather, human civilization will be severely challenged by the necessity of mitigating and adapting to future warming, which make anthropogenic climate change a climate crisis. Aware of this existential threat, the international community agreed in 2015 on the common goal of keeping global warming well-below +2 K by the end of this century compared to the pre-industrial era. To achieve this, humanity must undertake drastic mitigation measures. Current policies and actions are projected to lead to a warming path of +2.7 K by the end of the century [Stockwell et al., 2021], although warming will not have stopped by then. Furthermore, adaptation measures need to be implemented to address the consequences of ongoing climate change. Both mitigation and adaptation are tremendous challenges for society as a whole. Interdisciplinary research approaches could help find solutions to the threats of extreme events and climate crisis.

3 Modeling economic impacts

Weather extremes do not only impact regions directly affected, rather they can cause significant economic repercussions. On the one hand, production and supply disruptions may cause shortages or surplus along supply chains. On the other hand, demand for goods from unaffected regions could increase sharply during a disaster and in the aftermath. Furthermore, hysteresis effects might cause extreme weather to impact long-term economic development. Socio-economic models can simulate these cascade effects. In the following, I briefly depict prominent model families with which indirect economic effects can be computed and discuss their scope and limitations.
Closed economy models simulate macroeconomic patterns of an isolated economy. They reflect the interaction of price, demand, production channels, and GDP within a self-sufficient economic cycle. Among others, standard closed economy models address inflation (e.g. Lucas island model [Lucas Jr, 1975]), growth (e.g. Solow-Swan model [Solow, 1956]), or interest rates (e.g. IS-LM model [Hicks, 1937]). These approaches are useful to describe qualitative effects in macro-economy, especially for industrialized economies with low trade levels as it was rather typical during and after World War II [Ortiz-Ospina and Beltekian, 2018]. However, international trade has grown dramatically (faster than national GDPs) in the last 60 years [OWD, 2021], resulting in a need for a more interconnecting economic theory.
Leontief [1951] pioneered the development of input-output (IO) models, which couple economic production, trade flows, and final demands in a linear mathematical relationship. Using this, trade changes and associated economic impacts caused by perturbations can be computed. Analyses based on IO models are useful for computing first-order (cascading)

impacts. However, the coupling of economic variables is too inflexible and calculated damages are likely to be overestimated.

Comparable to IO models, computable general equilibrium (CGE) models simulate economic variables and their relation to each other, which are initially in general equilibrium [Hertel, 1997; Walras, 2013]. An external perturbation disturbs this state and causes the economic system to transition to a new general equilibrium state. The transition decision is usually based on price adjustments and cost minimization as a constraint. Economic systems modeled with CGE are highly flexible and adaptive. However, CGE models are mostly calibrated on long-term equilibriums, which neglects the inertia of adaptation processes, resulting in underestimating damages and costs of external impacts.

Workhorses of climate policy assessments are integrated assessment models (IAMs) [Rose et al., 2017]. They couple socio-economic and environmental models into one framework. There, anthropogenic processes (e.g. unsustainable agriculture) drive environmental changes (e.g. rise in GHG concentration). Corresponding changes (e.g. desertification) then backlash on human activities (e.g. harvest failure). Thus, policies and possible feedback can be evaluated, and future impacts caused by past actions can be linked to each other. Based on this, the social cost of carbon (SCC) – the long-term societal cost of one additional ton emitted CO_2 – can be computed. SCCs are included into cost-benefit analyses of mitigation efforts, adaptation measures, and their mutual cost trade-offs [Tol, 2005, 2007, 2011]. Though widely used, IAMs have the disadvantage that they do not properly account for short-term extreme events due to coarse temporal resolution [Otto et al., 2020; Pindyck, 2020]. Therefore, IAMs rather underestimate direct and indirect losses due to weather extremes.

Another approach to model social or economic processes is agent-based modeling, where discrete decision-making agents interact. An agent-based model (ABM) can be a network of individuals [Cuevas, 2020], collectives [Gurgone et al., 2018], or a mixture of different sized groups [Ermolova et al., 2021]. By modeling a network of autonomous agents, each agent's particular physical, economic, or social environment can be addressed. Furthermore, ABMs can operate at a high temporal resolution. A main drawback of ABMs are model calibration and validation, although methods improve for both [Lamperti et al., 2018; Fagiolo et al., 2019]. In economic studies based on ABMs, stylized facts and market dynamics have been reproduced [Gualdi and Mandel, 2016; Dosi et al., 2018]. A network of autonomous agents with microeconomic decision rationales can simulate macroeconomic patterns [Stiglitz and Gallegati, 2011; Dawid et al., 2019]. ABMs can be used to analyze loss propagation along supply chains [Gualdi and Mandel, 2016].

In this thesis, I mainly use the ABM *Acclimate* [Otto et al., 2017], which is designed to study loss propagation through the economic network caused by short-term economic impacts. The model simulates the behavior of myopic and locally optimizing economic agents on a daily resolution and thus allows an assessment of possible regional and sectoral responses to weather extremes. Feedback processes in both directions along the supply

chain are integrated, similarly to other ABMs [Jaumotte and Osorio, 2015]. Through downstream effects, supply deviations are passed down the supply chain. In upstream effects, shifted demands and prices propagate up the supply chain. Economic agents in *Acclimate* can flexibly adjust their daily actions, e.g. demand and supply allocation, to repercussions. Endogenous price dynamics account for short-term adaptation costs and constrain trade choices. Finite transportation times and inventories reflect the inertia of the trade system. Due to high regional and sectoral resolution, sub-national, national and international economic processes can be simulated.

4 Research questions

For my doctoral thesis, I identify three research questions, with whose answers I aim to achieve further scientific insights on the role of weather extremes on local economies and their interconnected supply chains. That might contribute to solutions for the major social challenges arising from weather extremes and climate crisis.
In my research, I lean on various tools from different scientific fields. Economic processes and decision rationales are derived from experiences in microeconomics and macroeconomics, e.g. utility maximization. To calculate the occurrence and patterns of weather extremes, I use insights from climate physics, e.g. statistical distribution of tropical storms. Furthermore, I make use of statistical measures to explore correlations between physical drivers and societal impacts, e.g. Lorenz-curves and Gini-coefficients to describe shock heterogeneity of extreme events. By referring to findings from classical mechanics, socio-economic phenomena are explained, e.g. loss amplification due to resonance effects within the economic network. It is important to me to examine the socio-economic repercussions explicitly from the point of view that the intrinsic temporal dynamics are resolved. The dynamic modeling and the computer-based simulation of these processes are built on my modeling experience in theoretical physics.
In the following three sections, I formulate my research questions (figure 1) and give a short outline of how my research, laid out in articles A to F, provides answers.

4.1 Impact

The subject of my thesis is the economic consequences of extreme weather events. To unfold this topic, my first research question addresses direct effects.

How do weather extremes impact local economic performance?

To answer this, I focus on three disaster categories: heat stress, river floods, and tropical cyclones. The disaster category heat stress is examined in articles A and C. To compute the economic impact in an area affected by heat stress, I use a linear temperature-productivity correlation found by Hsiang [2010]. The functional dependency is sector-specific and can

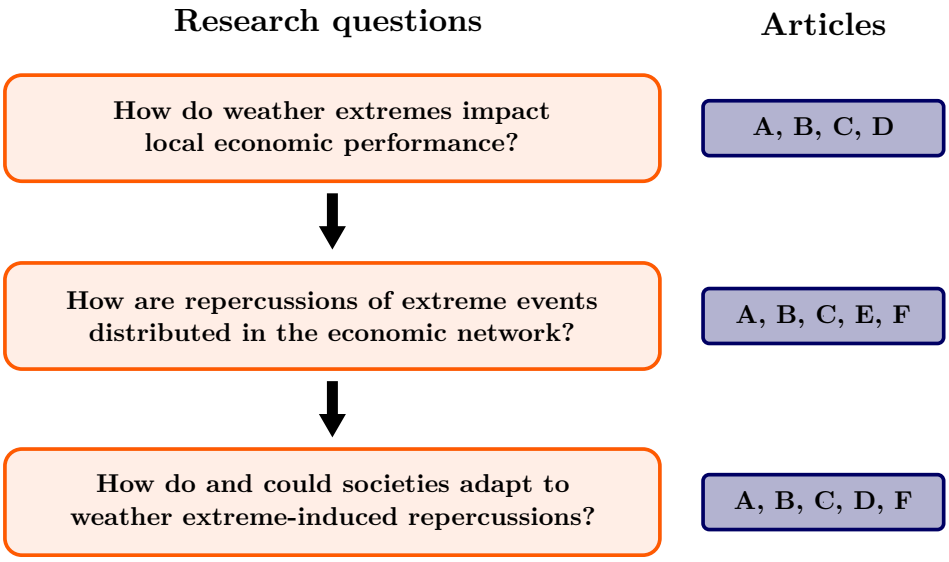

Figure 1: Schema of my thesis. Research questions (left) and corresponding articles of my thesis (right).

be applied beyond a daily mean temperature threshold of 27°C. I compute local economic productivity changes due to heat stress using gridded temperature data based on CMIP5's GCMs driven by RCP2.6 and RCP6.0 and the temperature-productivity correlation. Regional output reductions are aggregated weighted by gridded population data as a proxy of the productivity of an area.
To compute economic impacts of river floods [C], I use results of Willner et al. [2018a], which base on five hydrological models, driven by the four GCMs of CMIP5 and RCPs 2.6 and 6.0. I calculate the regional production failure by assuming that a flooded area stops its production in non-service sectors for the duration of a flood. In the disaster aftermath, the production recovers depending on the flood depth.
I further compute the economic impacts of tropical cyclones by using three different approaches. In article B, the production failures due to Hurricane Sandy (2012) are derived from the estimated business interruption in the most affected US states, New York and New Jersey. In article C, tropical cyclone trajectories simulations are based on methods from Geiger et al. [2018, 2021] and are driven again by mentioned GCMs and RCPs. Analog to river floods, I assume that non-service production in the tropical cyclone-affected area stops and that productivity recovery is wind speed dependent. In article D, the impact of damaged capital due to landfalling hurricanes on economic growth is calculated by using a modified closed economy growth model. The computations are based on historical events and their variation of shock sizes. I implement the Gini index as a metric of shock heterogeneity and show that the variation of individual shock sizes affects economic growth.

By overlapping the time series of productivity reduction caused by different disaster categories, I compute the direct impact of consecutive disasters of all three disaster categories [C].

4.2 Distribution

My second research question focuses on indirect effects of weather extremes within the complex economic network.

How are repercussions of extreme events distributed in the economic network?

To answer this question, I use the agent-based loss-propagation model *Acclimate*, which computes responses in regional and global supply, demand, and prices due to local production changes or transport perturbations. The *Acclimate* model consists of a complex network of 26 sectors, i.e. representative firms, and one consumer per region. The network is built by 268 regions – 186 nations, 31 Chinese provinces, and 51 federal US states, including the District of Colombia. The complex trading network has over 1.8 million linkages between 7,236 economic agents. The 26 trading goods and services are non-substitutable. Firms (consumers) locally optimize their profit (consumption) in response to short-term production, price, or supply changes. These changes are depicted as deviations from the economic baseline, which is derived from the Eora database, a static multi-regional input-output table [Lenzen et al., 2012]. The economic agents decide myopically, and the price dynamics is endogenous. The model was described by Otto et al. [2017].
As one indicator of how economic repercussion propagates through the complex economic network, I focus on regional and global consumption of goods and services. Since consumers are at the end of supply chains, conclusions can be drawn about the distribution of supply shortages and price changes. In article A, I examine price and consumption changes due to heat stress-induced local production reduction and project near-future loss intensification due to global warming. In article B, I focus on a single event, Hurricane Sandy (2012), to outline the repercussion propagation mechanism of extreme events and describe the emerging three-phased ripple within the complex economic network. In article C, resonance effects of ripples in the trading network due to consecutive disasters and consequences for consumers are analyzed.
Domestic and inter-regional trade are in the focus of articles E and F, as they are additional indicators of distribution of economic impact in a trading network. For this, I extend the *Acclimate* model with a geographical transportation route network, which consists of land entities, maritime entities, and ports. Economic agents autonomously compute their best transportation route based on a developed cost algorithm. This extension enables to obstruct the flow of goods through trade hubs. Network repercussions due to trading perturbation caused by a hypothetical no-deal Brexit [E] or observed typhoons [F] are examined. Important to note that no firm reduces production directly due to external perturbation in those studies. Thus, there are no direct output losses contrary to studies

A, B, and C. The daily product flows between ~1.8 million linkages are aggregated to reasonable trade flows between summarized economic regions or economic blocs.

4.3 Adaptation

My third and final research question addresses possibilities for adaptation strategies.

How do and could societies adapt to weather extreme-induced repercussions?

I study under which conditions the network of economic agents can mitigate or even overcome external disturbances. In article F, I focus on the changes in trade due to typhoon-induced transport perturbations. In my study, I find that different economic baselines show a trend in regional trade responses. To understand the reason for these deviations, I use network metrics like share of network flow and node inter-connectivity. The latter is measured in the number of outside connections normalized to the number of firms of a region. Here, an outside connection refers to a linkage to a firm or consumer which does not belong to the same region. I study how these network metrics influence trade responses and potential trade resilience.
In article D, I analyze how hurricane-induced capital damage affects economic growth while explicitly resolving individual landfalling tropical storms. I extend a classic Solow-Swan growth model by including a time-dynamic insurance scheme. Thereby, an economy uses previously reserved disaster funds for reconstruction in shock aftermaths. The insured capital is not paid out instantaneously, but rather the dynamic is adapted to the sigmoidal disbursement pattern of real-life payout processes. An insured capital stock reduces economic growth in the first place but triggers a faster recovery in the disaster aftermath. Using this, I examine such insurance scheme's societal benefit and adaptation potential on a historical observed impact level. I also explore if a basic insurance scheme may mitigate possible climate change-induced increased losses. For this, I project capital damages for a +2 K world (barely Paris-compatible) and a +2.7 K world (pathway of current mitigation policies and actions) using a wind speed approach and a surge index approach. For the former, I map historical damages of tropical storms to SSHWS categories and change the relative frequency of categories 0-3 (decrease) and categories 4-5 (increase) as Knutson et al. [2013] project. For the latter, I find a positive correlation between capital damage and surge index. Using this correlation and the surge index increase per degree of global warming (empirically found by Grinsted et al. [2013]), I project capital damages for a warmer world. Thus, I study the adaptation possibilities of an insurance scheme under different climate change projections.
Regarding the unfolding of the climate crisis for the next 20 years, mitigation measures are already too late. Therefore, besides further mitigation efforts, near-future adaptation measures are urgently needed. To find further potential adaptation advice, I refer to the insights of my first two research questions and interpret them in a connected-world framework. While computed impacts in articles A, B, and C are based on different direct

loss approaches, I analyze similarities and differences in the network's responses to these and present possible coping mechanisms like crisis-conscious trading corporations.

Articles

My thesis is built on six scientific articles. Four of them are published in peer-review journals and two are submitted to journals at the time of submission of this thesis. Each article by itself is a stand-alone contribution, which consist of an introduction, methods, results, discussion, and respective references. The supplementary information of each article can be found in the appendix of this thesis. As a short overview, I provide information on authors, journal, content, and my contribution to each article.

Article A

Future heat stress to reduce people's purchasing power

Authors

Kilian Kuhla, Sven N Willner, Christian Otto, Leonie Wenz, Anders Levermann

Status

Published in *PLOS ONE* in June 2021,
doi: 10.1371/journal.pone.0251210.

Capsule summary

Under near-future climate change, the frequency of local heat waves increases, which leads to intensified heat stress pressure on society. In this study, the impact on productivity due to heat stress for the first four decades of this century is computed. The resulting propagation of supply shortages and regional responses along the trading network are examined by using the network-based model *Acclimate*. Higher prices may increase the profit value of firms but reduce consumption for the vast majority of regions. The trend of the results is robust for different economic baselines. The analysis even implies that a more inter-linked network adapts worse to regionally and temporally widely distributed heat stress.

Author contributions

Sven N Willner, Anders Levermann and Kilian Kuhla designed the research. Kilian Kuhla conducted the analysis and made the visualization. Sven N Willner and Kilian Kuhla wrote the manuscript with contributions from all other authors. Kilian Kuhla discussed the results with all authors.

PLOS ONE

RESEARCH ARTICLE

Future heat stress to reduce people's purchasing power

Kilian Kuhla[1,2], **Sven Norman Willner**[1]*, **Christian Otto**[1], **Leonie Wenz**[1,3,4], **Anders Levermann**[1,2,5]

1 Potsdam Institute for Climate Impact Research, Potsdam, Germany, **2** Institute of Physics, Potsdam University, Potsdam, Germany, **3** Mercator Research Institute on Global Commons and Climate Change, Berlin, Germany, **4** Department of Agricultural and Resource Economics, University of California, Berkeley, California, United States of America, **5** Columbia University, New York, New York, United States of America

* sven.willner@pik-potsdam.de

Citation: Kuhla K, Willner SN, Otto C, Wenz L, Levermann A (2021) Future heat stress to reduce people's purchasing power. PLoS ONE 16(6): e0251210. https://doi.org/10.1371/journal.pone.0251210

Editor: Giray Gozgor, Istanbul Medeniyet University: Istanbul Medeniyet Universitesi, TURKEY

Received: February 1, 2021

Accepted: April 21, 2021

Published: June 10, 2021

Data Availability Statement: The implementation of the Acclimate model is available as open source on https://github.com/acclimate/acclimate with identifier 10.5281/zenodo.853345, the implementation of the disaggregation algorithm can be found on https://github.com/swillner/libmrio (10.5281/zenodo.832052). All further code used for data processing and plotting is available from the authors on request.

Funding: This research has received funding from the German Academic Scholarship Foundation, the

Abstract

With increasing carbon emissions rising temperatures are likely to impact our economies and societies profoundly. In particular, it has been shown that heat stress can strongly reduce labor productivity. The resulting economic perturbations can propagate along the global supply network. Here we show, using numerical simulations, that output losses due to heat stress alone are expected to increase by about 24% within the next 20 years, if no additional adaptation measures are taken. The subsequent market response with rising prices and supply shortages strongly reduces the consumers' purchasing power in almost all countries including the US and Europe with particularly strong effects in India, Brazil, and Indonesia. As a consequence, the producing sectors in many regions temporarily benefit from higher selling prices while decreasing their production in quantity, whereas other countries suffer losses within their entire national economy. Our results stress that, even though climate shocks may stimulate economic activity in some regions and some sectors, their unpredictability exerts increasing pressure on people's livelihood.

Introduction

Anthropogenic greenhouse gas emissions have already led to an increase in global mean temperature by about 1˚C compared to pre-industrial levels [1–3]. Due to inertia in the climate system, the planet will continue to warm over the next two decades even under possible emission reductions [4]. With global mean temperature rising, the number and intensity of extreme heat events are expected to increase [5, 6]. A growing body of empirical literature suggests that rising temperatures have various socio-economic impacts by affecting, for example, agricultural output [7], human health [8], energy supply [9, 10], income [11, 12], and labor productivity [13, 14]. Nevertheless, on a global scale there is not yet satisfying coverage on the overall production loss estimates due to heat stress [15].

Labor productivity, which is strongly impacted by heat stress [16], has been shown to decrease quasi-linearly with daily mean temperatures exceeding 27˚C [17, 18]. Possible relations to physiological heat stress make this particularly relevant for outdoor sectors such as

German Federal Ministry of Education and Research (BMBF) under the research projects CLIC (FKZ: 01LA1817C) and SLICE (FKZ: 01LA1829A), the Horizon 2020 Framework Programme of the European Union (grant agreement 820712), and from the Volkswagen foundation. The publication of this article was funded by the Open Access Fund of the Leibniz Association.

Competing interests: The authors have declared that no competing interests exist.

forestry, mining, and construction, where workers are strongly exposed to ambient temperature [19–21]. Stronger efforts to mitigate climate change are needed to avoid further increase in heat stress [22–24], but warming is unlikely to be halted in the next two decades. Without specific adaptation measures—which come at their own costs [25]—an increasing number of hot days due to globally rising temperatures will thus lead to temporarily reduced productivity of these sectors.

These losses can be substantial; for instance, the Russian heat wave in 2010 caused output losses of about USD 15bn in the Russian economy alone [26]. The business interruptions associated with such a strong shock to a local economy ("direct losses") can additionally spread to other sectors and regions via demand and supply cascades as well as associated price signals [27–30]. Resulting indirect losses [31, 32] can be particularly high in today's densely connected global economic network. However, there can also be gains through market adjustments, which effectively redistribute production in the short run [33–35]. Thus, depending on the structure of the economic network [36], the flexibility of the economic actors within that network [37], and the strength and regional pattern of the heat stress signal, direct losses can be both, amplified and mitigated through economic response dynamics.

In this study, we estimate the short-term effects of heat stress-induced reduction in labor productivity and corresponding output losses for 2020–2039 in comparison to 2000–2019. The effects are short-term in the sense that they are on the scale of days to weeks arising from direct productivity reduction beyond a daily temperature threshold on each individual day. In particular, we show the short-term repercussions of these specific shocks in the global economic network in terms of indirect production losses, price changes, and effects on consumption on a national and global scale. We show that the latter can be substantial and are likely to increase in many regions. We add up these daily economic repercussions to annual values and depict a long-term trend of these aggregated short-term effects for the next double decade. For that, we employ a loss-propagation model including a total of 7, 236 economic agents which form a network of about 1.8 million interconnections. Results are thus under the economic structure of 2012 in the absence of adaptation.

Materials and methods

Temperature data

We use time series of daily mean temperature for the period 2000–2039 as a physical driver for economic outages. The projected temperature data are provided by four global climate models (GCMs) of the CMIP5 [38] ensemble (HadGEM2-ES [39], IPSL-CM5A-LR [40], MIROC5 [41], GFDL-ESM2M [42]), which have been bias-corrected within ISIMIP [43] (project phase 2b) towards an observation-based data set using a trend-preserving method [44] at a spatial resolution of $0.5^\circ \times 0.5^\circ$. Using a bias-correction, extreme weather phenomena, which in the GCMs tend to be averaged out, can be better represented in the time series; thus, the daytime temperatures do not correspond to the historical values, but are well represented in their statistics over the ensemble (for consistency we also use ISIMIP2b output (historical scenario) for the historic period). For each model we use the representative concentration pathways (RCPs) 2.6 and 6.0. This combination results in an ensemble of eight daily temperature time series and thus eight direct output loss time series. Although the emission path for the next two decades is largely determined due to the inertia of the climate system, the usage of different RCPs provides a larger simulation ensemble.

Population data for distribution of production

Population data rely on the Population Count v4.11 for the year 2015 of the GPW data set [45] aggregated to the resolution of the physical input data ($0.5^\circ \times 0.5^\circ$). We use these population data as a proxy for the distribution of production of a region over a gridded area, meaning that a cell where x% of a region's population lives accounts for x% of its production as well. Thus, a heat wave over a densely populated area causes a higher direct loss of production than over sparsely populated area. As a region mask we use GADM data [46], which we rasterize to the same resolution ($0.5^\circ \times 0.5^\circ$) advanced in coastal areas to account for inaccuracies at shape boundaries.

Direct output losses due to heat stress

To obtain a region and sector specific damage function, we employ the empirical relationship between daily temperature and production capacity derived by Hsiang et al [17]. The production reduction bases solely on short-term performance shortfalls and not on longer-term structural damage, such as destroyed infrastructure. Though originally focuses on Caribbean countries, we transfer the productivity-temperature-correlation to all countries in the world. In our study, we take a look at the spatio-temporal responses of the global economic network. For this, a linear temperature-productivity-relation approach for every region makes slightly less assumptions than a non-linear relation. We translate the local daily mean temperature to direct output production losses within a regional sector. Every grid cell r where the daily mean temperature $T_r(t)$ at day t surpasses 27°C suffers a linear reduction α_s in its productivity $p_{s,r}(t)$ per °C beyond 27°C for the sectors $\{s\}$:

- agriculture (−0.8 p.p./°C),
- fishing (−0.8 p.p./°C),
- mining and quarrying (−4.2 p.p./°C),
- hotels and restaurants (−6.1 p.p./°C),
- wholesale trade (−6.1 p.p./°C),
- and others (−2.2 p.p./°C)

(the unit p.p./°C corresponds to percent points per additional degree Celsius).

Thereby we only consider sectors for which statistically significant results in reduction of labor productivity have been found [17] as well as the agriculture and fishery as important sectors (impact on these is comparatively small, though). Thus, we exclude the sectors transport, communications, construction and manufacturing for which the empirical results were not statically significant.

Thus, we have a perturbed productivity of

$$p_{s,r}(t) = 1 - \alpha_s(T_r(t) - 27\ ^\circ\mathrm{C}) \quad \text{for} \quad T_r(t) \geq 27\ ^\circ\mathrm{C}. \tag{1}$$

The perturbed productivity per sector s of each cell r, which belongs to a region R, is aggregated to the daily perturbed productivity per sector s of a region R weighted by the population distribution:

$$p_{s,R}(t) = \frac{\sum_{r \in R} p_{s,r}(t) P_r}{\sum_{r \in R} P_r},$$

with P_r being the population of cell r.

Absolute output losses are then determined by multiplying the perturbed productivity with the baseline production of that region (see next section).

Economic network

As the underlying baseline for the global economic network, we use multi-regional input-output (MRIO) tables of the EORA simplified data set v199.82 [47]. The build-up and harmonization of the input-output table base on certain assumptions, which barely affect the general structure of the flows, but rather their details. In our sensitivity analysis we show that our results are stable with respect to changes of individual flows. The commodity flows in the MRIO table are provided as monetary flows (in USD of the data year) between regional sectors. The economic baseline network is build from the EORA MRIO table for the year of 2012. Flows smaller than 1000$/year and regional sectors with negative value added are removed from the network. A few regions (Belarus, Guyana, Moldova, Zimbabwe) with inaccurate data basis, causing partially an extremely unrealistic temporal evolution, were neglected in our analysis. Because of their large economic power, we further disaggregate [48] the United States of America and China into 51 states and 32 provinces using gross regional product (GRP) data [49, 50] of the individual states and provinces, respectively. We thereby split the flows of goods and services from and to a subregion according to the share of the subregion's GRP of the total country's GDP. Each economic sector in a nation, US state or Chinese province, which we refer to as regions for simplicity, forms an individual agent or "regional sector" in the loss-propagation model Acclimate (see below). In addition to mapping the flows of goods and services, the EORA MRIO table is used to calculate the baseline production of each regional sector. The resulting economic network comprises 27 sectors (including one consumer sector) and 268 regions, a total of 7, 236 agents.

Indirect production losses—The Acclimate model

We use the agent-based loss-propagation model Acclimate [51] to project the dynamics of the global economic network and derive overall production and consumption losses. This anomaly model revolves around the economic baseline given by the multi-regional input-output data. The direct output losses, given as short-term production reduction, impact this economic baseline network; Acclimate then simulates the behavior of firms (regional sectors) and consumers when perturbed from the baseline by a demand, supply, or price shock. In that, each regional sector, represented by a node in the input–output network, individually maximizes its profit by choosing the optimal production level and corresponding upstream demand as well as the optimal distribution of this demand among its suppliers.

In more detail, every time step consists of three subsequent decision points for each agent. In the first sub-step, a firm calculates its current production level in order to maximize its profit (difference between revenue and costs) under the current supply and demand circumstances. Any restrictions, such as limited production capacity or limited number of input goods, are taken into account. In particular, production costs increase non-linearly if firms extend their production beyond baseline quantities. In their sales prices firms are bound by the demanded requests and price offers received from their purchasers. Ordering these orders by descending price results in a concave revenue curve. Similar to firms, consumers decide on their consumption, but following the perceived prices according to their respective consumption elasticity. In the second sub-step agents update their expectations for the next time step according to goods received in the first sub-step. In the last sub-step, each agents decides via cost-minimization the distribution of demand among its suppliers in terms of quantity and price. This is based on supplier's offer prices as well as expectations on their cost curves. Thus

prices are endogenous non-equilibrium prices that are can differ locally for each supplier-purchaser pair. Supplied goods are transported between agents following a distance-based delay. Together with storage inventories, these transport pathways act as buffers for supply shocks.

Overall, the model dynamics focuses on the perturbations around a baseline equilibrium. Whereas this baseline is assumed to be optimal on longer time scales the endogenous local price changes as well as supply and demand mismatches are resolved explicitly over time. In the disaster aftermath, these relax back to the unperturbed baseline equilibrium over a timescale determined by the market. Computed losses thus account for price effects such as demand surge and supply shortages. With its focus on short-term perturbation dynamics the model does not include structural changes in the global trade network, such as investments, relocation of production or the establishment of new trade relations. A comprehensive model description of Acclimate is provided in Otto et al [51].

Consumer price elasticity

The consumers' reaction to price changes depends on consumed commodity and services as well on their own economic background. To reflect this in our model, the consumer price elasticity differs among regions and sectors. For that, we divide the regions into four groups, income levels, corresponding to their gross national income (GNI) per capita (GNI/pc) (S2 Table) (low, lower-middle, upper-middle, high income level). As income rises, the flexibility to react to prices increases which enables countries with a higher GNI/pc to respond more resiliently to price changes. The World Bank provides an annually and inflation-adjusted definition of income levels and country-specific data [52], which we use as a basis for our classification for the year 2012. We do not consider other national socio-economic structures (education, wealth distribution, etc.) in this study. Accordingly, we base the classification on average income only.

Within the Global Trade Analysis Project (GTAP) [53], target income elasticities of demand have been calculated for 140 regions and 10 commodity classes [54]. The regions of EORA and GTAP do not match perfectly. For non-GTAP-countries we assign the consumption price elasticities via the respective income level group specific parameter. To link the different sectoral resolutions, we map our economic sectors to the GTAP classes and then group them into three categories: vital, relevant, and other. The categorization of the sectors used is given in S1 Table. The more life essential goods or services are, the less flexible consumers can be in responding to price fluctuations. Using the three sector categories and the World Bank's country classification, we assign a specific consumer price elasticity from the GTAP data set [55] for any pair of level income and sector category (S3 Table). We do not consider cross-sector elasticity as one can assume low to no substitutability for the large sector classes we use (S1 Table).

Limitations

Into this short-term loss-propagation model labor productivity shocks enter as direct reductions in productivity, but do not take into account longer-term damage, such as destroyed infrastructure. As we focus on these short-term shocks and the corresponding economic repercussions, we assume that there is no investment and no explicit capital on these time scales. Also neither firms nor consumers have the explicit notion of savings. However, on a daily time scale, the effects of corporate growth or relocation of production are small compared to external production constraints [35]. With its agent-based short-term dynamics, the Acclimate model is particularly suited to assess the global distribution of consequences of unanticipated short-term shocks such as those caused by heat stress. Nevertheless, this study only focuses on a single impact channel of climate change disturbing the global economy. Naturally, this

occurs additional to other economic activity. Our results should thus not be interpreted as quantitative projections, but show trends between the last and upcoming double decades.

Results

We find (i) increases in direct output losses, (ii) a very heterogeneous distribution of overall total production losses and gains when incorporating price changes and other indirect effects (with gains in a majority of countries), and (iii) a differently distributed consumption response with almost all regions reducing consumption while increasing expenditure. In the following, we give detailed results for the median of the ensemble of four climate models and two representative concentration pathways each. These results should not be interpreted as literal projections, but show trend and magnitude of the higher-order effects of this one particular impact channel of climate change—under the current economic structure and in absence of adaptation.

Direct output losses

According to global climate models, global mean temperature increases by about 0.8˚C between 2000 and 2039 and as a consequence direct output losses increase by 47%—if no further adaptation measures are taken (Fig 1A and 1C). Within the next two decades, the global direct output loss will increase by 24% (in 2039 compared to 2020). This corresponds to an increase in global direct output losses of about USD 127bn per degree of global warming. These local heat stress-induced losses are heterogeneously distributed across regions (Fig 1b).

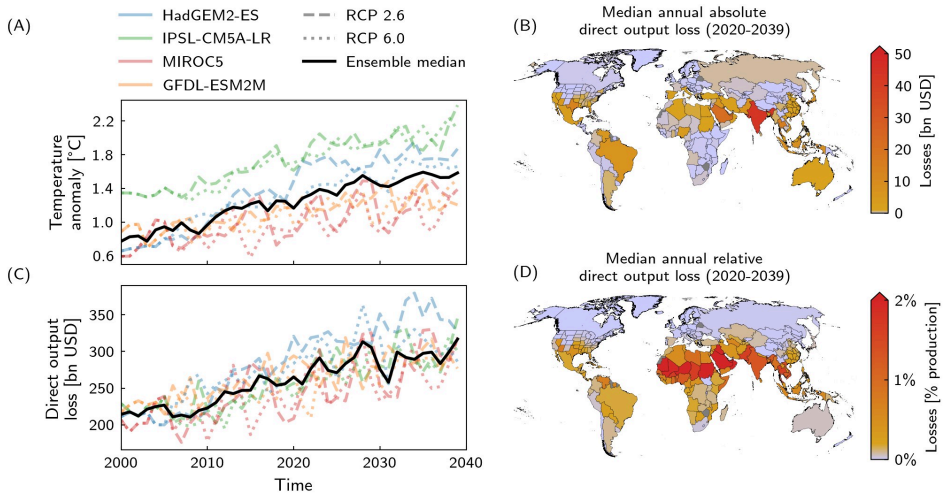

Fig 1. Global mean temperature anomaly and heat stress-induced direct output losses. A,C: Temporal evolution of A global mean temperature anomaly relating to pre-industrial level and C heat stress-induced direct output losses for the four climate models, HadGEM2-ES (blue), IPSL-CM5A-LR (green), MIROC5 (red), GFDL-ESM2M (orange) and RCP2.6 (dashed) and RCP6.0 (dotted), and ensemble median (black line). The higher temperature anomaly of climate model IPSL-CM5A-LR compared to the other climate models is due to the relatively lower model-internal pre-industrial temperature. B,D: Regional maps of B absolute and D relative annual direct output loss due to heat stress based on the respective regional projected median for 2020–2039. Regions with an absolute or relative direct annual output loss below USD 1bn or 0.2% of baseline (unperturbed) production are depicted in light purple.

https://doi.org/10.1371/journal.pone.0251210.g001

For all maps shown in this paper, shapes of countries are based on GADM data [46]. About 84% of all regions exhibit an annual median output loss of less than USD 1bn p.a. in 2020–2039 whereas several major economies experience substantially higher output losses. Among those are Saudi Arabia (USD 22bn p.a.), China (USD 29bn p.a.), USA (USD 40bn p.a.), and India (USD 44bn p.a.). In terms of relative losses, i.e. a percentage of a country's overall production level, countries of the Sahel, the Arabian Peninsula, and South Asia are impacted the strongest (Fig 1d). The global rise in temperature leads regionally to an increase in direct losses in the billions USD (e.g. in India, Saudi Arabia, or Mexico) or nearly double the direct output losses (e.g. in Northern America or Europe) within the next decades (S1 and S2 Figs).

Total production losses and gains. These direct output losses evoke a market response locally as well as across country borders. The heat stress-induced scarcity inflates prices of intermediate goods and services as well as consumer prices. On a global level, the increase in value of produced goods rises from 0.23% p.a. in 2000 to 0.36% p.a. in 2039 (Fig 2a). Again, there are large differences between countries. Some sectors in some countries even profit from heat stress-induced outages of their competitors when scarcity inflates the prices for their product and/or they receive more demand requests. For example, the US state of Texas and the country of Iraq have to cut back their production in the petroleum and non-metallic mineral sector, while Iran and Russia are ramping up their production in this sector. Many countries, including most G20 countries, are able to increase the value of their goods and services due to price effects despite direct output losses (Fig 2b). Economic relations are a relevant factor here. Although Spain and Greece suffer significant direct output losses (Fig 1), they are still increasing their production value through the European Single Market (Fig 2b). This is in contrast to Arizona and Texas failing to convert their direct output losses within the US economic system into total production gains. A few countries (e.g. Saudi Arabia, India, Thailand), suffer from many hot days in a year and therefore cannot benefit from a positive change in total production as well (Fig 3).

Consumption losses and change in expenditure

Facing higher prices, consumers have a certain willingness and ability to increase their expenditure in order to reduce consumption losses. This behavior determines the increase in household expenditures alongside a price-driven reduction in material consumption. In our model, consumers' willingness and ability to adjust their expenditures in response to rising prices is described by the consumption price elasticity. Since economic well-being and necessity of goods and services have a crucial role on consumption decision, we use a country and sector-specific consumption price elasticity (see Methods for a detailed description).

As a consequence, as global output decreases and prices inflate, consumption is diminished. However, our results show that this occurs regardless of the question if the country itself actually gains from increased prices in production value or not (Fig 3)—only a few economically small states show (very small) consumption gains. This is due to the strong global interconnectedness transferring heat-stress losses in terms of consumption also to countries not affected themselves. Though some of these countries can benefit in their production values, the consumption reduction can only partiality be compensated for; in most countries there is a higher share of production gain than consumption loss (Fig 3). Although in the three largest economic regions, USA, China, and the European Union, the heat stress-induced direct production losses are distributed heterogeneously within their regions (Fig 1B and 1D), the EU exhibits an enhanced consumption loss and total production gain (Fig 3). This may be due to the strong economic connection among US states and among provinces of China. These connections make it easier to compensate for production losses within these countries. Compared

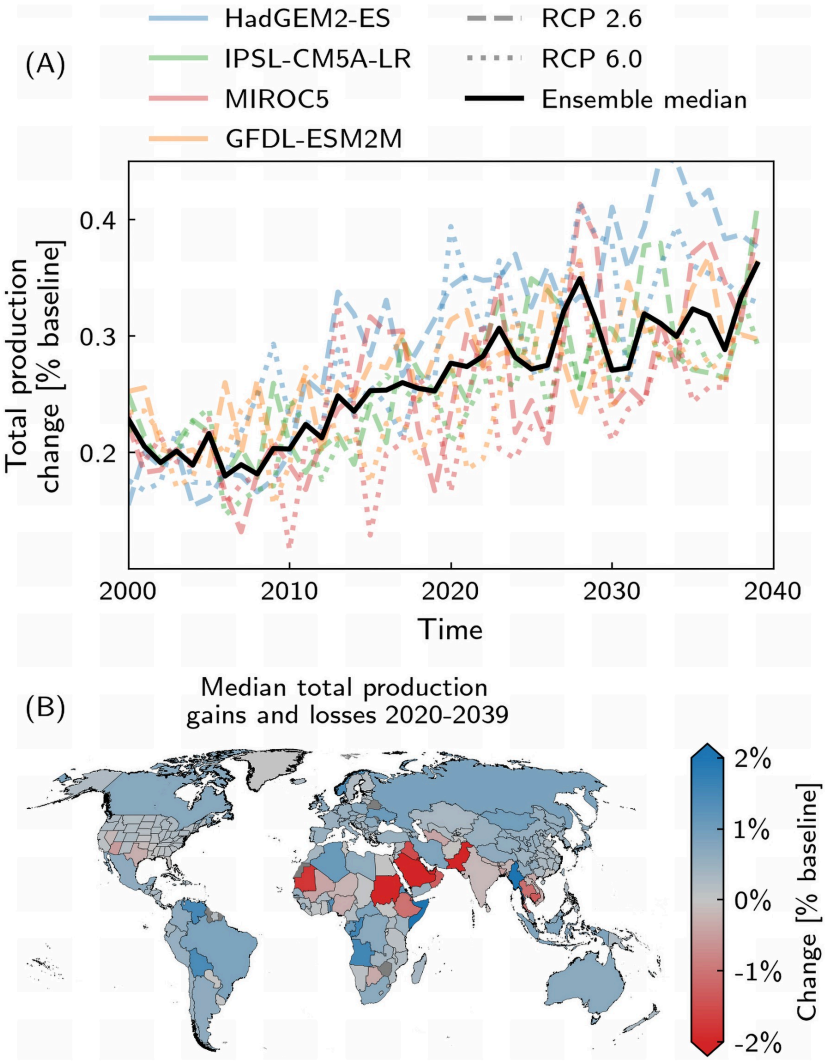

Fig 2. Total production losses and gains. A: Temporal evolution of global total production change for the four climate models, HadGEM2-ES (blue), IPSL-CM5A-LR (green), MIROC5 (red), GFDL-ESM2M (orange), and RCP2.6 (dashed) and RCP6.0 (dotted), and ensemble median (black line). B: Regional map of total production gains and losses based on the respective regional projected median for 2020–2039 and the full GCM–RCP ensemble. Quantities are given relative to the baseline (unperturbed) production.

https://doi.org/10.1371/journal.pone.0251210.g002

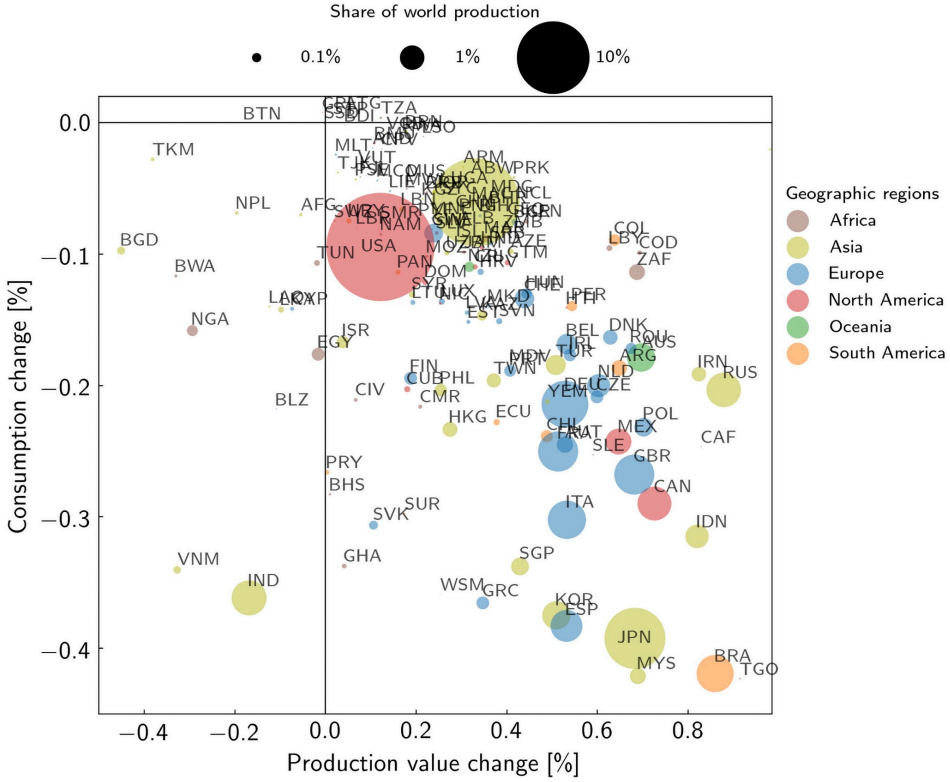

Fig 3. Consumption and total production change per country for the time period 2020–2039. The area of each dot is proportional to the corresponding country's baseline (unperturbed) production. The dot colours denote the geographic regions (see S2 Table). Quantities are given relative to the baseline (unperturbed) production and consumption, respectively.

https://doi.org/10.1371/journal.pone.0251210.g003

to the historical period (2000–2019), gains and losses of total production and consumption increase moderately in the future, but the qualitative pattern of the countries remains similar (Fig 3 and S3 Fig).

Global consumption decreases, i.e. heat stress-induced consumption losses increase from 0.15% p.a. in 2020 to 0.30% p.a. in 2039 (Fig 4A). These quantitative losses come at a higher consumer expenditure, which increases from 0.11% p.a. in 2020 to 0.16% p.a. in 2039 (Fig 4C). Per degree of warming, expenditure thus rises by 0.06 percentage points as consumption falls by 0.18 percentage points. These results are regionally fairly homogeneous (Fig 4B); about 93% of the global population lives in a region where consumer expenditures increase (Fig 4D). The pattern of pressure on consumers does not change between historical and future periods (S4B and S4C Fig).

Neglecting other economic benefits such as potentially higher wages because of increased production value (as most, though not all, countries with diminished consumption show), this

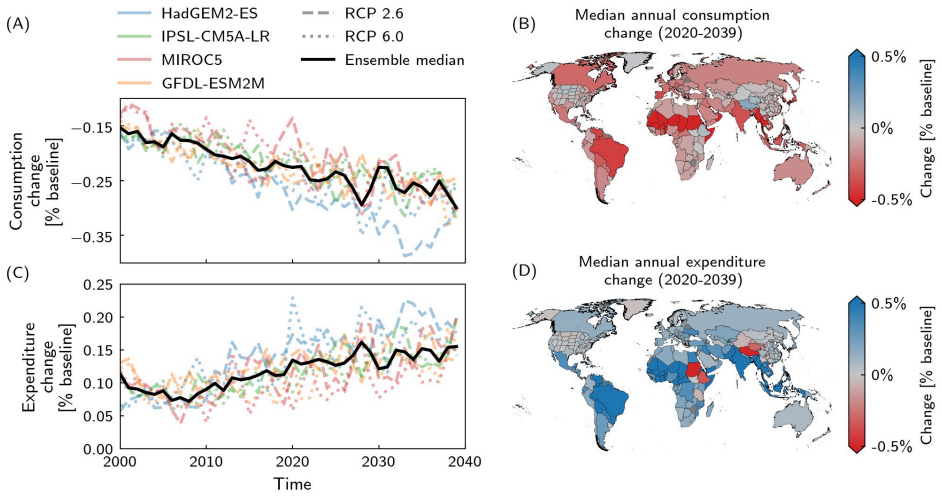

Fig 4. Consumption and expenditure change. A,C: Temporal evolution of A global consumption change and C global expenditure change for the four climate models, HadGEM2-ES (blue), IPSL-CM5A-LR (green), MIROC5 (red), GFDL-ESM2M (orange), and RCPs 2.6 (dashed) and 6.0 (dotted), and ensemble median (black line). B,D: Regional maps of B annual consumption change and D annual expenditure change based on the respective regional projected median for 2020–2039 and the full GCM–RCP ensemble. Quantities are given relative to the baseline (unperturbed) consumption and expenditure, respectively.

https://doi.org/10.1371/journal.pone.0251210.g004

comes at a decrease of household welfare. Overall, one can say that the heat stress shocks on productivity lead to a reduced overall economic efficiency which cannot be fully mitigated by market flexibility.

Changing the underlying economic network

The results above all assume a constant baseline structure of the global economic network, i.e. they are to be interpreted "given the world economy of 2012". Nevertheless, our results are qualitatively robust to the network used when compared to results with the network structures of 1992 and 2002 (Fig 5). Quantitatively, however, earlier network structures show a smaller response, in particular in the total production changes, due to their much smaller interconnectedness [36]. Interestingly, consumer expenses are similar for all three networks, though consumption losses are by far highest for the 2012 network (Fig 5B and 5C). For the future world economy assuming further globalization of supply and trade chains, one would thus expect an even stronger response to heat stress even without climate change.

Results robust against parameter choice

Central to the overall consumer behavior in our model is the consumption price elasticity. To assess its influence on our results, we conduct a sensitivity analysis sampling this parameter for every consumer in a range from −1.0 (highly flexible to price changes) to −0.1 (almost disregarding price changes) (Fig 6A). In the analysis, all consumers have the same consumption parameter so that results are directly comparable. In our parameter study, we use the eight direct output loss time series to shock Acclimate and we focus on the global consumption

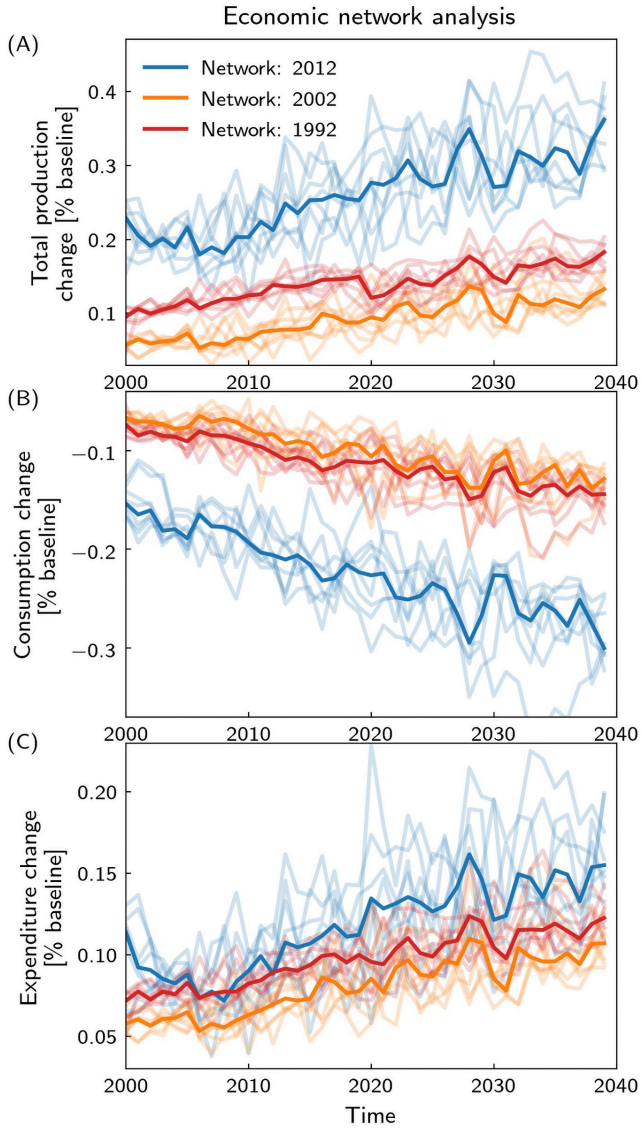

Fig 5. Total production, consumption, and expenditure change for economic networks of 2012, 2002, and 1992. Temporal evolution of A total production changes, B consumption change and C expenditure change for economic networks of 2012 (blue), 2002 (orange) and 1992 (red). Ensemble members and median are depicted in light and thick lines, respectively.

https://doi.org/10.1371/journal.pone.0251210.g005

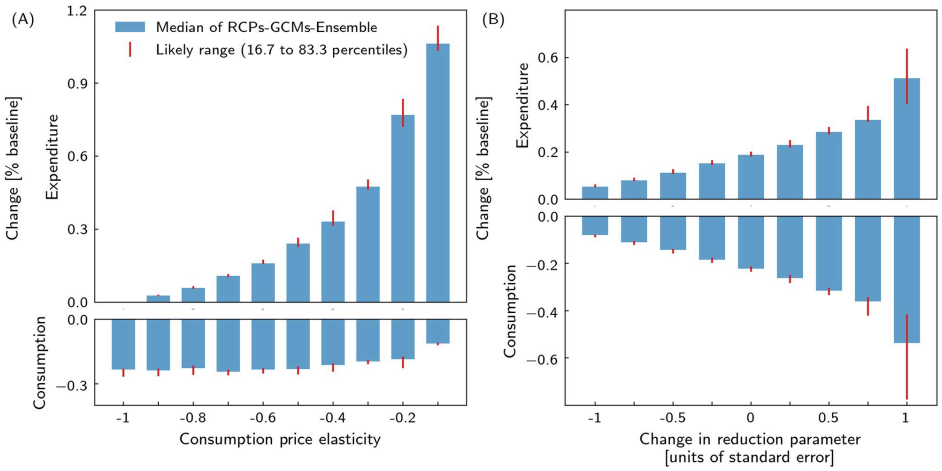

Fig 6. Results are robust against choice of consumption price elasticity and temperature-productivity-uncertainty. Median of RCPs-GCMs-Ensemble and likely range (16.7 to 83.3 percentiles) of heat stress-induced changes in consumer expenditure and consumption in 2039 relative to unperturbed baseline for A different consumption price elasticities and B change in intensity of productivity reduction due to heat stress.

https://doi.org/10.1371/journal.pone.0251210.g006

losses and expenditure raise in 2039. On the one hand, global expenditure rises with increasing inflexibility. This is reasonable to expect as consumers are less likely to accept price increases with greater flexibility. On the other hand, global consumption losses due to heat stress hardly change. So the future heat stress-related pressure on people's purchasing power is largely insensitive to the choice of the consumption price elasticity.

This study uses quasi-linear direct production reduction based on empirical econometric values [17]. A sensitivity analysis of this functions shows that the trend of our results persists against changes in the direct production reduction (Fig 6B). For that, the damage function parameters are sampled in their standard error range [17]. Global consumption losses and expenditure rise increase with higher direct output reduction. An increased sensitivity to heat stress leads to more disturbed production. The higher price increase due to greater scarcity is passed on to the consumer, who spends more and consumes less. Overall, our qualitative results are robust under a wide range of values of those parameters.

Discussion

Our results are in line with studies looking at the direct effect of heat stress [17, 18] and its consequences on the local economy [56]. We hereby give an additional global perspective including the impact of heat stress on short-term price changes as well as supply and trade chains. Besides a chance for "building back better" after an economic shock as suggested by other studies [57], we also identify a potential positive side effect for many less affected regions when considering shifting of demand and supply. We show that this effect, however, comes at the expense of the consumer. On a longer time scale, e.g. by affecting economic growth, also production might be affected negatively [58]. A stimulating effect of productivity shocks would also cease for stronger disasters, such as floods, which have an overall negative effect on directly as well as indirectly affected regions [37]. It is important to note that our study focuses

on consecutive extreme events [59] rather than singular shocks; locally, heat stress constitutes many small but lasting background shocks to the economy, partly even simultaneously at different regions, and thus puts a persistent pressure on the global supply network. Building on our results, further studies could provide estimates on sub-national distribution of heat induced consumption losses as well as on economic impacts due to heat stress for the mid- and end-century.

Since the interaction between consumption, production, and price is based on a complex chain of measurable factors (e.g. income) and psychological factors (e.g. expectations) [60], any modeling of these variables is necessarily based on generalizing assumptions. Here, we specify the main assumptions of our study and and discuss their adequacy. Regional daily temperatures from climate projections and resulting possible heat-related losses are not exact forecasts but rather serve as exemplary conditions here. For that, we use an ensemble of individual loss time series derived from eight different RCPs–GCMs combination. Since the trend and magnitude of the results are consistent within the ensemble, we observe that our results are robust with respect to the uncertainties of climate projections and independent of individual daily weather conditions. In this study we focus specifically on the impact on the economy and consumers due to short-term heat stress-related production losses. Therefore we opt a daily temperature-production-correlation. In particular, we generalize a heat impact shown only for Caribbean countries [17] to every region of the world. This assumption is supported by research showing that climatic conditions have non-linear effects on human productivity in any country [18, 21]. Similar to Hsiang et al [17], other studies are limited to a specific region as well [61]. With this damage function we show the trend evolution of consumption losses in the past and future double decade.

Apart from physical and econometric uncertainties, there are also constraints on economic and human behavior modeling due to their complexity. In order to properly interpret our results in the light of the limits of our study, we clarify the main boundaries of our modeling in the following. For one, we are simulating short-term economic repercussions, so we do not need to consider longer-term socio-economic changes, such as investment strategies of firms or new trade linkages. In particular, we use the economic trade network of 2012 as the fixed socio-economic baseline. Our sensitivity analysis on the networks depict that the trend of our results is robust against different economic networks. Additionally, the results of our analysis imply that in a more interconnected world trade the impact of heat stress is likely to increase. Furthermore, we explicitly neglect adaptation, since we do not want to make assumptions on possible adaptation measures and their effects. Thus we can interpret our results as a more direct response of the global supply network. In this respect, our results indicate that adaptation measures to heat stress in production are necessary. Global warming makes such measures even more vital.

Conclusion

Our results must not be interpreted as literal and comprehensive predictions of the effects of future heat stress events. They may rather serve as a qualitative prediction with quantitative predictive skill limited to the order of magnitude of the signal. Overall, they highlight that heat stress will, without adaptation measures, increase direct output production losses, regionally and globally. Those unexpected climatic events such as heat waves can reduce the welfare of consumers, even if economic key indicators such as production value, and thus nominal GDP, suggest beneficial economic effects in many regions. This indicates that intensified and more frequent heat waves constitute an increasing threat to prosperity of nations in the near future.

Supporting information

S1 Fig. Heat stress-induced median annual direct output losses for the historic time period 2000–2019. Regional maps of A absolute and B relative annual direct output loss due to heat stress based on the respective regional bias-corrected median for 2000–2019. Regions with an absolute or relative direct annual output loss below USD 1bn or 0.2% of baseline (unperturbed) production are depicted in light purple, respectively.
(TIF)

S2 Fig. Projected increase of heat stress-induced annual direct output losses between historic (2000–2019) and future (2020–2039) period. A Absolute annual increase of regional direct output losses of period 2020–2039 compared to 2000–2019. B Increase of direct output losses in the future period in terms of losses in the historic period.
(TIF)

S3 Fig. Consumption and total production change per country for the historic period 2000–2019. The area of each dot is proportional to the corresponding country's baseline (unperturbed) production. The dot colors denote the geographic regions (see S2 Table). Quantities are given relative to the baseline (unperturbed) production and consumption, respectively.
(TIF)

S4 Fig. Total production, consumption, and expenditure change for the historic period 2000–2019. Median annual change of A total production, B consumption and C expenditure relative to the unperturbed baseline.
(TIF)

S1 Table. Sectors used in the simulations. For sectors prone to heat stress-induced productivity loss the respective reduction factor (see Methods) is given in the last column.
(PDF)

S2 Table. Regions used in the simulations. Income level corresponds to Gross National Income per capita (GNIpc) of 2012.
(PDF)

S3 Table. Consumption price elasticities per income level and sector category. Values are based on GTAP [55].
(PDF)

Author Contributions

Conceptualization: Sven Norman Willner, Anders Levermann.

Formal analysis: Kilian Kuhla.

Investigation: Kilian Kuhla, Sven Norman Willner, Christian Otto, Anders Levermann.

Resources: Christian Otto, Leonie Wenz.

Writing – original draft: Kilian Kuhla, Sven Norman Willner.

Writing – review & editing: Christian Otto, Leonie Wenz, Anders Levermann.

References

1. Team G. GISS Surface Temperature Analysis (GISTEMP), version 4; 2021. https://data.giss.nasa.gov/gistemp/.

2. Lenssen N, Schmidt G, Hansen J, Menne M, Persin A, Ruedy R, et al. Improvements in the GISTEMP uncertainty model. J Geophys Res Atmos. 2019; 124(12):6307–6326. https://doi.org/10.1029/2018JD029522
3. Hansen J, Ruedy R, Sato M, Lo K. Global surface temperature change. Reviews of Geophysics. 2010; 48(4). https://doi.org/10.1029/2010RG000345
4. Stocker TF, Qin D, Plattner GK, Tignor M, Allen SK, Boschung J, et al. Climate Change 2013—The Physical Science Basis. Cambridge: Cambridge University Press; 2014. Available from: http://ebooks.cambridge.org/ref/id/CBO9781107415324.
5. Meehl GA, Tebaldi C. More intense, more frequent, and longer lasting heat waves in the 21st century. Science. 2004; 305(5686):994–997. https://doi.org/10.1126/science.1098704 PMID: 15310900
6. Rahmstorf S, Coumou D. Increase of extreme events in a warming world. PNAS. 2011; 108(44):17905–17909. https://doi.org/10.1073/pnas.1101766108 PMID: 22025683
7. Deryng D, Conway D, Ramankutty N, Price J, Warren R. Global crop yield response to extreme heat stress under multiple climate change futures. Environmental Research Letters. 2014; 9(3):034011. https://doi.org/10.1088/1748-9326/9/3/034011
8. Kovats RS, Sari Kovats R, Hajat S. Heat Stress and Public Health: A Critical Review. Annual Review Public Health. 2008; 29(1):41–55. https://doi.org/10.1146/annurev.publhealth.29.020907.090843 PMID: 18031221
9. Wenz L, Levermann A, Auffhammer M. North-south polarization of European electricity consumption under future warming. PNAS. 2017; 114(38):E7910–E7918. https://doi.org/10.1073/pnas.1704339114 PMID: 28847939
10. Auffhammer M, Baylis P, Hausman CH. Climate change is projected to have severe impacts on the frequency and intensity of peak electricity demand across the United States. PNAS. 2017; 114(8):1886–1891. https://doi.org/10.1073/pnas.1613193114 PMID: 28167756
11. Deryugina T, Hsiang SM. Does the Environment Still Matter? Daily Temperature and Income in the United States. National Bureau of Economic Research; 2014. 20750. Available from: http://www.nber.org/papers/w20750.
12. Dell M, Jones BF, Olken BA. Temperature and Income: Reconciling New Cross-Sectional and Panel Estimates. American Economic Review. 2009; 99(2):198–204. https://doi.org/10.1257/aer.99.2.198
13. Zander KK, Botzen WJW, Oppermann E, Kjellstrom T, Garnett ST. Heat stress causes substantial labour productivity loss in Australia. Nature Climate Change. 2015; 5(7):647–651. https://doi.org/10.1038/nclimate2623
14. Dunne JP, Stouffer RJ, John JG. Reductions in labour capacity from heat stress under climate warming. Nature Climate Change. 2013; 3(6):563–566. https://doi.org/10.1038/nclimate1827
15. Auffhammer M. Quantifying Economic Damages from Climate Change. Journal of Economic Perspectives. 2018; 32(4):33–52. https://doi.org/10.1257/jep.32.4.33
16. Roson Roberto; Van der Mensbrugghe D. Climate change and economic growth: impacts and interactions. International Journal of Sustainable Economy. 2012; 4(3). https://doi.org/10.1504/IJSE.2012.047933
17. Hsiang SM. Temperatures and cyclones strongly associated with economic production in the Caribbean and Central America. PNAS. 2010; 107(35):15367–15372. https://doi.org/10.1073/pnas.1009510107 PMID: 20713696
18. Burke M, Hsiang SM, Miguel E. Global non-linear effect of temperature on economic production. Nature. 2015; 527(7577):235–239. https://doi.org/10.1038/nature15725 PMID: 26503051
19. Cachon G, Gallino S, Olivares M. Severe Weather and Automobile Assembly Productivity. SSRN Electronic Journal. 2012;.
20. Graff Zivin J, Zivin JG, Neidell M. Temperature and the Allocation of Time: Implications for Climate Change. Journal of Labor Economy. 2014; 32(1):1–26. https://doi.org/10.1086/671766
21. Graff Zivin J, Zivin JG, Hsiang SM, Neidell M. Temperature and Human Capital in the Short and Long Run. Journal of the Association of Environmental and Resource Economists. 2018; 5(1):77–105. https://doi.org/10.1086/694177
22. Fang J, Gozgor G, Lu Z, Wu W. Effects of the export product quality on carbon dioxide emissions: evidence from developing economies. Environmental Science and Pollution Research. 2019; 26(12):12181–12193. https://doi.org/10.1007/s11356-019-04513-7 PMID: 30835064
23. Alam MS, Apergis N, Paramati SR, Fang J. The impacts of R&D investment and stock markets on clean-energy consumption and CO2 emissions in OECD economies. International Journal of Finance & Economics. 2020;.

24. Malerba D. The Trade-off Between Poverty Reduction and Carbon Emissions, and the Role of Economic Growth and Inequality: An Empirical Cross-Country Analysis Using a Novel Indicator. Social Indicators Research. 2020; 150(2):587–615. https://doi.org/10.1007/s11205-020-02332-9

25. Takakura J, Fujimori S, Takahashi K, Hijioka Y, Hasegawa T, Honda Y, et al. Cost of preventing workplace heat-related illness through worker breaks and the benefit of climate-change mitigation. Environmental Research Letters. 2017; 12(6):064010. https://doi.org/10.1088/1748-9326/aa72cc

26. Kim L, Levitov M. Bloomberg—Are you a robot?; 2010. http://www.bloomberg.com/news/2010-08-10/russia-may-lose-15-000-lives-15-billion-of-economic-output-in-heat-wave.html.

27. Acemoglu D, Carvalho VM, Ozdaglar A, Tahbaz-Salehi A. The network origins of aggregate fluctuations. Econometrica. 2012; 80(5):1977–2016. https://doi.org/10.3982/ECTA9623

28. Okuyama Y, Chang SE. Modeling Spatial and Economic Impacts of Disasters. Springer Science & Business Media; 2013.

29. Levermann A. Make supply chains climate-smart. Nature. 2014; 506:27–29. https://doi.org/10.1038/506027a PMID: 24499903

30. Inoue H, Todo Y. Propagation of negative shocks across nation-wide firm networks. PLoS One. 2019; 14(3):e0213648. https://doi.org/10.1371/journal.pone.0213648 PMID: 30870470

31. Rose A. Economic Principles, Issues, and Research Priorities in Hazard Loss Estimation. Modeling Spatial and Economic Impacts of Disasters. 2004; p. 13–36. https://doi.org/10.1007/978-3-540-24787-6_2

32. van der Veen A. Disasters and economic damage: macro, meso and micro approaches. Disaster Prevention and Management. 2004; 13(4):274–279. https://doi.org/10.1108/09653560410556483

33. Henriet F, Hallegatte S, Tabourier L. Firm-network characteristics and economic robustness to natural disasters. Journal of Economic Dynamics and Control. 2012; 36(1):150–167. https://doi.org/10.1016/j.jedc.2011.10.001

34. Haile MG, Kalkuhl M, von Braun J. Worldwide Acreage and Yield Response to International Price Change and Volatility: A Dynamic Panel Data Analysis for Wheat, Rice, Corn, and Soybeans. Food Price Volatility and Its Implications for Food Security and Policy. 2016; p. 139–165. https://doi.org/10.1007/978-3-319-28201-5_7

35. Hallegatte S. An adaptive regional input-output model and its application to the assessment of the economic cost of Katrina. Risk Analysis. 2008; 28(3):779–799. https://doi.org/10.1111/j.1539-6924.2008.01046.x PMID: 18643833

36. Wenz L, Levermann A. Enhanced economic connectivity to foster heat stress-related losses. Science Advances. 2016; 2(6):e1501026. https://doi.org/10.1126/sciadv.1501026 PMID: 27386555

37. Willner SN, Otto C, Levermann A. Global economic response to river floods. Nature Climate Change. 2018; 8(7):594–598. https://doi.org/10.1038/s41558-018-0173-2

38. Taylor KE, Stouffer RJ, Meehl GA. An Overview of CMIP5 and the Experiment Design. Bulletin of the American Meteorological Society. 2012; 93(4):485–498. https://doi.org/10.1175/BAMS-D-11-00094.1

39. Jones CD, Hughes J, Bellouin N, Hardiman S, Jones G, Knight J, et al. The HadGEM2-ES implementation of CMIP5 centennial simulations. Geoscientific Model Development (GMD). 2011; 4(3). https://doi.org/10.5194/gmd-4-543-2011

40. Dufresne JL, Foujols MA, Denvil S, Caubel A, Marti O, Aumont O, et al. Climate change projections using the IPSL-CM5 Earth System Model: from CMIP3 to CMIP5. Climate Dynamics. 2013; 40(9-10):2123–2165. https://doi.org/10.1007/s00382-012-1636-1

41. Watanabe M, Suzuki T, O'ishi R, Komuro Y, Watanabe S, Emori S, et al. Improved Climate Simulation by MIROC5: Mean States, Variability, and Climate Sensitivity. Journal of Climate. 2010; 23(23):6312–6335. https://doi.org/10.1175/2010JCLI3679.1

42. Dunne JP, John JG, Adcroft AJ, Griffies SM, Hallberg RW, Shevliakova E, et al. GFDL's ESM2 Global Coupled Climate–Carbon Earth System Models. Part I: Physical Formulation and Baseline Simulation Characteristics. Journal of Climate. 2012; 25(19):6646–6665. https://doi.org/10.1175/JCLI-D-11-00560.1

43. Frieler K, Lange S, Piontek F, Reyer CPO, Schewe J, Warszawski L, et al. Assessing the impacts of 1.5˚C global warming—simulation protocol of the Inter-Sectoral Impact Model Intercomparison Project (ISIMIP2b). Geoscientific Model Development. 2017; 10:4321–4345. https://doi.org/10.5194/gmd-10-4321-2017

44. Hempel S, Frieler K, Warszawski L, Schewe J, Piontek F. A trend-preserving bias correction—the ISI-MIP approach. Earth System Dynamics. 2013; 4(2):219–236. https://doi.org/10.5194/esd-4-219-2013

45. Center for International Earth Science Information Network—CIESIN – Columbia University. Gridded Population of the World, Version 4 (GPWv4): Population Count; 2016.

46. Global Administrative Areas. GADM database of Global Administrative Areas, version 3.6; 2018. Available from: http://www.gadm.org.

47. Lenzen M, Moran D, Kanemoto K, Geschke A. Building Eora: a global multi-region input–output database at high country and sector resolution. Economic Systems Research. 2013; 25(1):20–49. https://doi.org/10.1080/09535314.2013.769938

48. Wenz L, Willner SN, Bierkandt R, Levermann A. Acclimate—a model for economic damage propagation. Part II: a dynamic formulation of the backward effects of disaster-induced production failures in the global supply network. Environment Systems and Decisions. 2014; 34:525–539. https://doi.org/10.1007/s10669-014-9521-6

49. U S Bureau of Economic Analysis. Gross regional product of the states of the USA; 2010. https://apps.bea.gov/itable/iTable.cfm?ReqID=70.

50. National Bureau of Statistics of China. Gross regional product of the provinces of China; 2010. http://data.stats.gov.cn/english/easyquery.htm?cn=E0103.

51. Otto C, Willner SN, Wenz L, Frieler K, Levermann A. Modeling loss-propagation in the global supply network: The dynamic agent-based model acclimate. Journal of Economic Dynamics and Control. 2017; 83:232–269. https://doi.org/10.1016/j.jedc.2017.08.001

52. Khokhar T. Chart: Global Wealth Grew 66% Between 1995 and 2014; 2019. http://datatopics.worldbank.org/world-development-indicators/stories/the-classification-of-countries-by-income.html.

53. Ianchovichina E, McDougall R. Theoretical Structure of Dynamic GTAP. Global Trade Analysis Project (GTAP); 2000. 17. Available from: https://www.gtap.agecon.purdue.edu/resources/res_display.asp?RecordID=480.

54. Reimer J, Hertel TW. International Cross Section Estimates of Demand for Use in the GTAP Model. GTAP Technical paper. 2004; 23.

55. Hertel T, van der Mensbrugghe D. Behavioral Parameters. In: G BN, Aguiar A, McDougall R, editors. Global Trade, Assistance, and Production: The GTAP 9 Data Base. Department of Agricultural Economics, Purdue University, West Lafayette, IN: Purdue University; 2016. p. 14–1–14–20. Available from: https://www.gtap.agecon.purdue.edu/resources/res_display.asp?RecordID=5138.

56. Zhang P, Deschenes O, Meng K, Zhang J. Temperature effects on productivity and factor reallocation: Evidence from a half million chinese manufacturing plants. Journal of Environmental Economics and Management. 2018; 88(C):1–17. https://doi.org/10.1016/j.jeem.2017.11.001

57. Mannakkara Sandeeka; Wilkinson S. Re-conceptualising "Building Back Better" to Improve Post-Disaster Recovery. International Journal of Managing Projects in Business. 2014; 7(3). https://doi.org/10.1108/IJMPB-10-2013-0054

58. Poledna S, Hochrainer-Stigler S, Miess MG, Klimek P, Schmelzer S, Sorger J, et al. When does a disaster become a systemic event? Estimating indirect economic losses from natural disasters; 2018.

59. de Ruiter MC, Couasnon A, van den Homberg MJC, Daniell JE, Gill JC, Ward PJ. Why We Can No Longer Ignore Consecutive Disasters. Earth's Future. 2020; 8(3):e2019EF001425. https://doi.org/10.1029/2019EF001425

60. Boulding KE. The Consumption Concept in Economic Theory. The American Economic Review. 1945; 35(2).

61. Orlov A, Sillmann J, Aaheim A, Aunan K, de Bruin K. Economic Losses of Heat-Induced Reductions in Outdoor Worker Productivity: a Case Study of Europe. Economics of Disasters and Climate Change. 2019; 3(3):191–211. https://doi.org/10.1007/s41885-019-00044-0

Article B

Wave-like global economic ripple response to Hurricane Sandy

Authors

Robin Middelanis, Sven N Willner, Christian Otto, Kilian Kuhla, Lennart Quante and Anders Levermann

Status

Published in *Enviromental Research Letters* in December 2021,
doi: 10.1088/1748-9326/ac39c0.

Capsule summary

Hurricane Sandy (2012) was the fourth-costliest hurricane in the history of the USA. Here, the global economic repercussion due to Sandy is simulated using the agent-based model *Acclimate*. By doing this, a three-phased ripple in the global trade network is detected and analyzed. First, an initial demand reduction causes corresponding consumption prices to decline. Second, as economic agents are under-supplied, prices rise locally. Finally, after the ripples are propagated through the economic network, price, production, and supply changes relax to their initial state during a recovery phase. Regional responses to ripples depend on the link strength to directly affected network nodes, meaning firms in New York and New Jersey.

Author contributions

Kilian Kuhla provided regionally and sectorally resolved consumer price elasticities to analyze regional consumption price dependencies. Robin Middelanis and Kilian Kuhla reviewed different direct damage dynamics. All authors discussed the results and wrote the manuscript.

IOP Publishing Environ. Res. Lett. 16 (2021) 124049 https://doi.org/10.1088/1748-9326/ac39c0

ENVIRONMENTAL RESEARCH
LETTERS

OPEN ACCESS

RECEIVED
12 October 2021

REVISED
11 November 2021

ACCEPTED FOR PUBLICATION
15 November 2021

PUBLISHED
6 December 2021

LETTER

Wave-like global economic ripple response to Hurricane Sandy

Robin Middelanis[1,2], **Sven N Willner**[1,*], **Christian Otto**[1], **Kilian Kuhla**[1,2], **Lennart Quante**[1,2] and **Anders Levermann**[1,2,3]

[1] Potsdam Institute for Climate Impact Research, Telegrafenberg A56, Potsdam, Germany
[2] University of Potsdam, Potsdam, Germany
[3] Columbia University, New York, NY, United States of America
[*] Author to whom any correspondence should be addressed.

E-mail: sven.willner@pik-potsdam.de

Keywords: supply chains, Hurricane Sandy, economic ripples, extreme weather impacts, loss propagation, natural disasters

Supplementary material for this article is available online

Abstract

Tropical cyclones range among the costliest disasters on Earth. Their economic repercussions along the supply and trade network also affect remote economies that are not directly affected. We here simulate possible global repercussions on consumption for the example case of Hurricane Sandy in the US (2012) using the shock-propagation model *Acclimate*. The modeled shock yields a global three-phase ripple: an initial production demand reduction and associated consumption price decrease, followed by a supply shortage with increasing prices, and finally a recovery phase. Regions with strong trade relations to the US experience strong magnitudes of the ripple. A dominating demand reduction or supply shortage leads to overall consumption gains or losses of a region, respectively. While finding these repercussions in historic data is challenging due to strong volatility of economic interactions, numerical models like ours can help to identify them by approaching the problem from an exploratory angle, isolating the effect of interest. For this, our model simulates the economic interactions of over 7000 regional economic sectors, interlinked through about 1.8 million trade relations. Under global warming, the wave-like structures of the economic response to major hurricanes like the one simulated here are likely to intensify and potentially overlap with other weather extremes.

1. Introduction

Globally, tropical cyclones range among the costliest and deadliest natural disasters. While they constitute only 16.5% of all recorded billion-dollar events in the United States between 1980 and 2018, they are responsible for more than half of the costs resulting from all extreme weather events combined [1, 2]. Their frequency is expected to decrease or to remain static under global warming but most projections anticipate an increase in intensity of the most extreme tropical cyclones [3], especially in the Atlantic basin [4] (where tropical cyclones are called hurricanes). In consequence, economic losses in hurricane-prone regions are expected to increase in the future due to climate change [5–8] through higher storm intensity [9] and sea level rise [10] but also due to changes in the economic values at risk [11, 12]. Local economies can be affected through destroyed capital stock (stock losses or damages) or through lost production output (flow losses). Since we do not consider damages in this work, we here generally imply lost production in the notion of loss. In particular, we refer to losses in a region that is directly affected by a hurricane as direct losses. However, losses can spread through the supply network, which is then referred to as higher-order losses [13–15]. We here refer to the latter as indirect losses. These may represent a substantial or even dominant share of total economic disaster losses [16–18]. Indirect losses can result from supply shortages due to direct losses that propagate downstream along supply chains. Direct losses and an associated production decrease may also lead to reduced demand (production demand, generally in contrast to final demand for household consumption) which propagates upstream in the

supply network. These downstream and upstream effects are also called forward and backward propagation [19] or ripple effects [20]. Here, we investigate the possible ripple response to Hurricane Sandy (2012) and its effect on global consumption expenditure.

There is good consensus in the literature that extreme weather events have adverse effects on household consumption [21], which is commonly used in economic models as a measure for societal welfare [22] and is therefore often regarded in disaster impact analyses. In this study, we refer to the latter as final consumption or simply consumption where we also include government spending. In a globalized world, local disasters can have global economic repercussions [23], one prime example being the COVID-19 pandemic [24] with huge estimated indirect consumption losses worldwide [25]. However, most studies [26–29] on the impacts of historic extreme weather events focus on the local economic impacts of the disaster and therefore miss the global dimension [23].

With this work, we choose a different scope of analysis and investigate a single historic hurricane's possible impact on consumption on a global scale. We simulate the potential global indirect impacts on consumption that a major hurricane in the United States can have globally, using an agent-based network model. We choose a modeling approach because this allows us to investigate aspects of higher-order effects of a single event that cannot be found in historic data. While local effects of hurricanes are — in large parts — well-studied [30–32], higher-order effects and the way they propagate in the trade network are still poorly understood. Lenzen [14] conducted a study on the higher-order indirect effects of a single hurricane in Australia but focus on national spillover effects. Other studies [7, 33, 34] give a global perspective but cannot link effects to single historic events or do not consider indirect losses. We here propose one means to study loss propagation and global effects on consumption after a single historic major hurricane. As a case study, we choose Hurricane Sandy which made landfall in the US in 2012.

Sandy severely hit the US and in particular the states of New York (NY) and New Jersey (NJ) in 2012. It was the fourth-costliest hurricane in history and caused an estimated total damage of $65bn [35] (in 2012 US Dollar), predominantly by driving a storm surge into the coastlines of NY and NJ [36]. Given the magnitude of this local economic shock and the importance of the economically strong regions of NY and NJ in the global trade network, Hurricane Sandy most likely also entailed indirect effect in regions not directly affected. To understand how these repercussions may have spread in the global supply and trade network, we here simulate global consumption expenditure across the global economy in the direct aftermath of the strong economic shock in NY and NJ after Sandy.

We thereby add to the discussion on the welfare impacts of extreme weather events in two major points. First, by taking a modeling approach, we can go beyond a local case study and simulate consumption impacts globally as a result of production shortages and price effects propagating in the global supply network. This allows us to investigate effects that are otherwise hidden in coarse and noisy data. We find that although directly affected regions show the strongest effects, we observe an overall impact on consumption on the global level. Regions with strong trade relations to the US are affected most. Second, our approach allows us to analyze the underlying propagation effects inside our model that lead to the observed global consumption anomalies. The propagation follows a three-phase ripple of prices. An initial upstream effect results in price decreases and associated consumption increases. The following downstream effect leads to price increases and reduced consumption, followed by a normalization phase.

2. Method overview

Our simulations are carried out using the dynamic agent-based model *Acclimate* [37] which models loss-propagation on the global supply network, assuming a demand-driven economy. In this model, economic sectors (in case of the United States and China on a state and province level respectively, otherwise on a national level) are modeled as agents that are interlinked through trade flows, with each agent maximizing its own profit. The economy of each region is divided into 27 sectors, including the final consumer. With a total of 268 modeled regions, this results in over 7000 agents. By applying an external shock in the form of a reduction in the production capacity of one or more agents, the initial baseline state of equilibrium can be disturbed. We model this production shock to represent the direct losses due to Hurricane Sandy in the affected areas of New York and New Jersey. We use a disaggregated [38] version of the EORA MRIO dataset for the year 2012 [39] as economic baseline. *Acclimate* then simulates anomalies around this baseline state that result from the production capacity reduction by profit-maximization of each individual agent on a daily time scale. Prices in the model are endogenous variables which account for local scarcities and transport costs. They always reflect price changes relative to baseline prices and do not represent absolute prices of traded goods (which are unknown since they are not contained in the EORA dataset).

The conceptual approach of this study is summarized in figure 1. We model the direct economic impact from Hurricane Sandy for NY and NJ only (orange and blue, respectively), although another ten

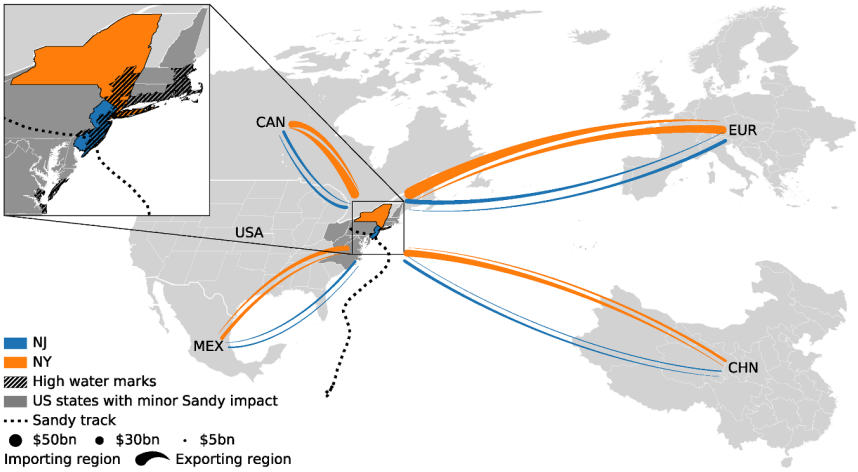

Figure 1. Conceptual design of the study. Hurricane Sandy (track shown as dotted line) resulted in physical damages in multiple US states. New York (orange) and New Jersey (blue) received the largest damages. Dark gray shaded states were affected in a comparatively minor way (see main text) and production shocks in these states therefore are not considered. We derive a disaster-driven reduction of production capacity for New York and New Jersey based on the GRP of counties with reported high water marks (hatched areas) and estimated recovery duration from business interruptions. We simulate the resulting impacts on global consumption through loss propagation in the global trade network. As an example, we here show import and export volumes of New York and New Jersey with Europe, China, Canada, and Mexico, aggregated over all sectors. Trade flows are directed from the sharp end to the large end of a wedge. The width of the large end shows the trade flow magnitude. Note that in the actual model, there are potentially trade flows between any two of the over 7000 economic agents, consisting of 27 sectors in 268 simulated regions. All region shape files retrieved from GADM [41], storm track from IBTrACS [42].

states and the District of Columbia (DC) were also affected (hatched areas). However, NY and NJ were most affected, receiving more than 96% of Congress' Disaster Relief Appropriations Act funds from January 2013 ($50.5bn in total) [40]. And according to estimates of the National Oceanic and Atmospheric Administration [1], the damage share for all other areas is less than 5% of the total damage. We derive production shocks for NY and NJ (supplementary figure 1, supplementary table 1 (available online at stacks.iop.org/ERL/16/124049/mmedia)) based on estimated business interruption (BI) due to the disaster. In this, we assume all sectors to be affected in the same way. While this is generally a strong assumption, we find it reasonable for the short time in the immediate aftermath of the hurricane. We then analyze the resulting global levels of final consumption and related prices as well as production levels, production prices, and demands communicated in the network to assess the higher-order repercussions of Hurricane Sandy. These result from the inter-linkages of NY and NJ within the global trade network (exemplary trade flows in figure 1). For a detailed description of the approach, see appendix A.

3. Three-phase consumption ripple

We compute the relative consumption change in the first 100 d after the disaster for all regions globally (figure 2, supplementary table 2). A region's consumption change is computed as the ratio between the absolute aggregated difference from baseline consumption and the consumption that these regions would exhibit in the unperturbed baseline scenario during this time (equation (5) in appendix A).

A normalisation of consumption and consumption prices in the United States of America occurs about 100 d after the event (figure 3). On a national level, the US show the strongest consumption decrease of all regions within our study. However, on a US state level we find both consumption increases as well as losses (figure 2(b)) in our simulations. Within the US, there is a strong correlation between the gross regional production (GRP) of a state and its consumption change. Economically strong states like California, Texas, or Florida exhibit strong consumption decreases whereas consumption increases in states with a lower GRP like Vermont, Wyoming, or Montana.

Both increases and reductions in consumption are a result of consumption price changes. The consumption level depends directly on the consumption price with sector and region specific consumption price elasticities (see appendix A, supplementary tables 2–4). The latter reflect the sensitivity of consumption (quantity) to price changes. Of course, post-disaster price elasticities might deviate from those during normal times. However, this is

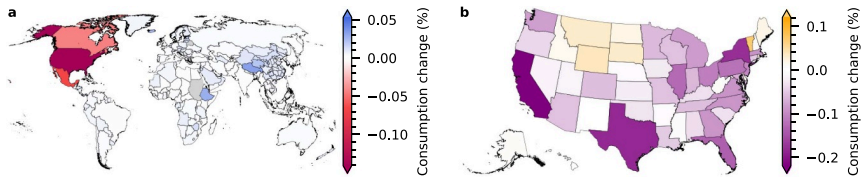

Figure 2. Consumption changes in the direct aftermath of Hurricane Sandy. Changes relative to baseline values during the first 100 d after the disaster (equation (5)) are shown (a) globally and (b) for the US only. Red and purple shading indicate a consumption decrease compared to baseline consumption, blue and yellow shading indicate a consumption increase. Grey areas are excluded from the calculation due to low data quality.

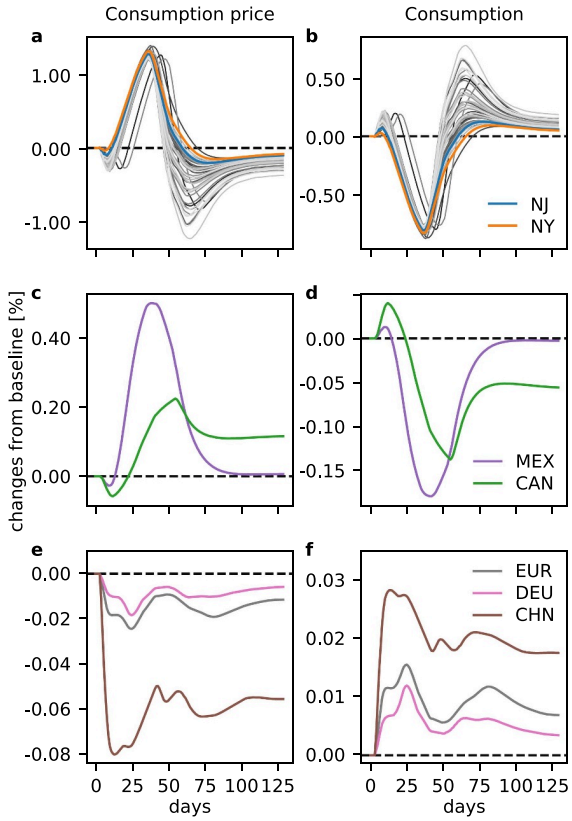

Figure 3. Changes of consumption and consumption prices relative to baseline values. All values are in percent compared to baseline levels (dashed lines). (Left column) Relative consumption price change. (Right column) Relative consumption change. (Upper panels) Results for the directly affected US states NY and NJ and all remaining US states and DC (in grey shades). (Middle panels) Results for Mexico and Canada. (Lower panels) Results for Europe, Germany and China.

difficult to estimate and only relevant for the final consumption in the directly affected states NY and NJ. Consumption in all other regions can be assumed to follow normal elasticities. Previous sensitivity analysis [43] on model-internal price elasticities showed that this parameter choice has no significant impact on results derived via *Acclimate*.

In all regions, we observe an initial consumption price drop directly after the disaster, resulting in a consumption level above baseline. This initial price drop results from a reduction in the (production) demand of the directly affected states of NY and NJ and its quick upstream propagation along the global supply chains. Therefore, reducing demand

instantaneously results in a situation of surplus supply, which causes prices to decline and consumption to rise. However, direct production losses in NY and NJ simultaneously propagate downstream through the global supply network and result in scarcity situations also in other regions that are not directly affected. As a result, shortly after the initial small consumption increase, consumption prices rise again with prices in US states reaching values above baseline level only few days after the hurricane and a maximum peak at over +1.3% about 30 d after the disaster. In case of the United States, the initial price drop associated with increased consumption is therefore quickly reversed by a scarcity driven price inflation resulting in a reduction in consumption. While the upstream effect happens without time delay, the downstream propagation of scarcities is initially buffered by the agents' inventories but also by transport chains through which goods are delivered. Therefore, in contrast to demand shortages propagating upstream, the downstream propagation of scarcities only shows effects with some lag time. The persisting shortage of supply leads to price inflation of intermediate goods that are passed on to the final consumers. As a consequence, the latter have to decrease their consumption. A normalization of US prices and consumption occurs about 100 d after the event. While the US are most impacted by the event, changes from the baseline economic state due to the hurricane event occur globally. A similar development with an initial small consumption increase followed by a stronger counter effect of decreasing consumption can be observed — yet with smaller magnitude — in Mexico and Canada, which have strong trade relations with the United States.

Generally, consumption shows a three-phase wave pattern of an initial price drop due to upstream effects, followed by a price increase attributable to downstream effects and finally a normalization phase where prices develop back towards baseline values. Depending on how strong the upstream and downstream effects are with regards to a particular region, average prices range above or below baseline. For example, the upstream effect for Canada and Mexico is small compared to the downstream effect, leading to higher average prices. In Europe and its strongest economy Germany as well as China, the initial price drop due to the fast upstream effect is large enough to permanently keep prices below baseline (figure 3(e)).

4. Regions' trade with the US

In the simulated disaster aftermath, the magnitude of the effect on a region's consumption depends on the trade relations of that region with the US (i.e. the sum of all imports and exports, figure 4(a)), following a power law relationship. Both high import and export trade flows result in a strong consumption changes (supplementary figure 2). Linear regression in the log-log space indicates an exponent that is below 1, i.e. the absolute consumption difference increases less than linearly with growing trade volume with the US. Regions with strong trade relations experience a stronger price effect. However, due to the prescribed negative price elasticities, this price effect affects consumption less than linearly.

Whether or not a region experiences total gains or losses in consumption depends on the country-specific shape of the three-phase ripple, i.e. whether the upstream or downstream effects is dominant. To show this, we analyze additional simulations with longer recovery times (80, 100, 120 d, figure 4), which mainly intensifies the slower propagating downstream effect (supplementary figure 3). Initially, most regions (with the exception of Mexico, Canada and the Philippines) show consumption gains. With longer duration, the latter decrease and consumption losses increase. With a recovery time extension of 20 d (figure 4(b)), additional regions transitions from gains to losses (e.g. Australia, Venezuela, Ireland, Singapore, Hong Kong). The initially small consumption loss increases with further recovery time extension (panels (c) and (d)). Likewise, regions like Canada, Mexico and the Philippines that show losses already with the original recovery time further increase their losses. In the case of Mexico and Canada, this can supposedly be explained by the geographic and economic proximity of the regions to the US, resulting in a faster downstream propagation to these countries. This suggests that each region has an individual threshold where the direct impact in NY and NJ becomes too strong and a dominating downstream effect results in overall consumption losses. This threshold is already crossed for the Philippines as well as Mexico and Canada with the original recovery time of 60 d.

Generally, the consumption reaction of all regions to the shock duration in NY and NJ appears to follow an inverted U-shape. Without a shock, all regions consume at their baseline level. Short shocks result in consumption gains that increase with the shock duration at first. At some point—depending on the trade relations with the US—consumption gains decrease and eventually transition into losses. Regions with a large trade volume tend to transition sooner than those with smaller trade to the US.

5. Price dynamics

So far we analyzed the consumption price and resulting consumption levels on a regional level and found a three-phased ripple that can result in both overall gains and losses of consumption. In the following, we investigate the underlying price dynamics that lead this ripple which originates in the directly affected regions NY and NJ. For this, we look at changes of

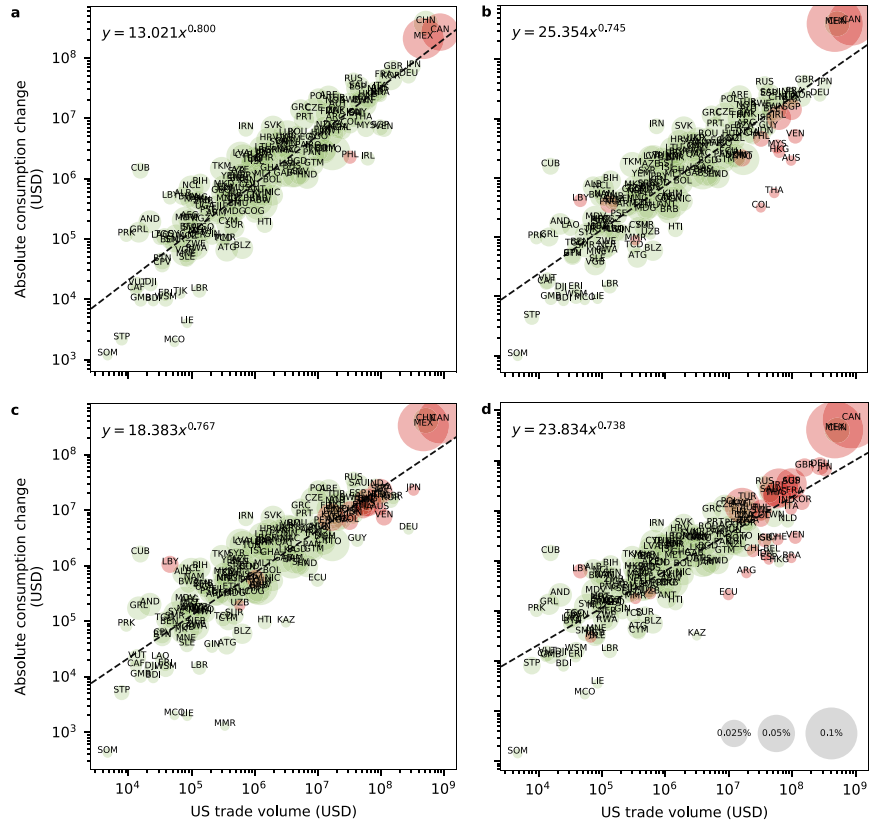

Figure 4. Consumption change over total trade volume with the US with varied recovery times. Consumption changes are cumulated for the first 100 d after the hurricane. US trade volume is the sum of a region's total exports and imports with the United States. Size of the scatters indicates the consumption change relative to what regions would consume under baseline conditions during this time. Green and red colors indicate consumption gains and losses, respectively. The dashed line is the linear fit in the log-log space. Recovery time is set to (a) 60 (default recovery), (b) 80, (c) 100 and (d) 120 d.

production prices and levels of incoming demand as well as changes of the capacity utilization in NY and NJ as well as the rest of the US. We use the economic notion of capacity utilization [44] that is defined as the ratio of actual output to the output that would minimize production costs. This measure quantifies if and by how much a region is in a state of overproduction, relative to the actual production capacity. For the directly affected regions, we need to first adjust production capacity for the applied production shock. We also calculate the similarly adjusted demand exceedance which indicates if fulfilling the entire incoming demand at a given time step would drive the agent into overproduction, i.e. by how much current incoming demand exceeds the production capacity (for both adjusted capacity utilization and demand exceedance see appendix A). Time series for production prices, demand exceedance and capacity utilization in our simulations are shown in figure 5 for the directly affected US states NJ and NY as well as an aggregate over all other US states and DC. We refer to the latter in the following as USA-OTH.

In the *Acclimate* model, production prices and ultimately consumption prices are driven by the demand that agents receive. In the immediate aftermath of the disaster, NY and NJ cannot satisfy their incoming demand due to the applied external reduction of production capacity. This is reflected by a high demand exceedance. As a result, the directly affected states switch to overproduction directly after the disaster, similarly indicated by an increased capacity utilization. At the same time, NY and NJ reduce their demand towards other regions. Due to the resulting initial upstream propagation, the remainder of the US does not fully use the available production capacity and production prices decrease at first (note that the apparent contradiction for the pooled region USA-OTH of positive demand exceedance

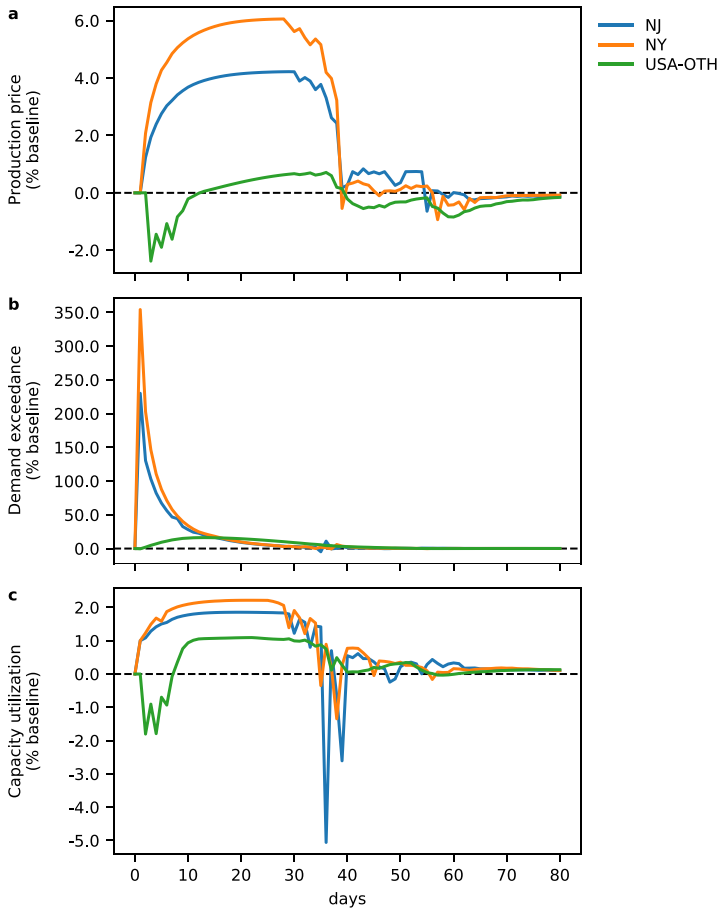

Figure 5. Production price, demand exceedance and capacity utilization for the United States. Directly affected states NJ and NY are shown individually, remaining 48 states and DC are aggregated as USA-OTH. Dashed lines represent baseline values. (a) Changes of the production price from baseline values. (b) Demand exceedance relative to baseline values. (c) Relative change in capacity utilization from baseline values.

and simultaneous low capacity utilization during the first days after the disaster is simply a result of the aggregation that we perform over the US regions and their individual sectors, see appendix A). However, the longer the disruption prevails, the more of the lost production in NY and NJ propagates downstream in the economic network, resulting in scarcity of goods. This scarcity is compensated by other US states and also the latter eventually switch to overproduction. Yet, overproduction comes at the cost of production prices increasing super-linearly with the production level and average prices rise above baseline levels during this upstream phase. In the situation of scarcity in the disaster aftermath, agents in the network are willing to pay these higher-than-usual prices and producing agents keep their increased production level.

We observe this behavior of rising production prices until about 45 d after the disaster, when production prices rapidly drop again. This drop marks the beginning of the normalization phase. Note that it coincides with a change of the capacity utilization change from positive to negative values, causing agents to switch from an overproduction state to a normal production regime. The sudden price drop results from the fact that now production prices no longer depend super-linearly on the produced quantity. Two factors lead to the end of the overproduction regime: (1) many purchasing firms decide simultaneously to reduce their demand due to the high level of prices, and (2) the reduction of production capacity in the directly affected states is released enough so that the new, reduced incoming demand can be satisfied without overproduction.

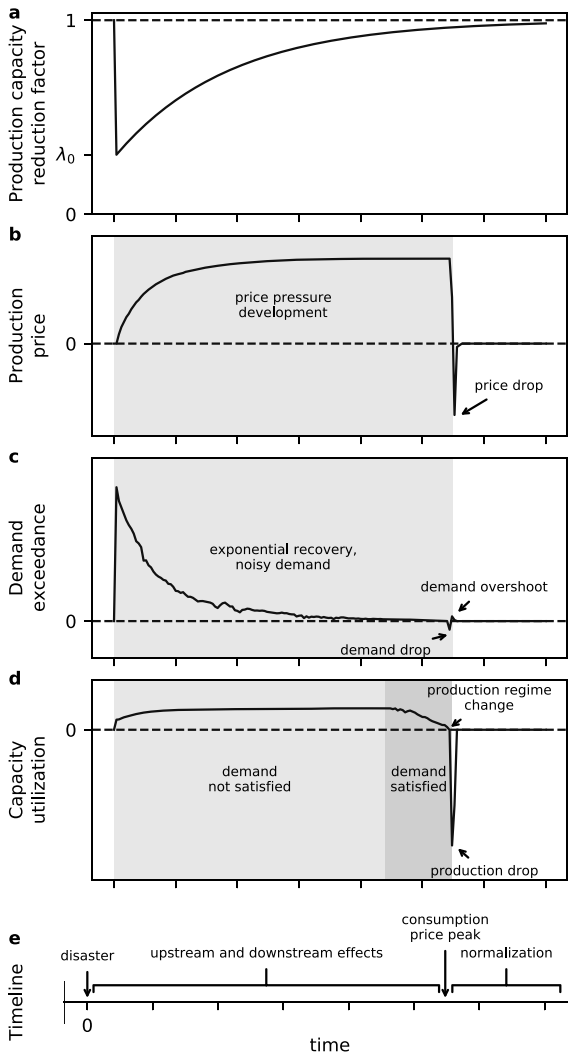

Figure 6. Schematic time evolution of a directly affected agent. Dashed lines represent baseline values. Explicit values and durations are not given because magnitudes and time scales differ between disasters. (a) Production capacity reduction factor with initial production shock λ_0. (b) Relative production price change. Grey shaded area denotes the price pressure development time until the price drop. (c) Demand exceedance. Grey shaded area denotes the time during which the economic shock has not decayed enough for demand variations to end the overproduction regime. Noise is due to demand fluctuation from the profit maximization and associated demand shifts of all agents. When the production capacity has recovered enough, this noise can be strong enough to make an agent switch from an overproduction to a normal production regime (production regime change). (d) Relative change in capacity utilization. Light grey area denotes the time during which the agent does not fulfill the incoming demand while in a state of overproduction. The dark grey shaded area is the time during which the entire demand can be satisfied with overproduction. (e) Timeline with the initial disaster impact, the consumption price peak and upstream, downstream and normalization phases.

As can be seen in figure 5, the demand exceedance for NY and NJ decreases exponentially after the disaster, which is simply due to the defined exponential economic recovery. About 45 d after the event, when we observe the production price drop, the production capacity reduction has released enough for smaller demand variations to cause the demand exceedance to drop below 0. Such variations are a result of the complex dynamics of the model. Since each agent may redistribute its demand in each time step and will do so in order to maximize its profit, the incoming demand (and hence, the demand exceedance) is

subject to some fluctuation. The price tension that previously built up in the network releases and prices drop back towards baseline levels.

A schematic time evolution for the analyzed quantities of a directly affected agent is shown in figure 6 (panels (a)–(d)) with coincident events and phases in the aftermath of the hurricane (panel (d)). While we expect the general behavior of directly affected agents to may be similar for other natural disasters that show an exponential BI recovery, time scales and magnitudes may well be different and are therefore omitted in the figure.

6. Discussion

In this study, we modeled the impact that a severe disaster like Hurricane Sandy (2012) can have on global consumption, resulting from economic forward and backward loss propagation in the global supply network. We find a three-phase economic ripple in the supply chain network. This ripple is characterized by an initial upstream effect and resulting consumption increase, followed by an opposing and slower downstream effect and associated reduced consumption. The last phase is a price normalization.

The magnitude of consumption effects on a region depends on its trade volume with the US. Whether a region experiences overall gains or losses depends on which of the upstream or downstream effect during the ripple is dominating. In our simulations, most regions experience slight consumption gains. With longer duration of the direct impact, these regions show a tendency of decreasing consumption gains and eventually a transition to consumption losses. Many regions experience these losses already with an additional recovery time of only 20 d. This is important for two reasons. First, direct losses of hurricanes must be expected to increase in the future due to climate change [8, 45], resulting in potentially longer recovery durations. Second, the recovery from BI was particularly quick after Hurricane Sandy and it can take much longer for other economies subjected to different natural disasters to recover. In the case of Hurricane Katrina in 2005, the economic activity recovered to pre-disaster levels only about one year later [46].

Of course, results from socioeconomic models like the one used in this study are subject to uncertainties due to the necessary assumptions on which the model builds. In particular, these uncertainties concern the absolute magnitudes of the reported results which may appear small at first sight. We emphasize that these values result from only one local, isolated extreme weather event and are therefore still considerable. Previous research [47] has also shown that economic ripples from disasters can amplify each other. More importantly however, we stress the *qualitative* nature and importance of our findings regarding the economic ripple. Our finding of a three-phase ripple and related consumption changes is qualitatively robust against variations of the local production disruption (supplementary figures 3–5).

While we focused on the specific regions of New York and New Jersey in the United States for this study, similar ripple waves can be expected for major shocks in other regions of the world. Besides hurricanes, we also expect other categories of extreme weather events to have similar economic impacts on consumption. Consecutive and compound events (e.g. the 2020 flood in China and the concurrent heat wave in Europe as recent examples) will likely further increase the magnitudes of the observed indirect effects. Since all these extremes are projected to intensify—at least on a local level—under global warming [48], we believe that modeling approaches like the one we conducted here can contribute valuable insights for necessary mitigation by allowing to simulate and better understand higher-order effects that otherwise cannot be studied.

Data availability statement

The data that support the findings of this study are available from the corresponding author upon request. GADM region shape files can be found at www.gadm.org. Storm track retrieved from IBTrACS database at http://ibtracs.unca.edu/.

The data that support the findings of this study will be openly available following an embargo at the DOI: 10.5281/zenodo.5682128. Data will be available from 01 December 2021.

Code availability

The implementation of the *Acclimate* model is available as open source on https://github.com/acclimate/acclimate with identifier 10.5281/zenodo.853345. The code for data processing and analysis scripts is available from the corresponding author upon request.

Acknowledgments

This research has received funding from the Horizon 2020 Framework Programme of the European Union project RECEIPT (Grant Agreement 820712), the German Academic Scholarship Foundation and the German Federal Ministry of Education and Research (BMBF) under the research projects CLIC (01LA1817C), SLICE (01LA1829A), and QUIDIC (01LP1907A). The authors gratefully acknowledge the European Regional Development Fund (ERDF), the German Federal Ministry of Education and Research, and the Land Brandenburg for supporting this project by providing resources on the high performance computer system at the Potsdam Institute for Climate Impact Research.

Author contributions

R M, S W, and C O designed the method. S W and C O developed the Acclimate model. K K provided the price elasticities. R M conducted the analysis. R M, S W, C O, and A L analysed and interpreted the results. R M, S W, C O, K K, L Q, and A L discussed the results and wrote the manuscript.

Conflict of interest

The authors declare that they have no competing interests.

ORCID iDs

Robin Middelanis https://orcid.org/0000-0001-8848-3745
Sven N Willner https://orcid.org/0000-0001-6798-6247
Christian Otto https://orcid.org/0000-0001-5500-6774
Kilian Kuhla https://orcid.org/0000-0002-8698-1246
Lennart Quante https://orcid.org/0000-0003-4942-8254
Anders Levermann https://orcid.org/0000-0003-4432-4704

References

[1] NOAA National Centers for Environmental Information (NCEI) 2020 U.S. billion-dollar weather and climate disasters (available at: www.ncdc.noaa.gov/billions/) (Accessed 10 June 2020)
[2] Münchener Rückversicherungs-Gesellschaft 2020 NatCatSERVICE (available at: https://natcatservice.munichre.com/) (Accessed 20 March 2020)
[3] Nicholls N *et al* 2012 Changes in climate extremes and their impacts on the natural physical environment *Managing the Risks of Extreme Events and Disasters to Advance Climate Change Adaptation* (Cambridge: Cambridge University Press) pp 109–230
[4] Walsh K J *et al* 2016 Tropical cyclones and climate change *Wiley Interdiscip. Rev. Clim. Change* **7** 65–89
[5] Knutson T R *et al* 2010 Tropical cyclones and climate change *Nat. Geosci.* **3** 157–63
[6] Hallegatte S 2012 The rising costs of hurricanes *Nat. Clim. Change* **2** 148–9
[7] Mendelsohn R, Emanuel K, Chonabayashi S and Bakkensen L 2012 The impact of climate change on global tropical cyclone damage *Nat. Clim. Change* **2** 205–9
[8] Knutson T *et al* 2020 Tropical cyclones and climate change assessment: part II: projected response to anthropogenic warming *Bull. Am. Meteorol. Soc.* **101** E303–22
[9] Emanuel K 2011 Global warming effects on us hurricane damage *Weather Clim. Soc.* **3** 261–8
[10] Maloney M C and Preston B L 2014 A geospatial dataset for us hurricane storm surge and sea-level rise vulnerability: development and case study applications *Clim. Risk Manage.* **2** 26–41
[11] Pielke Jr R A *et al* 2008 Normalized hurricane damage in the United States: 1900–2005 *Nat. Hazards Rev.* **9** 29–42
[12] Weinkle J *et al* 2018 Normalized hurricane damage in the continental united states 1900–2017 *Nat. Sustain.* **1** 808–13
[13] Rose A 2004 Economic principles, issues and research priorities in hazard loss estimation *Modeling Spatial and Economic Impacts of Disasters* (Berlin: Springer) pp 13–36
[14] Lenzen M *et al* 2019 Economic damage and spillovers from a tropical cyclone *Nat. Hazards Earth Syst. Sci.* **19** 137–51
[15] Inoue H and Todo Y 2019 Firm-level propagation of shocks through supply-chain networks *Nat. Sustain.* **2** 841–7
[16] Hallegatte S 2008 An adaptive regional input–output model and its application to the assessment of the economic cost of Katrina *Risk Anal.* **28** 779–99
[17] Noy I 2009 The macroeconomic consequences of disasters *J. Dev. Econ.* **88** 221–31
[18] Willner S N, Otto C and Levermann A 2018 Global economic response to river floods *Nat. Clim. Change* **8** 594–8
[19] Okuyama Y and Santos J R 2014 Disaster impact and input–output analysis *Econ. Syst. Res.* **26** 1–12
[20] Hallegatte S 2014 Economic resilience : definition and measurement. policy research working Paper (World Bank) **6852** (https://openknowledge.worldbank.org/handle/10986/18341)
[21] Hallegatte S and Przyluski V 2010 The economics of natural disasters: concepts and methods *Policy Research Working Paper* No. WPS 5507
[22] Deaton A and Zaidi S 2002 Guidelines for constructing consumption aggregates for welfare analysis. working paper (World Bank) **135** (https://openknowledge.worldbank.org/handle/10986/14101)
[23] Levermann A 2014 Climate economics: make supply chains climate-smart *Nature* **506** 27–29
[24] Guan D *et al* 2020 Global supply-chain effects of covid-19 control measures *Nat. Hum. Behav.* **4** 577–87
[25] Lenzen M *et al* 2020 Global socio-economic losses and environmental gains from the coronavirus pandemic *PLoS One* **15** e0235654
[26] Sawada Y 2007 The impact of natural and manmade disasters on household welfare *Agric. Econ.* **37** 59–73
[27] Pauw K, Thurlow J, Bachu M and Van Seventer D E 2011 The economic costs of extreme weather events: a hydrometeorological CGE analysis for Malawi *Environ. Dev. Econ.* **16** 177–98
[28] Markhvida M, Walsh B, Hallegatte S and Baker J 2020 Quantification of disaster impacts through household well-being losses *Nat. Sustain.* **3** 538–47
[29] Walsh B and Hallegatte S 2020 Measuring natural risks in the Philippines: socioeconomic resilience and wellbeing losses *Econ. Disasters Clim. Change* **4** 249–93
[30] Strobl E 2011 The economic growth impact of hurricanes: evidence from us coastal counties *Rev. Econ. Stat.* **93** 575–89
[31] Hsiang S M and Jina A S 2014 The causal effect of environmental catastrophe on long-run economic growth: evidence from 6,700 cyclones *Technical Report* (National Bureau of Economic Research)
[32] Elliott R J, Liu Y, Strobl E and Tong M 2019 Estimating the direct and indirect impact of typhoons on plant performance: evidence from Chinese manufacturers *J. Environ. Econ. Manage.* **98** 102252
[33] Neumayer E, Plümper T and Barthel F 2014 The political economy of natural disaster damage *Glob. Environ. Change* **24** 8–19
[34] Bakkensen L and Barrage L 2018 Climate shocks, cyclones, and economic growth: bridging the micro-macro gap *Technical Report* (National Bureau of Economic Research)
[35] National Hurricane Center 2018 Costliest us tropical cyclones tables updated (available at: www.nhc.noaa.gov/news/UpdatedCostliest.pdf) (Accessed 25 July 2020)
[36] Blake E S, Kimberlain T B, Berg R J, Cangialosi J P and Beven J L 2013 Tropical Cyclone Report: Hurricane Sandy **12** (National Hurricane Center) 1–10
[37] Otto C, Willner S N, Wenz L, Frieler K and Levermann A 2017 Modeling loss-propagation in the global supply network: the dynamic agent-based model acclimate *J. Econ. Dyn. Control* **83** 232–69

[38] Wenz L et al 2015 Regional and sectoral disaggregation of multi-regional input–output tables—a flexible algorithm *Econ. Syst. Res.* **27** 194–212
[39] Lenzen M, Kanemoto K, Moran D and Geschke A 2012 Mapping the structure of the world economy *Environ. Sci. Technol.* **46** 8374–81
[40] Henry D K et al 2013 *Economic Impact of Hurricane Sandy: Potential Economic Activity Lost and Gained in New Jersey and New York* (Washington, DC: US Department of Commerce)
[41] Global Administrative Areas 2018 GADM database of global administrative areas, version 3.6 (available at: www.gadm.org) (Accessed 16 December 2020)
[42] Knapp K R, Diamond H J, Kossin J P, Kruk M C and Schreck C J 2018 Int. best track archive for climate stewardship (IBTrACS) project, version 4 (NOAA National Centers for Environmental Information) (available at: https://doi.org/10.25921/82ty-9e16) (Accessed 8 August 2020)
[43] Kuhla K, Willner S N, Otto C, Wenz L and Levermann A 2021 Future heat stress to reduce people's purchasing power *PLoS One* **16** e0251210
[44] Berndt E R and Morrison C J 1981 Capacity utilization measures: underlying economic theory and an alternative approach *Am. Econ. Rev.* **71** 48–52
[45] Grinsted A, Moore J C and Jevrejeva S 2013 Projected atlantic hurricane surge threat from rising temperatures *Proc. Natl Acad. Sci.* **110** 5369–73
[46] Federal Reserve Bank of Philadelphia 2005 Coincident economic activity index for Louisiana (FRED, Federal Reserve Bank of St. Louis) (available at: https://fred.stlouisfed.org/series/LAPHCI) (Accessed 27 April 2021)
[47] Kuhla K, Willner S N, Otto C, Geiger T and Levermann A 2021 Ripple resonance amplifies economic welfare loss from weather extremes *Environ. Res. Lett.* **16** 114010
[48] Rahmstorf S and Coumou D 2011 Increase of extreme events in a warming world *Proc. Natl Acad. Sci.* **108** 17905–9

Article C

Ripple resonance amplifies economic welfare loss from weather extremes

Authors

Kilian Kuhla, Sven N Willner, Christian Otto, Tobias Geiger and Anders Levermann

Status

Published in *Enviromental Research Letters* in October 2021,
doi: 10.1088/1748-9326/ac2932.

Capsule summary

In this study, the regional productivity failures due to heat stress, river floods, tropical cyclones, and their overlapping occurrence are computed. Further, the repercussions within the global economic network using the loss-propagating model *Acclimate* are examined. Economic ripples of extreme events propagate within the economic network and may overlap, triggering a nonlinear economic response. This economic ripple resonance causes global and regional consumption losses to increase. The loss enhancement for consumers even amplifies over-proportionally with increasing direct local production losses. This study describes the economic ripple resonance effect of consecutive disasters within an economic network for the first time. The results imply that welfare losses from extreme weather events could be underestimated if overlapping economic ripples are not considered. Furthermore, the ongoing climate crisis may raise losses for consumers even more than previously assumed due to resonating repercussions within the trading network.

Author contributions

Sven N Willner, Christian Otto, Anders Levermann, and Kilian Kuhla designed the research. Kilian Kuhla conducted the analysis. Kilian Kuhla analyzed and interpreted the results with the help of Sven N Willner, Christian Otto, and Anders Levermann. Kilian Kuhla made the visualization. The manuscript was written with contributions from all authors.

IOP Publishing Environ. Res. Lett. 16 (2021) 114010 https://doi.org/10.1088/1748-9326/ac2932

ENVIRONMENTAL RESEARCH
LETTERS

OPEN ACCESS

RECEIVED
13 August 2021

REVISED
20 September 2021

ACCEPTED FOR PUBLICATION
22 September 2021

PUBLISHED
27 October 2021

LETTER

Ripple resonance amplifies economic welfare loss from weather extremes

Kilian Kuhla[1,2], Sven Norman Willner[1], Christian Otto[1], Tobias Geiger[1,3] and Anders Levermann[1,2,4,*]

[1] Potsdam Institute for Climate Impact Research, Telegrafenberg A56, Potsdam, Germany
[2] Institute of Physics, Potsdam University, Karl-Liebknecht-Str. 24, Potsdam, Germany
[3] Deutscher Wetterdienst, Klima und Umwelt, Potsdam, Germany
[4] Columbia University New York, New York, NY, United States of America
[*] Author to whom any correspondence should be addressed.

E-mail: anders.levermann@pik-potsdam.de

Keywords: consecutive disasters, economic ripple resonance, repercussion resonance, weather extremes, supply network, climate impacts, climate change

Supplementary material for this article is available online

Abstract

The most complex but potentially most severe impacts of climate change are caused by extreme weather events. In a globally connected economy, damages can cause remote perturbations and cascading consequences—a ripple effect along supply chains. Here we show an economic ripple resonance that amplifies losses when consecutive or overlapping weather extremes and their repercussions interact. This amounts to an average amplification of 21% for climate-induced heat stress, river floods, and tropical cyclones. Modeling the temporal evolution of 1.8 million trade relations between >7000 regional economic sectors, we find that the regional responses to future extremes are strongly heterogeneous also in their resonance behavior. The induced effect on welfare varies between gains due to increased demand in some regions and losses due to demand or supply shortages in others. Within the current global supply network, the ripple resonance effect of extreme weather is strongest in high-income economies—an important effect to consider when evaluating past and future economic climate impacts.

1. Introduction

Climate change due to anthropogenic greenhouse gas emissions is likely to intensify both weather extremes [1] and their impact on society [2, 3]. Disruptions by extreme weather events impact the health sector [4, 5] as well as the economy through perturbations of income [6], employment [7], economic growth [8, 9], energy supply [10, 11], and food security [12, 13]. In the aftermath of an extreme weather event, regions react in a variety of ways. Some might not manage to recover in between subsequent events [14] others might even profit from disasters when the economy is build back more resilient or more efficient after the shock [15, 16]. On an inter-regional level, local production shocks induced by extreme events can, via price and demand fluctuations in the highly interconnected global trading network, result in losses or gains in production or consumption elsewhere in the world [17–19].

The short and long-term economic impact of each of individual disaster categories by themselves have been studied in regional case studies [20–22] as well as on the individual regional or even at the global level [23–25]. Additionally, events such as heat stress, fluvial floods, and tropical storms, can also overlap spatially as well as temporally, often referred to as compound events [26]. This paper contributes to this literature, which so far mostly focuses on the natural science perspective or regards only local direct economic consequences [27]. We here focus on how local and cross-regional economic repercussions

of such events can interact due to trade and production supply linkages in a non-linear way [28] either amplifying or mitigating the economic losses caused by the individual events. Additionally, disasters due to extreme weather events (e.g. flooding of factories) can lead not only to *direct* local (production) output losses, but also to *indirect* losses due to the propagation of losses in the global trade network causing economic ripple effects [29]. Thus, the question arises of whether accounting for the interaction of these losses is important, and whether doing so amplifies or mitigates overall losses at a global level.

2. Methods summary

Here we model the response of the global supply network to heat stress [30, 31], river floods [25, 32], and tropical cyclone events [33, 34] for the years 2020–2039. The daily time series of the events are derived from an ensemble of four global climate models, each forced by two representative concentration pathways for all three event categories, as well as five hydrological models for river floods and five tropical cyclones realizations (8 time series for heat stress, 40 time series for river floods and tropical cyclones; see section 2 for details). From these we derive direct output losses. For heat stress, we use a linear reduction in local labor productivity for selected economic sectors for every degree warmer than a daily local temperature of 27 °C [30]. For the duration of a river flood in an area, production capacity is reduced by the relative amount of affected area for all non-service sectors. Similarly, the productivity of all non-service sectors vanishes when an area is on the track of a hurricane with wind speed exceeding 64 knots. This translation is rather simplistic and does not take account for short-term adaptation only by allowing for limited efforts to use additional production capacity at higher costs. During the short actual duration of each event we believe this linear translation to be a valid assumption. After the disaster has ceased, direct production capacity recovers depending on on flood depth and wind speed, respectively, thereby accounting for additional cleanup efforts. The production recovery of an affected area is exponential (80% per day). By overlapping the direct output loss time series (i.e. local impacts) of those three extreme event types we generate a direct output loss time series, where individual extreme events can overlap spatially and/or temporally. Following [28], we refer to these as *consecutive* disasters (200 time series for consecutive disaster scenarios).

We translate these regional direct output losses into *overall* losses (direct plus indirect losses) using the loss-propagation model Acclimate [18], which includes a complex network of 26 sectors per region, i.e. representative firms, and one consumer within each of the 256 regions of the model (184 nations as well as 51 US-states and 32 Chinese provinces). Each consumer consumes each of the 26 goods independent of the others. Similar to firms each good in general is supplied by many firms producing that good in different regions. This results in about 1.8 million interconnections between 7236 economic agents. Local profit optimization, causing demand and production changes, enables firms to react to short-term production, supply, or price shocks. Those economic shocks are depicted as deviations from the baseline, which rely on static multi-regional input-output data from the Eora database[5] [35] for the year 2015. Perturbed supply can lead to regional economic benefits through temporary production extension or result in loss cascades along supply chains. Inventories and transport delay may buffer this loss propagation as supply shortages do not directly constrain other firms' production. Consumption optimization by each regional consumer causes demand shifts which cast back to the firms' production behavior. There is hence a two-way feedback between consumers and producers. With its endogenous prices and agent-based daily dynamics, the Acclimate model is particularly suited to assess the global distribution of the consequences of unanticipated short-term shocks such as those by the three disaster types considered here.

3. Results

Due to inertia in the climate system the different carbon emission scenarios yield temperature scenarios that are well within model uncertainty within the next two decades [1]. Accordingly, we combine the individual years of the different scenarios into a full ensemble to improve statistics similar to previous publications [25, 32]. For that, we derive annual values of indirect losses from daily losses as computed by Acclimate. We then compare two situations. On the one hand, we use simulations with all three classes of weather extremes occurring together (i.e. consecutive disaster scenarios). The corresponding quantities, such as the consumption losses and production losses, are referred to as *total* quantities. On the other hand, we sum the results of three separate simulation classes with each having only one category of weather extremes. Their resulting quantities are denoted as *aggregated*. For direct losses, generally, the sum of the direct output losses of the three classes of weather extremes (aggregated direct losses) equals the losses of consecutively occurring disasters (total direct losses) (see section 2 for details). Using an ensemble of projected weather extremes of three disaster categories, enables us to get a broad range of consecutive disaster events, spatially as well as temporally. Accordingly, in the ensemble we observe disasters of very different sizes and combinations.

[5] www.worldmrio.com.

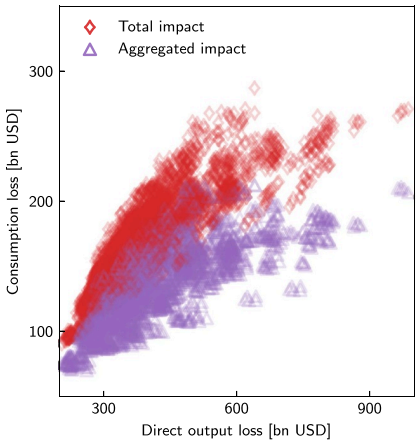

Figure 1. Global consumption losses are higher when impacts interact. Global annual consumption losses as they depend on annual direct output losses. For the *total* impact (red diamond) consumption losses are higher than for the *aggregated* sum of independent impacts (purple triangle) also for the same direct losses. This amplification is shown in figure 2. Each data point represents one year within the ensemble. Consumption and direct output losses are with respect to the baseline consumption and production, respectively.

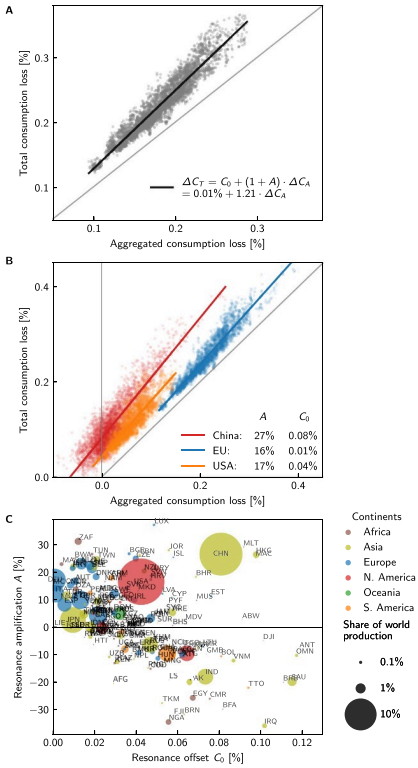

Figure 2. Economic ripple resonance—consumption losses of consecutive disasters are increased in comparison to losses of aggregated single disasters. (A), (B) Annual consumption losses for the *total* impact over those for the *aggregated* sum of independent impacts, globally ((A), grey dots) as well as for China, EU, and the USA ((B), colored dots). Each data point represents one year within the ensemble. Losses are relative to the (unperturbed) baseline consumption. The solid lines depict the resonance analysis with *resonance amplification factor A* and *resonance offset* C_0. (C) Resonance amplification factor and offset per country. The area of each circle represents the country's share of the world production, its color depicts the geographic region. A few extreme outliers (of economically small countries) are not in the visual range.

3.1. Consecutive disasters increase global consumption losses

Global welfare, measured as the sum of the final consumption of all regions, decreases in response to the direct losses in both cases, the aggregated as well as the total case (figure 1). The local production reductions are passed on via the supply network as supply and price shocks up to the final consumer. The latter usually just has the option to consume less, because of lack of supply or in response to increasing prices. Thus, price inflation of goods and services decreases consumption in the disasters aftermath (see section 2 for details).

Globally, we observe an *economic ripple resonance* of extreme weather events. We define this resonance as the amplification of regional and global economic disruptions that result from the interaction of the economic repercussions of individual event impacts. Here, total annual consumption losses are larger than the aggregated losses from single disaster scenarios for the whole simulated ensemble (figures 1 and 2(A)). Specifically, the resonance leads to both an additional consumption losses that is independent of the level of direct losses (the *resonance offset* C_0), and a linear amplification of consumption losses with increasing direct losses (the *resonance amplification factor* A). Consequently, losses from consecutive disasters are always larger than the sum of their individual scenarios, and this difference grows with the size of direct losses, e.g. for stronger disruptive events. We thus observe an increase of global total consumption losses ΔC_T compared to aggregated consumption losses ΔC_A with, on average, $\Delta C_T = (1 + A) \cdot \Delta C_A + C_0$. The global resonance offset $C_0 = 0.01\%$ indicates the extent to which consumption losses in the global trading network are intensified for consecutive disasters (figure 2(A)). The resonance amplification factor $A = 21\%$ of global losses implies that an increase of 10bn USD of aggregated consumption losses yield to an increase of more than 12bn USD of total consumption losses. In order to help modelers account for this effect, we provide tables of the amplification factors and resonance offsets for regions commonly used in integrated assessment models in the

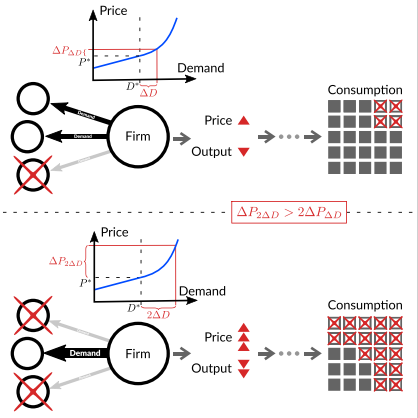

Figure 3. Non-linear price increase due to increasing demand—consumption response to ripple resonance. Upper panel: due to a supplier outage, a firm shifts its demand to other suppliers (of the same commodity/service). Consequent prices ($P^* + \Delta P_{\Delta D}$) grow non-linearly with increasing demand ($D^* + \Delta D$) due to extra costs for additional production, potentially reducing the firm's output. This price increase and supply shortage propagates through the supply network and leads to fewer consumption goods and services for a higher price for the consumer. Lower panel: if more suppliers fail, the fewer remaining suppliers face more demand ($D^* + 2\Delta D$), which increases the price enormously ($P^* + \Delta P_{2\Delta D}$). In fact, a price change due to a doubling of the demand change is greater than twice the price change due to a demand change ($\Delta P_{2\Delta D} > 2\Delta P_{\Delta D}$). A firm therefore produces less but that for a significantly higher price. At the end of the supply chain, the high expenditure for less goods and services result in a drastic reduction in consumption.

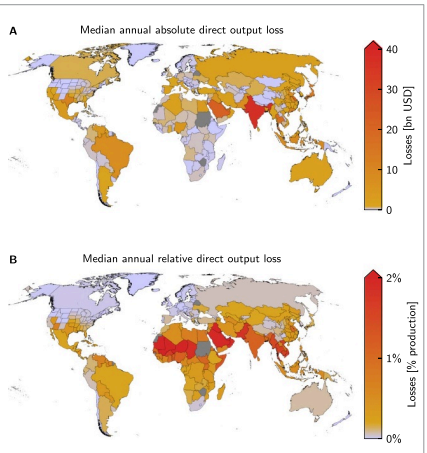

Figure 4. Median annual *direct* output losses due to heat stress, river floods, and tropical cyclones. Regional maps of (A) absolute and (B) relative median annual direct output losses due to heat stress, river floods and tropical cyclones. Regions with absolute or relative direct annual output losses below USD 1bn or 0.2% of baseline (unperturbed) production are depicted in light purple.

appendix (available online at stacks.iop.org/ERL/16/114010/mmedia).

The global enhancement of welfare losses via economic ripple resonance can be explained by non-linear price inflation due to rising demand (figure 3). If a firm increases its demand to some of its suppliers due to supply shortages elsewhere, the price increases non-linearly due to additional production costs. These higher prices and output losses are likely to be passed down the supply chain to the consumer, who has a lower consumption amount for a higher price. If other suppliers fail, due to economic repercussions of different weather extremes, these price deviations may interfere and the resulting declines in consumption can be intensified. Hence spatial and temporal consecutive disasters can amplify indirect consumer losses. It is important to note that individual extreme weather events are not responsible for the ripple resonance. Rather, the overlap of economic repercussions caused by several extreme events resonate and thus trigger the enhancement and amplification of consumption losses.

3.2. Regional welfare losses increase due to ripple resonance

Additionally, various regional direct losses (e.g. varying exposure to natural hazards), network effects (e.g. interference of demand anomalies), and market effects (e.g. strong price fluctuations) may result in regionally heterogeneous responses to the economic ripple resonance (figure 2(B)). In the following, we look at the summed results for the largest economic blocs, the United States of America, China, and the European Union, which consist of their federal states, provinces, and national states, respectively. Explicitly resolving their internal trade dynamics allows us to provide more specific insights for these economic blocs. They are of high economic relevance and exhibit robust sub-regional data resolution. Since we use the economic network of 2015, we refer to the EU as the former pre-Brexit European Union with 28 member states.

Locally, the EU experiences less relative direct output losses in contrast to the USA and China (figure 4). Nevertheless, production losses elsewhere can cause—via the supply network—local consumption losses. This is the case in the EU, where consumers experience higher total and aggregated consumption losses than Chinese or US consumers (figure 2(B)). Most other regions, except Canada and the northern US states, experience higher output losses than the EU. These production losses impact the EU via supply shortages. Additionally, the EU faces increased demand from outside as other regions seek substitutes for directly impact suppliers.

In response to this scarcity the EU increases its production and exports (figure S1) and, following market principle, this scarcity yields an increase in prices for EU products. These higher prices (on the 'world market' in our model) are not passed on solely to customers abroad, but also to customers inside the EU (figure S1). Since national supply is generally stronger than imports the non-EU consumers experience less of the price pressure from the EU than consumers within the union. The trade within the EU is about a factor 10 higher than with the outside. Due to this the EU consumer experiences the increased prices more clearly, because they are more directly dependent on the products and prices of the EU firms. Thus, the advantage of the EU firms—increased production and higher prices—becomes a disadvantage for their own consumers.

The ripple resonance further intensifies the EU's consumption losses with a resonance amplification factor similar to the USA, $A_{EU} = 16\%$ and $A_{USA} = 17\%$. Thus, domestic production losses and resulting demand shifts and price increases, due to stronger disasters, similarly intensify consumption losses for the USA and the EU. Hence, under climate change and without adequate adaptation measures, we expect more frequent heat stress and more intense tropical storms as well as their superposition to contribute to a larger welfare decline in the USA and EU.

For China, the ripple resonance of consecutive disasters has a crucial impact on its economy, which experiences significantly higher losses of consumption due to heat stress than due to flooding (figure 5). Nevertheless, the overlapping of event categories (total impact) causes an increase in consumption losses which exceeds the sum of the separate losses (aggregate impact). Here, China exhibits a resonance amplification factor of $A_{China} = 27\%$. This implies that a fourfold increase of aggregated consumption losses roughly translates to a fivefold increase in total consumption losses. Furthermore, China experiences one of the highest resonance offsets (0.08%). With such a high loss offset China is able to mitigate consumption losses for each disaster category individually; decreased foreign supply can be buffered by increasing domestic production.

However, this coping mechanism is less effective against consecutive disasters. In fact, Chinese consumption depicts a qualitative response shift; potential consumption gains (negative losses) of aggregated single disaster scenarios turn into consumption losses for consecutive disasters (figure 2(B)). In other words, measured by changes in consumption, China can change from a net-winner (aggregated impacts) to a net-loser (total impacts). This hints that single case assessments of extreme events may not only underestimate regional welfare losses but may even leave it undetected.

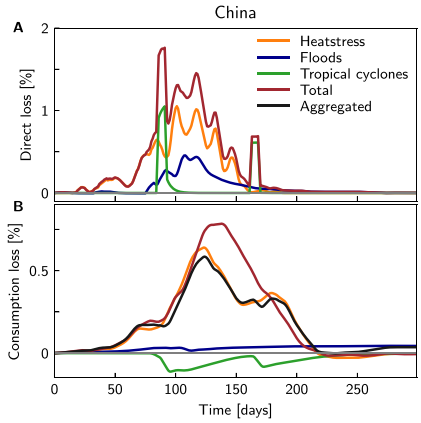

Figure 5. Ripple resonance of consecutive disasters has a crucial impact on the Chinese economy—sample time series of direct output losses and resulting changes in consumption. The disaster categories heat stress, river floods, tropical cyclones, the aggregation of them and consecutive disasters are depicted in orange, blue, green, black and red, respectively. Upper panel (A): temporal evolution of direct output losses for China due to different disaster categories for one sample year and sample bio-physical time series. Lower panel (B): temporal evolution of corresponding consumption losses. It is important to note that the consumption losses are not solely due to domestic production losses but rather reflect the repercussions on consumers of disrupted supply chains and global market effects.

Even for prominent global economic players, domestic trade has a much greater weight than foreign trade. Therefore, domestic production losses are largely redistributed in the internal market. Chinese firms have a strong exposure to all three extreme events (figure 5) especially compared to the EU and USA (figure 4). For isolated extreme events, the Chinese market is able to mitigate part of the direct output losses. However, when considering regional consecutive disasters, the economic repercussions are superimposed within the Chinese trade network—a domestic ripple resonance effect—which results in disproportionately higher consumption losses (figure 5). Thus, for consecutive disasters, the Chinese economy is no longer able to mitigate these overlapping losses; they are too severe to be compensated by non-domestic trading partners, even for a major trading power as China. Accordingly, when firms or policy makers prepare for disasters they should not only consider individual but also the interactions of several events.

In conclusion, the three biggest economic blocs, China, the European Union, and the United States of America are affected differently by the three disaster categories and the resulting economic repercussions. This follows from their different embedding within

the international trade network, their unequal balance of trade between one another, and their heterogeneous domestic economic structure. Accordingly, they exhibit different resilience to extreme events (figure 2(B)).

3.3. Heterogeneous response to economic ripple resonance among countries

Between individual countries a broader spectrum of response behavior emerges (figure 2(C)). Every country shows a positive resonance offset for total consumption losses. But, in contrast to China, the EU, and the USA, some economies, including Brazil, Canada, India, Mexico, Russia, and Sweden, exhibit a negative resonance amplification factor. In these regions, the discrepancy between total consumption losses and aggregated consumption losses shrinks with growing losses and therefore the increase in losses is mitigated in consecutive disaster scenarios (figure S2). Such a negative resonance amplification can be caused by competing producers experiencing higher indirect production outages for single disaster scenarios. These then lower their purchasing prices due to less demand of production and consumption goods.

Further analysis suggests that the resonance amplification tends to become smaller as the direct output losses relative to baseline production output increase (figure S3). Consecutive disasters cause more production than single disasters, which could partly lead to less demand and therefore to lower commodity prices. Countries which experience already high direct output losses from single events, e.g. heat stress in India, may benefit from these lower prices due to consecutive disasters compared to single disaster events. We also compare the regions' response for different income levels as well as to economic output (figure S4). This shows that, mostly low-income countries tend to exhibit a negative resonance amplification factor, whereas higher-income countries tend to perceive positive amplification. A distinct correlation between resonance offset or amplification factor, on the one hand, and national share of world production, on the other hand, has not been identified. However, there is a trend that countries with stronger mitigation reactions (negative amplification factor) are prone to a higher resonance offset (figure 2(C)).

It is important to note that all countries have a positive resonance offset and total consumption losses exceed aggregated consumption losses in most countries. From this follows that a comprehensive consideration of extreme events reveals higher national welfare losses which are caused by economic ripple resonance. Even if some nations depict a negative amplification rate, the majority of economic production (82% of global production) lies in regions with a positive amplification factor.

The resonance offsets and amplification factors for all regions used in the simulations are given in table S2. In order to help estimate the economic costs of extreme events, we also apply our estimation of quantifying the ripple resonance to the regions of different Integrated Assessment Models (see tables S3–S8). We hope this helps to transfer aggregated consumption losses of various studies to their corresponding losses for consecutive disasters.

4. Discussion

Our study shows an economic ripple resonance within the global supply network, which causes consecutive disasters to trigger higher consumption losses compared to separate single disaster categories. In general, this loss intensification becomes even more amplified for increasing losses. However, the extent or even the trend of loss amplification can vary substantially across regions. The three biggest economic blocs (China, EU, USA) exhibit strong amplification due to ripple resonance of consecutive disasters, despite different exposure to extreme events. On a national level, China's economic wealth, which grew outstandingly in recent decades, is particularly at risk due to China's exposure to several natural hazards. Apart from this, nations with small direct output losses from extreme weather events should become aware of their embedding in the global trade network. They also experience an increase in consumption losses due to overlapping extreme events in other countries. While we find first hints regarding the source of different resonance behavior—there is a trend indicating that high-income countries experience a higher resonance amplification—the underlying cause of different regional responses requires further in-depth research. The high resolution of the economic data from China, the EU, and the USA enables us to resolve their internal dynamics in more depth.

Socioeconomic modeling is subject to the inherent limitations of its assumptions and to certain uncertainties—nevertheless, this study explores and stresses the *qualitative* effect of ripple resonance. In this study, we focus on only three event categories, heat stress [30], floods [25], and tropical cyclones [33, 34], as well as on one particular economic network of 2015. Repeating our analysis on the economic network of 2012 reproduces the magnitude and trend of our results (figure S5). Previous studies indicate that reduced trade tends to hinder the mitigation of economic losses due to weather extremes [25]. New trade agreements or protectionist measures would likely alter the overall economic response to extreme weather events and thus could lead to a different ripple resonance effect. As the economic ripple resonance is a non-linear effect, further extreme event categories and different baseline networks may lead to

different resonance quantities. With the overall effect of an increase in losses when considering the total impact, we would further expect a stronger ripple resonance with more event categories. The same argumentation holds for a stronger increase in disaster frequency and severity than in the period we consider here (2020–2039). In order to consider a full range of potential meteorological time series, we here use an ensemble of four global climate models, two representative concentration pathways, five hydrological models, and five tropical cyclones realizations, overall minimizing outlier effects.

Numerous profound studies assess the economic impacts of individual extreme weather events. The results of our study suggest that considering only individual damages or event categories likely leads to an underestimation of their overall economic losses. On that line, our study potentially even underestimates this effect, as we only focus on three disaster categories. Also, the economic interactions studied here happen on top of other economic activity and shocks. Thus, in reality, further interactions will occur; we can here, naturally, only show this effect in its isolation.

Overall, our study demonstrates the importance of considering the interaction of the economic response to consecutive events in order to grasp the full picture of the economic impacts of climate change. As human-induced climate change progresses, the frequency and intensity of extreme weather events is likely to increase, leading to a high probability of increasing direct production losses and consequently to higher consumption losses. Thus, resonating economic effects leading to insufficient adaptation and a false sense of preparedness—these kinds of resonances should be considered for further adaptation measures and mitigation efforts.

Data availability statement

The data that support the findings of this study are openly available at the following URL/DOI: https://zenodo.org/record/4935179. The implementation of the *Acclimate* model is available as open source on https://github.com/acclimate/acclimate with identifier 10.5281/zenodo.853345, the implementation of the disaggregation algorithm can be found on https://github.com/swillner/libmrio (10.5281/zenodo.832052).

Acknowledgments

This research has received funding from the German Academic Scholarship Foundation and the German Federal Ministry of Education and Research (BMBF) under the research Projects CLIC (FKZ: 01LA1817C), QUIDIC (01LP1907A), and SLICE (FKZ: 01LA1829A), from the Horizon 2020 Framework Programme of the European Union (Grant Agreement No. 820712), as well as from the Leibniz foundation under the research Project ENGAGE (SAW-2016-PIK-1).

Author contributions

K K, S W, C O, and A L designed the research. T G and S W provided the tropical cyclone and river flood input data, respectively. S W and C O developed the Acclimate model. K K conducted the analysis. K K, S W, C O, and A L analyzed and interpreted the results, wrote the manuscript with contributions from all authors. All authors discussed the results.

Conflict of interest

The authors declare that they have no competing interests.

ORCID iDs

Kilian Kuhla https://orcid.org/0000-0002-8698-1246
Sven Norman Willner https://orcid.org/0000-0001-6798-6247
Christian Otto https://orcid.org/0000-0001-5500-6774
Tobias Geiger https://orcid.org/0000-0002-8059-8270
Anders Levermann https://orcid.org/0000-0003-4432-4704

References

[1] IPCC 2021 *AR6 Climate Change 2021: The Physical Science Basis. Contribution of Working Group I to the Sixth Assessment Report of the Intergovernmental Panel on Climate Change* (Cambridge: Cambridge University Press)
[2] IPCC 2014 *AR5 Climate Change 2014: Impacts, Adaptation and Vulnerability* vol 1 (Cambridge: Cambridge University Press)
[3] IPCC 2009 *Managing the Risks of Extreme Events and Disasters to Advance Climate Change Adaptation* (Cambridge: Cambridge University Press)
[4] Anderson B G and Bell M L 2009 Weather-related mortality *Epidemiology* **20** 205–13
[5] Rhodes J, Chan C, Paxson C, Rouse C E, Waters M and Fussell E 2010 The impact of hurricane Katrina on the mental and physical health of low-income parents in New Orleans *Am. J. Orthopsychiatry* **80** 237–47
[6] Dell M, Jones B F and Olken B A 2009 Temperature and income: reconciling new cross-sectional and panel estimates *Am. Econ. Rev.* **99** 198–204
[7] Wu X, Xu Z, Liu H, Guo J and Zhou L 2019 What are the impacts of tropical cyclones on employment? An analysis based on meta-regression *Weather Clim. Soc.* **11** 259–75
[8] Dell M, Jones B F and Olken B A 2012 Temperature shocks and economic growth: evidence from the last half century *Am. Econ. J. Macroecon.* **4** 66–95
[9] Winsemius H, Aerts J and van Beek L 2016 Global drivers of future river flood risk *Nat. Clim. Change* **80** 381–5
[10] Wenz L, Levermann A and Auffhammer M 2017 North–south polarization of European electricity consumption under future warming *Proc. Natl Acad. Sci. USA* **114** E7910–8

[11] Auffhammer M, Baylis P and Hausman C H 2017 Climate change is projected to have severe impacts on the frequency and intensity of peak electricity demand across the United States *Proc. Natl Acad. Sci. USA* **114** 1886–91
[12] Gbegbelegbe S, Chung U, Shiferaw B, Msangi S and Tesfaye K 2014 Quantifying the impact of weather extremes on global food security: a spatial bio-economic approach *Weather Clim. Extremes* **4** 96–108
[13] Sietz D, Mamani Choque S E and Lüdeke M K 2011 Typical patterns of smallholder vulnerability to weather extremes with regard to food security in the Peruvian altiplano *Reg. Environ. Change* **12** 489–505
[14] Marto R, Papageorgiou C and Klyuev V 2018 Building resilience to natural disasters: an application to small developing states *J. Dev. Econ.* **135** 574–86
[15] Mannakkara S and Wilkinson S 2014 Re-conceptualising "building back better" to improve post-disaster recovery *Int. J. Manag. Proj. Bus.* **7** 327–41
[16] Hallegatte S, Rentschler J and Walsh B 2018 Building back better: achieving resilience through stronger, faster, and more inclusive post-disaster reconstruction *Technical Report* (Washington, DC: World Bank)
[17] Levermann A 2014 Climate economics: make supply chains climate-smart *Nature* **506** 27–29
[18] Otto C, Willner S, Wenz L, Frieler K and Levermann A 2017 Modeling loss-propagation in the global supply network: the dynamic agent-based model acclimate *J. Econ. Dyn. Control* **83** 232–69
[19] Inoue H and Todo Y 2019 Propagation of negative shocks across nation-wide firm networks *PLoS One* **14** e0213648
[20] Yiou P, Ribereau P, Naveau P, Nogaj M and Brázdil R 2006 Statistical analysis of floods in Bohemia (Czech republic) since 1825 *Hydrol. Sci. J.* **51** 930–45
[21] Baade R A, Baumann R and Matheson V 2007 Estimating the economic impact of natural and social disasters, with an application to hurricane Katrina *Urban Stud.* **44** 2061–76
[22] Zander K K, Botzen W J, Oppermann E, Kjellstrom T and Garnett S T 2015 Heat stress causes substantial labour productivity loss in Australia *Nat. Clim. Change* **5** 647–51
[23] Ranson M, Kousky C, Ruth M, Jantarasami L, Crimmins A and Tarquinio L 2014 Tropical and extratropical cyclone damages under climate change *Clim. Change* **127** 227–41
[24] Burke M, Hsiang S M and Miguel E 2015 Global non-linear effect of temperature on economic production *Nature* **527** 235–9
[25] Willner S N, Otto C and Levermann A 2018 Global economic response to river floods *Nat. Clim. Change* **8** 594–8
[26] Zscheischler J *et al* 2018 Future climate risk from compound events *Nat. Clim. Change* **8** 469–77
[27] Zscheischler J *et al* 2020 A typology of compound weather and climate events *Nat. Rev. Earth Environ.* **7** 333–47
[28] Ruiter M C, Couasnon A, Homberg M J, Daniell J E, Gill J C and Ward P J 2020 Why we can no longer ignore consecutive disasters *Earth's Future* **8** e2019EF001425
[29] Hallegatte S 2014 *Economic Resilience: Definition and Measurement* (Washington, DC: The World Bank)
[30] Hsiang S 2010 Temperatures and cyclones strongly associated with economic production in the Caribbean and central America *Proc. Natl Acad. Sci. USA* **107** 15367–72
[31] Kuhla K, Willner S N, Otto C, Wenz L and Levermann A 2021 Future heat stress to reduce people's purchasing power *PLoS One* **16** e0251210
[32] Willner S N, Levermann A, Zhao F and Frieler K 2018 Adaptation required to preserve future high-end river flood risk at present levels *Sci. Adv.* **4** eaao1914
[33] Geiger T, Frieler K and Bresch D N 2018 A global historical data set of tropical cyclone exposure (TCE-DAT) *Earth Syst. Sci. Data* **10** 185–94
[34] Geiger T, Gütschow J, Bresch D N, Emanuel K and Frieler K 2021 Double benefit of limiting global warming for tropical cyclone exposure *Nat. Clim. Change* (https://doi.org/10.1038/s41558-021-01157-9)
[35] Lenzen M, Kanemoto K, Moran D and Geschke A 2012 Mapping the structure of the world economy *Environ. Sci. Technol.* **46** 8374–381

Article D

Incomplete recovery to enhance economic growth losses from US hurricanes under global warming

Authors

Christian Otto†, Kilian Kuhla†, Tobias Geiger, Jacob Schewe, Katja Frieler
† with equal contributions

Status

Submitted to *Nature Communications*,
preprint doi: 10.21203/rs.3.rs-654258/v2.

Capsule summary

The impact of hurricanes on long-term economic growth is computed using an event-based macroeconomic growth model, which resolves the dynamic response to each individual hurricane. A basic insurance scheme is included in this model to examine potential adaptation measures. The results depict that growth losses depend on an ensemble's shock size distribution of landfalling hurricanes, although the number of events and total damage remain constant. Incomplete recovery – subsequent shock repercussion during the recovery process to a former shock – has been identified as the cause. This highlights the relevance of (short-term) impact resolution to economic growth. Further, the results depict that growth losses can be mitigated, even under certain circumstances concerning climate change.

Author contributions

All authors designed the research. Christian Otto and Kilian Kuhla conducted the analysis. Kilian Kuhla implemented the model code and made the visualization for the study. Kilian Kuhla developed the climate change projections with contributions of Christian Otto and Tobias Geiger. Christian Otto and Kilian Kuhla wrote the manuscript with contributions from all authors.

Incomplete recovery to enhance economic growth losses from US hurricanes under global warming

Christian Otto[†a,*], Kilian Kuhla[†a,b], Tobias Geiger[a,c],
Jacob Schewe[a], Katja Frieler[a]

[a]Potsdam Institute for Climate Impact Research, Telegrafenberg A56, Potsdam, Germany
[b]Institute of Physics, Potsdam University, Karl-Liebknecht-Str. 24, Potsdam, Germany
[c]Deutscher Wetterdienst, Klima und Umwelt, Potsdam, Germany
[†] with equal contributions
[*]Correspondence to: christian.otto@pik-potsdam.de

Abstract

Ongoing global warming is likely to increase the return frequency of very intense hurricanes in the North Atlantic. Here, we analyse how this frequency increase may impact on economic growth. To this end, we introduce an event-based macroeconomic growth model that temporally resolves how growth depends on the heterogeneity in timing and intensity of hurricane impacts. We calibrate the model to the United States and find that economic growth losses scale super-linearly with their heterogeneity. We explain this by a disproportional increase of indirect losses with event severity which can lead to an incomplete recovery of the economy between consecutive intense landfall events. Based on two different methods to estimate the future frequency increase of intense hurricanes compared to the period 1980-2014, we estimate annual growth losses to increase between 10% and 146% in a Paris-compatible 2°C world and even up to 522% in a 2.7°C world in compliance with the median end-of-century warming under currently implemented or enacted policies. We finally study the efficacy of disaster insurance as an adaptation strategy and find that higher insurance coverage may higher insurance coverage may be a viable means to mitigate these climate change-induced increases in growth losses.

Introduction

Already in the present climate, hurricanes in the North Atlantic cause substantial economic losses in the United States (US). Between 1980 and 2019, these storms caused on average losses about US$ 31 billion in direct economic losses per year, peaking at US$ 266.5 billion in 2005 according to MunichRe's NatCatSERVICE database[1]. Moreover, there is increasing empirical evidence that, in addition to these direct losses, tropical cyclones can substantially reduce economic growth of affected countries for more than a decade[2;3;4]. These long-term growth impacts may have important implications for the adaptation to, and coping with, the impacts of tropical cyclones under global warming, since there is strong evidence that the proportion of very intense storms may increase[5;6;7]. There are at least two mechanisms through which this increase could overcompensate a possible mild decline of the overall number of tropical cyclones[5] driving up economic losses. First, the most intense storms cause dis-proportionally larger direct economic losses than smaller storms. For instance, major hurricanes of the two highest categories 4–5 on the Saffir-Simpsons scale[8] have accounted for almost half of normalised economic damage from all hurricanes that made landfall in the US in the period 1900-2005 despite representing only about 6% of landfall events[9]. Second, an increase of the return frequency implies that, on average, there is less time for the economy to recover in between consecutive events; incomplete recovery has been identified as one main factor that may increase the vulnerabilities of the economy to climate extremes and thereby drive up losses[10;11].

Catastrophe insurance is discussed as a means to reduce vulnerabilities of the economy to extreme weather events by shortening the recovery time in the disaster aftermath[12;13;14;15], and it may thereby even promote economic growth on the macroeconomic level[16]. These promising findings may explain the rising popularity of multilateral climate risk insurance schemes and the G20 InsuResilience Global Partnership initiative[17]. However, it remains an open question whether higher insurance coverage and better insurance schemes will be sufficient to counteract climate change impacts in a warming world[18;19].

Progress in answering this question has been also made difficult by the limitations of state-of-the-art climate integrated assessment models (IAMs). These standard workhorses for climate policy assessments (see[20;21] for detailed reviews of IAMs)) – such as the seminal DICE model[22] which is used by the US government to estimate the cost of carbon

emissions to society – have been criticised for not being able to appropriately account for the impacts of climate extremes[23;24]. The main reason is that the coarse temporal resolution of most models (typically 1–10 years) simply does not allow for the representation of individual extreme weather events; potentially important non-linearities arising from a disproportional increase of total economic losses with impact intensity or from incomplete recovery between consecutive events cannot be resolved. In consequence, IAM-based studies usually report relatively small, or even negligible, impacts of climate extremes on the economy[25;26] which are at odds with recent estimates in the climate econometric literature[27;3;2].

Main

Here, we first study how the heterogeneity of US hurricane impacts has affected economic growth in the period 1980–2014. We then project increases in growth losses that would arise from changes in the return frequencies of the storms and associated changes in storm number and impact heterogeneity in a Paris-compatible 2°C world as well as in a world, which is 2.7°C warmer than in preindustrial times corresponding to the median warming estimate by 2100 under the currently implemented or enacted policies ("current policy path")[28]. Since there is substantial uncertainty on how the return frequencies of hurricanes will change with global warming, and the magnitude of the effect strongly depends on the underlying methodology used to estimate this change[5], we consider two different approaches at both ends of the uncertainty range. In addition, we assess the efficacy and limits of disaster insurance in mitigating the climate change-induced increase in growth losses. To this end, we build a simple – and transparent – event-based neoclassical growth model for a national economy. The model accounts for losses to the stock of physical assets that result from individual landfall events. Reconstruction investments can be capped in the disaster aftermath to describe inefficiencies slowing down the economic recovery such as scarcity of trained labour and building materials and other financial and technical constraints in the reconstruction process[29;30]. Further, we integrate a compulsory non-profit hurricane insurance financed by a flat fee on all citizens, regardless of their individual risk[12]. This insurance scheme represents a precautionary

savings mechanism where premiums accumulated in normal times are issued to affected households in the disaster aftermath.

In the standard calibration of the model, the insurance ratio is set to 50% the average ratio of insured losses in the US between 1980 and 2014 according to the NatcatSERVICE database[1] and reconstruction investments are capped to 0.2% of weekly output following ref.[29]. This model calibration allows us to obtain average annual output growth losses that are comparable to those reported in the recent climate econometric literature[2;4] when driving the model with the direct asset losses of the 88 hurricanes that made landfall in the US in the period 1980–2014 according to the NatCatSERVICE database[1].

Insurance accelerates economic recovery

To illustrate the interplay of insurance payouts and limits of reconstruction investments, we first study the economic recovery dynamics in the aftermath of an individual storm that destroys 1% of the physical capital stock in month 3 (Fig. 1**A**). Besides the "realistic" standard calibration of the model (or scenario) (green full lines), we consider two limiting scenarios, one without insurance (red lines) and one with full insurance coverage of all losses (blue lines). Further, to test the sensitivity of the model with regard to the construction investment cap, we consider a 1% reconstruction investment cap (dashed lines) in addition to the 0.2% reconstruction investment cap (solid lines) and contrast both to a limiting case where all available investments (difference between output and savings) can be used for reconstruction ("no investment cap", dotted lines) (Fig. 1**B**). Since insurance premiums depend on insurance coverage, each growth trajectory is normalised to the balanced growth path of an unperturbed economy with the same insurance premium. To account for delays in insurance payouts, we fit data on cumulative insurance payouts of the Reinsurance Association of America[31] indicating that 60% (90%) of the insured losses are paid out after one (three) year(s) with a sigmoidal function (see Methods for details). The resulting weekly payouts are shown in the inset of Fig. 1**B**.

Generally, the recovery of the economy can be divided into a first phase of rapid reconstruction of destroyed capital, and a second phase, where the economy slowly approaches the balanced growth path of the unperturbed system. The recovery speed in the first phase is reduced when the reconstruction investment cap is lowered. For the

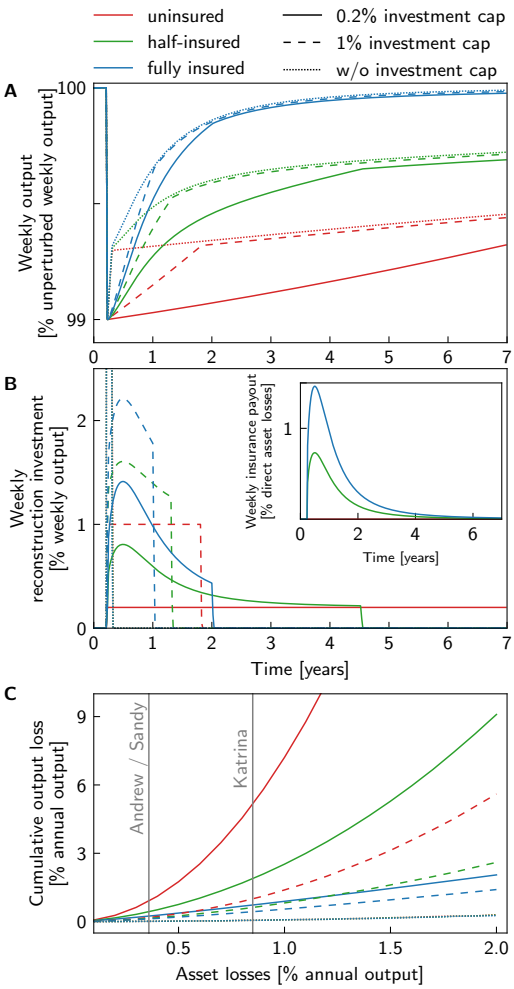

Fig. 1. The contribution of insurance and reconstruction investment on the economic recovery dynamics in the aftermath of an individual hurricane with landfall. Response dynamics in the aftermath of a 1% shock to the capital stock with no (red), 50% (green), and full (blue) insurance coverage, for scenarios where maximum weekly reconstruction investment is not limited (dotted lines) as well as limited to 0.2% (solid lines) and 1% (dashed lines) of weekly output, respectively. **A** Time series of weekly output relative to the output of an unperturbed economy on the balanced growth path. **B** Time series of weekly reconstruction investment (in % of weekly output) and weekly insurance payout (in % of direct asset losses to the capital stock, inset). **C** Cumulative output losses until full recovery of production capacity as a function of the direct asset losses (both in terms of annual output in the year before the landfall). Vertical grey lines indicate the asset losses caused by the historical major hurricanes Sandy, Andrew, and Katrina according to the NatCat-SERVICE database[1].

scenario with the lowest reconstruction investment cap and no insurance, the cap even limits the recovery dynamics in the slow second phase (red solid lines in Fig. 1**A**). In line with empirical findings, recovery speed increases with insurance coverage for two reasons[32;33]: First, since insurance provides additional financial means for reconstruction, the reconstruction investment cap can be temporarily exceeded, e.g., to compensate for scarcity driven wage increases[34]. This accelerates the recovery process especially in the first reconstruction phase. Second, the larger the insurance coverage the lower is the share of the output that has to be reinvested in reconstruction efforts. In consequence, more output can instead be invested in new capital. This fosters output growth especially in the slow recovery phase. Except in the limiting, overly optimistic, case of full insurance coverage and no reconstruction investment cap, cumulative output losses increase super-linearly with the size of the direct asset losses, i.e. *indirect losses* increase faster than shock size (Fig. 1**C**). In consequence, in the aftermath of intense hurricane shocks it can take multiple months or even years for the economy to recover. For instance, in the standard scenario, it takes more than 5 months for the production capacity to recover after the major hurricanes Andrew and Sandy that struck Florida and Louisiana in 1992 and New York and New Jersey in 2012, respectively, both causing asset losses equivalent to about 0.4% of the US's annual output in the years of landfall, respectively (grey vertical lines in Fig. 1**C**). Further, our modelling suggests that in the aftermath of the largest historical loss event, the landfall of hurricane Katrina in New Orleans in 2005, that caused asset losses equivalent to 0.8% of the US's annual output in this year, it took more than one year and a half for the production capacity to recover.

Growth losses increase with shock heterogeneity

Next, we study how the economic response dynamics depends upon the heterogeneity of hurricane shocks (Fig. 2). For that, we assume that landfall events are Poisson[35] distributed within the US hurricane season (June–November). Further, we assume that direct asset losses (relative to the gross domestic product (GDP) in the year of landfall) are log-normally distributed (see supplementary Fig. S5 for a log-normal fit of the data). This yields conservative damage estimates as even power law distributions with higher tail risk are currently discussed for US hurricane damages[36;37]. In the remainder of this paper,

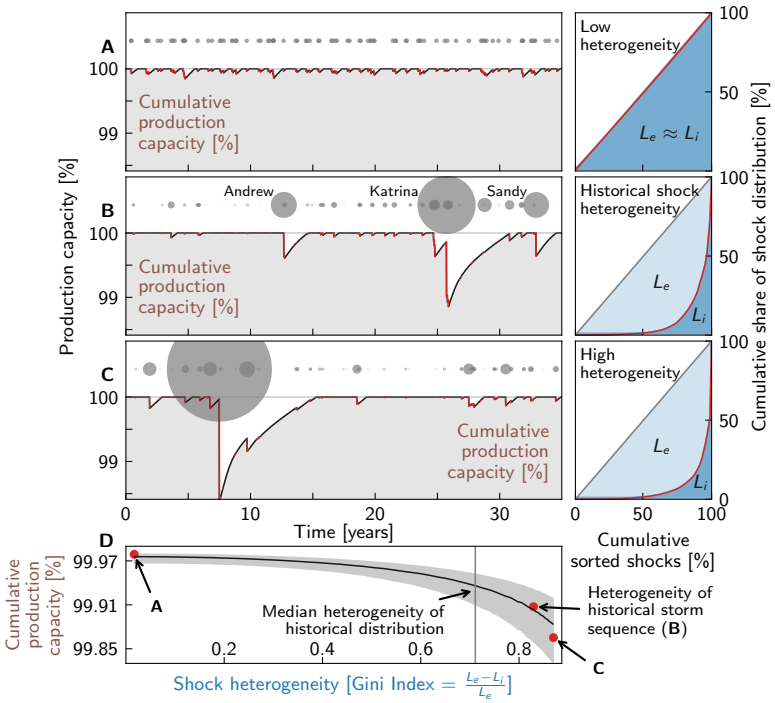

Fig. 2. Recovery dynamics of production capacity in dependence of hurricane shock heterogeneity. Economic impacts of hurricane shocks for a period of 35 years. The heterogeneity of shocks increases from **A** to **C**. Hurricane number and relative cumulative asset losses are fixed to the 88 hurricanes that reportedly made landfall in the United States in the period 1980-2014 and caused 3.24% of cumulative asset losses (relative to the growth domestic product of the years the hurricanes made landfall) according to the NatCatSERVICE database[1]. **B** depicts the impacts of the observed historical time series of hurricanes with landfall. **Left panel:** Exemplary time series of available production capacity (in % of full production capacity (grey horizontal lines)). Periods of reduced capacity in the disaster aftermaths are marked in red and shocks are marked by grey dots with the size of the dots indicating the shock size. **Right panel:** Lorenz curves to illustrate the heterogeneity of the shock distribution. Red lines indicate the cumulative share of production capacity losses as a function of the cumulative share of the shocks. Grey diagonal lines indicate the Lorenz curves for equally distributed shocks. The Gini index $G \equiv \frac{L_e - L_i}{L_e}$ as measure for shock heterogeneity is determined by the ratio of the areas under the red (L_e, light blue shading) and blue lines (L_i, dark blue shading). **D** Mean cumulative available production capacity (in % of the production capacity of unperturbed system) as a function of the Gini index. Red dots and grey shaded areas indicate the values of the Gini index obtained for the runs in **A**–**C** and the 16.7-83.3 percentile confidence interval, respectively. The grey vertical line indicates the median Gini index of the historical shock distribution (see Methods). Other parameters: Insurance coverage 50%; reconstruction investment cap 0.2% of weekly output.

we will refer to the distribution of relative asset losses as *shock distribution*. As detailed in Sec. A.3 of the Methods, drawing from this shock distribution allows us to generate synthetic time series of asset losses with defined length, event number, and value for the cumulative relative asset losses. To isolate the impact of shock heterogeneity, we then vary the heterogeneity of the asset losses – measured by the Gini index (G) of the event distribution – but keep the number of hurricanes with landfall (88) (and thus average hurricane return frequency) as well as relative cumulative direct asset losses (3.24% of cumulative output) at their values reported in the NatCatSERVICE database[1] fixed for the study period 1980–2014 (35 years). Here, normalization of direct asset losses relative to real national GDP in the year of impact allows us to generate representative synthetic time series irrespective of the year of occurrence of each underlying event. Note that we thereby adjust losses for inflation and economic growth but assume no changes in vulnerability (e.g., due to adaptive measures taken on the ground), see refs.[38;39;40] for a discussion on different normalization approaches with respect to hurricane damages.

For a nearly homogeneous shock distribution ($G = 0.018$), asset losses (grey circles in (Fig. 2**A**–**C**) are relatively small and production capacity can mostly recover between loss events and stays close to the one of the unperturbed system for the whole study period (Fig. 2**A**). For higher values of the Gini index, we obtain many small but few high intensity loss events. Since cumulative output losses increase dis-proportionally with event intensity (cf. Fig. 1**C**), also the risk for incomplete recovery between events increases for higher values of the Gini index (cf. Fig. 2**B** and **C** for $G = 0.83$ and $G = 0.87$). For instance, when driving the model with the historical sequence of landfall events, we find that the US economy may not have recovered in between the major hurricanes Katrina and Sandy (Fig. 2**B**).

To gain a systematic understanding on how production capacity depends upon shock heterogeneity, we study the cumulative production capacity over 35 years as a function of shock heterogeneity. For a given shock distribution, cumulative production capacity in general differs between event realisations due to differences in the timing and the size of the shocks. To account for this uncertainty, we generate a large ensembles of 20,000 realisation for each shock distribution. The cumulative production capacity is then plotted as a function of the median Gini index as obtained across all realisations (see Sec. A.2 of Methods) (Fig. 2**D**). (Note that values of the Gini index for individual realisations may

substantially deviate from the median Gini index. For instance, the Gini index for the observed historical storm sequence ($G = 0.83$) is substantially higher than the median value of the Gini index across all realisations for the historical storm distribution ($G = 0.71$) (compare red dot to vertical grey line in Fig. 2**D**).) We find that the available production capacity reduces super-linearly with increasing shock heterogeneity. The reduction is strongest in the high heterogeneity range to the right of the median Gini index for the historical period (grey line in Fig. 2**D**), where incomplete recovery becomes more likely.

Similarly, economic growth declines super-linearly with increasing shock heterogeneity (Fig. 3). Besides the standard scenario with a 0.2% reconstruction investment cap and 50% insurance coverage (red line in Fig. 3**B**), we again consider scenarios with a 1% and no investment cap (green and blue lines in Fig. 3) as well as the limiting cases of no and complete insurance (Fig. 3**A** and Fig. 3**C**). We find that the dependence of economic growth on shock heterogeneity increases when i) the reconstruction investment cap and ii) the insurance coverage is lowered.

For low values of the investment cap, the growth reduction with increasing shock heterogeneity can be quite substantial. For instance, for the standard scenario, annual growth losses increase by more than 16% from 0.0238 percentage points (p.p.) for the lowest to 0.0275 p.p. for the highest value of the Gini index (red line in Fig. 3**B**). While these growth rate reductions may appear small, they imply that for the highest value of the Gini index output losses accumulate over three and a half decade to 16,218 US$ per-capita, an additional 2,196 US$ per-capita compared to the lowest value of the Gini index. The dependence of growth on shock heterogeneity can again be understood by the disproportional increase of indirect losses with shock intensity making incomplete recovery between events more likely with increasing Gini index (cf. Fig. 1**A**). In line with this reasoning, we find that, in the scenario without construction investment cap, where the recovery time is substantially shorter then in the scenarios with caps (cf. Fig. 1), growth losses are nearly independent of the Gini index.

Further, for each fixed level of shock heterogeneity, growth losses decrease with increasing insurance coverage which can be understood as follows: Insurance provides additional financial means for reconstruction and thereby mitigates the impact of shocks that are large compared to the reconstruction investment cap by reducing the recovery time and therefore suppressing incomplete recovery. For instance, for the standard scenario

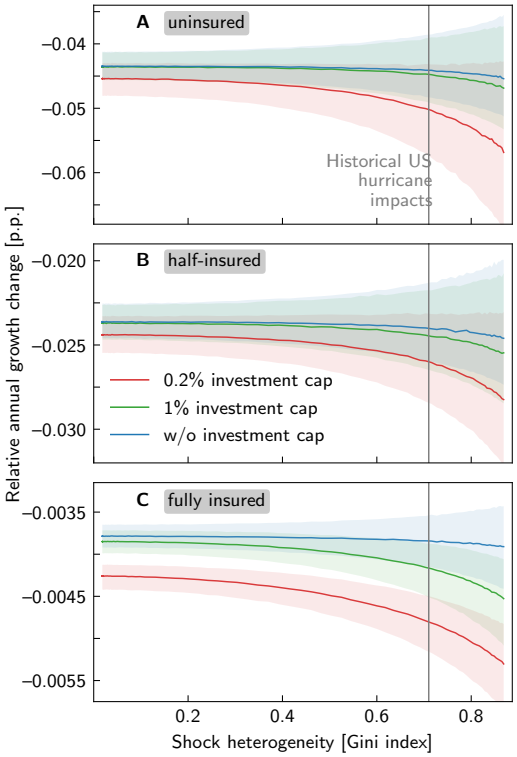

Fig. 3. Impact of hurricane shock heterogeneity on annual output growth rate. Median annual growth rate change of the economy under hurricane shocks relative to the growth rate of the corresponding unperturbed economy, as a function of shock heterogeneity – measured by the Gini index – for no (**A**), half (**B**), and full (**C**) insurance coverage. Blue, green, and red lines depict median growth rate changes for scenarios where reconstruction investment is not limited, limited to 0.2%, and 1% of weekly output, respectively; shaded areas mark the corresponding 16.7-83.3 percentile confidence intervals. The grey vertical line indicates the median Gini index of the historical distribution of relative direct asset losses.

and the median Gini index of the historical period (grey vertical line in Fig. 3), output losses accumulate over three and a half decades to 14,904 US$ per-capita. They are therefore, on average 832 US$ per-capita and 1,121 US$ per-capita higher than for the corresponding scenarios with a 1% and without reconstruction investment cap, respectively.

The greatest benefit of insurance is, however, that it strongly mitigates the magnitude of growth losses. For the median Gini index of the historical period and the lowest investment cap, hurricanes reduce annual growth on average by 0.048 p.p. in the uninsured scenario. These losses are already roughly halved to 0.025 p.p. for the standard scenario with 50% insurance coverage and reduced by a magnitude larger than ten to 0.0045 p.p. in the fully insured scenario. Accordingly, output losses accumulate over three and a half decade decrease from 28,807 US$, over 14,904 US$, to 2,746 US$ per-capita. Critically, there is a tradeoff between the increase in consumption in the disaster aftermath in the presence of insurance and consumption and economic growth losses due to lower capital accumulation in normal times. We find that the studied insurance scheme only fosters economic growth (supplementary Fig. S7) and national consumption when large indirect losses arise, i.e. when the reconstruction process is slow and shocks are heterogeneously distributed as this likely was the case in the historical period. Thereby, the benefit of insurance for national consumption (averaged over many shock realisations) increases with insurance penetration and shock heterogeneity (supplementary Fig. S8 and Fig. S9)). Insurance premiums increase with insurance coverage but remain small compared to average per-capita consumption. For instance, for the standard scenario of 50% insurance and the mean shock heterogeneity of the historical period, mean annual insurance premiums equal 110 US$ which is only a tiny fraction (about 0.003%) of US households' average annual consumption in the historical period. (supplementary Fig. S10)

To set all these numbers into context, it is important to keep in mind that our model, by construction, computes growth losses borne by the US in total. Local growth losses in the affected counties may be much larger.

Better insurance coverage can help mitigate climate change-induced growth losses

To account for the substantial uncertainty on how climate change will impact on hurricane climatology, we employ two different approaches estimating climate change-induced

changes in the return frequencies of hurricanes, one at the lower and one at the upper end of the impacts reported in the recent literature[5]. Both approaches consistently predict an increase of the proportion of very intense storms, though the magnitude of this change – and in consequence the resulting changes to direct asset losses – differs substantially between the two approaches. Importantly, in contrast to the last section, where only the heterogeneity of events was mutable, these climate change-induced frequency increases may additionally translate into changes of the distribution of direct asset losses with respect to i) the number of hurricanes and ii) the cumulative direct asset losses during the study period (Fig. 4) (see Methods for details). Knutson et al. report a moderate increase of the

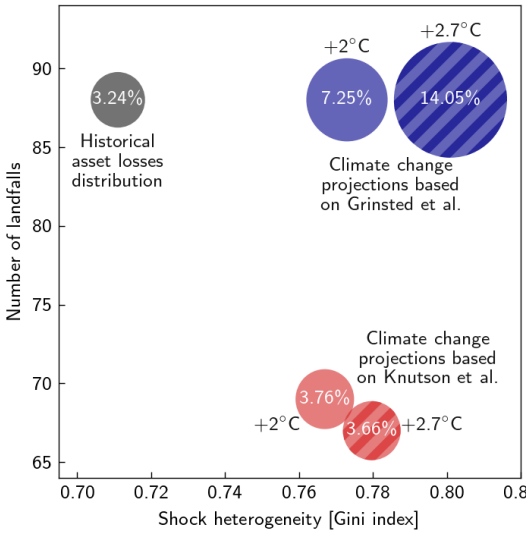

Fig. 4. Visualisation of climate change-induced shifts of the hurricane shock distribution. Under global warming, the historical distribution of the direct asset losses caused by the $N_s = 88$ historical hurricanes that made landfall in the US in the 35-years period from 1980 to 2014 (black filled circle) according to the NatCatSERVICE database[1] is projected to change along three dimension: i) the median shock heterogeneity measured by the Gini index (x-axis), ii) the number of landfalls for a 35 years period (y-axis) and iii) the median cumulative direct asset losses (size of circles). Blue and red circles indicate estimates for +2˚C (filled) and +2.7˚C (hashed) worlds (above pre-industrial levels) based on Grinsted et al.[6] and Knutson et al.[7], respectively. The numbers in the circles refer to the median cumulative relative asset losses for a 35 years period (see Methods for details).

return frequency of the most intense (Cat. 4-5) hurricanes by 45% in a 2˚C world (2.7˚C: 39%) but a reduction of the overall number of hurricanes (of all categories) by 22% (2.7˚C: 24%), which the authors derive from changes in the maximum lifetime wind speeds of the storms obtained from dynamical down-scaled global circulation model runs[7] ("wind speed-based" estimate). In contrast, Grinsted et al. use observational storm surge data and estimate a considerable increase of relative return frequencies ranging from 1.4 fold (2.7˚C: 1.6 fold) for storms with a small surge index to a 6.4 fold (2.7˚C: 15.2 fold) for the

most intense storms[6] ("surge-based" estimate). The authors' statistical analyses cannot distinguish whether this frequency increase is caused by an overall increase in the number of storms or merely implies a shift of the distribution of storm surges to higher intensity events. However, since there is relatively good agreement in the literature that the average number of hurricane per season will not strongly change with global warming[5], in our derivation of future direct asset losses according to Grinsted's surge-based estimate, we assume that the number of storms does not change compared to the historical study period (see Methods for details).

For both, the wind speed- and surge-based estimates, we obtain a moderate increase of shock heterogeneity with the median Gini index increasing from its historical value of 0.71 to 0.77 (2.7˚C: 0.78) and 0.77 (2.7˚C: 0.80), respectively. For the latter, the hurricane number (88) remains unchanged compared to the historical period, whereas it decreases to 69 (2.7˚C: 67) for the latter. Further, under the assumption of constant adaptation levels, the estimated cumulative relative asset losses over 35 years increase only moderately from 3.24% for the historical period to 3.76% (2.7˚C: 3.66%) for the wind speed-based estimate but more than double (7.25%) (2.7˚C: 14.05%) for the surge-based estimate. In terms of median annual growth losses, we obtain a moderate increase by 10% (for 2˚C as well as 2.7˚C) compared to the historical standard scenario for the wind field-based estimate but a strong increase by 146% (2.7˚C: 522%) for the storm surge-based estimate (Fig. 5**A**). The reason is that for the former the additional growth losses due to the increases of shock heterogeneity and cumulative direct asset losses are partially compensated by the reduction of growth losses due to the reduced absolute number of hurricanes; whereas for the latter the increases of shock heterogeneity, cumulative direct asset losses, and hurricane number all enhance growth losses. Since we always consider growth losses relative to a baseline scenario with the same reconstruction investment cap (and insurance coverage), these findings are robust with regard to changes in the reconstruction investment cap (cf. Fig. 5**B** and Fig. 5**C**).

We finally address the question whether an increase in insurance coverage would be sufficient to compensate for the additional global warming-induced growth losses. We find that, to this end, the historical insurance coverage of 50% would have to be substantially raised to 84% (2.7˚C: 99%) according to the surge-based estimate, whereas a moderate increase to 58% for 2˚C as well as 2.7˚C would suffice according to the wind field-based

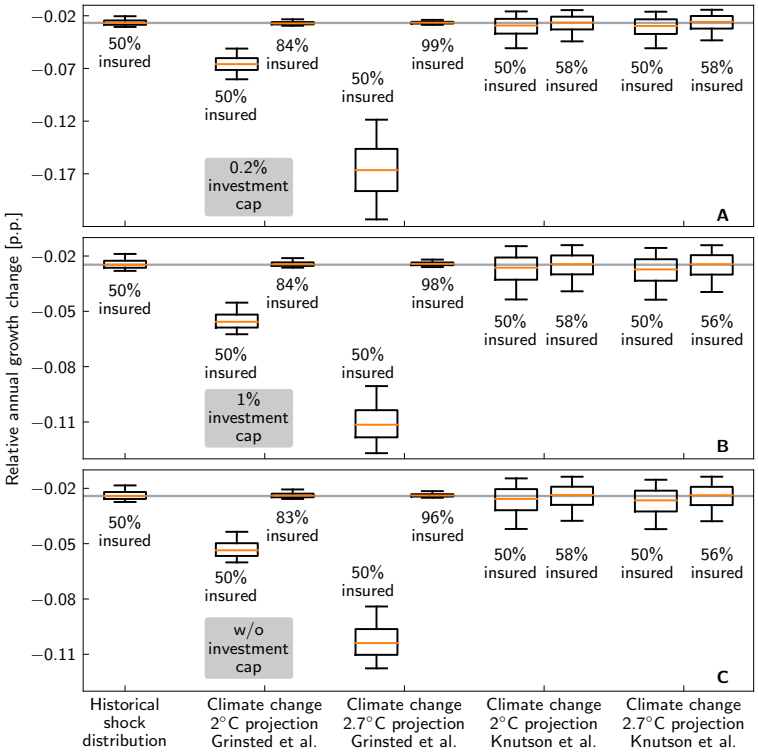

Fig. 5. Projected impacts of hurricanes on economic growth in 2°C and 2.7°C worlds and the effectiveness of insurance as coping strategy. Annual growth losses (relative to the corresponding unperturbed economies evolving on the balanced growth paths) as obtained for the historical shock distribution (50% insurance coverage, period 1980-2014; 1st column), for Paris-compatible +2°C warming above pre-industrial levels (2nd , 3rd , 6th and 7th column) and +2.7°C warming in compliance with current policies (4th , 5th , 8th and 9th column) for reconstruction investment caps of 0.2% (**A**, standard scenario), 1% (**B**) and without reconstruction investment cap (**C**). Climate change projections of growth losses are derived from two different methods to estimate climate change-induced changes in the return frequencies of hurricanes by Grinsted et al.[6] and Knutson et al.[7] (50% insurance coverage, 2nd and 4th column, respectively). Additionally, for both estimates and warming levels the insurance coverages that would be necessary to reduce growth losses to the historical level are shown (3rd , 5th , 7th and 9th column). Orange lines, boxes, and whiskers indicate median loss estimates as well as the 25th-75th and 5th-95th percentile ranges, respectively.

estimate for the standard scenario (cf. columns 2 and 6 with columns 3 and 7 (2.7°C: 5 and 9) in Fig. 5). Again, these findings are fairly robust with regard to different values of the construction investment cap.

Discussion

These numbers suggest that a better insurance coverage could indeed be a viable means to compensate for climate change-induced increases in tropical storm-related losses, even in the absence of other adaptation measures. However, we caution that we do not account for several drivers of losses in the future projections, which may lead to an over- or underestimation of future losses. On the one hand, we assume no future changes in the vulnerability of the economy to tropical cyclone impacts. While this may result in an overestimation of future losses, since vulnerability may be reduced by additional adaptation efforts, there also exists empirical evidence that the vulnerability of the US economy to tropical cyclone strikes has rather increased over the past decades[41;42]. Assuming constant vulnerability thus provides a balanced perspective. On the other hand, our estimates of climate-induced changes in direct asset losses are based on estimates for the changes in the return frequencies of the storms only; other potential channels through which climate change may impact on the economic losses caused by tropical cyclones, such as increasing storm surge risk due to sea level rise[43;44], and stronger precipitation associated with hurricanes[45] are neglected. Neglecting these additional drivers as well as non-economic losses such as lives lost most likely results in an underestimation of future economic losses[46;47].

Further, using a simple macroeconomic growth model with only one homogeneous output good, our analysis cannot provide information on the recovery dynamics of individual sectors and may therefore underestimate delays arising from the scarcity of intermediate goods from strongly affected sectors needed for production in other sectors and the associated scarcity-induced price inflation in the disaster aftermath. In consequence, we may underestimate recovery costs[48;49;50] and, in turn, growth losses. Finally, we do not discuss moral hazard issues that may arise from the considered mandatory precautionary savings scheme and may require the introduction of deductibles, for instance, to de-incentive the construction of new buildings in storm-surge prone locations[51]. This might

provide an over-optimistic assessment of the efficacy of insurance in mitigating disaster losses.

Our research stresses the importance of non-linear economic responses to consecutive extreme weather events. In particular, our results suggest that only by i) resolving the response to individual events, and by ii) accounting for a realistic timing of the events (e.g., accounting for the hurricane season), it is possible to estimate the full economic impact of extreme events[23]. Further, these findings are key to assess the efficacy of adaptation and coping strategies. For instance, in our study the limited pace of insurance payouts delays reconstruction efforts in the disaster aftermath, but a similar reasoning holds for physical protection measures, which once damaged may take months or even years to be repaired[52]. Thus, temporally resolving the economic recovery phase is critical for the assessment and comparison of disaster response measures. This aspect becomes especially important since extreme weather events are projected to intensify and become more frequent with global warming, at least on a regional level[53]. In this regard, our findings may also encourage the climate integrated assessment modelling community to consider new approaches allowing to go beyond smooth damage functions translating changes in global mean temperature into aggregate output losses. As shown here, this common approach may underestimate the economic repercussions of extreme weather events since it neglects potentially important non-linearities in the economic response such as the disproportional increases of indirect losses with impact intensity or the case of incomplete recovery[23]. This may also explain the discrepancy between the loss estimates reported in the recent climate econometrics literature and the estimates of climate integrated assessment models.

While our estimates on how climate change may impact on economic losses caused by hurricanes in the US are subject to several sources of uncertainty, they nonetheless show that the mitigating effect of increased insurance coverage is of the same order of magnitude as the climate change-induced loss increase. Though insurance premiums may increase under global warming by up to a factor of four, they likely will remain affordable for US consumers. This suggests that insurance can be a major building block of future climate change adaptation strategies, at least in developed countries. For developing countries the hurdles to adapt to climate change are much higher since they are often more strongly affected by – and more vulnerable to – climate change impacts and lack the

financial means and strong institutions to implement comprehensive climate adaptation measures[54]. To illustrate this, we have analysed the tropical cyclone-prone Small Island Developing State of Haiti (Sec. B.2) and find that the tropical cyclone induced growth losses it suffers in the present climate are already by one magnitude larger than those of the US (cf. Fig. 3**B** with Fig. S12**A**). One reason is that Haiti's disaster insurance market is much less developed and nearly all of the past tropical cyclone losses were not insured[1]. Further, already in the present climate Haiti is affected so strongly that even in the idealistic limit of full insurance coverage, it would still suffer growth losses comparable in magnitude to those of the US today (cf. Fig. 3**B** with Fig. S12**C**), and tropical cyclone impacts are projected to further aggravate for Haiti under continued climate change (appendix B.2.1). To this end, our results stress the importance – for developing and developed countries alike – to complement insurance solutions with other measures to build resilience to extreme weather events such as investments into better housing standards and resilient infrastructure[55;56] or coping strategies such as managed retreat[57;58] in a risk-layering approach[59]. However, in contrast to rich developed countries of the Global North, strongly affected developing countries will be only able to successfully adapt to climate change impacts when national and international mechanisms and institutions providing concessional climate finance and expertise in climate adaptation such as the United Nations' Green Climate Fund are further strengthened by ensuring that they have both, the financial resources and the effective government, to fulfil their mandates.

A Methods

A.1 Modeling approach

As the standard neoclassical Solow-Swan growth model for a closed economy[60], our model InGroCIIM (Insured Growth under Climate Impacts) describes the growth of a per-capita stock of physical capital k for a unique indistinguishable good under investments and capital depreciation. Here, we neglect changes in labour market and population growth as drivers of capital growth. In extension to the standard model, we account for a non-profit insurance scheme and obtain two coupled differential equations for k and the per-capita capital stock of the insurance k_I reading

$$\dot{A}(t) = \Lambda A(t), \tag{1a}$$

$$\dot{k}(t) = sy(t) - [\delta + r_I]\, k(t) + F_I(t), \tag{1b}$$

$$\dot{k}_I(t) = r_I k(t) - F_I(t). \tag{1c}$$

Here, $\dot{(\cdot)}$ denotes the derivative with respect to time t. We assume that total factor productivity (TFP) A growth exponentially with trend growth rate Λ, and s, y, and δ denote savings rate, production function, and depreciation rate of capital, respectively. The insurance premium $r_I \equiv r_I(r_c)$ depends on the economy's insurance coverage r_c, and $F_I(t)$ denotes the insurance payouts in the disaster aftermaths. Both terms are detailed below. Further, we assume that the production process can be described by a Cobb-Douglas production function $y(t) \equiv A(t)k(t)^\alpha$, where $\alpha \in (0, 1]$ denotes the capital share of income. We model the impact of extreme weather events as shocks to the capital stock. Following[29], we describe the economic recovery in the disaster aftermath as the superposition of two different mechanisms: i) a fast reconstruction process of the damaged capital and ii) the comparably slow growth of the capital stock due to technological development. To this end, we write the capital stock as the product of the fraction of remaining production capacity $\xi(t) \in [0, 1]$ and a "potential capital stock" k_p,

$$k(t) \equiv \xi(t) k_p(t). \tag{2}$$

The Cobb-Douglas production function is derived from the assumption that the process of capital accumulation is optimal and the last unit of capital added is the least productive[61]. However, it appears unlikely that a disaster strikes in such a way that it "de-constructs" the capital in the same optimal way, starting with the least productive unit, and this method is likely to underestimate direct production losses (see discussion in[62] for details). Following previous works[29;30;62], we therefore assume that a shock does not merely destroy the least efficient capital, but equally affects all "productivity layers" of capital. For that, we may write y as a function of ξ and k_p,

$$y(t) \equiv y(\xi(t), k_p(t)) = \xi(t) A \left(k_p(t)\right)^{\alpha} . \tag{3}$$

Noteworthy, this implies that at the time of the shock t_s, y reads

$$y(t_s) = \xi(t_s) \lim_{t \nearrow t_s} \left[y(t)\right] = \xi(t_s) A \left(k_p(t_s)\right)^{\alpha} ,$$

where $\xi(t_s) < 1$, and $k_p(t_s)$ represents the pre-disaster value of the capital stock. Thus, production is reduced by the same factor $1 - \xi(t)$ as the capital stock, i.e. direct asset losses equal direct production losses, and the marginal productivity of capital remains unchanged.

To derive the dynamical equations for k_p and ξ, we first decompose total investment $I(t)$ into the sum of two different investment channels: short-term reconstruction investments $I_{\tilde{\xi}}(t)$, and regular investments increasing production capacity $I_k(t)$,

$$I(t) \equiv sy(t) + F_I(t) = I_k(t) + I_{\tilde{\xi}}(t). \tag{4}$$

By employing Eqs. (2), (3) and (4), we may then rewrite the dynamical equation for the capital stock (1b) as

$$\dot{\left(\xi(t) k_p(t)\right)} = \dot{\xi}(t) k_p(t) + \xi(t) \dot{k}_p(t) \tag{5a}$$

$$= I_k(t) + I_{\tilde{\xi}} - \left[\delta + r_I\right] \xi(t) k_p(t). \tag{5b}$$

By comparing the right-hand sides of Eqs. (5a) and (5b), we obtain the dynamical equations for k_p and ξ as

$$\dot{k}_p(t) = \frac{I_k(t)}{\xi(t)} - [\delta + r_I]\, k_p(t), \tag{6a}$$

$$\dot{\xi}(t) = \frac{I_\xi(t)}{k_p(t)}. \tag{6b}$$

Next, we derive an expression for $I_\xi(t)$ which then permits us to calculate I_k from Eq. (4). To this end, we have to make four assumptions: First, we assume that reconstruction investments yield higher returns compared to investments in the potential capital stock and are therefore prioritised. Second, we assume that reconstruction efforts are limited by short-term constraints such as a lack of skilled labour or reconstruction materials, which may significantly slow down the economic recovery. In consequence, only a fraction $f_{\max} \in [0, 1]$ of the output available for investment $sy(t)$ can be used to finance reconstruction; the actual value of the investment cap $f_{\max}$ depends upon the economy under consideration[30]. Third, we assume that reconstruction efforts cease when the capital stock equals the potential capital stock, no overshoot is possible. Fourth, we assume that the insurance primarily finances reconstruction efforts. In the presence of insurance, the investment cap may be temporarily exceeded since the insurance provides additional financial means, e.g., to compensate for scarcity driven wage increases[34]. This assumption is motivated by empirical findings that higher insurance coverage can lead to a faster economic recovery[32;33]. However, if reconstruction is completed before all of the insured capital is reimbursed, the remaining insurance payout will be invested into the potential capital stock. With these assumption, we may express $I_\xi(t)$ as

$$I_\xi(t) \equiv \begin{cases} 0 & \xi(t) = 1, \\ \min\left[\min\left[f_{\max}, s\right] y(t) + F_I(t), I_r(t)\right] & \xi(t) < 1, \end{cases}$$

where $I_r(t) \equiv (1 - \xi(t))k_p(t)$ is the investment needed to reconstruct the capital stock in the present time step.

A.1.1 Insurance payout dynamics

We model insurance as a compulsory precautionary savings mechanism which may be implemented and managed on the national level by a public institution. To our knowledge, there are no empirical data on the payout dynamics of such an insurance scheme in the US. This is why we use observational data of insurance payouts of commercial providers of risk diversifying insurance by the Reinsurance Association of America (RAA)[31] arguing that the payouts dynamics of the insurance scheme discussed here and commercial (re-) insurers may be similar as main processing steps such as the filing of insurance claims and their eligibility assessment by the insurance provider would be identical for both insurance schemes. According to the RAA data, the reimbursement of insured losses $f_I(t)$ can spread over several years; 60% (90%) of the insured values are reimbursed with in one (three) year(s). This may significantly delay the reconstruction process. We describe the cumulative insurance payouts with a sigmoidal function,

$$f_I(t-t_s; r_c\Delta_s k_p(t_s)) \equiv r_c\Delta_s k_p(t_s)\beta \frac{\left(\frac{t-t_s}{\tau_I}\right)^{\beta-1}(a-1)\exp\left[-\left(\frac{t-t_s}{\tau_I}\right)^{\beta}\right]}{\tau_I\left(1+(a-1)\exp\left[-\left(\frac{t-t_s}{\tau_I}\right)^{\beta}\right]\right)^2}, \quad \forall t > t_s.$$

Here, t_s denotes the time of the shock, the insured losses are given by the product of the insurance coverage r_c, the asset loss Δ_s at time t_s relative to the pre-shock potential capital stock $k_p(t_s)$[1]. The three parameters a, τ_I and β[31] are specified in Tbl. 1 (see supplementary Fig. S2 for a fit of the observational data). The cumulative insurance payout in response to multiple successive asset losses $\{\Delta_{s_i}\}_i$ at times $\{t_{s_i}\}_i$ are then given by the sum of the individual payouts

$$F_I(t; \{t_{s_i}\}_i, \{\Delta_{s_i}\}_i) \equiv \sum_{i=1}^{N_s} f_I(t-t_{s_i}; r_c\Delta_{s_i}k_p(t_{s_i})),$$

where index i labels the shock number, and N_s denotes the total number of shocks.

[1] It is worthy to note, that according to Eq. (3) this is identical to expressing asset losses relative to the output in the year before the shock as done for the calibration of the model to empirical data in Sec. A.1.2

A.1.2 Model calibration

We assume that, in the absence of shocks, the economy evolves along its *balanced growth path* (BGP), where output growth is constant and only driven by TFP growth (growth rate Λ),

$$g \equiv \frac{\dot{y}}{y} = \frac{\dot{A}}{A} + \alpha\frac{\dot{k}}{k} = \Lambda + \alpha g \quad \Leftrightarrow \quad \Lambda = (1-\alpha)g, \tag{7}$$

where we have used in the second identity that if y growth constantly with rate g, k also growth constantly with the same rate[2]. Since in the absence of shocks $F_I(t) = 0 \quad \forall t \in [0, \mathcal{T}]$, where $\mathcal{T}$ denotes the length of the simulation, the dynamic equations for k and k_I decouple (cf. Eqs. (1)), it suffices to solve the equations of motions for the dynamic variables A and k along the BGP. The corresponding equation for k_I can then be derived from Eq. (1c). To this end, we insert the coordinate transformation

$$A(t) = e^{\Lambda t}\tilde{A}(t) \quad \& \quad k(t) = e^{gt}\tilde{k}(t),$$

into the dynamic equations for A and k yielding,

$$\dot{\tilde{A}}(t) = 0, \tag{8a}$$

$$\dot{\tilde{k}}(t) = s\tilde{y}(t) - (\delta + r_I + g)\tilde{k}(t), \tag{8b}$$

where we have introduced the output in BGP coordinates $\tilde{y}(t) \equiv A^0\tilde{k}^\alpha(t)$. Equating the right-hand-sides of Eqs. (8) to zero, yields the steady states for A and k in BGP coordinates

$$\tilde{A}^\star = A^0, \quad \& \quad \tilde{k}^\star = k^0 = \left(\frac{sA^0}{\delta + r_I + g}\right)^{\frac{1}{1-\alpha}}, \tag{9}$$

where $(\cdot)^\star$ and k^0 denote the steady state values of variables and k^0 initial capital stock, respectively. This allows to write the BGP solution of Eqs. (1) as

$$A(t) = e^{\Lambda t}A^0, \quad k(t) = e^{gt}k^0, \quad k_I(t) = \frac{r_I}{g}\left[k(t) - k^0\right] = \frac{r_I}{g}k^0\left[e^{gt} - 1\right]. \tag{10}$$

[2]This can be seen as follows: From the first identity in Eq. (7), it follows that the growth rate of the capital stock $\frac{\dot{k}}{k} = \frac{g-\Lambda}{\alpha}$ is constant when g is constant. From Eq. (2) it then follows that k and y have to grow with the same rate g.

To calibrate the model to the US, we set initial per-capita annual output y^0 and output growth rate g to the per-capita growth domestic product (GDP) and the GDP growth rate of the US in 2015 according to the World Banks' and OECD's National Accounts database[3], whereas capital depreciation rate δ, savings rate s, and capital share of income α are set to their standard values for developed economies[60]. Using the Cobb-Douglas relation for the production function $y = Ak^\alpha$ and the steady state relation for k^0 (cf. Eq. (9)) then allows to express initial TFP and initial per-capita stock as $A^0 = y^0 \left(\frac{\delta + r_I + g}{s}\right)^\alpha$ and $k^0 = sy^0(\delta + r_I + g)^{-1}$, respectively.

Table 1 lists all exogenous parameters used in the simulations. It is worthy to note that

Quantity	Symbol	Value	Unit
Initial GDP per capita	y^0	51638.1	US$
GDP growth rate	g	2.6%	year^{-1}
Savings rate	s	0.2	year^{-1}
Capital depreciation rate	δ	0.1	year^{-1}
Capital share of income	α	0.7	
Time step length	Δt	$\frac{1}{52}$	year
Insurance payout parameter one	a	10^9	
Insurance payout parameter two	β	0.0741	
Insurance payout parameter three	τ_I	$1.31 \cdot 10^{-18}$	year
Empirical insurance premium coefficient	ε	$4.046 \cdot 10^{-4}$	
Simulation period	$\mathcal{T}$	35	year
Cumulative relative historical asset losses	$\Delta_\mathcal{T}$	3.24	%
Number of historical landfalling hurricanes	N_s	88	
Standard deviation of historical log-normal asset loss distribution	σ_0	0.10654	

Tbl. 1. Exogenous parameters used in the numerical simulations.

our model results are very robust with regard to changes of the GDP growth rate g since we only consider changes of the perturbed economy relative to an unperturbed economy evolving along the BGP. Even large variations of $g \in [0.2\%, 4\%]$ result in changes of growth losses that are small compared to the climate uncertainties (cp. lines and shaded areas in supplementary Fig. S6)

[3] https://data.worldbank.org/indicator/NY.GDP.PCAP.CD

Modelling a non-profit insurance scheme, we have to ensure that, averaged over many realisations, the insurance does neither make profit nor losses. However, deriving an exact analytical formula for the corresponding insurance premium r_I is challenging since – as output losses and growth losses – it would depend upon shock heterogeneity. Instead, we here motivate a simple heuristic formula neglecting this dependence and show that the resulting average insurance profits or losses are negligible compared to the cumulative payouts of the insurance. In the worst case, the total relative asset losses occur at the last time step of the simulation. Covering this loss would require an insurance capital stock of $k_I(\mathcal{T}) = r_c \Delta_{\mathcal{T}} k(\mathcal{T})$, where $\mathcal{T}$ denotes the length of the simulation. Inserting this relation in the BGP solution for k_I (cf. Eq. (10)) provides us with the following expression for the insurance premium

$$r_I \equiv \varepsilon \frac{g r_c}{1 - e^{-g\mathcal{T}}},$$

where we have added an empirically determined factor ε ensuring that average insurance profits (or losses) are negligible. (cf. supplementary Fig. S4 revealing that average profits or losses of the insurance are about five magnitudes smaller than the insured capital.

A.2 Gini index as measure for shock heterogeneity

We fit the relative asset losses of the $N_s = 88$ historical hurricanes with landfall included in the NatCatSERVICE database[1] (cf. Tbl. S1) with a log-normal distribution (supplementary Fig. S3) with standard deviation σ_0. To change the heterogeneity of the loss events, we vary the standard deviation σ of the log-normal distribution from $\frac{\sigma_0}{100}$ to $4\sigma_0$. We use the Gini index $G \equiv \frac{L_e - L_i}{L_e} \in [0, 1]$ as measure for the shock heterogeneity, which is derived from the difference of the areas below the Lorenz-curves for a uniform distribution L_e and the given shock distribution L_i (cf. Fig. 2). Shock heterogeneity increases from small to large values of the Gini index. Noteworthy, the Gini index of the historical timeseries of hurricanes with landfall equals 0.829, whereas the median Gini index of the historical shock distribution – obtained by averaging over many synthetic realisations of asset loss time series (see Sec. A.3 for details) – equals 0.71.

A.3 Generation of synthetic time series of asset losses

In this section, we discuss the generation of synthetic time series of asset losses from their historical distribution as reported by the NatCatSERVICE[1] and TCE-DAT databases[63]. For the study period 1980–2014 of $\mathcal{T} = 35$ years, these databases list $N_s = 88$ hurricanes with landfall that have caused asset losses corresponding to at least 10^{-4} % of the GDP in the year of their landfall (see supplementary Tbl. S1). Over this period, relative asset losses accumulated to $\Delta_{\mathcal{T}} = 3.24\%$. We generate synthetic time series of asset losses of length $\mathcal{T}$ keeping N_s and $\Delta_{\mathcal{T}}$ at their historical values in three steps illustrated in supplementary Fig. S5. First, following ref.[35], we assume that the number of hurricanes with landfall n_a in each season a is Poisson distributed, $f_{\mathrm{P}}(n_a) \equiv \frac{\lambda^{n_a} e^{-\lambda}}{n_a!}$. Further, we assume that the mean number of landfalls per season λ is constant over the study period $\mathcal{T}$. To ensure that each synthetic track contains exactly N_s shocks, the shock number for the last season of the track is set to the remainder of available shocks $N_s - \sum_{a=1}^{\mathcal{T}-1} n_a$. To avoid that the last season always receives the remainder of available shocks, seasons are shuffled afterwards. Second, we assume that for each day of the season the likelihood of a hurricane making landfall is the same, but exclude the possibility that two hurricanes make landfall at the same day. Third, following ref.[36] (cf. Fig. S3 in SI), we assume that relative asset losses Δ_s are log-normally distributed, $f_{\mathrm{LN}}(\Delta_s) \equiv \frac{1}{s\Delta_s\sqrt{2\pi}} \exp\left[-\frac{(\ln(\Delta_s)-m)^2}{2s^2}\right]$, where we have introduced the parameters $s \equiv \left(\ln\left(\frac{\sigma^2}{\frac{\Delta_{\mathcal{T}}}{N_s}^2}+1\right)\right)^{\frac{1}{2}}$, $m \equiv \ln(\frac{\Delta_{\mathcal{T}}}{N_s}) - \frac{s^2}{2}$, and the standard deviation σ of the log-normal distribution. Similarly, to step one the size of the last shock of each realisation is set to the difference between $\Delta_{\mathcal{T}}$ and cumulative relative asset losses before the last shock in order to ensure that total cumulative relative asset losses equal $\Delta_{\mathcal{T}}$; then shock sizes are reshuffled.

A.4 Storm surge- and wind field-based climate change projections of asset losses

Storm surge-based projections of asset losses. Grinsted et al.[6] estimated the relative increase in the return frequency of hurricanes with landfall in dependence of the severity of their storm surge (measured by the surge index[64]) per degree of global mean temperature

(GMT) warming relative to the reference period 1980–2000. We employ these findings to project asset losses for a $+2^{\circ}$C increase of GMT above its pre-industrial level[4]. To this end, we first map the surge indices $\{\int_{s_i}\}$ of the $N_s = 88$ historical hurricanes that made landfall in the US between 1980–2014 to the corresponding relative asset losses $\{\Delta^h_{s_i}\}$ reported in the NatCatSERVICE database[1] (supplementary Tbl. S1). Next, we determine the statistical correlation between historical asset losses and surge indices, yielding the damage function $f(s)$ (supplementary Fig. S11). As discussed in the main text, we assume that the average number of hurricanes with landfall will not change compared to the historical study period. In consequence, we interpret the increases in return frequency reported by Grinsted et al. as increases solely in storm surge intensity, and not as an increase of the average number of hurricanes making landfall (in each season). This allows us to map the set of historical sure indices $\{\int_{s_i}\}$ to a set of estimated surge indices in a $+2^{\circ}$C world $\{\int^{cc}_{s_i}\}$. We then assume that each future relative asset loss $\Delta^{cc}_{s_i}$ can be written in terms of the corresponding historical asset loss. This allows to express future relative asset losses in terms of the historical relative asset losses as well as future and historical storm surge indices,

$$\Delta^{cc}_{s_i} \equiv \Delta_{s_i} + f(\int^{cc}_i) - f(\int^h_i). \tag{11}$$

Note that with this relationship historical asset losses are reproduced for $\int^{cc}_i = \int_i$. Employing Eq. (11), we project relative asset losses $\Delta_{\mathcal{T}}$ accumulated over $\mathcal{T} = 35$ years to increase substantially from their historical value of 3.24% to 7.25%. We then generate synthetic realisations of future asset loss time series by distributing the projected $N_s = 88$ relative asset losses over the simulation time of $\mathcal{T} = 35$ years as described in Sec. A.3.

Wind field-based projections of asset losses. Knutson et al.[7] analysed an ensemble of downscaled global climate models participating in the 5$^{\text{th}}$ phase of the Coupled Model Intercomparison Project (CMIP5). Based on the wind fields of the storms they estimated a median decrease of 22% in the overall number of all hurricanes but a median increase of the most intense Category 4 and 5 storms by 45% for an increase of GMT by $+2^{\circ}$C above its pre-industrial level under the Representative Concentration Pathway (RCP) 4.5. To estimate the associated changes in asset losses, we first divide the $N_s = 88$ historical

[4]Note that one degree of global warming compared to 1980–2000 corresponds to 1.5°C of warming compared to the pre-industrial level[65]

hurricanes that made landfall in the US in the period 1980–2014 into moderate (Category 0-3, 66 storms) and intense (Category 4-5, 22 storms) storms based on the IBTRaCS database[66]. Applying then the estimates of Knutson et al., we project that in a $+2^{\circ}$C degree world the number of all hurricanes and the number of moderate hurricanes decrease to 69 and 37, respectively, whereas the number of intense hurricanes increase to 32. This would lead to a minor change of relative cumulative asset losses $\Delta_{\mathcal{T}}$ from their historical value of 3.24% to 3.75%. Synthetic time series of future asset losses are finally generated as described for the surge-based estimate.

Code availability

The implementation of the InGroCIIM model is openly available on github (https://github.com/kuhla/InGroClIm or as zenodo repository 10.5281/zenodo.5017904).

Data availability

The authors thank Munich Re's NatCatSERVICE for providing assess to their natural catastrophes data base from which the direct asset losses of hurricanes with landfall and the insurance coverage employed in this study are derived. These data may be made available by the corresponding author upon request and after consultations with MunichRE. The InGroCIIM model is driven by asset losses of hurricanes with landfall relative to the growth domestic product of the US in the year of landfall as provided by the World Banks' and OECD's National Accounts database (https://data.worldbank.org/indicator/NY.GDP.PCAP.CD) (see supplementary Figs. Fig. S3 and Fig. S11). Intensities of the historical hurricanes on the Saffir-Simpsons scale are taken from the IBTRaCS database[66].

Acknowledgments

This research has received funding from the German Academic Scholarship Foundation and the German Federal Ministry of Education and Research (BMBF) under the research QUIDIC (01LP1907A), and SLICE (FKZ: 01LA1829A), as well as from the Leibniz foundation under the research project ENGAGE (SAW-2016-PIK-1) and the ERA4CS Joint

Call on Researching and Advancing Climate Services (ISIpedia, BMBF grant number 01LS1711A).

Author Contribution

All authors designed the research. CO and KK conducted the analysis and wrote the manuscript with contributions from all authors.

Competing Interests

The authors declare that they have no competing interests.

References

[1] NatCatSERVICE Natural catastrophe know-how for risk management and research (2016). URL https://www.munichre.com/site/corporate/get/documents_E673778764/mr/assetpool.shared/Documents/0_Corporate_Website/Publications/302-06733_en.pdf.

[2] Krichene, H. et al. The Impacts of Tropical Cyclones and Fluvial Floods on Economic Growth – Empirical Evidence on Transmission Channels at Different Levels of Development. World Development **144**, 105475 (2021). 10.1016/j.worlddev.2021.105475.

[3] Berlemann, M. & Wenzel, D. Hurricanes, economic growth and transmission channels: Empirical evidence for countries on differing levels of development. World Development **105**, 231–247 (2018). URL https://www.sciencedirect.com/science/article/abs/pii/S0305750X17304138. 10.1016/J.WORLDDEV.2017.12.020.

[4] Hsiang, S. M. & Jina, A. S. The causal effect of environmental catastrophe on long-run economic growth: Evidence from 6,700 cyclones. Tech. Rep., National Bureau of Economic Research (2014).

[5] Knutson, T. et al. Tropical cyclones and climate change assessment. Bulletin of the American Meteorological Society **100**, 1987–2007 (2019). 10.1175/BAMS-D-18-0189.1.

[6] Grinsted, A., Moore, J. C. & Jevrejeva, S. Projected Atlantic hurricane surge threat from rising temperatures. Proceedings of the National Academy of Sciences of the United States of America **110**, 5369–5373 (2013). 10.1073/pnas.1209980110.

[7] Knutson, T. R. et al. Dynamical downscaling projections of twenty-first-century atlantic hurricane activity: CMIP3 and CMIP5 model-based scenarios. Journal of Climate **26**, 6591–6617 (2013). 10.1175/JCLI-D-12-00539.1.

[8] Saffir-Simpson Hurricane Wind Scale. URL https://www.nhc.noaa.gov/aboutsshws.php.

[9] Pielke, R. A. et al. Normalized Hurricane Damage in the United States: 1900–2005. Natural Hazards Review **9**, 29–42 (2008). 10.1061/(asce)1527-6988(2008)9:1(29).

[10] de Ruiter, M. C. et al. Why We Can No Longer Ignore Consecutive Disasters. Earth's Future **8** (2020). 10.1029/2019EF001425.

[11] Raymond, C. et al. Understanding and managing connected extreme events. Nature Climate Change **10**, 611–621 (2020). 10.1038/s41558-020-0790-4.

[12] Kousky, C. The Role of Natural Disaster Insurance in Recovery and Risk Reduction. Annual Review of Resource Economics **11**, 399–418 (2019). 10.1146/annurev-resource-100518-094028.

[13] Botzen, W. J., Kunreuther, H. & Michel-Kerjan, E. Protecting against disaster risks: Why insurance and prevention may be complements. Journal of Risk and Uncertainty **59**, 151–169 (2019). 10.1007/s11166-019-09312-6.

[14] Peter, G. V., Dahlen, S. V. & Saxena, S. Unmitigated disasters? New evidence on the macroeconomic cost of natural catastrophes (2012).

[15] Michel-Kerjan, E. & Kunreuther, H. Redesigning flood insurance (2011). 10.1126/science.1202616.

[16] Arena, M. Does Insurance Market Activity Promote Economic Growth ? A Cross-Country Study for Industrialized and Developing Countries. The journal of Risk and Insurance **75**, 921–946 (2008). URL https://www.jstor.org/stable/25145316.

[17] Calliari, E., Surminski, S. & Mysiak, J. The Politics of the UNFCCC's Loss and Damage (Springer, 2019). 10.1007/978-3-319-72026-5_6.

[18] Krieger, K. & Demeritt, D. Limits of insurance as risk governance Market failures and disaster politics in German and British private flood insurance (2015). URL https://www.lse.ac.uk/accounting/assets/CARR/documents/D-P/Disspaper80.pdf.

[19] Charpentier, A. Insurability of climate risks. Geneva Papers on Risk and Insurance: Issues and Practice **33**, 91–109 (2008). 10.1057/palgrave.gpp.2510155.

[20] Rose, S. K., Diaz, D. B. & Blanford, G. J. Understanding the social cost of carbon: A model diagnostic and inter-comparison study. Climate Change Economics **8** (2017). 10.1142/S2010007817500099.

[21] Ortiz, R. A. & Markandya, A. Integrated Impact Assessment Models of Climate Change with an Emphasis on Damage Functions: a Literature Review. Basque Centre for Climate Change 1–35 (2009). URL http://ideas.repec.org/p/bcc/wpaper/2009-06.html#download.

[22] Nordhaus, W. D. The Climate Casino: Risk, Uncertainty, and Economics for a Warming World (Yale University Press, 2013).

[23] Otto, C., Piontek, F., Kalkuhl, M. & Frieler, K. Event-based models to understand the scale of the impact of extremes. Nature Energy **5**, 111–114 (2020). 10.1038/s41560-020-0562-4.

[24] Pindyck, R. S. The use and misuse of models for climate policy. Review of Environmental Economics and Policy **11**, 100–114 (2017). 10.1093/reep/rew012.

[25] Farmer, J. D., Hepburn, C., Mealy, P. & Teytelboym, A. A Third Wave in the Economics of Climate Change. Environmental and Resource Economics **62**, 329–357 (2015). 10.1007/s10640-015-9965-2.

[26] Pindyck, R. S. Pricing Carbon When We Don't Know the Right Price. Energy & Environment **87**, 166–167 (2013). 10.1089/acm.2010.0309.

[27] Carleton, T. & Hsiang, S. Social and Economic Impacts of Climate Change. Science (2016). 10.1126/science.aad9837.

[28] Global Update - Glasgow's 2030 credibility gap. Tech. Rep. November, Climate Action Tracker (2021). URL https://climateactiontracker.org/documents/997/CAT_2021-11-09_Briefing_Global-Update_Glasgow2030CredibilityGap.pdf.

[29] Hallegatte, S., Hourcade, J. C. & Dumas, P. Why economic dynamics matter in assessing climate change damages: Illustration on extreme events. Ecological Economics **62**, 330–340 (2007). 10.1016/j.ecolecon.2006.06.006.

[30] Hallegatte, S. & Dumas, P. Can natural disasters have positive consequences? Investigating the role of embodied technical change. Ecological Economics **68**, 777–786 (2009). URL http://dx.doi.org/10.1016/j.ecolecon.2008.06.011. 10.1016/j.ecolecon.2008.06.011.

[31] R.A.A. Catastrophe Loss Development Study: 2013 Edition (Createspace Independent Pub, 2013). URL https://books.google.de/books?id=TalNnwEACAAJ.

[32] Hallegatte, S. et al. Overview: Building the resilience of the poor in the face of natural disasters. Tech. Rep., World Bank (2016). 10.1596/978-1-4648-1003-9_ov.

[33] Hallegatte, S. et al. Shock waves - Managing the Impacts of Climate Change on Poverty. Tech. Rep., The World Bank (2016). URL http://www.journals.cambridge.org/abstract_S0022112081001535. 10.1017/S0022112081001535.

[34] Belasen, A. R. & Polachek, S. W. How hurricanes affect wages and employment in local labor markets. American Economic Review **98**, 49–53 (2008). 10.1257/aer.98.2.49.

[35] Xue, Z. & Neumann, C. J. Frequency and motion of western North Pacific tropical cyclones. Tech. Rep., NOAA (1984). URL https://repository.library.noaa.gov/view/noaa/7080.

[36] Blackwell, C. Power Law or Lognormal? Distribution of Normalized Hurricane Damages in the United States, 1900–2005. Natural Hazards Review **16**, 04014024 (2015). URL http://ascelibrary.org/doi/10.1061/%28ASCE%29NH.1527-6996.0000162. 10.1061/(ASCE)NH.1527-6996.0000162.

[37] Conte, M. N. & Kelly, D. L. An imperfect storm: Fat-tailed tropical cyclone damages, insurance, and climate policy. Journal of Environmental Economics and Management **92**, 677–706 (2018). URL https://doi.org/10.1016/j.jeem.2017.08.010. 10.1016/j.jeem.2017.08.010.

[38] Pielke, R. Economic 'normalisation' of disaster losses 1998–2020: a literature review and assessment. Environmental Hazards **20**, 93–111 (2021). URL https://doi.org/10.1080/17477891.2020.1800440. 10.1080/17477891.2020.1800440.

[39] Botzen, W. J., Estrada, F. & Tol, R. S. Methodological issues in natural disaster loss normalisation studies. Environmental Hazards **20**, 112–115 (2021). URL https://doi.org/10.1080/17477891.2020.1830744. 10.1080/17477891.2020.1830744.

[40] Grinsted, A., Ditlevsen, P. & Christensen, J. H. Normalized US hurricane damage estimates using area of total destruction, 19002018. Proceedings of the National Academy of Sciences of the United States of America **116**, 23942–23946 (2019). 10.1073/pnas.1912277116.

[41] Geiger, T., Frieler, K. & Levermann, A. High-income does not protect against hurricane losses'. Environmental Research Letters **11**, 084012 (2016). 10.1088/1748-9326/aa88d8.

[42] Bakkensen, L. A. & Mendelsohn, R. O. Risk and Adaptation: Evidence from Global Hurricane Damages and Fatalities. Journal of the Association of Environmental and Resource Economists **3**, 555–587 (2016). URL http://www.journals.uchicago.edu/doi/10.1086/685908. 10.1086/685908.

[43] Muis, S., Verlaan, M., Winsemius, H. C., Aerts, J. C. & Ward, P. J. A global reanalysis of storm surges and extreme sea levels. Nature Communications **7**, 12 (2016). 10.1038/ncomms11969.

[44] Li, M., Zhang, F., Barnes, S. & Wang, X. Assessing storm surge impacts on coastal inundation due to climate change: case studies of Baltimore and Dorchester County in Maryland. Natural Hazards **103**, 2561–2588 (2020). 10.1007/s11069-020-04096-4.

[45] Marto, R., Papageorgiou, C. & Klyuev, V. Building Resilience to Natural Disasters: An Application to Small Developing States 28 (2017). URL http://0-search.ebscohost.com.wam.city.ac.uk/login.aspx?direct=true&db=eoh&AN=1679041&site=ehost-live%0Ahttp://www.imf.org/external/pubs/cat/longres.aspx?sk=45329%0Ahttp://www.imf.org/external/pubs/cat/longres.aspx?sk=45329.

[46] Bakkensen, L. A., Park, D. S. R. & Sarkar, R. S. R. Climate costs of tropical cyclone losses also depend on rain. Environmental Research Letters **13**, 074034 (2018). 10.1088/1748-9326/aad056.

[47] Khanam, M. et al. Impact of compound flood event on coastal critical infrastructures considering current and future climate. Natural Hazards and Earth System Sciences **21**, 587–605 (2021). 10.5194/nhess-21-587-2021.

[48] Hallegatte, S. An adaptive regional input-output model and its application to the assessment of the economic cost of Katrina. Risk Analysis **28**, 779–799 (2008). 10.1111/j.1539-6924.2008.01046.x.

[49] Otto, C., Willner, S. N., Wenz, L., Frieler, K. & Levermann, A. Modeling loss-propagation in the global supply network: The dynamic agent-based model acclimate. Journal of Economic Dynamics and Control **83**, 232–269 (2017). URL https://doi.org/10.1016/j.jedc.2017.08.001. 10.1016/j.jedc.2017.08.001.

[50] Willner, S. N., Otto, C. & Levermann, A. Global economic response to river floods. Nature Climate Change **8**, 594–598 (2018). 10.1038/s41558-018-0173-2.

[51] Kousky, C. & Cooke, R. M. Climate Change and Risk Management (2009). URL http://citeseerx.ist.psu.edu/viewdoc/download?doi=10.1.1.860.6241&rep=rep1&type=pdf.

[52] Kates, R. W., Colten, C. E., Laska, S. & Leaterman, S. P. Reconstruction of New Orleas after Hurricane Katrina: A research perspective. Proceedings of the National Academy of Sciences **103**, 14563 (2006). 10.1073/pnas.0605726103.

[53] Herring, S. C., Hoerling, M. P., Peterson, T. C. & Stott, P. A. Explaining extreme events of 2019 from a climate perspective. Bulletin of the American Meteorological Society **102**, 115 (2019). 10.1175/1520-0477-95.9.s1.1.

[54] Hallegatte, S., Vogt-Schilb, A., Bangalore, M. & Rozenberg, J. Unbreakable - Building the Resilience of the Poor in the Face of Natural Disasters. Tech. Rep., World Bank (2016).

[55] Hallegatte, S., Rentschler, J. & Walsh, B. Building Back Better - Achieving resilience through stronger , faster , and more inclusive post-disaster reconstruction (2018). URL http://documents.worldbank.org/curated/en/420321528985115831/Building-

back-better-achieving-resilience-through-stronger-faster-and-more-inclusive-post-disaster-reconstruction.

[56] Climate-resilient Infrastructure. (2018). URL https://www.oecd.org/environment/cc/policy-perspectives-climate-resilient-infrastructure.pdf.

[57] Siders, A. R., Hino, M. & Mach, K. J. The case for strategic and managed climate retreat. Science Policy Forum **365**, 6455 (2019). 10.1126/science.

[58] Carey, J. & Writer, S. Managed retreat increasingly seen as necessary in response to climate change's fury. Proceedings of the National Academy of Sciences of the United States of America **117**, 13182–13185 (2020). 10.1073/pnas.2008198117.

[59] Martinez-Diaz, L., Sidner, L. & McClamrock, J. The Future of Disaster Risk Pooling for Developing Countries: Where Do We Go from Here? (2019). URL http://www.wri.org/publication/disaster-risk-pooling.

[60] Barro, R. J. & Sala-i Martin, X. Economic Growth (MIT Press, Cambridge, MA, 1999), second edn.

[61] Cohen, A. J. Prices, capital, and the one-commodity model in neoclassical and classical theories. History of Political Economy **21**, 231–251 (1989). 10.1215/00182702-21-2-231.

[62] Hallegatte, S. Economic Resilience – Definition and Measurement. Policy Research Working Paper **6852**, 1–46 (2014).

[63] Geiger, T., Frieler, K. & Bresch, D. N. A global historical data set of tropical cyclone exposure (TCE-DAT). Earth System Science Data **10** (2018). 10.5194/essd-10-185-2018.

[64] Grinsted, A., Moore, J. C. & Jevrejeva, S. Homogeneous record of Atlantic hurricane surge threat since 1923. Proceedings of the National Academy of Sciences **109**, 19601–19605 (2012). 10.1073/pnas.1209542109.

[65] Pachauri, R. K. & Meyer, L. (eds.) IPCC, 2014: Climate Change 2014: Synthesis Report. (IPCC, Geneva, 2014). URL https://www.ipcc.ch/report/ar5/syr/.

[66] Knapp, K. R., Kruk, M. C., Levinson, D. H., Diamond, H. J. & Neumann, C. J. The International Best Track Archive for Climate Stewardship (IBTrACS). Bulletin of the American Meteorological Society **91**, 363–376 (2010). 10.1175/2009BAMS2755.1.

Article E

Post-Brexit no-trade-deal scenario: Short-term consumer benefit at the expense of long-term economic development

Authors

Leonie Wenz, Anders Levermann, Sven N Willner, Christian Otto, Kilian Kuhla

Status

Published in *PLOS ONE* in September 2020,
doi: 10.1371/journal.pone.0237500.

Capsule summary

A hypothetical no-deal Brexit with abrupt and significant trade interruptions is analyzed. For this, the loss-propagation model *Acclimate* is extended with the first version of a new transportation module. As a first response to trade restrictions between the European Union (EU) and the United Kingdom (UK), commodity production in UK and Ireland decline sharply, originating in their formerly strong economic entanglement. Restricted borders and the relocation of purchasers caused prices to fall, resulting in short-term gains for consumers on the one hand and losses for the economy as a whole on the other hand.

Author contributions

Leonie Wenz, Sven N Willner, Christian Otto, and Kilian Kuhla elaborated the methodology. Kilian Kuhla developed and implemented the transport module of *Acclimate* and created the trade perturbation function. Leonie Wenz and Kilian Kuhla made the formal analysis. All authors contributed to the manuscript.

PLOS ONE

RESEARCH ARTICLE

Post-Brexit no-trade-deal scenario: Short-term consumer benefit at the expense of long-term economic development

Leonie Wenz[1,2,3]*, **Anders Levermann**[1,4,5], **Sven Norman Willner**[1], **Christian Otto**[1], **Kilian Kuhla**[1,5]

1 Potsdam Institute for Climate Impact Research, Potsdam, Germany, **2** Mercator Research Institute on Global Commons and Climate Change, Berlin, Germany, **3** Department of Agriculture and Resource Economics, University of California, Berkeley, CA, United States of America, **4** Columbia University, New York, NY, United States of America, **5** Institute of Physics, University of Potsdam, Potsdam, Germany

* leonie.wenz@pik-potsdam.de

Citation: Wenz L, Levermann A, Willner SN, Otto C, Kuhla K (2020) Post-Brexit no-trade-deal scenario: Short-term consumer benefit at the expense of long-term economic development. PLoS ONE 15(9): e0237500. https://doi.org/10.1371/journal.pone.0237500

Editor: Giorgio Fagiolo, Scuola Superiore Sant'Anna, ITALY

Received: November 8, 2019

Accepted: July 23, 2020

Published: September 3, 2020

Data Availability Statement: The implementation of the Acclimate model is available as open source on https://github.com/acclimate/acclimate/releases/tag/v3.2.0 (DOI: 10.5281/zenodo.2539089) and the implementation of the disaggregation algorithm can be found on https://github.com/swillner/libmrio (DOI: 10.5281/zenodo.832052). All further code used for data processing and plotting is available from the authors on request. Multi-regional input-output data were downloaded from www.worldmrio.com (EORA simplified dataset v199.82 for 2012). Data for

Abstract

After the United Kingdom has left the European Union it remains unclear whether the two parties can successfully negotiate and sign a trade agreement within the transition period. Ongoing negotiations, practical obstacles and resulting uncertainties make it highly unlikely that economic actors would be fully prepared to a "no-trade-deal" situation. Here we provide an economic shock simulation of the immediate aftermath of such a post-Brexit no-trade-deal scenario by computing the time evolution of more than 1.8 million interactions between more than 6,600 economic actors in the global trade network. We find an abrupt decline in the number of goods produced in the UK and the EU. This sudden output reduction is caused by drops in demand as customers on the respective other side of the Channel incorporate the new trade restriction into their decision-making. As a response, producers reduce prices in order to stimulate demand elsewhere. In the short term consumers benefit from lower prices but production value decreases with potentially severe socio-economic consequences in the longer term.

Introduction

If the Brexit transition periods ends without the United Kingdom and the European Union having agreed on a trade deal and arranged an orderly transition, trade across the English Channel is likely to undergo a sudden shock due to e.g. procedural complications at the borders [1, 2]. Although some preparation is underway, the ongoing negotiations, practical difficulties and resulting uncertainties make it highly unlikely that the administration and the private sector are prepared for the sudden implementation of required customs procedures. Here, we provide a numerical market shock simulation for a scenario in which the UK leaves the European single market and customs union at the end of the transition without a trade deal (referred to as "no-trade-deal event" hereafter) to shed light on its economic effects. These simulations are by no means a literal prediction of the full socio-economic consequences of

China, UK and USA were disaggregated by use of subnational GDP data; downloaded from the National Bureau of Statistics of China (http://data.stats.gov.cn/english/easyquery.htm?cn=E0103, accessed 2017-07-07, data for 2012), the U.K. Office for National Statistics (https://www.ons.gov.uk/economy/grossdomesticproductgdp/datasets/regionalgrossdomesticproductallnutslevelregions, accessed 2019-02-08, data for 2018) and the U.S. Bureau of Economic Analysis (BEA) (https://apps.bea.gov/itable/iTable.cfm?ReqID=70, accessed 2017-07-07, data for 2012). Further model input data, processed model output data and other data used for building figures and drawing conclusions are available as part of the Supporting Information. Maps were built by use of shapefiles provided by the GADM database of Global Administrative Areas, version 3.6 (https://gadm.org/).

Funding: LW: S.V. Ciriacy-Wantrup Fellowship programme at UC Berkeley LW:Volkswagen foundation (Europe and global challenges) SW & CO: German Federal Ministry of Education and Research (Grants 01LA1817C and 01LA1829A) KK: German Academic Scholarship Foundation The funders had no role in study design, data collection and analysis, decision to publish, or preparation of the manuscript.

Competing interests: The authors have declared that no competing interests exist.

Brexit as such a prediction is impossible. They can, however, serve as qualitative insights with quantitative predictive power limited to the order of magnitude of the economic response. We restrict our simulations to the 30 days following a no-trade-deal event.

The likely possibility of a relatively unprepared customs situation in the course of a no-trade-deal event requires numerical simulations with agents that follow a clear economic decision rationale in which they can be 'surprised' in the sense that they have informed expectations but do not foresee the future [3]. This necessitates a modeling approach that can dissolve economic dynamics at short timescales of days which is difficult to achieve with mainstream economic models such as gravity models, Computable General Equilibrium or Input-Output models that typically have much coarser temporal resolutions or lack dynamics. The theory of shock models has been developed in the context of extreme events and within the sphere of disaster impact studies; partly with focus on multi-regional spillover or short-term effects [4–14]. Here we build on and apply this theory by combining multi-regional Input-Output (MRIO) data with an agent-based modeling approach. MRIO data are well suited for investigating economic interdependencies [15, 16] but have so far only been used for static analyses of different Brexit scenarios [17–20]. Contrary to these works, we here provide a dynamic shock simulation of the days to weeks following a no-trade-deal event. Our numerical modeling framework depicts the economic response to such an event at day-level thereby accounting for important buffer mechanisms and market adjustments in the short-term such as stockpiling, use of idle capacities, and shifting of demand to unaffected suppliers [21]. We thus complement previous work that focused on longer-term adaptation to a Post-Brexit market (e.g. new trade deals [22]), analyzed the economic effects of a specific trade agreement [23] or identified key industries in the UK-EU trade relationships [20].

We use the numerical loss-propagation model Acclimate that was specifically designed to simulate the short-term global repercussions of unexpected local shocks [24]. It can be used to study the direct and indirect economic effects of a local disruption of infrastructure or productive capacity. Indirect effects thereby denote the spillover of economic losses and gains to initially unaffected sectors and regions because of ripple effects in the supply chain including price and demand changes [25]. The Acclimate model has, for example, been used for computations of future economic losses due to river flood extremes and heat-stress-induced production failure [26, 27]. At its core is the interaction of more than 6,600 heterogeneous economic agents, i.e. regional sectors (referred to as firms hereafter) and consumers, with more than 1.87 million flows between them, to account for the complex effects arising in trade networks [28]. In each time step, these economic agents form explicit expectations on the future. Based on these expectations, each agent then individually decides upon its optimal production level and upon its optimal strategy of distributing demand for input goods among suppliers by maximizing its future expected profit. Importantly, agents have only limited fore- and oversight. Their decisions reflect the information available to them at the time of decision-making and are not the result of an intertemporal optimization procedure. Since we assume a demand-driven economy, agents do not produce more than has been requested. Without external perturbation, the economy is assumed to be in equilibrium, i.e. supply matches demand. This baseline situation, which serves as our counterfactual, is given by the Eora MRIO data [29] that have been used for economic impact analysis in various other studies (e.g. [30, 31]).

Within the Acclimate modeling framework we simulate a no-trade-deal scenario by restricting trade between the UK and the remaining 27 EU countries from one day to the next and for the whole simulation period of 30 days. More precisely, we assume that only a certain percentage of the amount of goods that were previously traded between the UK and the EU can pass through in the days to weeks following a no-trade-deal event, referred to as '*border permeability*' hereafter. This reduced border permeability does not mean that all trade is

completely cut off nor does it represent the introduction of specific tariffs. Instead, it is supposed to mimic a relatively unprepared customs situation with e.g. administrative obstacles at the borders and harbors that result in delays such that only a certain amount of all previously traded goods transits in the same amount of time.

In total, we distinguish between four scenarios of border permeability and simulate the economic consequences during the first 30 days following the end of the transition period for a scenario in which no trade agreement has been agreed upon by the EU and the UK. We then analyze the time evolution of production and consumption in the UK, the EU and 240 other countries and regions around the globe during this period. Our simulation results highlight the importance of depicting economic response dynamics to market shocks such as the UK leaving the European single market without trade agreement on the same time scale as these events occur. We find that the value of both, production and consumption is reduced at the end of the simulation period and that this decrease is due to demand-side effects that occur immediately after the end of the transition period if no trade deal is put into place. These drops in demand and the resulting decreases in production and prices have received little attention compared to supply-side effects of Brexit (such as shortages of goods) and could aggravate the overall socioeconomic implications.

Materials and methods

Economic data

For the description of the global trade network, we use multi-regional Input-Output data in basic prices for the year 2012 as provided by the Eora World MRIO simplified dataset (v199.82 [32, 33]). These data describe annual monetary flows between 26 sectors and final demand in 188 countries. We interpret them as a measure of quantitative flows. Assuming that economic output is evenly generated throughout the year, we generate mean daily economic flow data (in USD). Using a disaggregation algorithm [34], we obtain state-level resolution for the USA and province-level resolution for China. Thus, the three biggest economies in the world–EU, China and the USA–are represented in a comparably detailed manner. In addition, we disaggregate the UK into England, Scotland, Wales and Northern Ireland which yields a total of 271 regions across the world (Fig 1 and S1 Table in S1 File). Because small flows are more likely to be subjected to large balancing adjustments in the data generating process [32], flows smaller than 1 Million USD (per year) are neglected in the computation. We thus obtain a globe-spanning network of daily economic flows between heterogeneous economic agents, i.e. regional sectors (firms) and final demand (consumers). This trade network serves as counterfactual in our simulations.

The numerical shock model Acclimate

The simulations are carried out with the numerical agent-based shock model Acclimate [24]. It is an anomaly model evolving around the baseline state of the global trade network as given by the MRIO data. Firms and consumers in this network are modeled as myopic agents with adaptive expectations. Their decision rationales are based on local optimization principles, e.g., firms maximize their expected profit to decide upon their production level and consumers maximize expected consumption to decide upon their purchases.

More specifically, every model time step is divided into three subsequent decisions points or sub-steps [24]. In the first sub-step, firms assess how much they should produce in the current time step to maximize their profits. They take possible constraints into account such as limits of productive capacity or limited input availability. The optimal production quantity is derived by maximizing the difference between revenues and costs. Since we assume a demand-

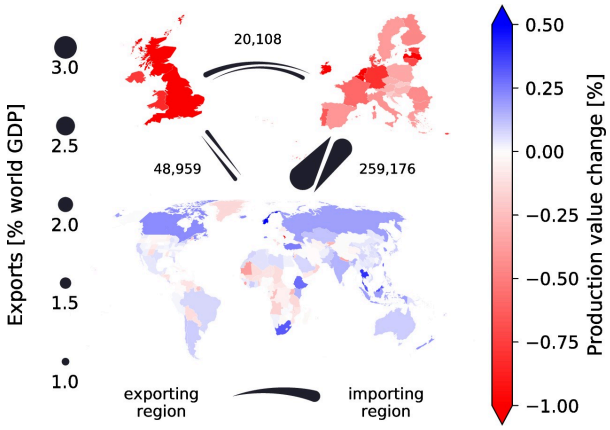

Fig 1. Production value changes after 30 days of a no-trade-deal event and trade relations between the UK, the EU and the rest of the world according to the underlying 2012 multi-regional Input-Output data. Maps show all countries and administrative units covered by our analysis. Thickness of arrows indicates how much is exported from one region to the other. Numbers above arrows state the number of trade connections between these two regions. In our simulations, we assume that trade between the UK and the EU is restricted to a certain percentage of the baseline values throughout the simulation period. Shading of colors is according to production value changes after 30 days of reduced border permeability. Changes shown here refer to a scenario of 70% border permeability. Complementary maps displaying changes in production quantities and prices after 30 days of a no-trade-deal event can be found in the Supplementary Materials (S2 Fig in S1 File).

https://doi.org/10.1371/journal.pone.0237500.g001

driven economy, revenues are known and reflect how much the firm's suppliers requested in the last time step and which prices they are willing to pay (reservation prices). Those suppliers that ordered at the highest unit prices are most likely to receive the full amount of goods they requested. In the second sub-step, firms form expectations for the next time step. Based on the demand requests they received in the last time step they estimate which production quantity might be profit-maximizing in the next time step. They then communicate corresponding offer prices, i.e. prices that customers will likely have to offer in order to receive the same amount of goods as before. This helps customers to correct their prices if they deviated hugely from the overall market situation. In the last sub-step, firms assess how many inputs they will presumably need to keep their production going at the optimal level, taking the amount of stockpiled goods into account. They then decide on the cost-minimizing way of distributing this demand among their suppliers under consideration of the respective offer prices that were just communicated. Similarly to firms, consumers decide upon their optimal consumption level, upon the optimal way of distributing their demand and upon the optimal reservation prices.

The model explicitly accounts for the principal factors determining the short-term flexibilities of production systems [21]: Idle capacities that can be activated in times of high demand, input and transport storages to buffer supply shocks, geographically-derived transport times, and price changes. For the simulations in this paper, sectors' idle capacities are set to 15% of their baseline output, and input storage sizes are set to 15 days of baseline production which means that agents have enough goods stored to uphold their baseline production/consumption quantity levels for 15 days without additional inflow. The model does not consider a restructuring of the global trade network, i.e., agents can only interact along trade relations that are

already established. Furthermore, substitution of input goods is not possible. Acclimate is a deterministic model and also in the simulations we adhere to one set of parameters which do not represent probability distributions. A range of likely outcomes can be examined via variation in the forcing. As detailed below, we here consider four different scenarios of border permeability to span a range of likely outcomes of a no-trade-deal event. Moreover, we conduct two additional analyses, each with a slightly different interpretation of a no-trade-deal event.

As detailed in refs. [24, 35], the Acclimate model differs from related modeling approaches such as Computable General Equilibrium (CGE) or Input-Output (IO) models in three important respects. First, the production system in Acclimate is more flexible than what IO models assume but more rigid than the highly flexible production systems in CGE approaches. Second, IO and CGE models are either static in the sense that they compare two different states or, in the case of dynamic CGEs, have coarse time steps of 5 to 10 years. Acclimate, to the contrary, operates on the timescale of days. Consequently, it can represent disequilibrium situations with local demand-supply mismatches that may occur in the immediate aftermath of an economic shock. Importantly, the agents in Acclimate are myopic and cannot foresee these shocks. This is the third major difference to dynamic CGEs with intertemporal optimization which assume perfect foresight of rational agents.

Modeling of Brexit

We simulate a no-trade-deal event after the transition period by assuming that trade flows between agents in the UK and agents in the 27 remaining EU member states are from one day to the next and for the whole simulation period restricted to a certain percentage of their baseline values. In our main modeling specification, this restriction applies to both, service and commodity sectors but we also provide results for a scenario where solely commodity flows are impacted by the trade restriction (see S2 Table in S1 File for an overview of service and commodity sectors). Furthermore, we conduct an additional analysis where trade flows between the UK and countries with which the EU has trade agreements are restricted as well. For our main modeling specification as well as for each of the two variants, we carry out four simulations with different values of border permeability between 70% and 85% (i.e. 70%, 75%, 80%, and 85%), meaning that only this percentage of the unperturbed trade volume can pass through. We consider different scenarios of trade flow restriction as it is impossible to anticipate the exact difficulties that will arise due to the no-trade-deal situation. Furthermore, we suppose that all economic agents have enough goods stored to uphold their baseline production/consumption quantity levels for 15 days without additional inflow. By embodying enhanced stockpiling of input/consumption goods, we account for some possible preparation measures.

Production and consumption quantity, prices and values

We look at changes in production and consumption quantities, prices and values over a period of 30 days (compared to the baseline state). The baseline production quantity of a firm is derived from the MRIO data by summing over all its outgoing flows. Production "value" denotes the product of the quantity that is produced and the price for which it is sold. Without loss of generality, all prices are assumed to equal one in the baseline state. In the presence of trade distortions, the value of a firms' production may change due to changes in the produced quantity or due to changes in prices. Similarly, consumption "value" denotes the product of the quantity that is actually consumed and its price. A negative consumption value change can hence indicate both, that consumption of goods decreases in terms of quantities (because of supply shortages and/or higher prices), or that goods are purchased at lower prices.

The Acclimate model accounts for one representative consumer in each region. Consumed goods are assumed to be perfect complements and consumption changes isoelastically with the consumer price. For each good, price elasticities are set to -0.5.

Results

For each scenario of reduced border permeability, we assess the short-term economic consequences within the UK, the EU, and the rest of the world by computing the temporal evolution of production and consumption during the first 30 days following a no-trade-deal event. We find that the qualitative results are independent of the specific value of border permeability. The direct economic response in the aftermath of Brexit follows a scenario-independent temporal evolution which strongly supports our confidence in the qualitative insights and in the order of magnitude of the results obtained here. For lower levels of border permeability, daily production seems to "fidget" around a general trend. This is due to the fact that agents have adaptive expectations, i.e. they update their supply and demand decisions at day level under consideration of the gain in information. The magnitude of this fidgeting is more pronounced for scenarios that deviate more strongly from the agents' baseline and it decreases with the aggregation level of the quantities considered (e.g. when aggregating across sectors of a country and/or across countries of a region). In case of consumption, the consumption elasticities smoothen the consumption response curves.

Economic effects in the UK and the EU

Specifically, we find a drop in the number of goods being produced in the UK and the EU immediately after a no-trade-deal event (Fig 2, first row). These short-term production losses cannot be due to supply shortages because at this point in time firms still have enough input goods in storage to keep their production going. They are, by contrast, *demand-side effects*. Firms on both sides of the English Channel have to reduce their production because they receive less demand from their customers on the respective other side of the Channel. These customers have realized that only a certain amount of the products they requested from their British/EU suppliers can pass through the newly established trade border. They hence decided to demand less from their Brexit-affected suppliers and instead refer to their inventories and other suppliers (compare S1 Fig in S1 File, first row). We find particularly high production losses in sectors that used to export a large share of their output to trading partners that are now on the other side of the UK-EU border (Fig 3).

Since, in relative terms, the EU is of higher importance for British exports than the other way around (Fig 1), we find larger production losses for UK sectors than for EU sectors. Ireland on the other hand heavily relies on the UK as sales market for its products and is even more affected than the UK (Fig 4, inlay and S1 Fig in S1 File). Also within the rest of the EU production losses are highest in those countries that previously exported larger shares of their production to the UK such as Belgium or the Netherlands (Fig 4). In response to the decline in demand, firms decide to sell their products at lower prices with the aim of stimulating demand for their products elsewhere (Fig 2, second row, and S1 Fig in S1 File). Consumers in the UK and the EU react to these lower prices by consuming more (Fig 2, third row). However, this increase in domestic consumption cannot offset the decline in demand from customer firms on the respective other side of the EU-UK border. Even though the amount of goods being produced starts recovering, prices do not rise accordingly and the value of production and consumption, i.e. the product of quantities and prices, remains below baseline levels throughout the simulation period. (S1 Fig in S1 File).

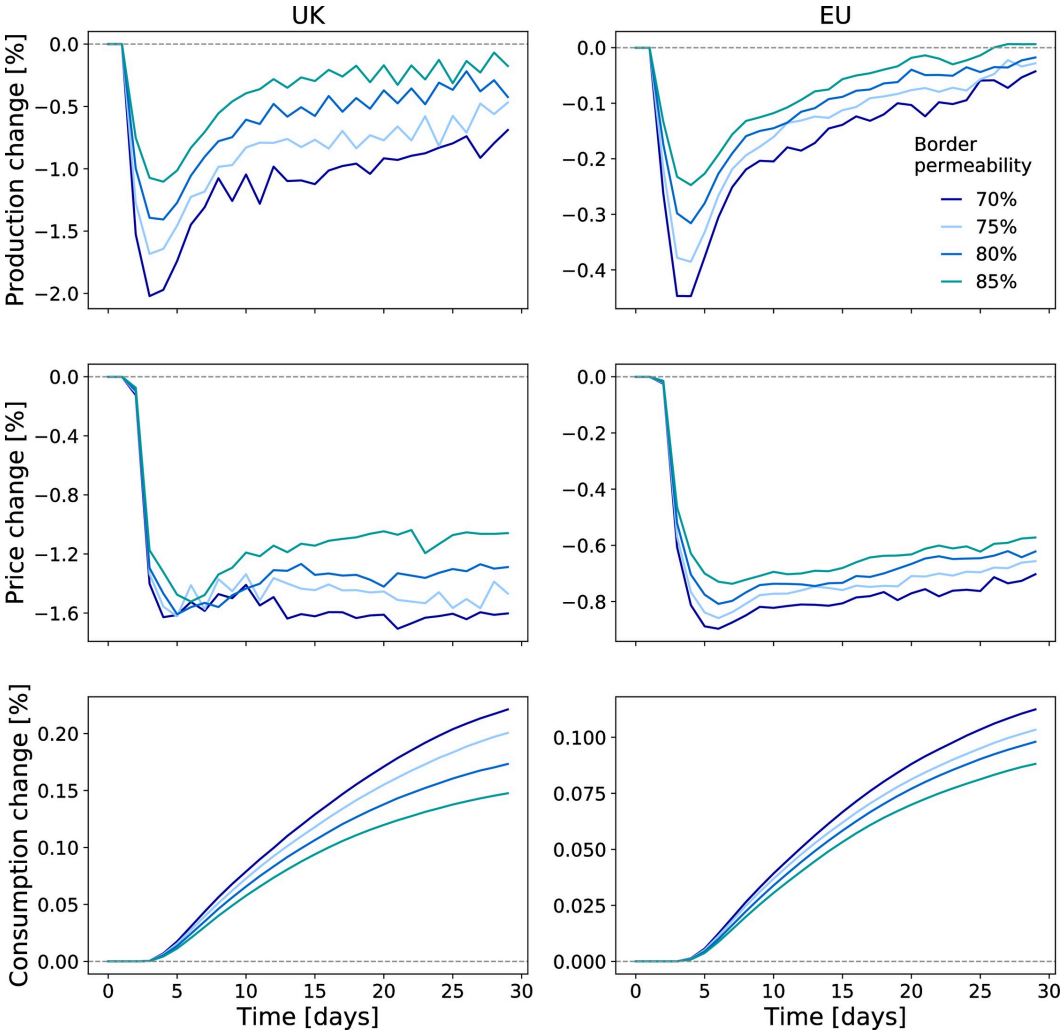

Fig 2. Changes in production, prices and consumption in the UK and the EU during the 30 days following a no-trade-deal event. The number of goods being produced declines in both, the UK and the EU shortly after a no-trade-deal event (first row) because customers on the respective other side of the UK-EU border demand less. Consequently, firms reduce production prices (second row). These lower prices stimulate demand for products slightly. Consumers respond to lower prices; consumption (quantities) rise (third row). In terms of value, i.e. the product of prices and quantities, production and consumption however remain below pre-Brexit levels throughout the simulation period (shown in S1 Fig in S1 File). All changes are depicted as relative deviation from the respective baseline values. Different scenarios of border permeability show similar dynamics. Reduced border permeability is assumed throughout the simulation period.

https://doi.org/10.1371/journal.pone.0237500.g002

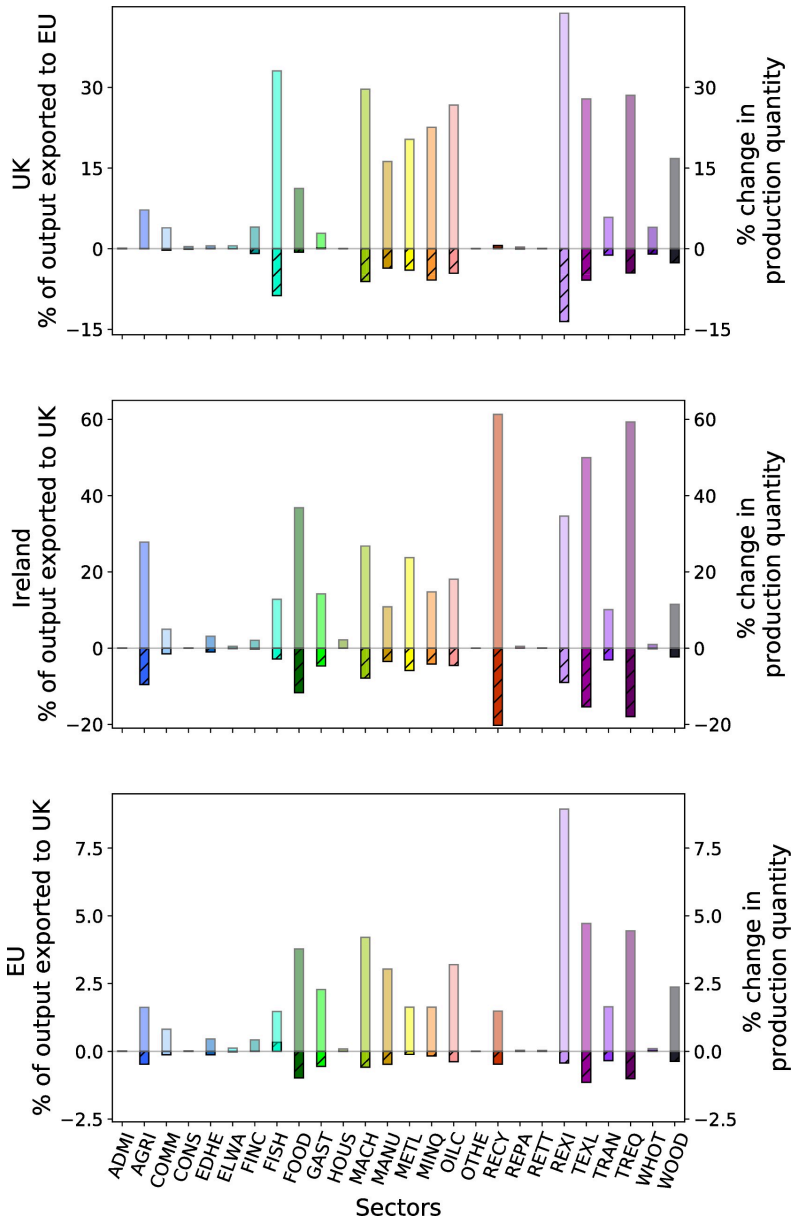
UK
% of output exported to EU
% change in production quantity
Ireland
% of output exported to UK
% change in production quantity
EU
% of output exported to UK
% change in production quantity
ADMI
AGRI
COMM
CONS
EDHE
ELWA
FINC
FISH
FOOD
GAST
HOUS
MACH
MANU
METL
MINQ
OILC
OTHE
RECY
REPA
RETT
REXI
TEXL
TRAN
TREQ
WHOT
WOOD
Sectors

Fig 3. Sectors exporting a large share of their output to customers directly affected by a post-Brexit no-trade-deal event are particularly prone to production losses. Transparently colored bars indicate how much of each sector's output was exported to the UK/EU in the baseline according to the underlying 2012 multi-regional Input-Output data. Hatched bars show production quantity changes after two days of reduced border permeability. Sectors that heavily rely on sales market on the other side of the UK/EU-border experience in general higher production losses. All sector abbreviations are spelled out in S2 Table in S1 File.

https://doi.org/10.1371/journal.pone.0237500.g003

Economic effects on the rest of the world

In our main simulations, we take a conservative approach in assuming that trade flows between the UK and countries with which the EU has trade agreements are not restricted. Countries outside the EU however can be indirectly affected–through up-stream and down-stream ripple effects in the supply chain as well as through the associated price signals. We find that several countries benefit from a no-trade-deal event in the sense that the value of their production increases (Fig 1 and S1 Fig in S1 File). This applies in particular to the non-

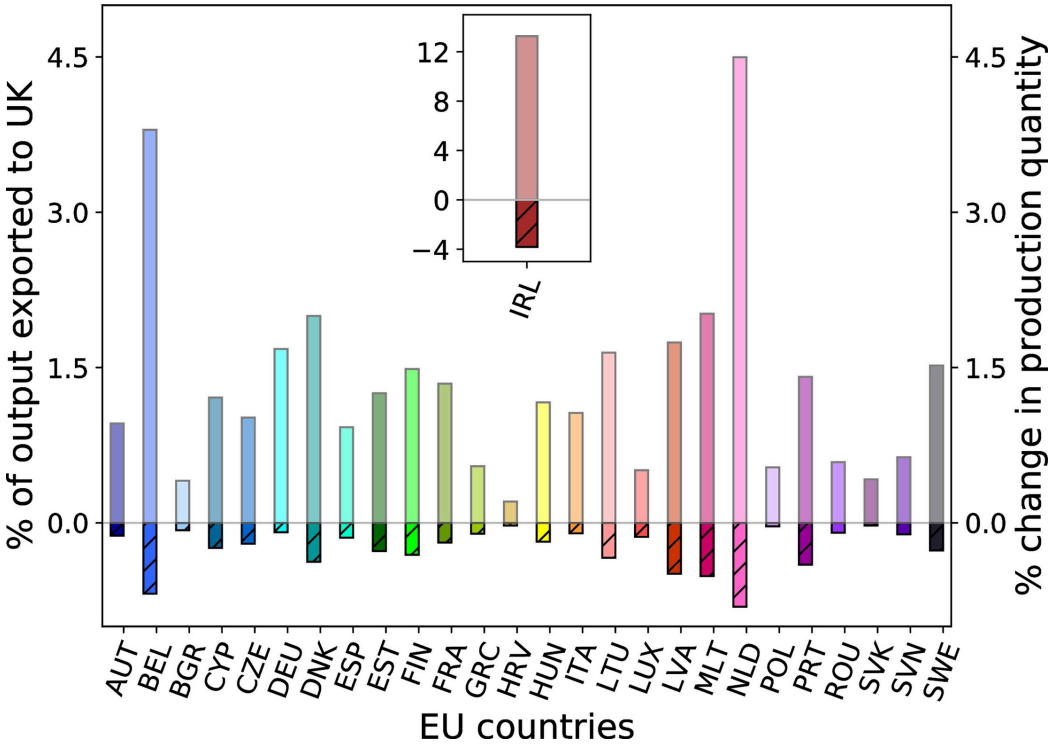

Fig 4. EU countries exporting a large share of their output to the UK experience highest production losses. Transparently colored bars indicate how much of each country's output was exported to the UK/EU in the baseline according to the underlying 2012 multi-regional Input-Output data. Hatched bars show production quantity changes after two days of reduced border permeability. Countries that export larger shares of their output to the UK experience in general higher production losses. Inlay: Close-up for Ireland.

https://doi.org/10.1371/journal.pone.0237500.g004

EU European countries Iceland, Norway and Switzerland as well as to several Commonwealth countries, e.g. Canada, Australia, India and South Africa. These countries are all in a good position to replace Brexit-affected suppliers due to strong existing trade relations. In most of these countries more goods are produced at slightly lower prices (S2 Fig in S1 File). After firms in the UK and the EU have reduced their prices, prices also fall in most of the other countries around the world (S1 Fig in S1 File) with the notable exception, again, of Norway and Switzerland (S2 Fig in S1 File). Conversely, in some countries, for instance in sub-Saharan Africa, the decline in prices is not offset by a respective increase in production quantities or production quantities even decline resulting in reduced production values (compare Fig 1 and S2 Fig in S1 File).

In terms of consumption changes, the amount of goods being consumed increases slightly in most of the countries (Fig 5, panel A). As firms around the world offer their goods at lower prices, people in many countries consume more in quantitative terms (S1 and S3 Figs in S1 File). However, the value of consumption remains below the baseline level in the majority of countries throughout the simulation period (Fig 5, panel B). Among those countries that benefit from a no-trade-deal event in terms of gains in consumption values are again several Commonwealth countries such as Canada or India.

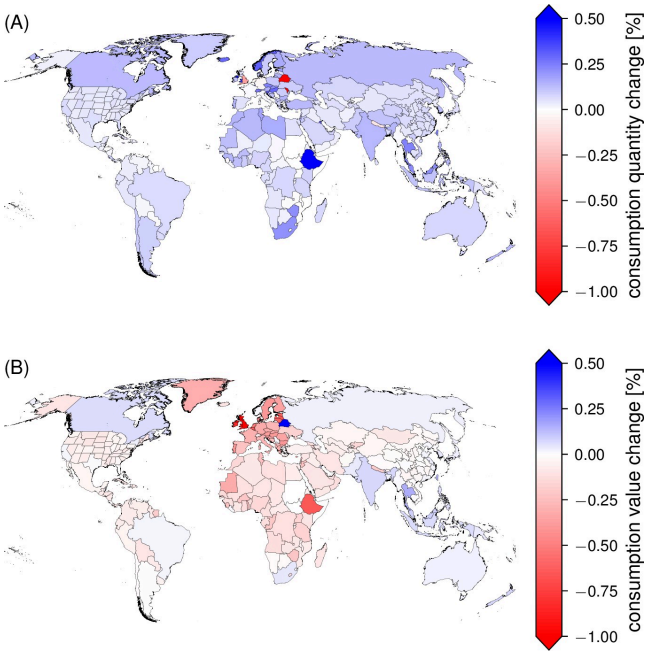

Fig 5. World map of consumption quantity and value changes after 30 days of a no-trade-deal event. Shading of colors is according to consumption quantity (panel A) and consumption value (panel B) changes after 30 days of reduced border permeability. Underlying scenario assumes 70% border permeability. Changes in consumers' prices are shown in S3 Fig in S1 File.

https://doi.org/10.1371/journal.pone.0237500.g005

Results for variants of a no-trade-deal post-Brexit event

In additional analyses, we consider two variants of our main modeling specification. First, we assume that only commodity sectors are affected by the no-trade-deal event as service sectors typically do not have to cross a geographical border. Second, we do not only restrict trade flows between the UK and EU member countries but also between the UK and countries with which the EU currently has trade agreements (see S1 Table in S1 File for a list). We do not include countries where trade agreements are only partly in place according to the European Commission (as to November 2019) such as Canada or Ukraine. In this model set-up, we again restrict trade flows of both, commodity and service sectors. The results for these two additional variants of a no-trade-deal event are qualitatively similar to those of our main modeling specification (S4 and S5 Figs in S1 File). If service sectors are not affected by the trade restriction, we see the most notable difference in simulation results for Ireland where production quantity is reduced less during the first days of trade restriction (S4 Fig in S1 File). Consecutively, production and consumption prices and values decline to a lesser extent as well whereas consumption (quantity) does not increase as much as in the main modeling specification. In the rest of the EU, the decline in consumption prices is also more moderate than in the main modeling specification.

In case the trade restriction also applies to all flows between the UK and countries with which the EU currently holds trade agreements, the effects on the UK are generally stronger (S5 Fig in S1 File). During the first days of trade restriction, production quantity, price and value decrease more than under the main modeling specification. As a consequence, consumption prices and value are more strongly reduced as well whereas consumption quantity increases more. Ireland, to the contrary, is a little less affected in this modeling specification. In the rest of the world, we observe less positive effects than in the main modeling specification. Here, production quantities do not go up as much in response to the trade restriction suggesting that producers in the rest of the world step in less for UK and EU firms. Consequently, prices fall. In the main modeling specification, production value in the rest of the world increases for all scenarios of border permeability. Here, the picture is less clear. On a more disaggregated level, we see that in particular countries with which the EU has trade agreements such as Norway, Switzerland, Iceland, South Africa, or Japan are now negatively affected in terms of production value changes (S6 Fig in S1 File). These countries were among the main beneficiaries in the main modeling specification.

Discussion

The major economic incision that a no-trade-deal event as conceptualized by our simulations presents to the UK and Ireland is likely to impact society profoundly. The short-term adverse effects on production we observe here can have a long-lasting impact on economic growth and development. Even though consumers benefit at first from declining prices, the unsustainable economic situation created by the UK leaving the European single market without a trade agreement is likely to affect them negatively in the long-run, e.g. due to labor market effects. The latter might also deepen intra-regional inequality. In general, an economic recession of this magnitude impedes social, ecological and infrastructural projects and innovation. Our simulations are restricted to a period of 30 days following a no-trade-deal event– a period, in which stockpiling is likely to buffer major supply shortages. These supply shortages might, however, hit the already struggling economy at a later point in time thus aggravating the overall situation.

Our simulations can naturally only depict certain aspects of a post-Brexit no-trade-deal scenario and can hence not provide a quantitatively accurate prediction of its real-world

consequences. For instance, in our modeling framework we assume that trade between Ireland and the EU is not perturbed. In reality, a large amount of the goods traded between these two partners passes through the UK. As a consequence, our simulations might underestimate the effect of a no-trade-deal event on Ireland and some European economies. Furthermore, our simulations are based on MRIO data for the year 2012. Since the structure of the global trade network changes over time [16, 26] with e.g. new trade agreements being negotiated [36], this represents a potential limitation. For example, the EU has established new or reinforced existing trade relations with several countries since 2012 via regional or bilateral trade agreements. Even though we consider these trade agreements in the additional model variant where trade between the UK and EU trade agreement partners is also affected, these agreements are likely not reflected in the structure of the global trade and supply network as given by the 2012 data. As a consequence, the countries in question might be affected to a stronger extent (positively or negatively) by a no-trade-deal event between the UK and the EU than our simulations predict. Yet, MRIO data are published with some time delay and the 2012 Eora data have the advantage of having already been used and tested in published work [37–39].

Finally, given the high level of complexity of modern-day economies with e.g. nested production processes [28], there are many "unknown unknowns" related to a no-trade-deal event that our modeling framework may or may not capture. Using a network approach that explicitly models the sectoral and regional interlinkages in the global trade and supply network allows us to study cascade effects that can be induced by an economic disintegration of the British economy from the EU single market. In particular, our modeling exercise illuminates an aspect of a no-trade-deal post-Brexit scenario that has received little attention so far and that could worsen its expected overall economic and societal implications. That is the shrinking of potential sales market on both sides of the Channel. We find that these short-term demand-side effects decrease the value of production and consumption and are hence likely to have a substantial negative impact on the British, Irish and, to a lesser degree, European economies.

Supporting information

S1 File.
(PDF)

S2 File.
(ZIP)

Acknowledgments

We thank Maximilian Auffhammer for discussions and extremely helpful comments on the manuscript.

Author Contributions

Conceptualization: Leonie Wenz, Anders Levermann.

Formal analysis: Leonie Wenz, Kilian Kuhla.

Methodology: Leonie Wenz, Sven Norman Willner, Christian Otto, Kilian Kuhla.

Software: Sven Norman Willner, Christian Otto.

Visualization: Leonie Wenz, Sven Norman Willner.

Writing – original draft: Leonie Wenz.

References

1. Dhingra S, Machin S, Overman H. Local economic effects of Brexit. Natl Inst Econ Rev. 2017; 242(1): R24—R36.
2. Alex Hunt & Brian Wheeler. Brexit: All you need to know about the UK leaving the EU [Internet]. BBC. 2019. Available from: https://www.bbc.com/news/uk-politics-32810887
3. Gualdi S, Mandel A. On the emergence of scale-free production networks. J Econ Dyn Control. 2016; 73:61–77.
4. Koks EE, Thissen M. A multiregional impact assessment model for disaster analysis. Econ Syst Res. 2016; 28(4):429–49.
5. Hallegatte S. An Adaptive Regional Input-Output Model and its Application to the Assessment of the Economic Cost of Katrina. Risk Anal [Internet]. 2008; 28(3):779–99. Available from: https://doi.org/10.1111/j.1539-6924.2008.01046.x PMID: 18643833
6. Levermann A. Make supply chains climate-smart. Nature. 2014; 504:27–9.
7. Kajitani Y, Tatano H. Applicability of a spatial computable general equilibrium model to assess the short-term economic impact of natural disasters. Econ Syst Res. 2018; 30(3):289–312.
8. Acemoglu D, Carvalho VM, Ozdaglar A, Tahbaz-Salehi A. The Network Origins of Aggregate Fluctuations. Econometrica. 2012; 80(5):1977–2016.
9. Ward PJ, Jongman B, Aerts JCJH, Bates PD, Botzen WJW, DIaz Loaiza A, et al. A global framework for future costs and benefits of river-flood protection in urban areas. Nat Clim Chang. 2017; 7(9):642–6.
10. in den Bäumen H, Moran D, Lenzen M, Cairns I, Steenge A. How severe space weather can disrupt global supply chains. Nat Hazards Earth Syst Sci. 2014; 14(10):2749–59.
11. Steenge AE, Bočkarjova M. Thinking about imbalances in post-catastrophe economies: an input—output based proposition. Econ Syst Res. 2007; 19(2):205–23.
12. Gabaix X. The Granular Origins of Aggregate Fluctuations. Econometrica. 2011; 79:733–72.
13. Carvalho VM, Nirei M, Saito Y. Supply Chain Disruptions: Evidence from the Great East Japan Earthquake. 2014.
14. Inoue H, Todo Y. Propagation of negative shocks across nation-wide firm networks. PLoS One. 2019; 14(3):e0213648. https://doi.org/10.1371/journal.pone.0213648 PMID: 30870470
15. Wiedmann T, Wilting HC, Lenzen M, Lutter S, Palm V. Quo Vadis MRIO? Methodological, data and institutional requirements for multi-region input–output analysis. Ecol Econ [Internet]. 2011; 70 (11):1937–45. Available from: http://linkinghub.elsevier.com/retrieve/pii/S0921800911002606
16. Maluck J, Donner R V. A Network of Networks Perspective on Global Trade. PLoS One. 2015; 10(7): e0133310. https://doi.org/10.1371/journal.pone.0133310 PMID: 26197439
17. Los B, Mccann P, Springford J, Thissen M, Mccann P, Springford J, et al. The mismatch between local voting and the local economic consequences of Brexit The mismatch between local voting and the local economic consequences of Brexit. 2017; 3404.
18. Chen W, Los B, McCann P, Ortega-Argilés R, Thissen M, van Oort F. The continental divide? Economic exposure to Brexit in regions and countries on both sides of The Channel. Pap Reg Sci. 2018; 97(1):25–54.
19. IJtsma P, Levell P, Los B, Timmer MP. The UK's Participation in Global Value Chains and Its Implications for Post-Brexit Trade Policy. Fisc Stud. 2018; 39(4):651–83.
20. Giammetti R, Russo A, Gallegati M. Key sectors in Input-Output Production Networks: an application to Brexit. World Econ. 2019;
21. Hallegatte S. Modeling the Roles of Heterogeneity, Substitution, and Inventories in the Assessment of Natural Disaster Economic Costs. Risk Anal. 2014; 34(1):152–67. https://doi.org/10.1111/risa.12090 PMID: 23834029
22. Brakman S, Garretsen H, Kohl T. Consequences of Brexit and options for a ' Global Britain.' 2018; (October 2017):55–72.
23. Sampson T. Brexit: the economics of international disintegration. J Econ Perspect. 2017; 31(4):163–84.
24. Otto C, Willner SN, Wenz L, Frieler K, Levermann A. Modeling loss-propagation in the global supply network: The dynamic agent-based model acclimate. J Econ Dyn Control [Internet]. 2017; 83:232–69. Available from: http://dx.doi.org/10.2139/ssrn.2888904
25. Rose AZ. Economic Resilience to Disasters. 2009;
26. Wenz L, Levermann A. Enhanced economic connectivity to foster heat-stress-related losses. Sci Adv. 2016; 2(6):e1501026. https://doi.org/10.1126/sciadv.1501026 PMID: 27386555

27. Willner SN, Otto C, Levermann A. Global economic response to river floods. Nat Clim Chang. 2018; 8:594–8.

28. Bardoscia M, Livan G, Marsili M. Statistical mechanics of complex economies. J Stat Mech Theory Exp. 2017; 2017(4):43401.

29. Lenzen M, Kanemoto K, Moran D, Geschke A. Mapping the structure of the world economy. Environ Sci Technol [Internet]. 2012 Aug 7; 46(15):8374–81. Available from: http://www.ncbi.nlm.nih.gov/pubmed/22794089 https://doi.org/10.1021/es300171x PMID: 22794089

30. Lenzen M, Moran D, Kanemoto K, Foran B, Lobefaro L, Geschke A. International trade drives biodiversity threats in developing nations. Nature. 2012; 486.

31. Oita A, Malik A, Kanemoto K, Geschke A, Nishijima S, Lenzen M. Substantial nitrogen pollution embedded in international trade. Nat Geosci. 2016; 9:111–5.

32. Lenzen M, Kanemoto K, Moran D, Geschke A, Kanemot K, Moran D, et al. Mapping the structure of the world economy. Environ Sci Technol. 2012; 46(15):8374–81. https://doi.org/10.1021/es300171x PMID: 22794089

33. Lenzen M, Moran D, Kanemoto K, Geschke A. Building Eora: a global multi-region input–output database at high country and sector resolution. Econ Syst Res. 2013; 25:20–49.

34. Wenz L, Willner SN, Radebach A, Bierkandt R, Steckel JC, Levermann A. Regional and Sectoral Disaggregation of Multi-Regional Input–Output Tables–a Flexible Algorithm. Econ Syst Res. 2015; 27 (2):194–212.

35. Wenz L, Willner SN, Bierkandt R, Levermann A. Acclimate—a model for economic damage propagation. Part II: a dynamic formulation of the backward effects of disaster-induced production failures in the global supply network. Environ Syst Decis [Internet]. 2014; 34(4):525–39. Available from: http://dx.doi.org/10.1007/s10669-014-9521-6

36. Maluck J, Glanemann N, Donner R V. Bilateral trade agreements and the interconnectedness of global trade. Front Phys. 2018; 6:134.

37. Han M, Yao Q, Liu W, Dunford M. Tracking embodied carbon flows in the Belt and Road regions. J Geogr Sci. 2018; 28(9):1263–74.

38. Chandrakumar C, McLaren SJ, Malik A, Ramilan T, Lenzen M. Understanding New Zealand's consumption-based greenhouse gas emissions: an application of multi-regional input-output analysis. Int J Life Cycle Assess. 2019;1–10.

39. Lenzen M, Sun Y-Y, Faturay F, Ting Y-P, Geschke A, Malik A. The carbon footprint of global tourism. Nat Clim Chang. 2018; 8(6):522–8.

Article F

Resilience of international trade to typhoon-related supply disruptions

Authors

Kilian Kuhla, Sven N Willner, Christian Otto, Anders Levermann

Status

Submitted to *Journal of Economic Dynamics and Control*,
preprint: https://ssrn.com/abstract=4014484.

Capsule summary

Several tropical storms pass over maritime East Asian trading routes within the West Pacific typhoon season. In this study, short-term transport perturbation in those maritime routes is modeled using observed typhoon tracks from 2000 to 2020. To analyze the trading network response, the agent-based model *Acclimate* is extended by a geographical transportation route system. The short-term constriction of multiple network connections leads to local oversupply and demand shifts. Shifted demand and supply cause an increase in network activity between and after interruptions; as a result, annual exports increase in most regions due to transport disturbances. Results reveal that this trade resilience increases with node inter-connectivity.

Author contributions

Kilian Kuhla developed and implemented the transport module of *Acclimate*. Kilian Kuhla created and implemented the typhoon-induced transport perturbation function. Kilian Kuhla discussed the methodology with Sven N Willner. Kilian Kuhla analyzed the results and discussed them with Sven N Willner and Anders Levermann. Kilian Kuhla made the visualization. Kilian Kuhla wrote the manuscript with contributions from all other authors.

Resilience of international trade to typhoon-related supply disruptions

Kilian Kuhla[a,b], Sven N Willner[a], Christian Otto[a], Anders Levermann[a,b,c]

[a] *Potsdam Institute for Climate Impact Research, Potsdam, Germany*
[b] *Institute of Physics, Potsdam University, Potsdam, Germany*
[c] *Columbia University New York, New York, USA*

Abstract

Shipping accidents and environmental disasters pose a challenge to the reliability of maritime supply chains. With international trade intensifying without a significant diversification of the supply routes the risk of perturbations is likely to increase, because higher atmospheric carbon dioxide provides more energy to tropical cyclones which tends to make them more destructive. In this study we analyze the regional and global economic repercussions of short-term transport disruptions of West Pacific trading routes during typhoon seasons. Using a numerical agent-based shock model with myopic local optimization, we compute the response of more than 7,000 regional economic sectors with more than 1.8 million trade- and supply relations. Disturbances due to typhoons observed between 2000–2020 are found to have caused local oversupply and scarcity situations as well as the associated regional price changes. In our model economic agents respond to these price signals and temporary supply bottlenecks by rescheduling and increasing their demand. As a consequence we find annual average export volume to increase in all trade blocs due to a decrease of export prices, but substantial regional differences emerge. Resilience of export to typhoon induced perturbations is increased in China, ASEAN, East Asia, and Europe. We trace this back to an increase of the inter-connectivity of these trade blocs to their foreign trade partners.

Keywords: agent-based modeling, trade modeling, transport disruptions, trade resilience

1. Introduction

Since the end of World War II, international trade has grown immensely [1] and even the COVID-19 pandemic has only shortly interrupted this trend [2]. With the increase of global exports to production, the exposition of the global economy to supply chain risks has increased. To date, up to 90% of the national exposition to insecurities in water, energy, and land resources derive from international trade [3].

Over 80% of the world trade volume is transported on sea [4], rendering disruptions of maritime trade routes a substantial threat to global supply chain security. This was impressively demonstrated by the blockage of the Suez-Canal by the container vessel "Evergreen" in Spring 2021. This resulted in substantial delivery delays and associated production shortfalls, especially in Europe and Asia [5]. Besides straits and canals [6], ports are major bottlenecks of the maritime trade network [7]. In addition to socioeconomic factors such as accidents [8] or congestion during loading and unloading [9, 10], storm surge and strong winds from extreme weather is one of the main source of transport delays through ports [11].

The increase in the concentration of carbon dioxide in the atmosphere is increasing the energy that is accumulating in the ocean [12, 13]. The emergence of tropical cyclones such as hurricanes and typhoons follows a complicated mechanism that is subject to energy constraints and shear wind strength. The amount of energy that is accumulating within a tropical cyclone that has already developed is physically constraint by the amount of energy available in the upper ocean layers. Thus under future warming the number of tropical cyclones as a whole is difficult to predict, but it is clear that the number of strong typhoons and hurricanes will statistically increase under future warming [14, 15, 16]. This combination of intensifying trade volume and increased risk of perturbations by typhoons motivates an investigation of the economic responses of these transportation interruptions.

Linking major Asian exporters such as China and Japan to their European

and American trade partners, the West Pacific basin is of predominant importance for international maritime shipping. For instance, the maritime trade of the world's largest (national) exporter [17] — China — relies exclusively on West Pacific shipping routes through the South China and East China Sea. During June and December, maritime transport in the region is put at risk by typhoons. Strong winds, high swells, and poor visibility of these events can cause transport delays due to port closures and re-direction of transport vessels [18, 19].

In this study we extend the agent-based global supply chain model Acclimate[20] by a global network of maritime trade routes. We employ the model to study the economic repercussions of transport disruptions of recurrent typhoons. Immediate responses of trading partners to transportation perturbations caused by typhoons are referred to as direct impacts. Further, we compute and analyze *indirect* or *higher-order* impacts, which arise due to economic ripple propagation along supply chains, e.g, through price fluctuation or demand shifts.

Including the shocks by the typhoons of 2000–2015 in the model, we find average export volumes to increase in all major trade blocs due to a decrease of export prices. However, substantial regional differences occur. In all but one trade blocs the decrease in export prices is overcompensated by the increase in export volume resulting in an increase of the value of exported goods; in China as the most strongly affected trade bloc a moderate increase in export volume is overcompensated by the decline in export prices. We also study how the topography of the underlying trade network affects the resilience of international trade to typhoon strikes. Using exports as a measure for international trade, we find that that its resilience to typhoon strikes has increased over the period 2000–2015 especially in China, ASEAN, East Asia, and Europe. We explain these gains in resilience by an increase of the inter-connectivity of these trade bloks to foreign trade partners within the study period.

This paper is organized as follows. We first review the related literature in Sec. 2, before presenting our modeling approach in Sec. 3. In Sec. 4 we present our modeling and before discussing them in Sec. 5.

2. Related literature

2.1. Supply chain risks

The modeling of supply chains is typically carried out on either on the macroeconomic level, i.e. nations and their bilateral trade relations, or on a microeconomic level, i.e. regional firms or the multinational corporations and their networks (cf. Johnson [21] for a comprehensive review). Here, we focus on the macro level, where two modeling frameworks are well established: input-output (I-O) models and computable general equilibrium (CGE) models (see van der Veen [22] and Okuyama et al. [23] for a comprehensive introduction). Both approaches can reflect the economic dependencies in high detail [24]. However, when it comes to describing and temporally resolving the indirect economic effects of disasters due to the cascading of losses along supply chains — the main focus of this paper — both approaches, I-O and CGE, may not be able to realistically describe the economic responses in the period of days to months following a disaster [25, 26, 27]. Whereas the production system in I-O models is fixed, rendering short-term adaptation impossible [28], that of CGEs is highly adaptive and flexible due to price responsiveness and a high degree of substitutability among commodities. CGEs are calibrated such that supply and demand elasticities as well as the elasticities of substitution are suitable to describe an economy in long-term equilibrium. Consequently, in contrast to I-O models that tend to overestimate losses, CGEs are prone to mitigate losses unrealistically well [25].

Attempts to represent a system's complex dynamics from the bottom up are undertaken by use of agent-based models (ABMs), e.g., [29, 30]. Here, the stylized facts of macroeconomic systems emerge from the interplay of individual heterogeneous agents [31, 32]. This may in particular include non-equilibrium dynamics. For instance, micro-economically founded agent-based growth models have been shown to reproduce exponential growth [33, 34] and myopic decision rationals have been shown to induce far-sighted inter-temporal optimization [35]. In recent years, ABMs have been frequently applied to study the implications of

specific policies [36]. Further, similar to static methods, a focus has been put on systemic risk by studying bankrupt avalanches and their dependence on network topology [37, 38, 39, 40, 41]. However, ABMs still struggle to gain broader recognition from the mainstream neoclassical economic community [42]. Regarding the analysis of production loss cascades along supply-chains, ABM approaches appear promising. With their help, loss-propagation can be very naturally discussed in a setting where the economy is described by heterogeneous interacting agents yielding a production system with well tuneable flexibilities [43]. For example, Gualdi et al. [44] presented an ABM of an evolutionary network of monopolistically competitive firms, which is able to reproduce important stylized facts of real-world firm networks. They can allocate the scale-free topology of firm networks to the competition among the firms. Further, as in the static theory [45], their model permits to ascribe aggregate volatility to the fat-tailed distribution of firm sizes.

A foray in the description of disaster-induced losses in supply networks was undertaken by Hallegatte [25] with the introduction of an agent-based dynamic model, the ARIO model. A more recent version of the model accounts for inventories acting as buffer-stock, which are essential for the assessment of indirect losses in the disaster aftermath [46]. This model has been successfully employed in several empirical disaster impact studies such as Hallegatte [47], Ranger et al. [48], and Hallegatte et al. [49]. Further, Henriet et al. [50] extended the model to study how the robustness of a firm network to micro-shocks depends on the structure of the network as well as the heterogeneity of direct losses. Moreover, the authors provided an algorithm to disaggregate I-O tables such that a firm network with realistic size distribution is obtained.

In the most recent model generation, Otto et al. [20] implemented endogenous price dynamics between the economic agents. Thereby, the relevance of inventories and idle capacities as adaptation measures to repercussions in the economic network was elaborated. Using the *Acclimate* model, Willner et al. [51] examined direct and higher-order impacts of river floods. The study reveals that China suffer by far the highest direct flood-induced production losses, which

increase even further under near-future warming projections. Additionally it highlights that the USA exhibit significantly high indirect losses compared to their direct impact of river floods. Besides effects on regional and global production, Kuhla et al. [52] computed the resulting impact on consumption regarding productivity reduction caused by heat stress. Within the first four decades of the century, the direct production losses are projected to increase by 47% while losses for consumers double. A qualitative analysis on the repercussion of hurricane Sandy revealed that local disaster impact propagates as ripples with three phases through supply chains [53]. Further results of the study suggest that regional higher-order economic impacts increase with higher inter-connectivity to disaster area.

The ABM and explicit non-equilibrium dynamics approach of the model further allowed to assess the economic repercussions of several events and how they interact. Here, Kuhla et al. [54] showed that the interaction of indirect economic effects of heat stress, flooding, and tropical cyclone events can lead to an economic ripple resonance intensifying regional and globel consumption losses . While climate-related direct losses rise, e.g. under global warming, additional consumer losses amplify disproportional, which stresses the importance of in more-depth assessment of consecutive disaster and global adaptation measures.

Risk for supply chains may arise from internal or external factors [55, 56] or from operational disruptions [57, 58]. Furthermore, managing decisions of firms like just-in-time-policy or lean production may increase risk for stable supply chains [59]. On the demand side, uncertainties and unforeseen changes of demand are additional potential supply chain risks [60]. Regarding a firm's bankruptcy and resulting supply chain effects, the analysis of Yang et al. [61] depicted that competitors could be put under higher pressure and affected suppliers could even partly benefit. Also, Giannakis et al. [62] identified and evaluated 30 sustainability-related risks, where greenhouse gases and natural disasters score highest. Next to firm-related supply chain risks, trading effects, like currency fluctuations or restriction of information, can affect demand and supply [63]. In order to mitigate trade disturbances due to (short-term) ex-

change rate fluctuations Günay et al. [64] developed a stochastic optimization model. With this, they find nation-depending fluctuation range thresholds for product architecture selection. Durowoju et al. [65] used entropy theory to depict that disrupted information flow puts more pressure on managing inventories, which drives cost on producer side and may lead to interruption in the supply chain. Regarding evaluation of manufacturing and supply information, the review work of Ivanov et al. [66] suggests that digitalization and big data analyses pose promising technologies helping to reduce ripple effects along supply chains.

Additional to business and trading supply risks, problems in transport pose substantial risks on the logistics side of supply chains. Here, Morris et al. [67] found that the last part of a transport supply chain — the delivery to the costumer — is often impeded by congestion, theft, and availability of fast parking facilities. Tatikonda et al. [68] found that supply via road comes with risks of truck accidents and that improved working conditions, e.g. team-based drivers, could reduce such risks and improve drivers health. The transition from transport via road to sea and vice versa can further be delayed by port strikes, which lead to additional transport costs and congestions along the whole supply chain [69]. Similar, quitting ship crew members stresses supply chains, which emphasizes the necessity of better working conditions for employees as shown by Jiang et al. [70]. For goods transported via sea, potential pirate attacks can increase transport costs and stress the affected supply chains as Martínez et al. [6] depicted.

2.2. Maritime transport at risk due to climatic conditions

Climatic extremes, like heavy winds or rainfall caused by storms, delay transportation via sea [71]. For ports, and thus overall maritime trade, the most frequent natural threats are posed by tropical storms [72]. Using a dynamic I-O model, Thekdi et al. [73] depicted that a hurricane reduces shipping activities which again cause economic losses in transportation and fossil fuel sectors. Cao et al. [74] estimated that the worst-case economic losses at a port due to a single

typhoon can add up to roughly USD0.9 bn. Examining the impact of tropical cyclones further, Zhang et al. [75] found that four major Chinese ports exhibit on average 0.9–2.6 disruption days per year in the most typhoon-prone months. Further, their computations stressed the importance to include disruption time and port throughput within the economic loss assessment.

Being aware of such disruptive maritime events, frameworks for optimally rescheduling liner shipping are developed, e.g. by Brouer et al. [76] or Li et al. [77]. These aim to adapt transportation plans and to reduce resulting costs. Negative impacts on maritime transport will continue and even intensify. This increases the necessity of deep adaptation as Monios et al. [78] elaborated. Likewise, Lam et al. [79] concluded that there are still some research gaps to be filled regarding disruptions in maritime transport and their consequences.

2.3. Global trade — risks and resilience

Global supply chains experience operational, logistic, and physical threats, which puts global trade at a whole at risk. Despite these risks, international trade has grown faster than national GDPs in the last 60 years [80] and up to 80% of this trade is shipped via sea [4]. Inter-connectivity of global trade, measured in different metrics like supply propagation connectivity [81] or link density [82], has increased since the beginning of the century. Next to discussions about benefits and harms of global trade [83, 84, 85], there is an ongoing scientific debate about the adaptation and resilience capacity of the highly-interconnected global trade network toward larger shocks. In general, work from Fyodorov et al. [86] suggests that a coupled system of nonlinear ordinary differential equations increases stability with complexity, which could be applied to trade networks. Further, the information theory-based network flow analyses of Kharrazi et al. depicted that more interconnected global trade has become more resilient towards economic shock despite lowering overall efficiency [87].

Contrary to that, findings of Kummu et al. [88] suggest that resilience towards trade risk has decreased over the last three decades. In particular, they analyzed multiple indicators of international food system resilience and found

that regional food import dependency mostly increase while number of trading decreases. Wenz et al. [81] found that higher inter-connectivity of international trade network increase vulnerability towards climate extremes. Similar, Moran et al. [89] evaluated, using random matrix theory, that a complex system of firms decreases its stability with increasing size in term of number of firms or connectivity.

3. Modeling approach

3.1. Loss-propagation model Acclimate

In this study, we compute direct and higher-order economic impacts due to typhoon-induced transport delays using the agent-based loss-propagation model Acclimate. This model consists of around $7,000$ economic agents, firms and consumers, who maximize myopically and locally their profit or consumption, respectively. Flows of goods and services — between 27 economic sectors of 268 regions (186 nations as well as 51 US-states and 31 Chinese provinces) — connect these agents, which form a network of around 1.8 million linkages. The sectors and regions used in our simulation are listed in Table S1 and Table S2, respectively. The 26 consumption commodities are not substitutable. The model has endogenous price dynamics and explicitly distinguishes between quantity, price, and value of goods and services. Due to exogenous (direct impacts) and endogenous (indirect impacts) production, trading and transport anomalies, the model computes daily economic repercussions, which are deviations from the baseline state. As an economic baseline we use the static multi-regional input-output data from the Eora database [90] of the year 2015. Further model assumptions and local economic mechanisms are described in detail by Otto et al. [20].

3.2. Product transport in Acclimate

In this section we describe the transport of commodities and products in Acclimate. In the following, we will only to transportation between firms as it is the same for a firm and a consumer. Every firm, or "regional sector", ir is

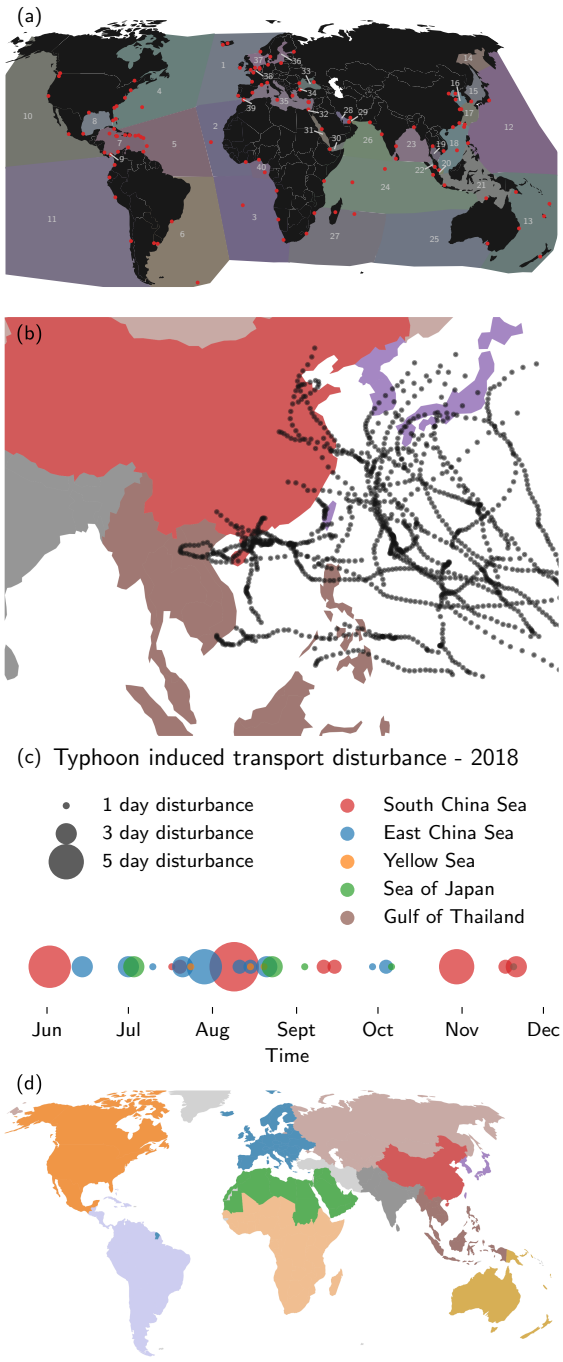

Figure 1: **West Pacific typhoon seasons affects East Asian maritime routes**

(a) Modeled maritime entities (colored areas on water) which form the maritime trading network are connected to land routes via the ports (red dots). Names of maritime trading routes are listed in Table 2.

(b) Zoom into West Pacific regions. Black dotted lines depict trajectory of tropical storms (wind speed $\geq$ 22 kn) in the period 2000–2021.

(c) Scheme of typhoon-induced transport disturbances in South China Sea (red), East China Sea (blue), Yellow Sea (orange), Sea of Japan (green), and Gulf of Thailand (brown) for the season 2018. Diameters of circles proportional to the number of days of disturbance.

(d) Blocs used for analyses in this paper: China (red), Europe (blue), NAFTA (orange), ASEAN (brown), Latin America (light purple), SAARC (grey), East Asia (purple), Arab League (green), Post-Soviet states (light brown), Australia & Oceania (ochre), Sub-Saharan Africa (light orange), and Rest of the World (light grey).

described by its economic sector i, in which it produces, and by the region r in which it is located. The economic linkage between firm ir (supplier) and firm

js (purchaser) is referred to as business connection. The economic network — the set of all business connections — lies on a geographical transport network, which is described in detail below.

A business connection consists of one or more transport chain links. In every time step t the product flow $Z^{(t)}_{ir\to js}$ between ir and js is transferred from one transport chain link to the next. Thus, the number of transport chain links of a business connection equals the transport time τ_{rs} between regions r and s measured in time steps. Service or non-service economic sectors (Table S1) transfer their products between supplier ir and purchaser js differently. On the one hand, economic products, which are assigned to the service sector, are not physical commodities and are delivered between firms within the next time step, e.g., Financial Intermediation & Business Activities. On the other hand, non-service products are delivered between supplier ir and purchaser js with a finite transport time along a business connection.

In the former version of Acclimate, the length and transport time of a non-service business connection was defined by the distance Δ^c_{rs} between the centroids c_r and c_s of region r and s, respectively. Using the exogenous delivery velocity v^c and the distance Δ^c_{rs} between the regions, each business connection had a fixed transport time τ_{rs} measured in time steps.

Here, we extend Acclimate with the geographical transportation network. Each business connection between non-service supplier ir and purchaser js has a transportation route $\mathcal{T}_{ir\to js}$, which may include transportation via land, sea, or aviation. Each business connection with its transport chain links lies on a particular transportation route. This means that the length of the transport, and thus the number of transport chain links, is based on the transportation route. With this, an economic linkage is bound to the physical trading route it uses. How a transportation route is set up depends on whether the commodity is an aviation-good or non-aviation-good. In the former, the transport route consists of the centroids of the respective regions r and s. Their distance Δ^c_{rs} is passed by aviation speed v^a. The transport by aviation can be compared with the previous transport modeling only at higher speed. Since our sectoral reso-

lution is rather coarse and up to 90% of the merchandise goods are transported by ship, there are no products transported by aviation in this study.

Transportation routes of non-aviation goods are based on a geographical entity network, which consists of land entities, maritime entities, and ports. The former comprise the model regions and are spatially depicted via regions' centroids c_r. Each land entity has a connection to their adjacent land entity. Transport between neighboring regions progresses at land velocity v^l and takes transport time $\tau_{rs} = \frac{\Delta^c_{rs}}{v^l}$, where Δ^c_{rs} is the distance between centroids of r and s. If regions r and w are not directly connected but both are adjacent to region s, the transportation route is $r \rightarrow s \rightarrow w$. For this, the distance (transport time) between r and w is the sum of the distances (transport times) between r and s, and s and w: $\Delta^c_{rw} = \Delta^c_{rs} + \Delta^c_{sw}$ ($\tau_{rw} = \tau_{rs} + \tau_{sw}$). As long as there is a contiguous chain of land entities between a region r and w, there can be a transportation route via land between those regions (even if there is more than one region between them). The total distance and transport time is calculated from the sum of the distances and transport times of the connected sub chain links, as in the example above. If a set of transport routes $\{\mathcal{T}_{irjs}\}$ is possible between firm ir and js , the one with the shortest distance is used for the transportation route via land. For example, the transportation route between a firm in Denmark and Italy consists of the land entities Denmark, Germany, Austria and Italy and not Denmark, Germany, France and Italy, even if this connection would be possible. Since continents are not connected to each other, there is no transportation route for each pair of regions that uses only land entities. For this we explicitly model sea routes using maritime entities.

For the maritime entities we split the relevant navigable seas into single areas with unique centroids[1] (Fig. 1a). Each maritime entity α is connected to their adjacent maritime entities $\{\beta\}$. The transport between them via sea has a velocity of v^s and takes transport time $\tau_{\alpha\beta} = \frac{\Delta^c_{\alpha\beta}}{v^s}$, where $\Delta^c_{\alpha\beta}$ is the distance between the centroids of α and β. Analog to land entities, maritime entities

[1]The centroids of the maritime entities are listed in 10.5281/zenodo.5807332

that are not directly connected are connected via neighbor or next-neighbor (or next-next-neighbor and so on). As well as for land entities, distance or transport time between those not-directly connected entities aggregate the distance or transport time of the connected sub chain links between them. Likewise, if there are multiple options, the shortest transportation via sea route is chosen.

Land and maritime entities are not directly connected. Rather, a land entity and a maritime entity can both have a connection to a port h (Fig. 1a). Ports are characteristic geographic points and therefore have a longitude and latitude coordinate. At the port as the common 'interface' between land and sea entity, transport on land (sea) changes to transport by sea (land) and thus the velocity changes to v^s (v^l). The turnaround time at a port can be set exogenously and is fixed at one time step in this study ($\tau_h = 1$). If the transportation route $\mathcal{T}_{ir\to js}$ of firms ir and js consist of land and maritime entity, the total distance Δ^c_{rs} can be calculated by

$$\Delta^c_{rs} = \sum_{\{ww'\}} \Delta^c_{ww'} + \sum_{\{\alpha\alpha'\}} \Delta^c_{\alpha\alpha'} + \sum_{\{wh\}} \Delta^c_{wh} + \sum_{\{\alpha h\}} \Delta^c_{\alpha h}, \tag{1}$$

where ww', $\alpha\alpha'$, wh, and αh are the set of connected and used land–land connections, sea–sea connections, land–port connections and sea–port connections, respectively. Analogously, the total transport time adds up to

$$\tau_{rs} = \sum_{\{ww'\}} \frac{\Delta^c_{ww'}}{v^l} + \sum_{\{\alpha\alpha'\}} \frac{\Delta^c_{\alpha\alpha'}}{v^s} + \sum_{\{wh\}} \frac{\Delta^c_{wh}}{v^l} + \sum_{\{\alpha h\}} \frac{\Delta^c_{\alpha h}}{v^s} + \sum_{\{h\}} \tau_h, \tag{2}$$

where $\{h\}$ is the set of used ports of transportation route $\mathcal{T}_{ir\to js}$.

By using [91] and [92], we state that the price of one ton transported for one mile (a ton mile) on land is 3.7 times more expensive than transporting one ton-mile via sea. So the relative price per ton mile via sea is $p^s = 1$ and via land $p^l = 3.7$. Using this, we can calculate the cost of a transport route. The relative costs $\mathcal{C}_{rs}$ of transportation route $\mathcal{T}_{ir\to js}$ are

$$\mathcal{C}_{rs} = \sum_{\{ww'\}} \Delta^c_{ww'} p^l + \sum_{\{\alpha\alpha'\}} \Delta^c_{\alpha\alpha'} p^s + \sum_{\{wh\}} \Delta^c_{wh} p^l + \sum_{\{\alpha h\}} \Delta^c_{\alpha h} p^s, \tag{3}$$

where the set notation are the same as in eq. (1). If a set of transport routes $\{\mathcal{T}_{irjs}\}$ is possible between firm ir and js , the one with the *lowest* transportation

costs is used for the transportation route. Using this decision rationale, there is a unique transportation route that is autonomously chosen by the economic agents and that closely replicates real-world trade routes. Transportation routes using maritime entities can be longer but still are more cost efficient, i.e. cheaper.

For example, a commodity from Germany to Beijing is transported as follows. From Germany (centroid) via land to the Port of Hamburg and shipped via North Sea, English Channel, Northern Atlantic Ocean North East, Strait of Gibraltar, Mediterranean Sea, Suez Canal, Red Sea, Gulf of Aden, Arabian Sea, Bay of Bengal, Strait of Malacca, Strait of Singapore, South China Sea, East China Sea, Yellow Sea to the Port of Tianjin. The final path to Beijing is then covered by road again. In our transport network we implement the 188 most important continental ports and islands (Table S3). Important to note is, the transportation prices on land or sea, and the relative transportation costs have no relevance to the further economic analysis and are only used for the model-internal decision firms for the transportation route.

As we mentioned above, the business connection of firm ir and js is "embedded" in the transportation route of those firms. This means, the number of transport chain links per business connection equals the total transportation time (measured in time steps) of the transportation route. More precisely, the transport chain links are divided among the individual sub-paths. A sub-path, distance between two entities or an entity and a port, or a port turnaround, has as many transport chain links as it takes transport time to complete this sub-path. Newly introduced parameters (compared to Otto et al. [20]) are listed in Table 1.

3.3. Transport perturbations

We assume that the transportation route between two agents is fixed and cannot be changed within the short time scales of the model. Each geographic entity e — land entity, maritime entity or port — has a passage flow $\chi_e(t)$, which determines how much of the baseline flow can pass through this entity per time step. The size of the baseline flow $Z^*_{ir\to js}$ depends on the specific firms

Name	Symbol	Value	Unit
Time step	Δt	1	day
Land velocity	v^l	70	$\mathrm{km \cdot h^{-1}}$
Sea velocity	v^s	40	$\mathrm{km \cdot h^{-1}}$
Port delay	τ_h	1	day
Relative sea transport price	p^s	1	–
Relative land transport price	p^l	3.7	–

Table 1: **Transportation parameter**
A list of the transportation parameter of the Acclimate extension transport module.

ir and js . We assume that without perturbation a theoretically infinite volume of goods can flow through the land entities, maritime entities, or ports. The volume of flow of goods in a certain route segment can be exogenously disturbed. If an entity is disturbed, the flow of goods can be impeded by a factor $[0, 1]$. This means for entity e:

$$\chi_e(t) = \begin{cases} \infty & \text{, if no perturbation} \\ [0,1] & \text{, if perturbation} \end{cases} .$$

Each business connection between firms ir and js determines for each time step t the minimum passage flow $m_{ir\to js}(t)$ of all its associated geographic entities $\{e'\}$: $m_{ir\to js}(t) = \min \chi_e(t)|_{e\in\{e'\}}$. If the minimum passage flow is below 1 ($m_{ir\to js}(t) < 1$) it has two consequences for the business connection of firms ir and js .

First, in such a situation the flow of goods $(1-m_{ir\to js}(t))Z^*_{ir\to js}$ $(\equiv \mathcal{B}_e(t))$ is blocked at entity e. This blocked flow ($\mathcal{B}_e(t)$ accumulates over time

$$\mathcal{B}_e(t) = (1 - m_{ir\to js}(t_1))Z^*_{ir\to js} + (1 - m_{ir\to js}(t_2))Z^*_{ir\to js} + \cdots ,$$

as long as $m_{ir\to js}(t) < 1$. If the blockage is lifted and $m_{ir\to js}(t) > 1$, the blocked flow is released with $\mathcal{B}_e(t+1) = \mathcal{B}_e(t) - (m_{ir\to js}(t) - 1)Z^*_{ir\to js}$ per time step (until it is zero) and is transported further along the business connections. If $m_{ir\to js}(t) = \infty$, the blocked flow passes entirely through the entity e in one time step.

Second, as long as the minimum passage flow is below 1 ($m_{ir\to js}(t)< 1$), the purchaser js will reduce its demand $D_{ir\to js}(t)$ to ir by

$$D_{ir\to js}(t) = m_{ir\to js}(t)D^*_{ir\to js}, \quad \text{if } m_{ir\to js}(t) < 1. \tag{4}$$

Firm js does not have the foresight how long the disturbance will occur and thus reduces its demand to supplier with a perturbed business connection. On the one hand, supplier ir receives a lower demand if there is no compensating increased demand from other purchasers $\{j's'\}$. It has overproduced goods, which results in lower production and offering prices. On the other hand, to fulfill its demand (in order to produce the inquired products of other firms or consumers), firm js will distribute remaining demand $(1-m_{ir\to js}(t))D^*_{ir\to js}$ on its other supplier $\{i'r'\}$. Thus some suppliers $\{i'r'\}$ receive increased demand, which causes production and prices to rise. However, depending on their ability to do so, js's demand may not be entirely fulfilled.

Important to note is that the delayed commodities are not destroyed and their delivering continues after the local blockage ceases. Nevertheless, reacting to shifted demand, the economic agents change demand, production, prices, and supply, which causes repercussions within the economic network. Even if there is no (direct) production failures of firms (as it has been studied in [20, 51, 52, 53, 54]) the perturbations propagate through the supply chains.

3.4. Typhoon impact on transmissibility of sea routes

We focus on transport perturbation of the most affected maritime routes: South China Sea, East China Sea, Yellow Sea, Sea of Japan, and Gulf of Thailand. Tropical cyclones during a West Pacific typhoon season may restrict the navigability of these sea routes. Therefore, we assume that for the duration of a storm with more than 22 kn over those shipping routes, the flow of goods is constrained to 25% compared to baseline flow. The results in this study (in Section 4) are robust against these parameter choices as we depict in our sensitivity analysis in Section 4.6. Non-passed goods can be transported further via this sea route once the storm has passed or its wind speed is below the threshold of

	Sea entity		Sea entity
1	Northern Atlantic North East	21	Tiger Cub Sea
2	Northern Atlantic South East	22	Strait of Malacca
3	Southern Atlantic East	23	Bay of Bengal
4	Northern Atlantic North West	24	Indian Ocean North
5	Northern Atlantic South West	25	Indian Ocean South East
6	Southern Atlantic West	26	Arabian Sea
7	Caribbean Sea	27	Indian Ocean South West
8	Gulf of Mexico	28	Persian Gulf
9	Panama Canal	29	Strait of Hormuz
10	Northern Pacific East	30	Gulf of Aden
11	Southern Pacific East	31	Red Sea
12	Northern Pacific West	32	Suez Canal
13	Southern Pacific West	33	Black Sea
14	Sea of Okhotsk	34	Bosporus
15	Sea of Japan	35	Mediterranean Sea
16	Yellow Sea	36	Baltic Sea
17	East China Sea	37	North Sea
18	South China Sea	38	English Channel
19	Gulf of Thailand	39	Strait of Gibraltar
20	Strait of Singapore	40	Gulf of Guinea

Table 2: **Sea entity**

Maritime trading routes implemented in Loss-propagation model Acclimate. Numbering refers to Fig. 1a.

22 kn. That means

$$\chi_e(t) = \begin{cases} \infty, & \text{if wind speed} < 22 \text{ kn in } \mathcal{P}_e \\ 0.25, & \text{if wind speed} \geq 22 \text{ kn in } \mathcal{P}_e \end{cases}, \tag{5}$$

where $\mathcal{P}_e$ is the polygon that defines the area of maritime routes e, here, South China Sea, East China Sea, Yellow Sea, Sea of Japan, and the Gulf of Thailand[2]. From tropical storm trajectories (Fig. 1b), based on IBTrACS [93, 94], we derive time series of commodity passage for the East Asian maritime trade routes for the years 2000–2020. Exemplary time series for the disturbed trade routes are depicted in Fig. 1c.

[2]Definition of polygons are available under 10.5281/zenodo.5807332.

3.5. Regional and sectoral aggregation

Based on these time series of short-term transport delays the Acclimate model computes the resulting economic repercussions. We then analyze the direct and indirect impacts. In the following, the regional results are summarized to economic blocs (Fig. 1d): China, Europe, NAFTA[3] (North American Free Trade Agreement), ASEAN (Association of Southeast Asian Nations), Latin America (except Mexico), SAARC (South Asian Association for Regional Cooperation), East Asia (Japan, North Korea, South Korea, Taiwan), Arab League, Post-Soviet states, Australia & Oceania, Sub-Saharan Africa, and Rest of the World. The detailed grouping of the regions is listed in Table S2. We include Mongolia among the Post-Soviet states because of its historical economic close relationship to the Soviet Union, even though this is historically inaccurate. Furthermore, we include Mauritania and Sudan to the bloc Arab League, even if they would fit to the definition of Sub-Sahara Africa as well. The economic blocs are economically quite large, which is why individual sectors and their flows do not exhibit significant different patterns. Therefore, we aggregate all flows and production of the sectors together. We list in Table 3 how many trading links and which economic volume in bn USD per year pass the typhoon-impacted West Pacific trading routes per the economic bloc.

In our further analyses we mainly focus on China, ASEAN, East Asia, Europe and NAFTA. For the first three blocs, several close maritime trade routes are directly affected by West Pacific typhoon season. The last two are the largest global economic blocs next to China. Results for other aggregated blocs are given in the Supplementary Information.

[3]Our computations base on the economic network of 2015, therefore we use the economic bloc NAFTA, despite it was replaced in 2020 by he succession agreement USMCA.

	South China Sea		East China Sea		Yellow Sea		Sea of Japan		Gulf of Thailand	
	[links]	[bn USD]	[links]	[bn USD]	[links]	[bn USD]	[links]	[bn USD]	[links]	[bn USD]
China	2515	856.7	2810	1030.2	1865	603.8	26	89.2	80	54.5
	(47.1%)	(46.7%)	(52.6%)	(56.2%)	(34.9%)	(32.9%)	(0.5%)	(4.9%)	(1.5%)	(3.0%)
Europe	876	797.7	378	322.8	263	151.3	32	99.8	41	44.5
	(15.5%)	(25.8%)	(6.7%)	(10.5%)	(4.7%)	(4.9%)	(0.6%)	(3.2%)	(0.7%)	(1.4%)
NAFTA	624	107.3	1106	104.3	636	48.2	53	54.5	75	19.0
	(10.2%)	(8.3%)	(18.1%)	(8.1%)	(10.4%)	(3.7%)	(0.9%)	(4.2%)	(1.2%)	(1.5%)
ASEAN	834	559.6	141	152.9	103	60.5	9	65.7	437	272.7
	(53.4%)	(57.6%)	(9.0%)	(15.7%)	(6.6%)	(6.2%)	(0.6%)	(6.8%)	(28.0%)	(28.1%)
Latin	141	25.2	195	18.7	110	11.3	20	7.1	13	1.1
America	(5.6%)	(6.0%)	(7.7%)	(4.4%)	(4.4%)	(2.7%)	(0.8%)	(1.7%)	(0.5%)	(0.3%)
SAARC	169	59.8	51	19.5	34	7.6	5	7.5	3	0.2
	(15.5%)	(17.6%)	(4.7%)	(5.7%)	(3.1%)	(2.2%)	(0.5%)	(2.2%)	(0.3%)	(0.1%)
East Asia	342	685.3	274	572.2	81	150.9	226	467.5	17	81.3
	(42.3%)	(44.4%)	(33.9%)	(37.0%)	(10.0%)	(9.8%)	(28.0%)	(30.3%)	(2.1%)	(5.3%)
Arab League	428	150.4	178	63.1	122	7.6	16	52.0	17	8.0
	(23.0%)	(33.8%)	(9.5%)	(14.2%)	(6.5%)	(1.7%)	(0.9%)	(11.7%)	(0.9%)	(1.8%)
Post-Soviet	54	11.8	66	48.6	56	48.4	4	0.2	4	1.8
states	(7.0%)	(3.0%)	(8.5%)	(12.3%)	(7.2%)	(12.3%)	(0.5%)	(0.1%)	(0.5%)	(0.5%)
Australia	83	86.9	50	42.7	38	18.4	6	18.8	9	6.2
& Oceania	(15.3%)	(28.0%)	(9.2%)	(13.7%)	(7.0%)	(5.9%)	(1.1%)	(6.1%)	(1.7%)	(2.0%)
Sub-Saharan	352	31.8	171	18.6	113	8.5	19	6.3	21	1.0
Africa	(18.4%)	(18.1%)	(8.9%)	(10.6%)	(5.9%)	(4.8%)	(1.0%)	(3.6%)	(1.1%)	(0.6%)

Table 3: **Economic blocs and their dependency on West Pacific trading routes.** Used aggregated economic bloc used in post-simulation analysis (Fig. 1b) and their number of business connection through a West Pacific trading route as well as the economic size of those business connections in bn USD. The number in brackets depict the share of the trading route compared to the total links or exports of the bloc, respectively.

4. Results

In the following results are presented in changes of the economic values with respect to their unperturbed baseline. Unless otherwise stated, the economic network and baseline refer to the year 2015. In our analysis we distinguish between the *quantity* and the *value* of an economic variable. The former refers to the physical amount of traded goods or hours spent on services measured in fixed 2015-USD. The latter refers to the value of traded goods and services, which is composed of the quantity and the *price* of a commodity or service ($value = price \cdot quantity$). Thereby, in the model price is the relative deviation from the (unknown) baseline price (i.e. 1 for the baseline) and quantity as well as value are both measured in USD. The first relies on fixed prices within the baseline MRIO table of 2015. The second accounts for endogenous price changes in our model. The temporal evolution of quantity, price, and thus also of the value for each traded good, is computed by *Acclimate*, after which they are aggregated to annual values in the post-computing analysis. In the following we also distinguish between *internal* and *external* demand. The former refers to demand which comes exclusively from firms and consumers of the economic bloc itself, while the later corresponds to the demand from other economic blocs. Similarly, we refer to internal and external trade as flows of commodities and services where the receivers are inside or outside of the economic bloc, respectively. In this study we use external trade and export as synonyms.

4.1. Transport perturbations cause demand-supply mismatch

In order to clarify the economic dynamics during and after a transport disturbance due to a typhoon, we focus in this section on the typhoon seasons of 2018 and the simulated economic repercussions of the most affected bloc, China, and the biggest profiteer, NAFTA.

Tropical storms cause transport disturbances on West Pacific shipping routes from 1 to 8 days depending on their trajectory (Fig. 1c). Chinese maritime trading routes may be perturbed due to one of these typhoons, which causes

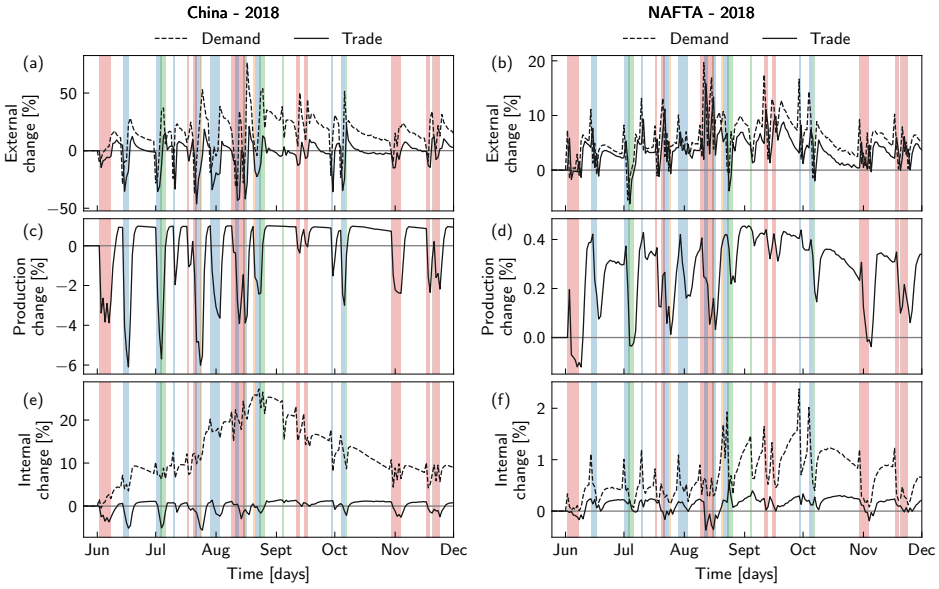

Figure 2: **Typhoon-induced transport disturbance induce demand shifts and furthermore production and trade changes.** The external (upper panels) and internal (middle panels) demand change (dashed line) with corresponding production change (middle pannels) and following trade change (solid line) due to transport disturbance in maritime trade routes for China (a,c,d) and (b,d,f) NAFTA. Changes are relative to baseline. The perturbed trading route is marked via same color scheme, which is used in Fig. 1d. The exemplary typhoon season shown is 2018.

short-term decrease of external demand (Fig. 2a). A decline of external demand yields a lower Chinese production (Fig. 2c) during a typhoon. In the aftermath of a transport disturbance external demand and therewith production in China increases.

In contrast to China, NAFTA maritime trading routes are just partially affected by the West Pacific typhoon season. As a result, they are used as substitute suppliers for other blocs and thus external demand increases at the beginning of the transport perturbation (Fig. 2b). But since production in other blocs decrease, external demand declines after some time steps while West Pacific transport disturbance. Thus, NAFTA's initial rise in external demand, trade, and production abates partly (Fig. 2b,d).

The demand and supply shocks during a typhoon cause Chinese production to decline, which causes that demand of the domestic market cannot be perfectly fulfilled as well. Thus, internal trade decreases during phases of production reduction. Less production causes a decline in inner-Chinese trade (internal trade), despite the fact that internal demand increased. As stated previously, in the disaster aftermath external demand increases. The lack of supply and a rise in production puts more pressure on the Chinese market externally and internally. Thus, internal demand increases even further (Fig. 2e). The same pattern occurs for every transport disturbance. However, previous economic repercussions are reflected in the dynamics (Fig. 2e), e.g. internal demand may rise after one typhoon and before the next. The high frequency of transport perturbations between June and end of August yield increased internal demand. In other words, the frequency of transport shocks is too high compared to the relaxation time of internal demand. For NAFTA, short-term production declines causes short internal supply shortages, but internal trade increases in the aftermath. Supply uncertainties are counteracted as well by increased demand from the domestic market (Fig. 2f).

4.2. Exports increase despite typhoon transport perturbations

In the following, our results are given in median annual changes of 21 West Pacific typhoon seasons (2000–2020) with corresponding likely ranges.

4.2.1. Exports increase in quantity

Despite imminent typhoon-induced maritime transport restrictions, China is able to increase its annual exports in quantity (Fig. 3a). In contrast to this, China depicts losses in exported value. The other economic blocs are able to increase their exports in quantity and value facing the typhoon-induced transport disruptions. In this regard, NAFTA is the biggest winner. Our results hint that inter-regional trade involving NAFTA might be boosted by typhoon-induced transport disruption (Fig. 3a). So the annual intra-regional trade of the economic blocs depict gains — at least in the amount of exports — even

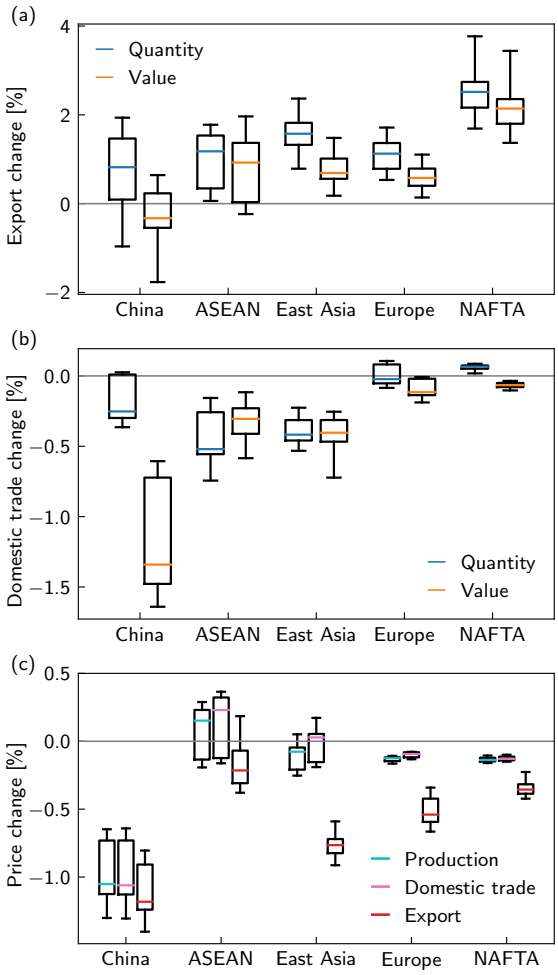

Figure 3: **Perturbed trading routes yield price changes which mostly intensify internal trading losses or decreases export gains in value.** Ensemble includes 21 typhoon seasons (2000–2020). Colored lines, boxes and whiskers indicate median changes for each estimate, the 25–75 and 5–95 percentile ranges, respectively. Changes are depicted for one year and are relative to the economic baseline.
(a) Typhoon disturbed inter-regional trade increases amount of exports (blue) but lower prices decreases gain in value (orange).
(b) Domestic trade decreases in quantity and value in most economic blocs. Raised demand increases production in NAFTA and thus the domestic trade also increases slightly in quantity.
(c) Prices of production (light blue), and goods and services traded internally (pink) or exported (red) decrease in most economic blocs.

if transport is disturbed. In the disaster aftermath, increased demand and trade lead to an rise of exports of every economic bloc. We interpret this positive feedback as resilience towards trade perturbation caused by maritime disturbances.

4.2.2. Internal trade mostly reduces

Trade inside each economic bloc does not depict such a perturbation resilience; trade within the domestic market decreases in most blocs (Fig. 3b).

Here, China has the largest losses in value and only NAFTA can strengthen its internal trade. However, the internally highly interconnected economic blocs of China and Europe show comparatively small impacts on the volume of internal trade.

4.2.3. Production and trading prices mostly decrease

In our study setup no good is destroyed by typhoons, nor do firms stop production due to direct impacts of a typhoon. Therefore, there is no direct global scarcity of commodities but rather a dislocation and delay of goods and services. As firms' inventories tend to be fuller and inter-regional buyers are absent, a regional oversupply is created, causing prices to fall (Fig. 3c). This effect occurs mainly in China. Since China is directly affected from typhoon-induced transport disruption, there is a larger oversupply of goods. Thus, production and domestic trade prices drop as well as offering prices for exporting commodities. However, the latter is likely to be beneficial for demand from abroad, allowing China to increase their exports in quantity (Fig. 3a). Lower export prices are common across the economic blocs, even for ASEAN which increases production and internal trade prices. Since the South China Sea is within the trade routes of the ASEAN region, internal trade between ASEAN countries is disrupted, resulting in no intra-regional oversupply and thus no price reductions but price increases instead (Fig. 3c).

4.3. Affected trading routes impact Chinese exports

In this study we focus on the transport obstructions through the South China Sea, East China Sea, Yellow Sea, Sea of Japan, and the Gulf of Thailand. China uses, depending on its trading partner, every single one of these five trading routes. Important trading routes are the first three ones, regarding number of trading connection and traded economic volume (Table 3). China depicts a different export change if only trading routes in East China Sea or South China Sea are disturbed compared to all five West Pacific trading routes (Fig. 4a). Transport blockages in East China Sea cause Chinese export losses in

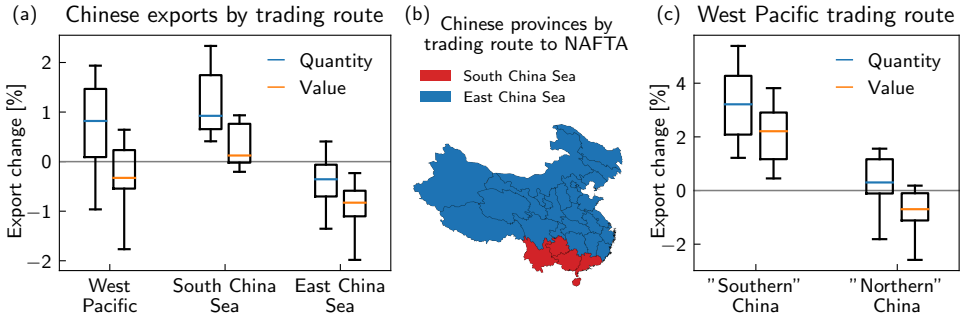

Figure 4: **Chinese export resilience to transport disruption depend on affected trading route.**

For (a) and (c): Ensemble includes 21 typhoon seasons (2000–2020). Colored lines, boxes and whiskers indicate median changes each estimates, the 25–75 and 5–95 percentile ranges, respectively. Changes refer to the economic baseline.

(a) Chinese export changes if typhoon seasons cause transport perturbation on all five West Pacific trading routes, only on South China Sea or only on East China Sea. Disruption of the latter causes export losses in quantity and value.

(b) Regarding maritime trading route to NAFTA, China provinces are divided into those using South China Sea (red) – "Southern" China – or East China Sea (blue) – "Northern" China.

(c) Regarding typhoon-induced transport perturbation on all five West Pacific trading routes, "Southern" China can benefit (more) from typhoon-induced transport perturbation on all five West Pacific trading routes compared to "Northern" China.

quantity and value. In contrast to that, Chinese firms are able to increase their exports from perturbation within the South China Sea. The reason for this is that one important receiving economic bloc from China is NAFTA — 22% of Chinese exports are to NAFTA (Table 4). Chinese provinces can be divided into "Northern" China that uses East China Sea to NAFTA and "Southern" China that uses South China Sea to export commodities to NAFTA (Fig. 4b). The total production of the former is about 5 times higher than the latter(Table 4). Regarding typhoon-induced West Pacific transport route perturbations "Southern" China profits, while "Northern" China exports in value decreases (Fig. 4c). As a result, China as a whole has more difficulties to compensate for export reductions going through East China Sea, which suggest that this maritime entity is crucial to Chinese economic well-being.

	GDP [tn USD]	China [bn USD]	Europe [bn USD]	NAFTA [bn USD]	ASEAN [bn USD]	Latin America [bn USD]	SAARC [bn USD]	East Asia [bn USD]	Arab League [bn USD]	Post-Soviet states [bn USD]	Australia & Oceania [bn USD]	Sub-Saharan Africa [bn USD]	Rest of World [bn USD]
China	24.6 (17.8%)	22,793	445 (24.3%)	398 (21.7%)	144 (7.9%)	49 (2.7%)	44 (2.4%)	319 (17.4%)	47 (2.6%)	20 (1.1%)	44 (2.4%)	18 (1.0%)	307 (16.7%)
Europe	35.3 (25.5%)	449 (14.5%)	32,201	780 (25.2%)	209 (6.8%)	235 (7.6%)	127 (4.1%)	288 (9.3%)	263 (8.5%)	215 (6.9%)	75 (2.4%)	123 (4.0%)	325 (10.5%)
NAFTA	34.1 (24.6%)	124 (9.7%)	434 (33.7%)	32,781	111 (8.6%)	195 (15.1%)	20 (1.6%)	227 (17.6%)	37 (2.9%)	12 (0.9%)	67 (5.2%)	12 (1.0%)	47 (3.7%)
ASEAN	5.0 (3.6%)	176 (18.2%)	186 (19.2%)	164 (16.9%)	4,016	13 (1.3%)	46 (4.7%)	238 (24.6%)	27 (2.7%)	3 (0.3%)	50 (5.2%)	8 (0.9%)	58 (6.0%)
Latin America	7.8 (5.6%)	34 (7.9%)	110 (26.0%)	210 (49.7%)	7 (1.7%)	7,353	4 (1.0%)	31 (7.3%)	6 (1.4%)	4 (0.9%)	4 (0.9%)	6 (1.5%)	7 (1.8%)
SAARC	4.1 (3.0%)	26 (7.7%)	99 (29.2%)	65 (19.1%)	29 (8.7%)	10 (2.8%)	3,762	21 (6.2%)	49 (14.5%)	4 (1.3%)	4 (1.3%)	15 (4.5%)	16 (4.7%)
East Asia	11.8 (8.5%)	440 (28.5%)	245 (15.9%)	321 (20.8%)	242 (15.7%)	41 (2.6%)	37 (2.4%)	10,284	37 (2.4%)	8 (0.5%)	48 (3.1%)	12 (0.8%)	113 (7.3%)
Arabic League	4.3 (3.1%)	23 (5.1%)	146 (32.9%)	43 (9.6%)	30 (6.8%)	9 (1.9%)	23 (5.2%)	129 (29.0%)	3,818	5 (1.1%)	6 (1.3%)	8 (1.9%)	23 (5.3%)
Post-Soviet states	4.0 (2.9%)	54 (13.8%)	231 (58.6%)	23 (5.8%)	6 (1.4%)	3 (0.8%)	11 (2.8%)	35 (9.0%)	3 (0.9%)	3,592	0 (0.0%)	1 (0.2%)	27 (6.8%)
Australia & Oceania	2.7 (2.0%)	51 (16.5%)	36 (11.6%)	34 (10.9%)	51 (16.5%)	5 (1.5%)	13 (4.2%)	90 (28.9%)	8 (2.6%)	2 (0.5%)	2,389	5 (1.5%)	16 (5.3%)
Sub-Saharan Africa	2.1 (1.5%)	24 (13.9%)	72 (41.1%)	32 (18.2%)	5 (3.1%)	6 (3.4%)	7 (4.0%)	18 (10.1%)	3 (1.8%)	1 (0.4%)	3 (1.6%)	1,923	4 (2.4%)
Rest of World	2.7 (1.9%)	95 (21.1%)	151 (33.5%)	61 (13.7%)	41 (9.2%)	11 (2.3%)	14 (3.1%)	30 (6.6%)	20 (4.5%)	15 (3.4%)	4 (1.0%)	7 (1.6%)	2,238
"Northern" China	20.6 (14.9%)	–	372 (20.3%)	333 (18.1%)	121 (6.6%)	41 (2.2%)	36 (2.0%)	267 (14.6%)	39 (2.1%)	17 (0.9%)	37 (2.0%)	15 (0.8%)	257 (14.0%)
"Southern" China	4.0 (2.9%)	–	73 (4.0%)	65 (3.6%)	23 (1.3%)	8 (0.4%)	7 (0.4%)	52 (2.8%)	8 (0.4%)	3 (0.2%)	7 (0.4%)	3 (0.2%)	50 (2.7%)

Table 4: **Economic volume of blocs in 2015.** Left side: Annual production in tn USD with share of world production below in brackets per bloc. Right side: Supply volume in bn USD internally and to others of economic blocs. The share of exports of a bloc to another is given below the corresponding supply. Self-supply of each bloc is roughly a magnitude higher than the total exports of a bloc.

4.4. Increased inter-connectivity supports short-term export adaptation

So far, our results and interpretations base on the trade structures of 2015. In this section, we examine export changes for other in order to reveal factors for the identified trade resilience. Using the same impact of 2000–2020 typhoon seasons, we compute the export changes to different economic baselines from 2000 to 2015 (Fig. 5). Overall, the economic blocs' exports increases with later economic baselines. The most directly affected blocs, China, ASEAN, and East Asia experience lower export losses or partly get net-export gains in later years. Especially ASEAN and East Asia turn into net-export winner in quantity and value. Next to them, Europe is able to become a net-export winner as well within later years. The positive export response of NAFTA is robust against different network years.

This increase in resilience to transport perturbations for most blocs cannot be explained by the export share of each economic bloc. While China more than doubles its export between 2000 and 2015, East Asia's and NAFTA's share decreases roughly by a third (Fig. 6a). At the same time ASEAN increases its share by 20% and Europe's share is more or less stable at a high level. Nevertheless, resilience increases collectively in the later economic networks.

We find that the reason that trade resilience increases for some blocs in recent years arises from the changes of number of trade connections. From the beginning of the millennium the number of connections to external purchasers per firm within a economic bloc develops different from the export share (Fig. 6b). We refer to the number of connections to external purchasers as the total number of trading links to the outside of each economic bloc. We normalize this number of outside connections with the economic bloc's number of firms to account for blocs' different economic sizes. From 2000 to 2015 China, Europe, East Asia, and ASEAN increased their number of outside connections per firm, while NAFTA is at a stable high level. A higher number of connections to other firms enables economic agents to shift supply and demand on non-disturbed trading routes. A higher number of outside connections can be interpreted as a more strengthened inter-connectivity of a bloc. Increasing inter-connectivity

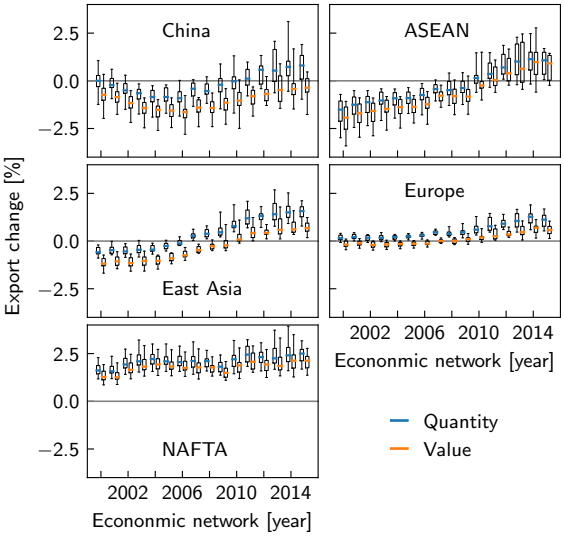

Figure 5: **Most blocs become over time more resilient against perturbations to West Pacific transport.**
Annual export change per quantity (blue) and value (orange) for economic network baselines for the years 2000–2015. The trend of results for the most affected economic blocs — China, ASEAN and East Asia — changes with underlying economic network. Export losses due to transport perturbations convert to export quantity gains for these blocs. Europe becomes a net-export value winner for later network years. Results for NAFTA are robust against changes in baseline network. Ensemble includes 21 typhoon seasons (2000–2020). Colored lines, boxes and whiskers indicate median changes each estimates, the 25–75 and 5–95 percentile ranges, respectively. Changes refer to the economic baseline.

supports to buffer export losses and may turn export losses to export gains (Fig. 6c). A diverse variety of links to other blocs supports export adaptation to demand and supply fluctuations. Other economic blocs show an increase in the number of outside connections since the beginning of the century as well (Fig. S3a). Likewise, their trade resilience towards maritime disturbance grow with higher trade-inter-connectivity (Fig. S3b).

4.5. Demands and supply shifts between blocs

After giving an explanation for trade resilience, we want to focus on changes in trade between the five main economic blocs. So in this section, our analysis

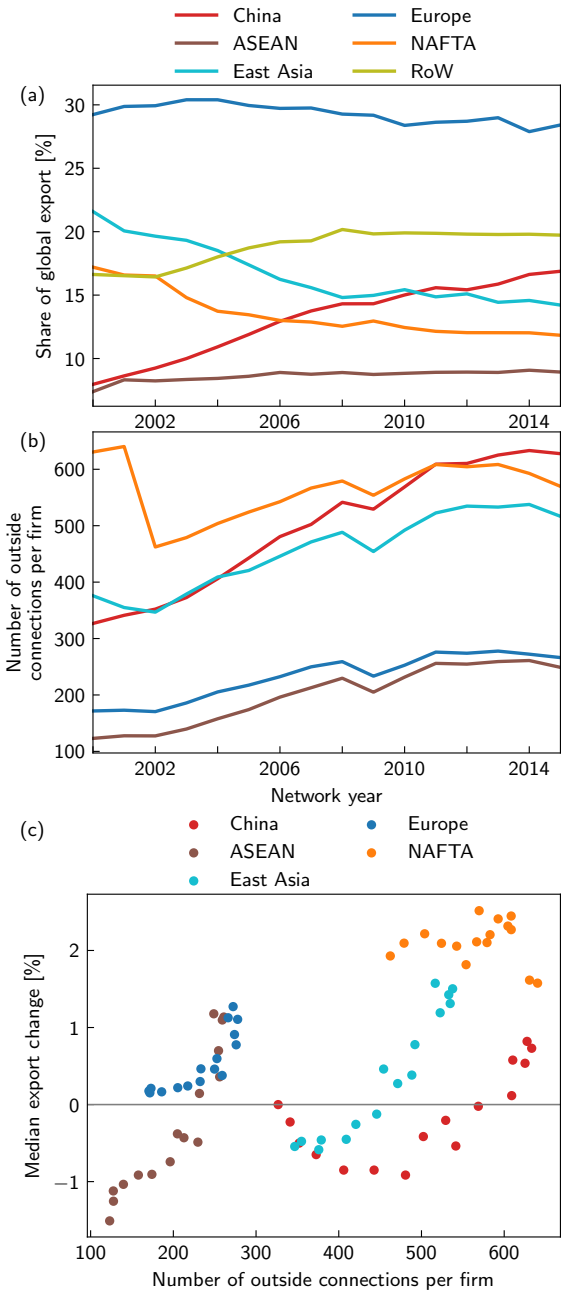

Figure 6: **Inter-connectivity of economic blocs change for different economic baselines.** China, ASEAN, East Asia, Europe, NAFTA, and Rest of the World (RoW) are depicted in red, brown, turkis, blue, orange, and lime, respectively.
(a) Annual export share changes regionally between 2000 and 2015.
(b) Number of foreign connections per firm within the economic bloc for different economic baselines.
(c) Median annual export change in quantity per region over number of foreign connections per firm. Export resilience tends to increase with more foreign connections.

bases again on the economic baseline of 2015. As we present changes in trade only for the five blocs considered so far (Fig. 7), trading results between any two blocs are listed in Table S4 and Table S5. The blocs' exports in the baseline and its corresponding share of exports can be found in Table 4.

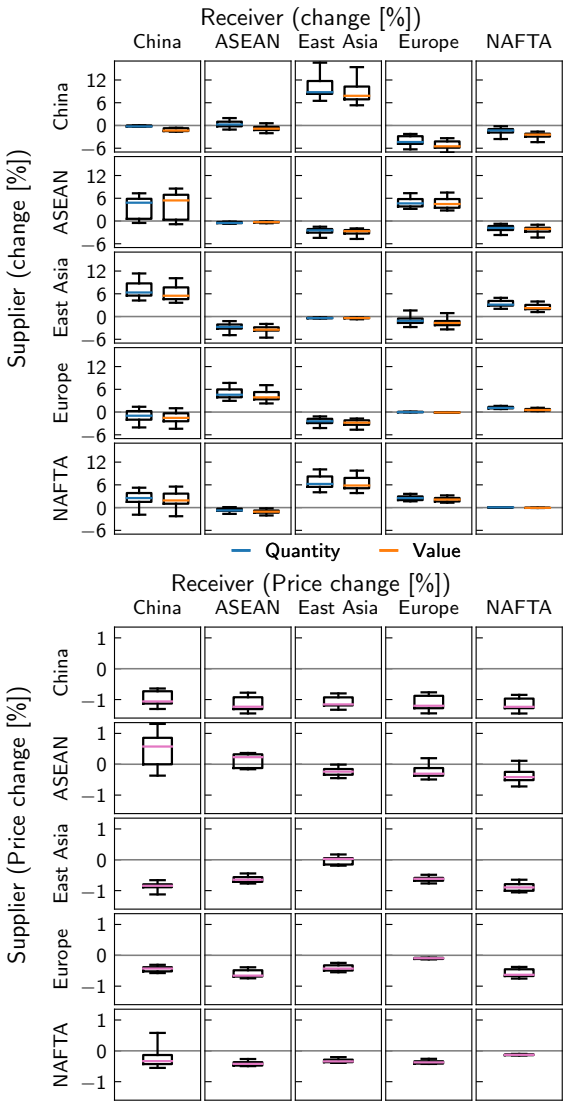

Figure 7: **Inter-connectivity increases except for NAFTA.** Ensemble includes 21 typhoon seasons (2000–2020). Colored lines, boxes and whiskers indicate median changes each estimates, the 25–75 and 5–95 percentile ranges, respectively. Changes refer to the economic baseline.
(a) Annual supply change per supplier (row) and purchaser (column) due to West Pacific typhoon season. Export between blocs increases (decreases) by quantity (value). Bloc-internal trade change is shown on the diagonal graphs.
(b) Annual price change of traded goods and services per supplier (row) and purchaser (column) due to West Pacific typhoon season. Bloc-internal (domestic) trade price change is shown on the diagonal graphs. China depicts the highest export price drop to any other economic bloc.

4.5.1. China's export losses and adaptation mechanism

China decreases its exports in quantity to almost any other economic bloc (Fig. 7a). Export losses are particularly severe for the largest customer (24%) of Chinese goods: Europe. However, the Chinese export reduction to other blocs is probably buffered by lower trading prices compared to other export prices of other blocs (Fig. 7b). Lower supply prices make Chinese goods more attractive for firms and consumers from outside of China. In particular, there are strong

Chinese export gains towards East Asia. East Asia is already a big purchaser of Chinese exports (about 17%) and can substitute for lack in supply and demand, especially when the trading route through South China Sea is perturbed.

4.5.2. East Asia intensifies its trade with China and NAFTA

Going the other way around, China has an even bigger share of East Asian exports (29%). By disturbing the trading route through South China Sea, East Asia trade relations with ASEAN and Europe are flagging. The East Asia's export share of these blocs add up to 32%. Demand and supply deficits are compensated for by China and NAFTA. The latter increases its trade as well when trading routes between East Asia and China is partly perturbed.

4.5.3. ASEAN's trade relocates to the west

During typhoons the ASEAN states are challenged by trade interruptions to East Asia and NAFTA. Both are significant buyers of ASEAN goods (25% and 17%, respectively). In order to sell their commodities ASEAN increases its exports to Europe and SAARC (Table S4). Exports to China are increasing as well, but ensemble results fluctuate widely. This may arise from the different connections to China. Some ASEAN states, like Vietnam or Thailand, have some trading route on land, which (in this study) are not affected by typhoon-induced transport disruption. Other states, like Philippines or Indonesia, are very much cut off from China regarding transport during a typhoon. Nevertheless, regarding ASEAN as a whole, export gains to China prevail.

4.5.4. Europe substitutes eastern Asian purchaser

During the West Pacific typhoon seasons, the globally largest exporting bloc, Europe, increases its exports to any other bloc (Table S4), except for China and East Asia. However, the losses in exports to China are marginal and do not occur for all seasons. Especially seasons with a low impact on the South China Sea may exert less pressure on the export problems between China and Europe.

4.5.5. NAFTA is net-export winner

NAFTA faces the biggest export gains in quantity and in value. It increases its export to any bloc except for ASEAN and Rest of the World (Table S4). The diversified export rise comes from the geographic benefit of the NAFTA countries. NAFTA can satisfy mostly increased demand from the west, east, and south without depending on interruptions in the Western Pacific trading routes, except for ASEAN states and some provinces of China. But even the partly limited trade to China is compensated for. Therefore, NAFTA can increase exports to China. As NAFTA has a negative trade balance with most other blocs, the export rise is even more favorable for it.

4.6. Sensitivity analysis

In this study we use a novel approach model for maritime transport disturbances due to typhoons. A typhoon that passes through a sea area reduces the ability to ship goods through this area. To implement this we assume, on the one hand, a passage limit (25%) on the amount of goods passing a route during a disturbance. On the other hand, we set a wind speed threshold (22 kn) when a sea route is perturbed by a tropical storm. Sensitivity analyses of those parameters depict that our results do not significantly change under these parameters (Fig. 8a). If the passage limit during a storm is attenuated (limit closer to 100%) more goods can be transported through the trading route. This causes that export changes decline slightly. A higher transport throughput yields to less economic repercussion, which changes the quantity of the results but not their general trend. When increasing the disturbance threshold, the export changes decrease as well, but do not show a trend shift (Fig. 8b). A higher wind speed threshold causes fewer days of transport perturbation, especially for South China Sea (Fig. S2). But even with fewer transport disturbances and thus less economic repercussion, the trend of export changes is preserved.

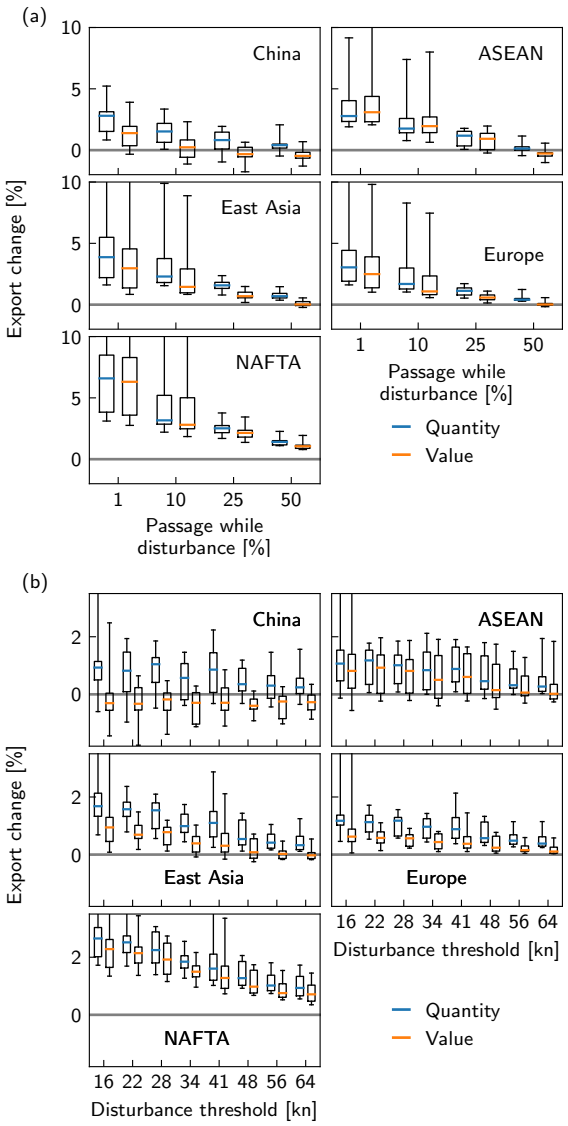

Figure 8: **Trends in result are robust against changes of disturbance modeling.**
Annual export change per quantity (blue) and value (orange) for different (a) passages – possible commodity flows through maritime trading route – and (b) wind speed thresholds while typhoon-induced disturbances. Ensemble includes 21 typhoon seasons (2000–2020). Colored lines, boxes and whiskers indicate median changes each estimates, the 25–75 and 5–95 percentile ranges, respectively. Results with full percentile ranges are depicted in Fig. S4. Changes refer to the economic baseline.
(a) Attenuate the passage limit yield that more commodities can go through sea route while disruption time. Note, that the x-axis is not true to scale. Since perturbations of trade becomes smaller for softer limits, export increase of each economic bloc is weakened but the trend persists.
(b) Higher thresholds of wind speed result in fewer days of transport perturbation. Since perturbations of trade becomes smaller for higher thresholds, export changes decline as well but trend of the response of economic blocs remains the same.

5. Discussion

In this study, we focus on transport perturbations induced by typhoons in the West Pacific. We find that during the perturbation directly affected trade blocs

such as China or East Asia become less attractive for the their trade partners, who partially reschedule their demand to other non-affected trade partners, e.g., Europe or NAFTA. This results in a decline of production in the directly affected blocs, which can translate into production declines in non-directly affected blocs due to reduced demand received from outside of the region. These production anomalies result in reductions in trade within the respective trade blocs as well. The resulting price drops lead to a temporal increase in demand, production, as well as internal and external trade above their pre-disaster levels once the perturbation has ceased.

Accounting for the last 21 West Pacific typhoon seasons, we find that, in absolute terms, annual average export volumes increase all trade blocs. This suggests that inter-regional trade is partially resilient against typhoon-induced transport disruptions. In relative terms, trade between Europe and East Asia, China, and East Asia, decreases, while trading between Europe and South Asia — SAARC and ASEAN — increases. Due to regional proximity, trade between China and East Asia is being strengthened, although the latter is increasingly relying on trade on the other side of the Pacific (NAFTA and Latin America). NAFTA is the overall net-export winner, which can be explained by its geographic advantage to reach most economic actors without transport disruption.

Further, we find that the resilience of the exports of the trade blocs are correlated with the number of outside connections per sector. Export gains increase with the number of connections to external trade partners of the firms within the block. Since the connectivity of firms in China, ASEAN and East Asia to external trade partners has substantially increased between 2000–2015, they shifted from net-export losers in the early 2000s to net-export winners in 2015.

By its very nature, economic modeling must always be understood in the context of its limitations due to the complexity of human behavior. Nevertheless, for reasonable assumptions, conclusions can be made within the limits drawn. In this study, we focus on short-term transport disruptions (a few days) due to typhoons and the resulting economic repercussions. For this, our assumption

of myopic economic agents with no long-term investment strategy is justifiable. Adaptation measures, such as the formation of new transport routes or trade links, are, however, not in the scope of our study.

The modeled maritime transport network consists of ocean sub-regions (e.g. Northern Atlantic North East or Southern Pacific East), seas (e.g. Red Sea), coastal bodies of water (e.g. Gulf of Mexico or Bay of Bengal), and artificial or natural sea straits (e.g. Suez Canal or Strait of Malacca). Thereby, the selection of the trade routes is a trade-off between computational effort and required resolution for this study. We include only possible and plausible routes that are also navigable throughout the year. For example, maritime routes across the partially ice-free Arctic Ocean are not taken into account. Furthermore, we assume that theoretically an infinite amount of commodities can pass through a land entity, maritime entity or port. This assumption is perhaps practical but rather less realistic, especially for ports. In our model, ships pass through the midpoints of the associated sea entities along a transport route and ships cannot adjust their maritime routes due to preceding transport obstructions. This is a constraint on the adaptation measures of the transportation planners, however, reasonable for the length of our simulated shocks. The Suez canal obstruction in early 2021 depicted that the most ships did not change transport routes for a short-term (daily scale) transport blockage.

Additionally, we have to make simplifying assumptions for the transport perturbation in the West Pacific sea routes. Here, the transport disruption over a wind speed threshold is based on studies referring to storm-induced delays for ports [11] or to container network analysis [95]. Next to this, our sensitivity analyses reveal, that the choice of disturbance threshold and intensity does not change the trend of our results. To tackle the problem with climate variability, our results base on an ensemble of 21 typhoon seasons (which included measured storm tracks).

At a first glance, our findings that exports increase in the disaster aftermath contrast with estimated export losses of previous studies [96, 97]. However, our analysis focuses on short-term transport delays and does not include the

destruction of production goods or the long-term destruction of infrastructure. Because tropical storms can cause both impacts — short-term transportation disruption and destruction of physical capital — further research should consider both effects in a joint setup.

While the underlying economic network evolves, the number of outside connections per firm of the economic blocs changes(Fig. 6). However, although the blocs exhibit divergent rates of change, the signs of change are uniform across the blocs (except in the early 2000s). That means that the trading density of the economic network increases or decreases homogeneously. In the literature, the debate [98] whether more dense and complex networks are more stable [99, 86] or less stable [99, 89] is still open. Assuming trade resilience to maritime disruptions as a measure of stability of a global trade network, our results suggest that more complex networks (more inter-connections) are more likely to be stable (more trade resilience). Nevertheless, this likely differs depending on location and size of the perturbation.

The transportation extension of Acclimate presented in this study can be used to examine economic repercussions of further short-term supply chain constraints. Tropical storms impede shipping even in other locations, and other extreme events can disrupt supply chains for short periods of time. For those regions, our analysis could be easily extended. The storm tracks used here vary widely between seasons and our results depict clear results in trends, which hints that we there is a more in-depth mechanism. The diversification of trading partners enables economies to counteract transport disruptions with increased export in the aftermath. In a world where extreme events are likely to increase, this trade resilience can mitigate local economic perturbations.

Data and materials availability

The implementation of the *Acclimate* model is available as open source on `https://github.com/acclimate/acclimate` with identifier 10.5281/zenodo.needed. The used data for categorization of the maritime entities and the

geographic network are available at 10.5281/zenodo.5807332).

Acknowledgments

This research has received funding from the German Academic Scholarship Foundation and the German Federal Ministry of Education and Research (BMBF) under the research projects CLIC (FKZ: 01LA1817C), QUIDIC (01LP1907A), and SLICE (FKZ: 01LA1829A), from the Horizon 2020 Framework Program of the European Union (grant agreement 820712), and by the Defense Advanced Research Project Agency under the World Modelers program (grant W911NF1910013).

References

[1] G. Federico, A. Tena-Junguito, A tale of two globalizations: gains from trade and openness 1800–2010, Review of World economics 153 (3) (2017) 601–626.

[2] WTO, Global trade rebound beats expectations but marked by regional divergences, accessed: 2021-11-05 (Oct 2021).
URL https://www.wto.org/english/news_e/pres21_e/pr889_e.html

[3] O. Taherzadeh, M. Bithell, K. Richards, Water, energy and land insecurity in global supply chains, Global Environmental Change 67 (2021) 102158. doi:https://doi.org/10.1016/j.gloenvcha.2020.102158.
URL https://www.sciencedirect.com/science/article/pii/S095937802030741X

[4] S. N. Sirimanne, J. Hoffman, W. Juan, R. Asariotis, M. Assaf, G. Ayala, H. Benamara, D. Chantrel, J. Hoffmann, A. Premti, et al., Review of maritime transport 2019, Tech. rep., tech. rep (2019).

[5] Ship still stuck in suez canal as backlog grows to 150 other ships — cbc news, accessed: 2021-11-05 (Mar 2021).

URL https://www.cbc.ca/news/business/suez-canal-egypt-ever-given-1.5963207

[6] I. Martínez-Zarzoso, S. Bensassi, The price of modern maritime piracy, Defence and Peace Economics 24 (5) (2013) 397–418.

[7] V. Wendler-Bosco, C. Nicholson, Port disruption impact on the maritime supply chain: a literature review, Sustainable and Resilient Infrastructure 5 (6) (2020) 378–394.

[8] M. Hassanzadeh, Port safety; requirements & economic outcomes, Marine Navigation and Safety of Sea Transportation: Maritime Transport & Shipping (2013) 117–121.

[9] H. S. Loh, Q. Zhou, V. V. Thai, Y. D. Wong, K. F. Yuen, Fuzzy comprehensive evaluation of port-centric supply chain disruption threats, Ocean & Coastal Management 148 (2017) 53–62.

[10] U. Gidado, Consequences of port congestion on logistics and supply chain in african ports, Developing Country Studies 5 (6) (2015) 160–167.

[11] J. Verschuur, E. Koks, J. Hall, Port disruptions due to natural disasters: Insights into port and logistics resilience, Transportation research part D: transport and environment 85 (2020) 102393.

[12] J. A. Church, N. J. White, L. F. Konikow, C. M. Domingues, J. G. Cogley, E. Rignot, J. M. Gregory, M. R. van den Broeke, A. J. Monaghan, I. Velicogna, Revisiting the earth's sea-level and energy budgets from 1961 to 2008, Geophysical Research Letters 38 (18).

[13] L. Cheng, K. E. Trenberth, J. Fasullo, T. Boyer, J. Abraham, J. Zhu, Improved estimates of ocean heat content from 1960 to 2015, Science Advances 3 (3) (2017) e1601545.

[14] K. Emanuel, Increasing destructiveness of tropical cyclones over the past 30 years, Nature 436 (7051) (2005) 686–688.

[15] K. A. Emanuel, Downscaling cmip5 climate models shows increased tropical cyclone activity over the 21st century, Proceedings of the National Academy of Sciences 110 (30) (2013) 12219–12224.

[16] K. Balaguru, G. R. Foltz, L. R. Leung, K. A. Emanuel, Global warming-induced upper-ocean freshening and the intensification of super typhoons, Nature communications 7 (1) (2016) 1–8.

[17] Exports of goods and services (current usd), accessed: 2021-11-05 (2020).
URL https://data.worldbank.org/indicator/NE.EXP.GNFS.CD?view=map

[18] B. D. Brouer, J. Dirksen, D. Pisinger, C. E. Plum, B. Vaaben, The vessel schedule recovery problem (vsrp)–a mip model for handling disruptions in liner shipping, European Journal of Operational Research 224 (2) (2013) 362–374.

[19] J. Wang, M. Li, Y. Liu, H. Zhang, W. Zou, L. Cheng, Safety assessment of shipping routes in the south china sea based on the fuzzy analytic hierarchy process, Safety Science 62 (2014) 46–57. doi:10.1016/j.ssci.2013.08.002.

[20] C. Otto, S. Willner, L. Wenz, K. Frieler, A. Levermann, Modeling loss-propagation in the global supply network: The dynamic agent-based model acclimate, Journal of Economic Dynamics and Control 83 (2017) 232–269. doi:10.1016/j.jedc.2017.08.001.
URL https://doi.org/10.1016/j.jedc.2017.08.001

[21] R. C. Johnson, Measuring global value chains, Annual Review of Economics 10 (2018) 207–236.

[22] A. van der Veen, Disasters and economic damage: macro, meso and micro approaches, Disaster Prevention and Management: An International Journal 13 (4) (2004) 274–279. doi:10.1108/09653560410556483.

[23] Y. Okuyama, J. R. Santos, Disaster Impact and Input–Output Analysis, Economic Systems Research 26 (1) (2014) 1–12. doi:10.1080/09535314.2013.871505.

[24] A. Rose, Economic Principles, Issues, and Research Priorities in Hazard Loss Estimation, in: Y. Okuyama, S. Chang (Eds.), Modeling Spatial and Economic Impacts of Disasters, Advances in Spatial Science, Springer Berlin Heidelberg, 2004, pp. 13–36. doi:10.1007/978-3-540-24787-6_2. URL http://dx.doi.org/10.1007/978-3-540-24787-6{_}2

[25] S. Hallegatte, An adaptive regional input-output model and its application to the assessment of the economic cost of Katrina, Risk Analysis 28 (3) (2008) 779–799. doi:10.1111/j.1539-6924.2008.01046.x.

[26] J. D. Farmer, D. Foley, The economy needs agent-based modelling, Nature 460 (7256) (2009) 685–686. doi:10.1038/460685a.

[27] J. D. Farmer, C. Hepburn, P. Mealy, A. Teytelboym, A Third Wave in the Economics of Climate Change, Environmental and Resource Economics 62 (2) (2015) 329–357. doi:10.1007/s10640-015-9965-2.

[28] J. M. Albala-Bertrand, Disasters and the networked economy, routledge Edition, Routledge, 2013.

[29] M. Gallegati, M. G. Richiardi, Agent Based Models in Economics, Complex Systems in Finance and Econometrics (2011) 30–53.

[30] R. L. Axtell, What economic agents do: How cognition and interaction lead to emergence and complexity, Review of Austrian Economics 20 (2-3) (2007) 105–122. doi:10.1007/s11138-007-0021-5.

[31] A. Caiani, A. Godin, E. Caverzasi, M. Gallegati, S. Kinsella, J. E. Stiglitz, Agent based-stock flow consistent macroeconomics: Towards a benchmark model, Journal of Economic Dynamics and Control 69 (2016) 375–408. doi:10.1016/j.jedc.2016.06.001.

[32] D. Delli Gatti, C. Di Guilmi, E. Gaffeo, G. Giulioni, M. Gallegati, A. Palestrini, A new approach to business fluctuations: heterogeneous interacting agents, scaling laws and financial fragility, Journal of Economic Behavior & Organization 56 (2005) 489–512. doi:10.1016/j.jebo.2003.10.012.

[33] D. Delli Gatti, E. Gaffeo, M. Gallegati, G. Giulioni, A. Kirman, A. Palestrini, A. Russo, Complex dynamics and empirical evidence, Information Sciences 177 (5) (2007) 1204–1221. doi:10.1016/j.ins.2006.08.003.

[34] A. Mandel, Agent-based dynamics in the general equilibrium model, Complexity Economics 1 (2012) 105–121. doi:10.7564/12-COEC6.

[35] Y. M. Asano, J. J. Kolb, J. Heitzig, J. D. Farmer, Emergent inequality and business cycles in a simple behavioral macroeconomic model, Proceedings of the National Academy of Sciences 118 (27).

[36] G. Dosi, G. Fagiolo, A. Roventini, Schumpeter meeting Keynes: A policy-friendly model of endogenous growth and business cycles, Journal of Economic Dynamics and Control 34 (9) (2010) 1748–1767. doi:10.1016/j.jedc.2010.06.018.

[37] G. Weisbuch, S. Battiston, From production networks to geographical economics, Journal of Economic Behavior and Organization 64 (3-4 SPEC. ISS.) (2007) 448–469. doi:10.1016/j.jebo.2006.06.018.

[38] D. Delli Gatti, M. Gallegati, B. Greenwald, A. Russo, J. E. Stiglitz, The financial accelerator in an evolving credit network, Journal of Economic Dynamics and Control 34 (9) (2010) 1627–1650. doi:10.1016/j.jedc.2010.06.019.

[39] L. Ricetti, A. Russo, G. Mauro, Leveraged network-based financial accelerator, Journal of Economic Dynamics and Control 37 (2) (2013) 404–421. doi:10.1016/j.jedc.2012.10.004.

[40] S. Vitali, S. Battiston, M. Gallegatti, Financial fragility and distress propagation in a network of regions, Journal of Economic Dynamics and Control 72 (March 2005) (2016) 141–154. doi:10.1016/j.jedc.2016.03.010.

[41] M. Wolski, M. van der Leur, Interbanks loans, collateral and modern monetary policy, Journal of Economic Dynamics and Control 72 (March 2005) (2016) 141–154. doi:10.1016/j.jedc.2016.03.010.

[42] R. Leombruni, M. Richiardi, Why are economists sceptical about agent-based simulations?, Physica A: Statistical Mechanics and its Applications 355 (1) (2005) 103–109. doi:10.1016/j.physa.2005.02.072.

[43] J. E. Stiglitz, M. Gallegati, Heterogeneous Interacting Agent Models for Understanding Monetary Economies, Eastern Economic Journal 37 (1) (2011) 6–12. doi:10.1057/eej.2010.33.

[44] S. Gualdi, A. Mandel, On the emergence of scale-free production networks, Journal of Economic Dynamics and Control 73 (2016) 61–77. arXiv:1509.01483, doi:10.1016/j.jedc.2016.09.012.

[45] D. Acemoglu, V. M. Carvalho, A. Ozdaglar, A. Tahbaz-Selehi, The Network Origins of Aggregate Fluctuations, Econometrica 80 (5) (2012) 1977–2016. doi:10.3982/ECTA9623.

[46] S. Hallegatte, Modeling the Role of Inventories and Heterogeneity in the Assessment of the Economic Costs of Natural Disasters., Risk analysis 34 (1) (2013) 152–167. doi:10.1111/risa.12090.

[47] S. Hallegatte, Strategies to adapt to an uncertain climate change, Global Environmental Change 19 (2) (2009) 240–247. doi:10.1016/j.gloenvcha.2008.12.003.

[48] N. Ranger, S. Hallegatte, S. Bhattacharya, M. Bachu, S. Priya, K. Dhore, F. Rafique, P. Mathur, N. Naville, F. Henriet, C. Herweijer, S. Pohit, J. Corfee-Morlot, An assessment of the potential impact of climate

change on flood risk in Mumbai, Climatic Change 104 (1) (2011) 139–167. doi:10.1007/s10584-010-9979-2.

[49] S. Hallegatte, N. Ranger, O. Mestre, P. Dumas, J. Corfee-Morlot, C. Herweijer, R. M. Wood, Assessing climate change impacts, sea level rise and storm surge risk in port cities: A case study on Copenhagen, Climatic Change 104 (1) (2011) 113–137. doi:10.1007/s10584-010-9978-3.

[50] F. Henriet, S. Hallegatte, L. Tabourier, Firm-network characteristics and economic robustness to natural disasters, Journal of Economic Dynamics & Control 36 (2012) 150 –167. doi:10.1016/j.jedc.2011.10.001.

[51] S. N. Willner, C. Otto, A. Levermann, Global economic response to river floods, Nature Climate Change 8 (7) (2018) 594–598.

[52] K. Kuhla, S. N. Willner, C. Otto, L. Wenz, A. Levermann, Future heat stress to reduce people's purchasing power, PloS one 16 (6) (2021) e0251210.

[53] R. Middelanis, S. N. Willner, C. Otto, K. Kuhla, L. Quante, A. Levermann, Wave-like global economic ripple response to hurricane sandy, Environmental Research Letters.

[54] K. Kuhla, S. N. Willner, C. Otto, T. Geiger, A. Levermann, Ripple resonance amplifies economic welfare loss from weather extremes, Environmental Research Letters 16 (11) (2021) 114010.

[55] P. Trkman, K. McCormack, Supply chain risk in turbulent environments—a conceptual model for managing supply chain network risk, International Journal of Production Economics 119 (2) (2009) 247–258.

[56] T. Wu, J. Blackhurst, V. Chidambaram, A model for inbound supply risk analysis, Computers in industry 57 (4) (2006) 350–365.

[57] A. R. Ravindran, R. Ufuk Bilsel, V. Wadhwa, T. Yang, Risk adjusted multicriteria supplier selection models with applications, International Journal of Production Research 48 (2) (2010) 405–424.

[58] C. S. Tang, Perspectives in supply chain risk management, International journal of production economics 103 (2) (2006) 451–488.

[59] S. M. Wagner, V. Silveira-Camargos, Managing risks in just-in-sequence supply networks: Exploratory evidence from automakers, IEEE Transactions on Engineering Management 59 (1) (2010) 52–64.

[60] A. Baghalian, S. Rezapour, R. Z. Farahani, Robust supply chain network design with service level against disruptions and demand uncertainties: A real-life case, European journal of operational research 227 (1) (2013) 199–215.

[61] S. A. Yang, J. R. Birge, R. P. Parker, The supply chain effects of bankruptcy, Management Science 61 (10) (2015) 2320–2338.

[62] M. Giannakis, T. Papadopoulos, Supply chain sustainability: A risk management approach, International Journal of Production Economics 171 (2016) 455–470.

[63] W. Ho, T. Zheng, H. Yildiz, S. Talluri, Supply chain risk management: a literature review, International Journal of Production Research 53 (16) (2015) 5031–5069.

[64] E. E. Günay, K. Park, G. E. O. Kremer, Integration of product architecture and supply chain under currency exchange rate fluctuation, Research in Engineering Design (2021) 1–18.

[65] O. A. Durowoju, H. K. Chan, X. Wang, Entropy assessment of supply chain disruption, Journal of Manufacturing Technology Management.

[66] D. Ivanov, A. Dolgui, B. Sokolov, The impact of digital technology and industry 4.0 on the ripple effect and supply chain risk analytics, International Journal of Production Research 57 (3) (2019) 829–846.

[67] A. G. Morris, A. L. Kornhauser, M. J. Kay, Getting the goods delivered in dense urban areas: a snapshot of the last link of the supply chain, Transportation Research Record 1653 (1) (1999) 34–41.

[68] M. V. Tatikonda, M. Frohlich, Human operators and supply chain disruptions: A longitudinal study of truck driver accidents, in: Academy of Management Proceedings, Academy of Management Briarcliff Manor, NY 10510, 2013, p. 17133.

[69] H. S. Loh, V. Van Thai, Cost consequences of a port-related supply chain disruption, The Asian Journal of Shipping and Logistics 31 (3) (2015) 319–340.

[70] B. Jiang, R. C. Baker, G. V. Frazier, An analysis of job dissatisfaction and turnover to reduce global supply chain risk: Evidence from china, Journal of operations management 27 (2) (2009) 169–184.

[71] J. Vilko, P. Ritala, J. Hallikas, Risk management abilities in multimodal maritime supply chains: Visibility and control perspectives, Accident Analysis & Prevention 123 (2019) 469–481.

[72] S. Re, Natural catastrophes and man-made disasters in 2015: Asia suffers substantial losses, Tech. rep., Swiss Re (2016).

[73] S. A. Thekdi, J. R. Santos, Supply chain vulnerability analysis using scenario-based input-output modeling: Application to port operations, Risk Analysis 36 (5) (2016) 1025–1039.

[74] X. Cao, J. S. L. Lam, Simulation-based catastrophe-induced port loss estimation, Reliability Engineering & System Safety 175 (2018) 1–12.

[75] Y. Zhang, K. Wei, Z. Shen, X. Bai, X. Lu, C. G. Soares, Economic impact of typhoon-induced wind disasters on port operations: A case study of ports in china, International Journal of Disaster Risk Reduction 50 (2020) 101719.

[76] B. D. Brouer, J. Dirksen, D. Pisinger, C. E. Plum, B. Vaaben, The vessel schedule recovery problem (vsrp)–a mip model for handling disruptions in liner shipping, European Journal of Operational Research 224 (2) (2013) 362–374.

[77] C. Li, X. Qi, D. Song, Real-time schedule recovery in liner shipping service with regular uncertainties and disruption events, Transportation Research Part B: Methodological 93 (2016) 762–788.

[78] J. Monios, G. Wilmsmeier, Deep adaptation to climate change in the maritime transport sector–a new paradigm for maritime economics?, Maritime Policy & Management 47 (7) (2020) 853–872.

[79] J. S. L. Lam, J. A. Lassa, Risk assessment framework for exposure of cargo and ports to natural hazards and climate extremes, Maritime Policy & Management 44 (1) (2017) 1–15.

[80] OWD, Trade as share of GDP – 1960 to 2020, accessed: 2021-12-19 (2021). URL https://ourworldindata.org/grapher/trade-as-share-of-gdp?tab=chart

[81] L. Wenz, A. Levermann, Enhanced economic connectivity to foster heat-stress-related losses, Science Advances 2 (6) (2016) e1501026. doi:10.1126/sciadv.1501026.

[82] J. Maluck, R. V. Donner, A network of networks perspective on global trade, PloS one 10 (7) (2015) e0133310.

[83] A. Costinot, A. Rodríguez-Clare, Trade theory with numbers: Quantifying the consequences of globalization, in: Handbook of international economics, Vol. 4, Elsevier, 2014, pp. 197–261.

[84] E. Ortiz-Ospina, D. Beltekian, Trade and globalization, accessed: 2021-11-05 (Nov 2018).
URL https://ourworldindata.org/trade-and-globalization

[85] N. Pavcnik, The impact of trade on inequality in developing countries, Tech. rep., National Bureau of Economic Research (2017).

[86] Y. V. Fyodorov, B. A. Khoruzhenko, Nonlinear analogue of the may- wigner instability transition, Proceedings of the National Academy of Sciences 113 (25) (2016) 6827–6832.

[87] A. Kharrazi, E. Rovenskaya, B. D. Fath, Network structure impacts global commodity trade growth and resilience, PloS one 12 (2) (2017) e0171184.

[88] M. Kummu, P. Kinnunen, E. Lehikoinen, M. Porkka, C. Queiroz, E. Röös, M. Troell, C. Weil, Interplay of trade and food system resilience: Gains on supply diversity over time at the cost of trade independency, Global Food Security 24 (2020) 100360.

[89] J. Moran, J.-P. Bouchaud, May's instability in large economies, Physical Review E 100 (3) (2019) 032307.

[90] M. Lenzen, K. Kanemoto, D. Moran, A. Geschke, Mapping the structure of the world economy, Environmental science & technology 46 (15) (2012) 8374–8381.

[91] T. E. Zabelsky, 2002 economic census: Transportation 2002 commodity flow survey, Tech. rep., U.S. Department of Commerce and U.S. Department of Transportation (2002).

[92] M. Research, Technology, Logistics costs and u.s. gross domestic product, accessed: 2019-02-02.
URL `https://ops.fhwa.dot.gov/freight/freight_analysis/econ_methods/lcdp_rep/index.htm#Toc112735358`

[93] K. R. Knapp, M. C. Kruk, D. H. Levinson, H. J. Diamond, C. J. Neumann, The international best track archive for climate stewardship (ibtracs) unifying tropical cyclone data, Bulletin of the American Meteorological Society 91 (3) (2010) 363–376.

[94] K. R. Knapp, H. J. Diamond, J. P. Kossin, M. C. Kruk, C. J. I. Schreck, International best track archive for climate stewardship (ibtracs) project, version 4.wp, https://doi.org/10.25921/82ty-9e16, accessed: 2020-03-03.

[95] J. Wu, D. Zhang, C. Wan, Resilience assessment of maritime container shipping networks–a case of the maritime silk road, in: 2019 5th Inter-

national Conference on Transportation Information and Safety (ICTIS), IEEE, 2019, pp. 252–259.

[96] Y. Okuyama, How shaky was the regional economy after the 1995 kobe earthquake? a multiplicative decomposition analysis of disaster impact, The Annals of Regional Science 55 (2) (2015) 289–312.

[97] S. E. Chang, Disasters and transport systems: loss, recovery and competition at the port of kobe after the 1995 earthquake, Journal of transport geography 8 (1) (2000) 53–65.

[98] P. Landi, H. O. Minoarivelo, Å. Brännström, C. Hui, U. Dieckmann, Complexity and stability of adaptive ecological networks: a survey of the theory in community ecology, Systems analysis approach for complex global challenges (2018) 209–248.

[99] C. van Altena, L. Hemerik, P. C. de Ruiter, Food web stability and weighted connectance: the complexity-stability debate revisited, Theoretical Ecology 9 (1) (2016) 49–58.

Conclusion

5 Results

The scope of this thesis is to reveal a deep and enriched understanding of the overall impacts of weather extremes on economic systems. This includes the computation of direct local effects and resulting higher-order repercussions, and the exploration of plausible adaptation strategies. To derive such insights, I develop and use highly regionally and temporally resolved dynamical models during my research. In the following, I present my research findings in comprehensive answers to my three research questions.

5.1 Impact

How do weather extremes impact local economic performance?

During climate-related extreme events, local production is reduced, which is referred to as direct losses. My results depict that regional occurrence of weather extremes and resulting impacts differ between disaster categories. Furthermore, the amplitude of direct losses is largely heterogeneously distributed in time and space depending on heat stress, tropical cyclones, or river floods. Using a temperature-productivity relation and near-future climate projections, I find that global direct output losses caused by heat stress increase by 47% between 2000–2039 [A]. This translates to a direct loss increase of about USD127 bn per K of global warming. However, heat stress-induced economic losses vary between regions. Across 84% of the regions, the annual economic output loss is less than one bn USD. In contrast, some economically strong nations are frequently affected by heat waves, such as Saudi Arabia, China, the USA, and India. Their estimated annual production losses range in the two-digit billions USD. Regarding direct output losses relative to GDP, countries of the Sahel, the Arabian Peninsula, and South Asia are affected the strongest.
Using a tropical cyclone emulator of Geiger et al. [2018], I find that tropical cyclones cause a short, strong peak in production losses of affected areas [C]. The single-case study on Hurricane Sandy [B] depicts similar results; here, hurricane-induced initial production

failures of 80.2% and 69.3% are estimated for US-states New York and New Jersey, respectively. However, while the short-term production reduction may be substantial for impacted regions, the annual global direct output losses due to tropical cyclones are on average about 20 times smaller than from heat stress [C].
A region affected by river floods exhibits a different pattern of production decline compared to tropical storm impacts [C]. River floods' resulting regional production reductions depict a broader time distribution. This may be explained by the geographic and temporal extent of the different disaster categories. According to my calculations, annual global and regional direct losses from river floods vary widely. Thus, global direct production losses are about 80 times larger in high-impact years than in low-impact years. In contrast, direct production losses from heat stress exhibit a smaller distribution range from -28% to +33% around average.
I compute the local economic impacts of consecutive disasters of the three disaster categories by aggregating the corresponding temporal and regional direct production losses. It is excluded that direct output losses can exceed 100% of the initial production. The computed annual global direct production losses due to consecutive disasters range from USD206 bn to USD985 bn and have a median value of USD361 bn. I further discuss the economic repercussions of extreme events within the complex trading network and their interactions with each other in section 5.2.

Besides local productivity reduction, capital may be damaged due to weather extremes as well. NatCatService of MunichRe reports that 88 hurricanes with landfall caused 3.24% of cumulative normalized capital damage over 35 years in the USA. To estimate resulting growth losses, I use a classical one-channel growth model, extended with a basic insurance scheme [D]. In this growth model, impacts of individual storms and productivity recoveries are temporally resolved. I find that the size and time point of a shock affect the temporal evolution of production and thus impact economic growth. Furthermore, I implement the Gini index[2] as a metric of shock heterogeneity (shock size imbalance). The more unequal shock sizes are distributed among the events, the more heterogeneous the ensemble is and the higher the corresponding Gini index. While simulating economic growth perturbed by shock ensembles with different shock size imbalances, I find that hurricane-induced growth losses increase with higher shock heterogeneity. That means that time series with (almost) equal-sized shocks cause lower growth losses than those with many tiny and a few huge shocks[3]. This arises from incomplete recovery. The probability that an extreme event occurs during the recovery phase of a former shock increases with the recovery time and thus with the shock size. By higher shock heterogeneity, those incomplete recovery events become more frequent. The results suggest that the particular

[2] One can compute the Gini index of a set of shock sizes by creating the corresponding Lorenz curve, calculating the area beneath this curve and compare the area to a perfect equally distributed Lorenz curve.

[3] The number of events and total cumulative capital damage are kept constant between simulations.

shock timing and size caused by weather extremes should be considered while calculating economic growth impact.

5.2 Distribution

How are repercussions of extreme events distributed in the economic network?

The main tool to answer this question is the loss-propagation model *Acclimate*, which simulates a complex network of economic agents (nodes) and their trading flows (linkages). The network can be perturbed by direct output losses of firms [A, B, C] or restrictions of product flows [E, F]. Locally optimizing economic agents react myopically to fluctuations in demand, supply, and prices, resulting in local market responses to direct losses and resulting indirect impacts at each time step (days). The responses are aggregated, analyzed, and interpreted at the level of firms, regions (e.g. Chinese provinces), nations (e.g. the USA), economic blocs (e.g. the EU), or globally.

Economic repercussions, caused by extreme weather-induced production reduction, propagate as ripples upstream and downstream along the supply chain [A, B, C]. During a disaster, the demand of affected firms declines due to direct production reduction. This virtually immediate demand reduction is a first-order upstream effect and causes a short-term decrease in trading and consumer prices, resulting in a brief higher consumption level. Subsequently, my computations show a significantly longer period of price inflation due to two identified network effects. On the one hand, production losses of directly affected firms downstream the supply chain, causing supply shortages and rising prices. On the other hand, firms with impaired supply try to substitute their failing suppliers, thus shifting their demand to less perturbed firms. This higher-order upstream effect causes local price inflation. As a result, substituting firms may increase their production in quantity and value (quantity to current prices). I find that even some countries with notable direct extreme weather impacts (e.g. Spain or Greece experiencing heat waves) are able to increase their production value due to higher prices [A]. Furthermore, my calculations depict that while the global temperature rises, heat stress-induced changes in global production value increase by 56% between 2000–2039.
Although there is a possible positive effect on the (regional) output value, the regions' welfare mostly declines [A, B, C]. Consumers, which are at the end of the supply chain, face shortages of goods and services, and inflation in prices. They can only adapt with certain flexibility to those changes[4] and thus decrease consumption. Economic repercussions due to heat stress are transferred through the economic network, causing (almost) every country's welfare to decline, even if some national production values increase [A]. I find that one K of additional global warming corresponds to an increase of heat stress-induced

[4] To reflect differences in regional and sectoral consumer price response, I use country and sector-specific consumption price elasticities.

consumption reduction by 0.18 percentage points (pp). That translates to a doubling in global consumption losses within the first four decades of this century, which is a disproportionate increase compared to +47% higher direct output losses. My results suggest that the ratio between direct production reduction and higher-order consumption losses is neither constant nor straightforward to assess. This applies globally as well as on a regional level. While the USA experiences four times higher direct output reductions per year than the EU, US consumers suffer fewer subsequent losses than consumers in the EU [C]. This is because prices in the EU increase particularly due to supply scarcity (downstream effect) and raised demand (upstream effect) and thus excessively affecting EU consumers. A region's cumulative loss (or gain) in consumption due to weather extremes depends on its trading connectivity to the affected firms [B]. A higher link strength tends to correlate with more losses.

Ripples of repercussions of different weather extremes may interact with each other in the economic network and enhance economic responses super-linear. In article C, I identify this effect and introduce the notion of *economic ripple resonance* to climate impact research. The effect arises, for example, if demand ripples, caused by two or more extreme events, coincide at a firm. The resulting demand for the firm adds up. But the additional costs for over-production to fulfill this demand increase non-linearly, making these extra costs disproportionately larger than the aggregated additional production costs of separate demands. Thereby, prices rise higher by overlapping ripples than by aggregation of separated ripples. Such economic ripple resonance mainly occurs by repercussions of consecutive disasters. Regarding regional and global consumption, my findings reveal that economic ripple resonance causes an enhancement in total consumption losses. That means that annual consumption losses caused by repercussions of consecutive disasters (total losses) are larger than the sum of annual consumption losses by the repercussions of individual disaster categories (aggregated losses)[5]. Further, the enhancement amplifies disproportionately with higher direct output losses respective consumption losses. That means that the discrepancy between total losses and aggregated losses increases with higher losses. The widening of this gap is defined by the loss amplification factor A. Globally I find that $A_{\text{global}} = 21\%$, i.e. an increase of 0.5 pp of aggregated consumption losses converts to a rise of ~0.6 pp in total consumption losses. While the intensity of economic ripple resonance is regionally heterogeneously distributed, every country depicts a loss enhancement and 82% of global production lies in regions with a positive amplification factor. The USA and the EU exhibit a similar loss amplification ($A_{\text{USA}} = 17\%$, $A_{\text{EU}} = 16\%$). China's economy responses intensely to overlapping ripples. On the one hand, China depicts a loss amplification of $A_{\text{CHN}} = 27\%$. On the other hand, in some simulation runs, China has negative aggregated losses (i.e. consumption gains), which turn into total consumption losses for consecutive disasters. That means economic ripple resonance may

[5] Important to note that the annual direct output losses of the corresponding simulation pairs are equal.

even trigger a shift in regional coping reactions to economic repercussions due to weather extremes.

Next to local production reduction, perturbed transport of products and commodities may cause repercussions in the economic network. To analyze resulting higher-order effects from those events, I extend *Acclimate* with a geographical transportation network, which enables me to perturb trading routes or connections. Using this, I focus on regional consequences of sudden transportation blockages caused by a no-deal Brexit scenario [E]. Further, I analyze transport disturbances by observed West Pacific typhoons[6] and resulting regional and inter-regional economic responses [F]. Transport perturbation causes affected trading partners to reduce and redistribute their mutual demand. Firms with a substantial share of their supply chains using the perturbed trading route receive a sharp drop in demand. This results in an immediate production reduction in particularly affected areas: UK and Ireland during a no-deal Brexit [E], and China during a West Pacific typhoon [F]. Due to the absence of purchasers, affected firms lower offering prices. Thus, domestic market prices decline and macroeconomic output value decreases. Another result is that less directly affected regions receive a higher demand, e.g. non-EU European countries [E] or NAFTA[7] [F], and therefore increase production in the short run.
After this initial increase, there is a decrease in demand due to two effects. First, directly affected firms reduce their production due to lower demand and thus reduce demand to other firms as well. Second, due to perturbed transport, firms globally expect less manufacturing supply and therefor lower production and demand. In the aftermath of a transport disturbance, I find that demand of inter-regional trading partners increases, followed by production to rise globally [F]. Economic blocs go through this trading pattern multiple times within a typhoon season, where economic repercussions may add up. In the following section, I examine inferred coping mechanisms of economic blocs and regions.

5.3 Adaptation

How do and could societies adapt to weather extreme-induced repercussions?

In my research, I find evidence that economic trade networks exhibit an intrinsic adaptation strategy to trade disruptions caused by storms [F]. While typhoons disturb East Asian maritime trading routes, causing initial prices in domestic markets to fall and international trade to decrease, medium-term responses of economic blocs depict a positive trend. Despite typhoon-induced impairment of inter-regional trade, all economic blocs are able to

[6] Using real typhoon trajectories of IBTrACS, I compute time series of transport disturbances for West Pacific typhoon seasons 2000–2020.

[7] Computations base on the economic network of 2015. At that time, the economic bloc of Canada, Mexico, and the USA was referred to as North American Free Trade Agreement (NAFTA). The agreement was replaced by the United States-Mexico-Canada Agreement (USMCA) in 2020.

increase their exports in volume to other blocs over the year, compared to the economic baseline of 2015. Even China, whose maritime transportation routes are strongly affected by West Pacific typhoon seasons, exhibits an increase in export quantity. This coping mechanism indicates a degree of trade resilience to weather-related transport disruptions. Since the adaptation emerges from the network of locally optimizing economic agents itself, it appears to be an intrinsic characteristic of the network. A network analysis reveals that trade resilience has tended to strengthen over the years (regarding 2000–2015). Further it depicts that this arises from a higher node inter-connectivity and not from changed shares of network flow. Most economic blocs increase their node inter-connectivity, i.e. number of trade connections to other blocs per firm. Thus, the set on possible substitutes for supply and demand grew. Asian regions like China, Association of Southeast Asian Nations (ASEAN), or South Asian Association for Regional Cooperation (SAARC) turn from net-export losers to gainers by expanding and diversifying their trading connections. However, trade resilience has its limitations. On the one hand, the export gain does not convert to export value gain (export at current prices) everywhere. For example, China and the Arab League have slight export value losses due to falling trade prices. Nevertheless, losses decrease as node inter-connectivity increases. On the other hand, there are too important trading links whose perturbation is too severe to adapt to. For example, Chinese firms use two sea routes to export to NAFTA: the East China Sea and the South China Sea. Most Chinese firms use the former maritime route to export to NAFTA. As a result, if the East China Sea is blocked, China will exhibit export losses that cannot be compensated. However, my research indicates that increasing network-connectivity by diversifying trading partners and trading routes is a potent measure to adapt to extreme weather-induced trade repercussions [E, F].

Regarding economic development, I find that long-term growth losses caused by hurricane-induced capital damage can be reduced by a macroeconomic insurance scheme [D]. Using a closed economy growth model, which I extend with insurance dynamics, I compare economies that face the same time series of weather extremes, with and without insurance coverage. My results depict that the former has significant growth benefits towards the latter. For example, for historical hurricane distribution in the USA (1980–2014), annual growth is reduced by 0.048 pp in the uninsured scenario, according to my calculations. Compared to this, insured damaged capital could decrease annual growth losses by factor two (half-insured) or even factor ten (fully insured). Even when the adverse pay-in effects on growth are considered, insurance coverage remains a macroeconomic reasonable adaptation measure. Within observed parameter sets[8], consumption losses due to hurricanes can be mitigated as well.

[8] For hypothetical, unobserved parameter sets, consumption disadvantages are possible which arise from non-linear growth response to shock heterogeneity.

Depending on the climate change projection approach and degree of warming, growth losses could increase by 10%, 146%, or even 522% compared to growth losses in historical settings. In order to cope with those additional losses, insurance coverage needs to increase by about 8 pp, 34 pp, or 49 pp, respectively. It is important to emphasize that growth losses do not vanish, but rather they are reduced to historical levels. The results point out that an insurance scheme may be an effective adaptation measure, although it cannot counteract all the perturbations.

In addition to intrinsic resilience within the trade network and potential coping strategies by insurance schemes, further adaptations mechanism to weather extremes can be drawn from my research. My derived conclusions, based on results of articles A, B, and C, should not been seen as strict advice for any economic or political actor but rather encourage to see adaptation efforts in a connected-world framework.
An economically tightly linked bloc, e.g. US states or Chinese provinces, can mitigate losses by using non or less affected firms as substitutes for perturbed firms within the bloc. This mechanism could be implemented by regions with returning disaster seasons and their trading partners, which creates a win-win situation. The unaffected trading partner increases production to substitute for deficits in the affected region. As a result, those suffer less from supply shortages. A stronger economic relationship where both partners are exposed to weather extremes, which occur at different times of the year, could be a possible adaptation strategy as well. This would ensure that one could provide economic substitution during local disasters to the other and vice versa.
A highly interlinked region (e.g. the EU) that is exposed to small direct output losses can be disproportionately affected by disasters elsewhere through upstream and downstream effects. In particular, substantial price increases cause higher consumption losses. On the surface, it could be presumed that a significant reduction in node connections, i.e. compartmentalization, would be an appropriate adaptation strategy for this. However, three of my insights argue against this possible assessment. First, if economically isolated regions suffer from a disaster, short-term supply substitution to ensure production and consumer supply is missing, probably leading to more devastating disaster aftermath. Second, in a strongly interconnected trading network, ripples can reach (almost) any point in the economic network via neighbor or super-neighbor nodes. Thus, complete secure isolation is not possible nor is it practical. Third, my results suggest that broader trading diversification could more effectively distribute repercussions among economic agents globally. However, diversifying purchasers and suppliers is not a panacea. While an extreme weather event with local and time-limited direct output losses (e.g. tropical cyclone) can be buffered in the trading network, longer-lasting and cross-regional direct production losses (e.g. due to consecutive disasters) cannot be mitigated in highly interconnected networks and rather amplify consumption losses.

Discussion of costs of adaptation measures must consider the loss enhancement and amplification by consecutive disasters caused by economic ripple resonance. Adaptation costs due to extreme events could be strongly underestimated if only considered by itself and by neglecting repercussions within the global economic network. Economic ripple resonance could influence cost-benefit analyses between mitigation and adaptation measures.
As mentioned, economic repercussions (and their interaction) may cause a variety of responses along the supply chain. Thus, explicit regional consequences are often hard to predict. Another option to mitigate network-related losses is to minimize the extent of repercussion entering the supply chain. Increased adaptation to local extreme events, such as dams against floods or storm-resistant infrastructure, can minimize local production damage. The less local production is perturbed, the lower resulting ripple effects along supply chains and impact on consumption elsewhere. In addition, a fast reconstruction contributes to a shorter persistence of ripples in the economic network. The current dense trading network makes the reduction of local impacts of weather extremes a global challenge. Hence, it appears to make economic sense that adaptation and rebuilding costs are borne at a global level.

6 Discussion

Weather extremes, isolated or as consecutive disasters, cause locally direct output losses that are regionally and temporally broadly spread and propagate as ripples along supply chains. Using weather-productivity relations, I compute resulting regional direct and indirect deviations of production, consumption, trade, and prices, which can reach the magnitude of some percent relative to the baseline. During economic ripple resonance, repercussions in the supply chain overlap and intensify consumption losses. From my findings, I conclude that preventing ripples in the supply chain (local disaster adaptation) and risk-aware and diversified trading have the potential to reduce welfare losses.
Disruptions of trade routes initially lead to demand and supply insecurities. However, I find that regions exhibit increased annual exports in the perturbation aftermath, which is interpreted as trade resilience and arises from a high diversification of network connections. Regarding economic development, I show that hurricane-damaged capital hinders long-term growth. Further, I reveal that a higher heterogeneity of a shock ensemble increases economic growth losses. Precautionary saving funds (e.g. insurance) can be a possible adaptation strategy against growth losses, although it does not compensate for all losses.

Limitations

Modeling processes, whether physical, socio-economic, or others, are always constrained by limitations. My model-based research is no exception; hence, I outline the main limitations

in the following. Boundaries of individual studies are discussed in detail in the respective articles.

The relations of sectoral and regional production and physical perturbation drivers are still a subject of research. Here, my approaches on weather extremes and economic performances enable me to estimate direct impacts, but they are bound to uncertainties of ongoing research topics. I generalize a temperature-productivity correlation only found for Caribbean countries [Hsiang, 2010] to every region [A, C]. Related studies depict as well that heat stress has an effect on productivity which is regionally bounded [Burke et al., 2015; Graff Zivin et al., 2018; Orlov et al., 2019]. Further, I derive the direct productivity impacts of weather extremes from affected areas and their corresponding population share [A, C]. Potentially required local recovery depends on the severity of the extremes, e.g. flood depth or wind speed. Therefore, damages to local infrastructure or workers' health are not explicitly considered. That means that the used conservative approach produces lower bounds for direct output losses. In article B, the production perturbation applies for every regional sector equally. This is justifiable since an at least once-in-a-century event like Hurricane Sandy will have an impact on all areas of work, even if it is just the interrupted trip to work. I show that destroyed capital and their rebuilding process affect the economy's evolution [D]. While neglecting the impact on potential other channels, e.g. labor, my results could underestimate growth losses. My novel approach to model typhoon-induced transport perturbation is based on reported experiences [F]. However, sensitivity analyses of perturbation parameters, wind speed threshold and passage flow, do not show significant changes in results.

Using the economic network model *Acclimate*, I examine short-term impacts due to weather extremes. Thereby, medium to long-term socio-economic processes, e.g. large-scale production allocation or social development, are not considered in the model design. This should be taken into account when assessing the elaborated adaptation measures. Further, two production assumptions in *Acclimate* are subject to discussion for my results. First, without perturbation, any firm produces its goods or services at the same rate for every time step (day). While this is quite reasonably valid for some producing industries, it is a simplification for the agricultural sector. Harvests are regionally distributed and take place at specific times of the year. Therefore, the timing of a local weather extreme determines the vulnerability of the regional agricultural sector. Due to this fact, the approach for *Acclimate* is a more conservative approach regarding the impact on the food sectors. Second, it is assumed that the daily changes of demand, products allocation, and supplies are done with very little logistical cost. Switching large production orders can imply price increases and medium to long-term supply shortages, e.g. 2020/21 global chip shortage [Wu et al., 2021]. Since microeconomic agents in *Acclimate* are very flexible, the network may respond to transportation perturbation with decreased instead of increased local prices. In my thesis, the complex economic networks I focus on should be understood as "reactive and flexible networks of well-functioning economies". This conservative

approach tends to underestimate the losses developed in the network. Hence, it points out the importance of adaptation measures to weather extremes and mitigation of climate change.
The main goal of my thesis is to derive an enriched understanding of the impacts of weather extremes in economic networks. For this, I focus on qualitative trends and deeper dynamical mechanisms. Hence my results shall not be seen as quantitative predictions. In this respect, the indicated limits of the physical-socio-economic relations and modeling are reasonable.

Further research

As discussed above, constraints on my conclusions arise from uncertain or insufficient correlations between physical drivers and short-term socio-economic impacts. While econometric studies have improved on such correlations in recent years, it still lacks comprehensive regional and sectoral coverage. Improvements in this research field could yield a more in-depth and precise analysis of weather extreme-induced impacts on the complex trading network.
The research presented in this thesis focuses mainly on ensembles of time series of weather extremes (except articles B and E). Thereby, general responses of the economic network to realistic sequences of natural disasters are evaluated. Network nodes, i.e. firms and consumers, are unequally embedded within the trade network. For example, while half of the firms have 59 or fewer purchasers, 1% of firms supply at least 2,000 other economic agents. Following complex network studies [Ravasz and Barabási, 2003; Park and Barabási, 2007], it can be assumed that the different inter-connectivity of nodes can lead to different response patterns and ripple propagation. Systematic studies on network nodes could illuminate this topic and define important node characteristics. Building on a single case event, like Hurricane Sandy in article B, and alternating the affected nodes could be a possible study design.
Regarding the economic network as a complex system, results of article F indicate that the more complex the network (higher node inter-connectivity), the more stable it is (trade resilience). This statement is still debated in recent complexity research [Landi et al., 2018; Fyodorov and Khoruzhenko, 2016; Moran and Bouchaud, 2019]. Further network analyses of *Acclimate* may find more parameters to (de-) stabilize the complex economic system. Additionally, studies could identify critical tipping points [Krönke et al., 2020; Kostanjčar et al., 2016; Guleva, 2020] for resilience or vulnerability with respect to direct output losses, trade disruptions, or other factors.
Qualitative analyses on regional heterogeneity of direct output losses or indirect network responses are main subjects of my research. A quantitative study of the disparity in vulnerability to weather extremes and their distribution in the network could lead to regionally differentiated adaptation measures. Further, every society consists of different income groups [Kuznets, 1955], which should be considered in forthcoming research.

Building on article C, the intensity of the economic ripple resonance effect on diverse consumer groups can be discussed. Research on possible amplification or mitigation of intra-regional and inter-regional inequality due to weather extremes gives insights on more effective and necessary adaptation measures.
My studies mostly address direct impacts of weather extremes on production or trade. In addition, the energy supply of firms and consumers can be directly affected as well [Turner et al., 2019; Byers et al., 2020]. The economic and energy networks can be modeled as two coupled complex networks. Thus, it could be examined how ripples transfer between these networks and whether there are energy-economic ripple resonance effects. Further, critical junctions and adaptation measures for the energy-economy system may be evaluated.
Regarding direct impacts, I focus in this thesis on the three separated economic quantities: regional production, capital, and transportation. However, an extreme event can affect more than one channel. Therefore, including more direct impact channels may enhance the comprehension of socio-economic responses to weather extremes. As a measure for those responses, I focus mainly on production, consumption, and trade. Thereby, other human needs or essential economic developments may be missed. Respecting this, further studies focusing on complementary socio-economic aspects are relevant to obtain a broader understanding of extreme weather impacts.

Final remarks

Although the body of studies on impacts of weather extremes grew in recent years, global but regionally disaggregated results on economic performances due to extreme events are still rare. In this thesis, I compute regional direct output losses caused by heat stress, river floods, and tropical cyclones. Further, I study the temporal and spatial distribution as well as the magnitudes of the resulting losses. By overlapping the three mentioned disaster categories, analyses on repercussions of consecutive disasters add newest insights to recent climate impact research. Using *Acclimate*, a complex network of myopically deciding economic agents with endogenous price dynamics, I simulate the resulting economic ripple propagation along supply chains. Regional net-winners and net-losers arise from resulting higher-order effects in production and consumption. Further, I reveal that the economic responses may change over time and depend on ripple amplitudes. This is in line with former studies that show that ripple effects in the trading network cause sectoral and regional loss spillovers [Hewings and Mahidhara, 2019; Kunimitsu et al., 2013]. Here, I give a qualitative description and explanation of the three phases of such economic ripples. The understanding of ripple dynamics is urgently needed as it seems that the economic ripple effect will increase under climate change [Zhang et al., 2018]. While examining consecutive disasters, I find that economic ripples may interact in the global trade network, causing an overall intensified economic response, like an enhancement of regional and global consumption losses. Further, my analysis reveals that additional direct losses, e.g. due to climate change, amplify consumption losses over-proportionally. My results suggest

that additional costs caused by economic ripple resonance should be priced into further adaptation cost calculations.

Political and economic actors rely their decisions on measures to combat the climate crisis partly on findings of IAMs [Rose et al., 2017]. However, these models lack proper extreme weather resolution and thus probably underestimate their effects [Hallegatte et al., 2007; Otto et al., 2020]. I implement a method that explicitly resolves the temporal dimension of hurricane impacts and aftermaths on capital, production, and growth. I point out that weather extremes' timing and shock severity have a non-linear impact on growth. Next to this, I introduce the Gini index as a characteristic of damage ensemble to explain how shock heterogeneity hinders economic development. My macroeconomic research implies that insurance is beneficial to consumers and can mitigate long-term growth losses to some extent, with which it contributes to adaptation research (e.g. particular on insurance effects [Charpentier, 2008; Krieger and Demeritt, 2015]).

Even though a no-deal Brexit was politically prevented [European Commission, 2020], UK leaving the EU causes severe damage to its economy in medium-term [OBR, 2021]. In my study on a hypothetical no-deal Brexit, I compute cascading effects caused by trade restrictions, resulting in economic disadvantages for the UK and the EU in the longer run. This adds onto other short to long-term scientific predictions, e.g. of Dhingra et al. [2016], Chang [2018], and Kierzenkowski et al. [2016].

Studies on perturbations of maritime transport often focus on port disruption [Thekdi and Santos, 2016; Zhang et al., 2020] and liner shipping scheduling [Brouer et al., 2013; Li et al., 2016]. However, Lam and Lassa [2017] argue that the research field still exhibits some gaps. My research partly fills these gaps by adding an analysis of typhoon-induced transportation disturbances and resulting repercussions along supply chains. In addition, computed inter-regional trade responses reveal coping mechanisms to overcome supply and demand shortfalls.

In summary, my dissertation focuses on regionally heterogeneous direct losses in production, capital, or transportation caused by weather extremes and their resulting higher-order impacts. On the one hand, those losses can add up in time and produce longer-term economic disadvantages. On the other hand, demand and supply ripples propagate along the economic network, causing deviations in consumption and trade. Network-intrinsic resilience mechanisms, lowering direct vulnerability towards extreme events, and coping mechanisms at the end of the supply chain may diminish losses but not completely compensate for them. My findings advocates that the dynamically and temporally resolution of processes is relevant for understanding and evaluating complex socio-economic systems. Further evolution of dynamic models in physical, socio-economic, and interdisciplinary areas and their coupling will be a key element in comprehending and improving societies within a highly interconnected world.

Bibliography

M. Ahern, R. S. Kovats, P. Wilkinson, R. Few, and F. Matthies. Global health impacts of floods: epidemiologic evidence. *Epidemiologic Reviews*, 27(1):36–46, 2005.

C. A. Anderson, K. B. Anderson, N. Dorr, K. M. DeNeve, and M. Flanagan. Temperature and aggression. In *Advances in Experimental Social Psychology*, volume 32, pages 63–133. Elsevier, 2000.

L. Andrade, J. O'Dwyer, E. O'Neill, and P. Hynds. Surface water flooding, groundwater contamination, and enteric disease in developed countries: A scoping review of connections and consequences. *Environmental Pollution*, 236:540–549, 2018.

M. Auffhammer. Quantifying economic damages from climate change. *Journal of Economic Perspectives*, 32(4):33–52, 2018.

M. Auffhammer, P. Baylis, and C. H. Hausman. Climate change is projected to have severe impacts on the frequency and intensity of peak electricity demand across the United States. *Proceedings of the National Academy of Sciences*, 114(8):1886–1891, Feb. 2017.

M. Berlemann and D. Wenzel. Hurricanes, economic growth and transmission channels: Empirical evidence for countries on differing levels of development. *World Development*, 105:231–247, 2018.

G. I. Bhaskara and V. Filimonau. The COVID-19 pandemic and organisational learning for disaster planning and management: A perspective of tourism businesses from a destination prone to consecutive disasters. *Journal of Hospitality and Tourism Management*, 46:364–375, 2021.

T. Bódai and T. Tél. Annual variability in a conceptual climate model: Snapshot attractors, hysteresis in extreme events, and climate sensitivity. *Chaos: An Interdisciplinary Journal of Nonlinear Science*, 22(2):023110, 2012.

T. A. Brás, J. Seixas, N. Carvalhais, and J. Jägermeyr. Severity of drought and heatwave crop losses tripled over the last five decades in Europe. *Environmental Research Letters*, 16(6):065012, 2021.

B. D. Brouer, J. Dirksen, D. Pisinger, C. E. Plum, and B. Vaaben. The Vessel Schedule Recovery Problem (VSRP)–A MIP model for handling disruptions in liner shipping. *European Journal of Operational Research*, 224(2):362–374, 2013.

M. Burke, S. M. Hsiang, and E. Miguel. Global non-linear effect of temperature on economic production. *Nature*, 527(7577):235–239, 2015.

E. A. Byers, G. Coxon, J. Freer, and J. W. Hall. Drought and climate change impacts on cooling water shortages and electricity prices in Great Britain. *Nature Communications*, 11(1):1–12, 2020.

W. W. Chang. Brexit and its economic consequences. *The World Economy*, 41(9):2349–2373, 2018.

A. Charpentier. Insurability of climate risks. *The Geneva Papers on Risk and Insurance-Issues and Practice*, 33(1):91–109, 2008.

V. N. Chau, J. Holland, S. Cassells, and M. Tuohy. Using GIS to map impacts upon agriculture from extreme floods in Vietnam. *Applied Geography*, 41:65–74, 2013.

Y. Chen, Z. Liao, Y. Shi, Y. Tian, and P. Zhai. Detectable increases in sequential flood-heatwave events across China during 1961–2018. *Geophysical Research Letters*, 48(6): e2021GL092549, 2021.

M. Claussen, L. Mysak, A. Weaver, M. Crucifix, T. Fichefet, M.-F. Loutre, S. Weber, J. Alcamo, V. Alexeev, A. Berger, et al. Earth system models of intermediate complexity: closing the gap in the spectrum of climate system models. *Climate Dynamics*, 18(7): 579–586, 2002.

CRED. The human cost of natural disasters: a global perspective, 2015. URL http://www.cred.be/sites/default/files/The_Human_Cost_of_Natural_Disasters_CRED.pdf.

CRED. CRED Crunch 62 - 2020 Annual Report , 2021. URL https://cred.be/sites/default/files/CredCrunch62.pdf.

E. Cuevas. An agent-based model to evaluate the COVID-19 transmission risks in facilities. *Computers in Biology and Medicine*, 121:103827, 2020.

H. Dawid, P. Harting, S. Van der Hoog, and M. Neugart. Macroeconomics with heterogeneous agent models: fostering transparency, reproducibility and replication. *Journal of Evolutionary Economics*, 29(1):467–538, 2019.

M. C. de Ruiter, A. Couasnon, M. J. Homberg, J. E. Daniell, J. C. Gill, and P. J. Ward. Why we can no longer ignore consecutive disasters. *Earth's Future*, 8(3):e2019EF001425, 2020.

M. Dell, B. F. Jones, and B. A. Olken. Temperature and income: reconciling new cross-sectional and panel estimates. *American Economic Review*, 99(2):198–204, 2009.

S. Dhingra, G. I. Ottaviano, T. Sampson, and J. v. Reenen. The consequences of Brexit for UK trade and living standards. *BREXIT*, 2016.

G. N. Doering, I. Scharf, H. V. Moeller, and J. N. Pruitt. Social tipping points in animal societies in response to heat stress. *Nature Ecology & Evolution*, 2(8):1298–1305, 2018.

G. Dosi, M. C. Pereira, A. Roventini, and M. E. Virgillito. The effects of labour market reforms upon unemployment and income inequalities: an agent-based model. *Socio-Economic Review*, 16(4):687–720, 2018.

F. Dottori, W. Szewczyk, J.-C. Ciscar, F. Zhao, L. Alfieri, Y. Hirabayashi, A. Bianchi, I. Mongelli, K. Frieler, R. A. Betts, et al. Increased human and economic losses from river flooding with anthropogenic warming. *Nature Climate Change*, 8(9):781–786, 2018.

J.-L. Dufresne, M.-A. Foujols, S. Denvil, A. Caubel, O. Marti, O. Aumont, Y. Balkanski, S. Bekki, H. Bellenger, R. Benshila, et al. Climate change projections using the IPSL-CM5 Earth System Model: from CMIP3 to CMIP5. *Climate Dynamics*, 40(9):2123–2165, 2013.

O. Dun. Migration and displacement triggered by floods in the Mekong Delta. *International Migration*, 49:e200–e223, 2011.

J. P. Dunne, J. G. John, A. J. Adcroft, S. M. Griffies, R. W. Hallberg, E. Shevliakova, R. J. Stouffer, W. Cooke, K. A. Dunne, M. J. Harrison, et al. GFDL's ESM2 global coupled climate–carbon earth system models. Part I: Physical formulation and baseline simulation characteristics. *Journal of Climate*, 25(19):6646–6665, 2012.

J. P. Dunne, R. J. Stouffer, and J. G. John. Reductions in labour capacity from heat stress under climate warming. *Nature Climate Change*, 3(6):563–566, 2013.

M. Ermolova, A. Leonidov, V. Nechitailo, H. Penikas, N. Pilnik, and E. Serebryannikova. Agent-based model of the Russian banking system: Calibration for maturity, interest

rate spread, credit risk, and capital regulation. *Journal of Simulation*, 15(1-2):82–92, 2021.

European Commission. EU-UK trade and cooperation agreement, Dec 2020. URL https://ec.europa.eu/commission/presscorner/detail/en/ip_20_2531. Accessed: 2021-12-16.

G. Fagiolo, M. Guerini, F. Lamperti, A. Moneta, and A. Roventini. Validation of agent-based models in economics and finance. In *Computer Simulation Validation*, pages 763–787. Springer, 2019.

W. G. Fernandez, S. Galea, J. Miller, J. Ahern, W. Chiang, E. L. Kennedy, and J. Garritano. Health status among emergency department patients approximately one year after consecutive disasters in New York City. *Academic Emergency Medicine*, 12(10):958–964, 2005.

C. B. Field, V. Barros, T. F. Stocker, and Q. Dahe. *Managing the risks of extreme events and disasters to advance climate change adaptation: special report of the intergovernmental panel on climate change*. Cambridge University Press, 2012.

Y. V. Fyodorov and B. A. Khoruzhenko. Nonlinear analogue of the May-Wigner instability transition. *Proceedings of the National Academy of Sciences*, 113(25):6827–6832, 2016.

T. Geiger, K. Frieler, and D. N. Bresch. A global historical data set of tropical cyclone exposure (TCE-DAT). *Earth System Science Data*, 10(1):185–194, 2018.

T. Geiger, J. Gütschow, D. N. Bresch, K. Emanuel, and K. Frieler. Double benefit of limiting global warming for tropical cyclone exposure. *Nature Climate Change*, 11(10): 861–866, 2021.

A. Gissing, M. Timms, S. Browning, R. Crompton, and J. McAneney. Compound natural disasters in Australia: a historical analysis. *Environmental Hazards*, pages 1–15, 2021.

P. A. Gonzalez-Rivas, S. S. Chauhan, M. Ha, N. Fegan, F. R. Dunshea, and R. D. Warner. Effects of heat stress on animal physiology, metabolism, and meat quality: A review. *Meat Science*, 162:108025, 2020.

J. Graff Zivin, S. M. Hsiang, and M. Neidell. Temperature and human capital in the short and long run. *Journal of the Association of Environmental and Resource Economists*, 5 (1):77–105, 2018.

A. Grinsted, J. C. Moore, and S. Jevrejeva. Projected Atlantic hurricane surge threat from rising temperatures. *Proceedings of the National Academy*, 110(14):5369–5373, 2013.

S. Gualdi and A. Mandel. On the emergence of scale-free production networks. *Journal of Economic Dynamics and Control*, 73:61–77, 2016.

D. Guha-Sapir. EM-DAT: The Emergency Events Database, 2017. URL www.emdat.be. Accessed: 2021-12-05.

V. Y. Guleva. Estimation of tipping points for critical and transitional regimes in the evolution of complex interbank network. In *International Conference on Computational Science*, pages 432–444. Springer, 2020.

A. Gurgone, G. Iori, and S. Jafarey. The effects of interbank networks on efficiency and stability in a macroeconomic agent-based model. *Journal of Economic Dynamics and Control*, 91:257–288, 2018.

S. Hallegatte, J.-C. Hourcade, and P. Dumas. Why economic dynamics matter in assessing climate change damages: illustration on extreme events. *Ecological Economics*, 62(2): 330–340, 2007.

T. W. Hertel. *Global trade analysis: modeling and applications*. Cambridge university press, 1997.

G. J. Hewings and R. Mahidhara. Economic impacts: lost income, ripple effects, and recovery. In *The great flood of 1993*, pages 205–217. Routledge, 2019.

J. R. Hicks. Mr. Keynes and the "classics"; a suggested interpretation. *Econometrica: Journal of the Econometric Society*, pages 147–159, 1937.

S. Hsiang. Temperatures and cyclones strongly associated with economic production in the Caribbean and Central America. *Proceedings of the National Academy of Sciences*, 107(35):15367–15372, 2010.

IBTrACS. International Best Track Archive for Climate Stewardship (IBTrACS) Project, Version 4.WP. URL https://www.ncei.noaa.gov/access/metadata/landing-page/bin/iso?id=gov.noaa.ncdc:C01552. Accessed: 2021-07-03.

IPCC. AR5 Climate Change 2013: The Physical Science Basis. Contribution of Working Group I. *Fifth Assessment Report of the Intergovernmental Panel on Climate Change*, 2013.

IPCC. AR6 Climate Change 2021: The Physical Science Basis. Contribution of Working Group I. *Sixth Assessment Report of the Intergovernmental Panel on Climate Change*, 2021.

M. F. Jaumotte and M. C. Osorio. *Inequality and labor market institutions*. International Monetary Fund, 2015.

A. Jones, J. Hughes, N. Bellouin, S. Hardiman, G. Jones, J. Knight, S. Liddicoat, F. O'connor, R. J. Andres, C. Bell, et al. The HadGEM2-ES implementation of CMIP5 centennial simulations. *Geoscientific Model Development*, 4(3):543–570, 2011.

R. Kierzenkowski, N. Pain, E. Rusticelli, and S. Zwart. The economic consequences of Brexit: a taxing decision. *OECD Economic Policy Papers*, 2016.

T. R. Knutson, J. J. Sirutis, G. A. Vecchi, S. Garner, M. Zhao, H. S. Kim, M. Bender, R. E. Tuleya, I. M. Held, and G. Villarini. Dynamical downscaling projections of twenty-first-century atlantic hurricane activity: CMIP3 and CMIP5 model-based scenarios. *Journal of Climate*, 26(17):6591–6617, 2013.

Z. Kostanjčar, S. Begušić, H. E. Stanley, and B. Podobnik. Estimating tipping points in feedback-driven financial networks. *IEEE Journal of Selected Topics in Signal Processing*, 10(6):1040–1052, 2016.

S. Kotak, J. Larkindale, U. Lee, P. von Koskull-Döring, E. Vierling, and K.-D. Scharf. Complexity of the heat stress response in plants. *Current Opinion in Plant Biology*, 10 (3):310–316, 2007.

R. S. Kovats and S. Hajat. Heat stress and public health: a critical review. *Annual Reviews Public Health*, 29:41–55, 2008.

H. Krichene, T. Geiger, K. Frieler, S. Willner, I. Sauer, and C. Otto. Long-term impacts of tropical cyclones and fluvial floods on economic growth–Empirical evidence on transmission channels at different levels of development. *World Development*, 144: 105475, 2021.

K. Krieger and D. Demeritt. Limits of insurance as risk governance. 2015.

J. Krönke, N. Wunderling, R. Winkelmann, A. Staal, B. Stumpf, O. A. Tuinenburg, and J. F. Donges. Dynamics of tipping cascades on complex networks. *Physical Review E*, 101:042311, Apr 2020.

Y. Kunimitsu, K. Takahashi, T. Furubayashi, and T. Nakata. Economic ripple effects of bioethanol production in ASEAN countries: Application of inter-regional input-output analysis. *Japan Agricultural Research Quarterly*, 47(3):307–317, 2013.

S. Kuznets. Economic growth and income inequality. *American Economic Review*, 45(1): 1–28, 1955.

J. S. L. Lam and J. A. Lassa. Risk assessment framework for exposure of cargo and ports to natural hazards and climate extremes. *Maritime Policy & Management*, 44(1):1–15, 2017.

F. Lamperti, A. Roventini, and A. Sani. Agent-based model calibration using machine learning surrogates. *Journal of Economic Dynamics and Control*, 90:366–389, 2018.

P. Landi, H. O. Minoarivelo, Å. Brännström, C. Hui, and U. Dieckmann. Complexity and stability of adaptive ecological networks: a survey of the theory in community ecology. *Systems Analysis Approach for Complex Global Challenges*, pages 209–248, 2018.

G. Leng, M. Huang, Q. Tang, and L. R. Leung. A modeling study of irrigation effects on global surface water and groundwater resources under a changing climate. *Journal of Advances in Modeling Earth Systems*, 7(3):1285–1304, 2015.

M. Lenzen, K. Kanemoto, D. Moran, and A. Geschke. Mapping the structure of the world economy. *Environmental Science & Technology*, 46(15):8374–8381, 2012.

W. W. Leontief. The structure of American economy, 1919-1939: an empirical application of equilibrium analysis. Technical report, 1951.

C. Li, X. Qi, and D. Song. Real-time schedule recovery in liner shipping service with regular uncertainties and disruption events. *Transportation Research Part B: Methodological*, 93:762–788, 2016.

J.-Z. Li, S. Li, W.-Z. Wang, L.-L. Rao, and H. Liu. Are people always more risk averse after disasters? Surveys after a heavy snow-hit and a major earthquake in China in 2008. *Applied Cognitive Psychology*, 25(1):104–111, 2011.

R. E. Lucas Jr. An equilibrium model of the business cycle. *Journal of Political Economy*, 83(6):1113–1144, 1975.

B. Merz, G. Blöschl, S. Vorogushyn, F. Dottori, J. C. Aerts, P. Bates, M. Bertola, M. Kemter, H. Kreibich, U. Lall, et al. Causes, impacts and patterns of disastrous river floods. *Nature Reviews Earth & Environment*, pages 1–18, 2021.

D. Mitsova, A.-M. Esnard, A. Sapat, and B. S. Lai. Socioeconomic vulnerability and electric power restoration timelines in Florida: the case of Hurricane Irma. *Natural Hazards*, 94(2):689–709, 2018.

J. Moran and J.-P. Bouchaud. May's instability in large economies. *Physical Review E*, 100(3):032307, 2019.

B. Morrow and J. Lazo. Effective tropical cyclone forecast and warning communication: Recent social science contributions. *Tropical Cyclone Research and Review*, 4(1):38–48, 2015.

MunichRe. Disastrous flooding in western Germany – did climate change play a role?: Munich Re Topics Online, Jul 2021. URL https://www.munichre.com/topics-online/en/climate-change-and-natural-disasters/natural-disasters/floods/disastrous-flooding-in-western-germany.html. Accessed: 2021-12-19.

NHC. Saffir-Simpson Hurricane Wind Scale, 2021. URL https://www.nhc.noaa.gov/pdf/sshws.pdf. Accessed: 2021-12-19.

OBR. Economic and fiscal outlook. *Office for Budget Responsibility – Her Majesty's Treasury*, October 2021. URL https://obr.uk/efo/economic-and-fiscal-outlook-october-2021/.

A. Orlov, J. Sillmann, A. Aaheim, K. Aunan, and K. De Bruin. Economic losses of heat-induced reductions in outdoor worker productivity: a case study of Europe. *Economics of Disasters and Climate Change*, 3(3):191–211, 2019.

E. Ortiz-Ospina and D. Beltekian. Trade and Globalization, Nov 2018. URL https://ourworldindata.org/weve-updated-our-entry-on-trade-and-globalization#licence. Accessed: 2021-11-05.

C. Otto, S. Willner, L. Wenz, K. Frieler, and A. Levermann. Modeling loss-propagation in the global supply network: The dynamic agent-based model acclimate. *Journal of Economic Dynamics and Control*, 83:232–269, 2017.

C. Otto, F. Piontek, M. Kalkuhl, and K. Frieler. Event-based models to understand the scale of the impact of extremes. *Nature Energy*, 5(2):111–114, 2020.

OWD. Trade as share of GDP – 1960 to 2020, 2021. URL https://ourworldindata.org/grapher/trade-as-share-of-gdp?tab=chart. Accessed: 2021-12-19.

J. Park and A.-L. Barabási. Distribution of node characteristics in complex networks. *Proceedings of the National Academy of Sciences*, 104(46):17916–17920, 2007.

C. H. Paxton. Overview of potential hurricane death and damage in the Tampa Bay Region. In *Hurricane Risk*, pages 89–121. Springer, 2019.

V. Petoukhov, A. Ganopolski, V. Brovkin, M. Claussen, A. Eliseev, C. Kubatzki, and S. Rahmstorf. CLIMBER-2: a climate system model of intermediate complexity. Part I: model description and performance for present climate. *Climate Dynamics*, 16(1): 1–17, 2000.

R. A. Pielke, J. Gratz, C. W. Landsea, D. Collins, M. A. Saunders, and R. Musulin. Normalized hurricane damage in the United States: 1900–2005. *Natural Hazards Review*, 9(1):29–42, 2008.

R. S. Pindyck. The use and misuse of models for climate policy. *Review of Environmental Economics and Policy*, 2020.

M. Pregnolato, A. Ford, S. M. Wilkinson, and R. J. Dawson. The impact of flooding on road transport: A depth-disruption function. *Transportation Research Part D: Transport and Environment*, 55:67–81, 2017.

E. Ravasz and A.-L. Barabási. Hierarchical organization in complex networks. *Physical Review E*, 67(2):026112, 2003.

A. Robinson, J. Lehmann, D. Barriopedro, S. Rahmstorf, and D. Coumou. Increasing heat and rainfall extremes now far outside the historical climate. *Climate and Atmospheric Science*, 4(1):1–4, 2021.

S. K. Rose, D. B. Diaz, and G. J. Blanford. Understanding the social cost of carbon: a model diagnostic and inter-comparison study. *Climate Change Economics*, 8(02): 1750009, 2017.

B. Saltzman and K. A. Maasch. Carbon cycle instability as a cause of the late Pleistocene ice age oscillations: modeling the asymmetric response. *Global Biogeochemical Cycles*, 2 (2):177–185, 1988.

J. D. Shakun, P. U. Clark, F. He, S. A. Marcott, A. C. Mix, Z. Liu, B. Otto-Bliesner, A. Schmittner, and E. Bard. Global warming preceded by increasing carbon dioxide concentrations during the last deglaciation. *Nature*, 484(7392):49–54, 2012.

R. M. Solow. A contribution to the theory of economic growth. *The Quarterly Journal of Economics*, 70(1):65–94, 1956.

A. Stechemesser, L. Wenz, M. Kotz, and A. Levermann. Strong increase of racist tweets outside of climate comfort zone in Europe. *Environmental Research Letters*, 16(11): 114001, 2021.

J. E. Stiglitz and M. Gallegati. Heterogeneous interacting agent models for understanding monetary economies. *Eastern Economic Journal*, 37(1):6–12, 2011.

C. Stockwell, A. Geiges, D. Ramalope, M. Gidden, B. Hare, M. J. de Villafranca Casas, M. Moisio, F. Hans, S. Mooldijk, N. Höhne, and et al. Warming projections global update November 2021, Nov 2021. URL https://climateactiontracker.org/documents/997/CAT_2021-11-09_Briefing_Global-Update_Glasgow2030CredibilityGap.pdf. Accessed: 2021-12-19.

K. E. Taylor, R. J. Stouffer, and G. A. Meehl. An Overview of CMIP5 and the Experiment Design. *Bulletin of the American Meteorological Society*, 93(4):485–498, 2012.

S. A. Thekdi and J. R. Santos. Supply chain vulnerability analysis using scenario-based input-output modeling: Application to port operations. *Risk Analysis*, 36(5):1025–1039, 2016.

A. S. Thomas, S. Mangubhai, C. Vandervord, M. Fox, and Y. Nand. Impact of Tropical Cyclone Winston on women mud crab fishers in Fiji. *Climate and Development*, 11(8): 699–709, 2019.

R. S. Tol. Adaptation and mitigation: trade-offs in substance and methods. *Environmental Science & Policy*, 8(6):572–578, 2005.

R. S. Tol. The double trade-off between adaptation and mitigation for sea level rise: an application of FUND. *Mitigation and Adaptation Strategies for Global Change*, 12(5): 741–753, 2007.

R. S. Tol. The social cost of carbon. *Annual Review of Resource Economics*, 3(1):419–443, 2011.

S. Tong. Flooding-related displacement and mental health. *The Lancet Planetary Health*, 1(4):e124–e125, 2017.

S. W. Turner, N. Voisin, J. Fazio, D. Hua, and M. Jourabchi. Compound climate events transform electrical power shortfall risk in the Pacific Northwest. *Nature Communications*, 10(1):1–8, 2019.

J. Vigdor. The economic aftermath of Hurricane Katrina. *Journal of Economic Perspectives*, 22(4):135–54, 2008.

L. Walras. *Elements of pure economics*. Routledge, 2013.

J. Wang, M. Li, Y. Liu, H. Zhang, W. Zou, and L. Cheng. Safety assessment of shipping routes in the South China Sea based on the fuzzy analytic hierarchy process. *Safety Science*, 62:46–57, 02 2014.

M. Watanabe, T. Suzuki, R. O'ishi, Y. Komuro, S. Watanabe, S. Emori, T. Takemura, M. Chikira, T. Ogura, M. Sekiguchi, K. Takata, D. Yamazaki, T. Yokohata, T. Nozawa, H. Hasumi, H. Tatebe, and M. Kimoto. Improved Climate Simulation by MIROC5: Mean States, Variability, and Climate Sensitivity. *Journal of Climate*, 23(23):6312–6335, 2010.

L. Wenz, A. Levermann, and M. Auffhammer. North–south polarization of European electricity consumption under future warming. *Proceedings of the National Academy of Sciences*, 114(38):E7910–E7918, Aug. 2017.

S. N. Willner, A. Levermann, F. Zhao, and K. Frieler. Adaptation required to preserve future high-end river flood risk at present levels. *Science Advances*, 4(1):eaao1914, 2018a.

S. N. Willner, C. Otto, and A. Levermann. Global economic response to river floods. *Nature Climate Change*, 8(7):594–598, 2018b.

X. Wu, C. Zhang, and W. Du. An analysis on the crisis of "chips shortage" in automobile industry–Based on the double influence of COVID-19 and trade friction. In *Journal of Physics: Conference Series*, volume 1971, page 012100. IOP Publishing, 2021.

S. Yang, F. Hu, and C. Jaeger. Impact factors and risk analysis of tropical cyclones on a highway network. *Risk Analysis*, 36(2):262–277, 2016.

K. K. Zander, W. J. Botzen, E. Oppermann, T. Kjellstrom, and S. T. Garnett. Heat stress causes substantial labour productivity loss in Australia. *Nature Climate Change*, 5(7): 647–651, 2015.

Y. Zhang, K. Wei, Z. Shen, X. Bai, X. Lu, and C. G. Soares. Economic impact of typhoon-induced wind disasters on port operations: A case study of ports in China. *International Journal of Disaster Risk Reduction*, 50:101719, 2020.

Z. Zhang, N. Li, H. Xu, and X. Chen. Analysis of the economic ripple effect of the United States on the world due to future climate change. *Earth's Future*, 6(6):828–840, 2018.

Acronyms

Acronym	Meaning
ABM	agent-based model
ASEAN	Association of Southeast Asian Nations
bn	billion (10^9)
$^\circ$C	degree Celsius
CGE	computable general equilibrium
CMIP5	Coupled Model Intercomparison Project Phase 5
EU	European Union
GCM	general circulation model
GDP	gross domestic product
GHG	greenhouse gas
IAM	integrated assessment model
IO	input-output
K	Kelvin
NAFTA	North American Free Trade Agreement
pp	percent points
RCP	representative concentration pathway
SAARC	South Asian Association for Regional Cooperation
SSC	social cost of carbon
SSHWS	Saffir-Simpson hurricane wind scale
UK	United Kingdom
USA	United States of America
USD	United States dollar

Appendix

Appendix of article A

Future heat stress to reduce people's purchasing power

Authors

Kilian Kuhla, Sven N Willner, Christian Otto, Leonie Wenz, Anders Levermann

Status

Published in *PLOS ONE* in June 2021,
doi: 10.1371/journal.pone.0251210.

Future heat stress to reduce people's purchasing power

Kilian Kuhla, Sven N Willner, Christian Otto, Leonie Wenz, Anders Levermann

Supplementary Materials

Table of contents

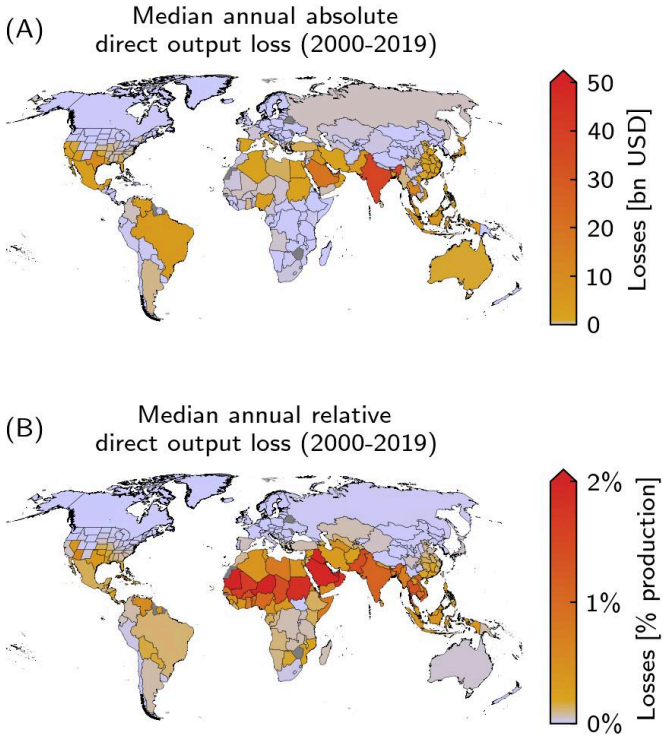

Fig. S1. Heat stress-induced median annual direct output losses for the historic time period 2000–2019. Regional maps of A absolute and B relative annual direct output loss due to heat stress based on the respective regional bias-corrected median for 2000–2019. Regions with an absolute or relative direct annual output loss below USD 1bn or 0.2% of baseline (unperturbed) production are depicted in light purple, respectively.

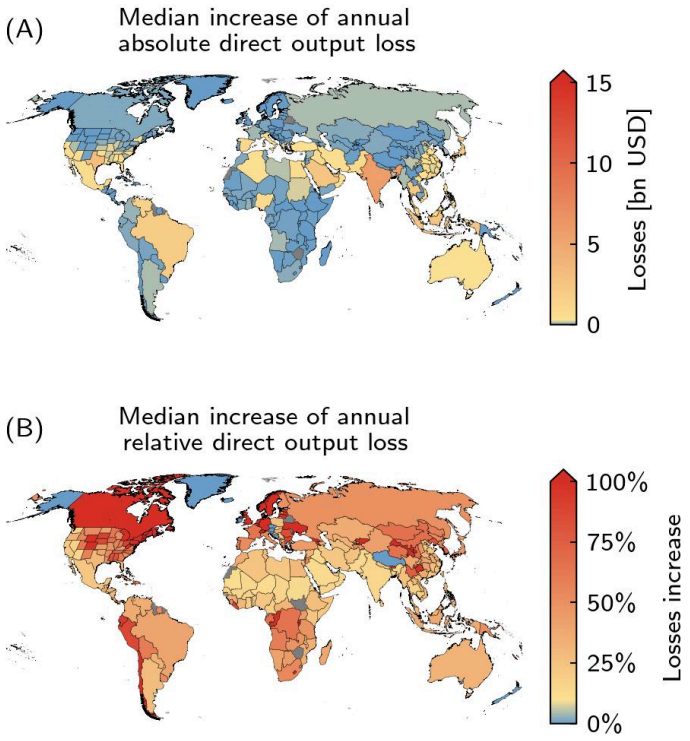

Fig. S2. Projected increase of heat stress-induced annual direct output losses between historic (2000–2019) and future (2020–2039) period. A Absolute annual increase of regional direct output losses of period 2020–2039 compared to 2000–2019. B Increase of direct output losses in the future period in terms of losses in the historic period.

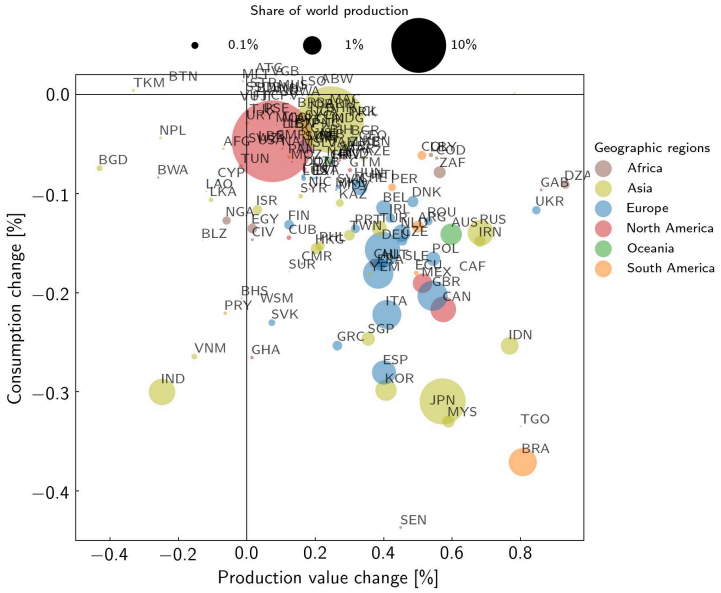

Fig. S3. Consumption and total production change per country for the historic period 2000–2019. The area of each dot is proportional to the corresponding country's baseline (unperturbed) production. The dot colors denote the geographic regions (see Tbl. S2). Quantities are given relative to the baseline (unperturbed) production and consumption, respectively.

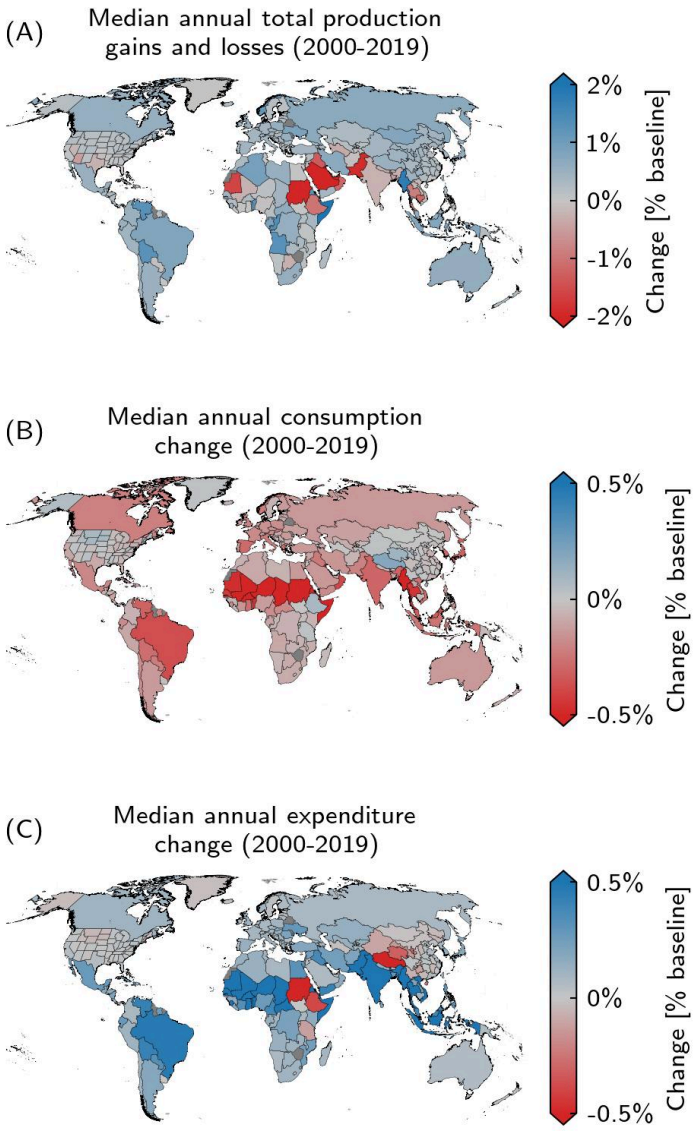

Fig. S4. Total production, consumption, and expenditure change for the historic period 2000–2019. Median annual change of A total production, B consumption and C expenditure relative to the unperturbed baseline.

Tbl. S1. Sectors used in the simulations. For sectors prone to heat stress-induced productivity loss the respective reduction factor (see Methods) is given in the last column.

Code	Name	Category	Production reduction factor
AGRI	Agriculture	vital	-0.8 p.p./°C
FISH	Fishing	vital	-0.8 p.p./°C
MINQ	Mining and quarrying	other	-4.2 p.p./°C
GAST	Hotels and restaurants	other	-6.1 p.p./°C
WHOT	Wholesale trade	relevant	-6.1 p.p./°C
OTHE	Others	other	-2.2 p.p./°C
REPA	Maintenance and Repair	other	/
RETT	Retail Trade	relevant	/
FOOD	Food and Beverages	vital	/
TEXL	Textiles and Wearing Apparel	relevant	/
TRAN	Transport	relevant	/
WOOD	Wood and Paper	relevant	/
OILC	Petroleum, Chemical & Non-Metallic Mineral Products	relevant	/
FINC	Financial Intermediation and Business Activities	other	/
METL	Metal Products	relevant	/
MACH	Electrical and Machinery	relevant	/
TREQ	Transport Equipment	relevant	/
MANU	Other Manufacturing	relevant	/
REXI	Re-export and Re-import	other	/
CONS	Construction	relevant	/
ADMI	Public Administration	other	/
EDHE	Education, Health and Other Services	vital	/
HOUS	Private Households	other	/
COMM	Post and Telecommunications	relevant	/
RECY	Recycling	other	/
ELWA	Electricity, Gas and Water	vital	/
FCON	Final consumption	relevant	/

Tbl. S2. Regions used in the simulations. Income level corresponds to Gross National Income per capita (GNIpc) of 2012.
Income level 1: GNIpc $< 1,305$ USD
Income level 2: $1,036$ USD $<$ GNIpc $< 4,085$ USD
Income level 3: $4,086$ USD $<$ GNIpc $< 12,615$ USD
Income level 4: $12,616$ USD $<$ GNIpc

ISO code	Name	Income level	Geographic region
AFG	Afghanistan	1	Asia
ALB	Albania	3	Europe
DZA	Algeria	3	Africa
AND	Andorra	4	Europe
AGO	Angola	3	Africa
ATG	Antigua and Barbuda	4	North America
ARG	Argentina	3	South America
ARM	Armenia	2	Asia
ABW	Aruba	4	South America
AUS	Australia	4	Oceania
AUT	Austria	4	Europe
AZE	Azerbaijan	3	Asia
BHS	Bahamas	4	North America
BHR	Bahrain	4	Asia
BGD	Bangladesh	1	Asia
BRB	Barbados	4	North America
BLR	Belarus	3	Europe
BEL	Belgium	4	Europe
BLZ	Belize	3	North America
BEN	Benin	1	Africa
BMU	Bermuda	4	North America
BTN	Bhutan	2	Asia
BOL	Bolivia	2	South America
BIH	Bosnia and Herzegovina	3	Europe
BWA	Botswana	3	Africa
BRA	Brazil	3	South America
VGB	British Virgin Islands	4	South America
BRN	Brunei Darussalam	4	Asia
BGR	Bulgaria	3	Europe
BFA	Burkina Faso	1	Africa
BDI	Burundi	1	Africa
KHM	Cambodia	1	Asia
CMR	Cameroon	2	Africa

ISO code	Name	Income level	Geographic region
CAN	Canada	4	North America
CPV	Cabo Verde	2	Africa
CYM	Cayman Islands	4	South America
CAF	Central African Republic	1	Africa
TCD	Chad	1	Africa
CHL	Chile	4	South America
CN.AH	Anhui	3	China, Asia
CN.BJ	Beijing	3	China, Asia
CN.CQ	Chongqing	3	China, Asia
CN.FJ	Fujian	3	China, Asia
CN.GS	Gansu	3	China, Asia
CN.GD	Guangdong	3	China, Asia
CN.GX	Guangxi	3	China, Asia
CN.GZ	Guizhou	3	China, Asia
CN.HA	Hainan	3	China, Asia
CN.HB	Hebei	3	China, Asia
CN.HL	Heilongjiang	3	China, Asia
CN.HE	Henan	3	China, Asia
CN.HU	Hubei	3	China, Asia
CN.HN	Hunan	3	China, Asia
CN.JS	Jiangsu	3	China, Asia
CN.JX	Jiangxi	3	China, Asia
CN.JL	Jilin	3	China, Asia
CN.LN	Liaoning	3	China, Asia
CN.NM	Nei Mongol	3	China, Asia
CN.NX	Ningxia Hui	3	China, Asia
CN.QH	Qinghai	3	China, Asia
CN.SA	Shaanxi	3	China, Asia
CN.SD	Shandong	3	China, Asia
CN.SH	Shanghai	3	China, Asia
CN.SX	Shanxi	3	China, Asia
CN.SC	Sichuan	3	China, Asia
CN.TJ	Tianjin	3	China, Asia
CN.XJ	Xinjiang Uygur	3	China, Asia
CN.XZ	Xizang	3	China, Asia
CN.YN	Yunnan	3	China, Asia
CN.ZJ	Zhejiang	3	China, Asia
COL	Colombia	3	South America
COG	Republic Congo	2	Africa
CRI	Costa Rica	3	North America

ISO code	Name	Income level	Geographic region
HRV	Croatia	4	Europe
CUB	Cuba	3	North America
CYP	Cyprus	4	Europe
CZE	Czech Republic	4	Europe
CIV	Côte d'Ivoire	2	Africa
PRK	North Korea	1	Asia
COD	Democratic Republic Congo	1	Africa
DNK	Denmark	4	Europe
DJI	Djibouti	2	Africa
DOM	Dominican Republic	3	North America
ECU	Ecuador	3	South America
EGY	Egypt	2	Africa
SLV	El Salvador	2	North America
ERI	Eritrea	1	Africa
EST	Estonia	4	Europe
ETH	Ethiopia	1	Africa
FJI	Fiji	3	Oceania
FIN	Finland	4	Europe
FRA	France	4	Europe
PYF	French Polynesia	4	Oceania
GAB	Gabon	3	Africa
GMB	Gambia	1	Africa
GEO	Georgia	2	Asia
DEU	Germany	4	Europe
GHA	Ghana	2	Africa
GRC	Greece	4	Europe
GRL	Greenland	4	North America
GTM	Guatemala	2	North America
GIN	Guinea	1	Africa
GUY	Guyana	2	South America
HTI	Haiti	1	North America
HND	Honduras	2	North America
HKG	Hong Kong	4	Asia
HUN	Hungary	3	Europe
ISL	Iceland	4	Europe
IND	India	2	Asia
IDN	Indonesia	2	Asia
IRN	Iran	3	Asia
IRQ	Iraq	3	Asia
IRL	Ireland	4	Europe

ISO code	Name	Income level	Geographic region
ISR	Israel	4	Asia
ITA	Italy	4	Europe
JAM	Jamaica	3	North America
JPN	Japan	4	Asia
JOR	Jordan	3	Asia
KAZ	Kazakhstan	3	Asia
KEN	Kenya	1	Africa
KWT	Kuwait	4	Asia
KGZ	Kyrgyz Republic	1	Asia
LAO	Lao PDR	2	Asia
LVA	Latvia	4	Europe
LBN	Lebanon	3	Asia
LSO	Lesotho	2	Africa
LBR	Liberia	1	Africa
LBY	Libya	3	Africa
LIE	Liechtenstein	4	Europe
LTU	Lithuania	4	Europe
LUX	Luxembourg	4	Europe
MAC	Macao	4	Asia
MDG	Madagascar	1	Africa
MWI	Malawi	1	Africa
MYS	Malaysia	3	Asia
MDV	Maldives	3	Asia
MLI	Mali	1	Africa
MLT	Malta	4	Europe
MRT	Mauritania	2	Africa
MUS	Mauritius	3	Africa
MEX	Mexico	3	North America
MCO	Monaco	4	Europe
MNG	Mongolia	2	Asia
MNE	Montenegro	3	Europe
MAR	Morocco	2	Africa
MOZ	Mozambique	1	Africa
MMR	Myanmar	1	Asia
NAM	Namibia	3	Africa
NPL	Nepal	1	Asia
NLD	Netherlands	4	Europe
ANT	Netherlands Antilles	4	Sout America
NCL	New Caledonia	4	Oceania
NZL	New Zealand	4	Oceania

ISO code	Name	Income level	Geographic region
NIC	Nicaragua	2	North America
NER	Niger	1	Africa
NGA	Nigeria	2	Africa
NOR	Norway	4	Europe
PSE	West Bank and Gaza	2	Asia
OMN	Oman	4	Asia
PAK	Pakistan	2	Asia
PAN	Panama	3	South America
PNG	Papua New Guinea	2	Asia
PRY	Paraguay	2	South America
PER	Peru	3	South America
PHL	Philippines	2	Asia
POL	Poland	4	Europe
PRT	Portugal	4	Europe
QAT	Qatar	4	Asia
KOR	South Korea	4	Asia
MDA	Moldova	2	Europe
ROU	Romania	3	Europe
RUS	Russian Federation	4	Asia
RWA	Rwanda	1	Africa
WSM	Samoa	2	Oceania
SMR	San Marino	4	Europe
STP	São Tomé and Principe	2	Africa
SAU	Saudi Arabia	4	Asia
SEN	Senegal	2	Africa
SRB	Serbia	3	Europe
SYC	Seychelles	3	Africa
SLE	Sierra Leone	1	Africa
SGP	Singapore	4	Asia
SVK	Slovak Republic	4	Europe
SVN	Slovenia	4	Europe
SOM	Somalia	1	Africa
ZAF	South Africa	3	Africa
SSD	South Sudan	1	Africa
ESP	Spain	4	Europe
LKA	Sri Lanka	2	Asia
SDN	Sudan	2	Africa
SUR	Suriname	3	South America
SWZ	Swaziland	2	Africa
SWE	Sweden	4	Europe

ISO code	Name	Income level	Geographic region
CHE	Switzerland	4	Europe
SYR	Syrian Arab Republic	2	Asia
TWN	Taiwan	4	Asia
TJK	Tajikistan	1	Asia
THA	Thailand	3	Asia
MKD	Macedonia	3	Europe
TGO	Togo	1	Africa
TTO	Trinidad and Tobago	4	South America
TUN	Tunisia	3	Africa
TUR	Turkey	3	Asia
TKM	Turkmenistan	3	Asia
UGA	Uganda	1	Africa
UKR	Ukraine	2	Europe
ARE	United Arab Emirates	4	Asia
GBR	United Kingdom	4	Europe
TZA	Tanzania	1	Africa
US.AL	Alabama	4	USA, North America
US.AK	Alaska	4	USA, North America
US.AZ	Arizona	4	USA, North America
US.AR	Arkansas	4	USA, North America
US.CA	California	4	USA, North America
US.CO	Colorado	4	USA, North America
US.CT	Connecticut	4	USA, North America
US.DE	Delaware	4	USA, North America
US.DC	District of Columbia	4	USA, North America
US.FL	Florida	4	USA, North America
US.GA	Georgia	4	USA, North America
US.HI	Hawaii	4	USA, North America
US.ID	Idaho	4	USA, North America
US.IL	Illinois	4	USA, North America
US.IN	Indiana	4	USA, North America
US.IA	Iowa	4	USA, North America
US.KS	Kansas	4	USA, North America
US.KY	Kentucky	4	USA, North America
US.LA	Louisiana	4	USA, North America
US.ME	Maine	4	USA, North America
US.MD	Maryland	4	USA, North America
US.MA	Massachusetts	4	USA, North America
US.MI	Michigan	4	USA, North America
US.MN	Minnesota	4	USA, North America

ISO code	Name	Income level	Geographic region
US.MS	Mississippi	4	USA, North America
US.MO	Missouri	4	USA, North America
US.MT	Montana	4	USA, North America
US.NE	Nebraska	4	USA, North America
US.NV	Nevada	4	USA, North America
US.NH	New Hampshire	4	USA, North America
US.NJ	New Jersey	4	USA, North America
US.NM	New Mexico	4	USA, North America
US.NY	New York	4	USA, North America
US.NC	North Carolina	4	USA, North America
US.ND	North Dakota	4	USA, North America
US.OH	Ohio	4	USA, North America
US.OK	Oklahoma	4	USA, North America
US.OR	Oregon	4	USA, North America
US.PA	Pennsylvania	4	USA, North America
US.RI	Rhode Island	4	USA, North America
US.SC	South Carolina	4	USA, North America
US.SD	South Dakota	4	USA, North America
US.TN	Tennessee	4	USA, North America
US.TX	Texas	4	USA, North America
US.UT	Utah	4	USA, North America
US.VT	Vermont	4	USA, North America
US.VA	Virginia	4	USA, North America
US.WA	Washington	4	USA, North America
US.WV	West Virginia	4	USA, North America
US.WI	Wisconsin	4	USA, North America
US.WY	Wyoming	4	USA, North America
URY	Uruguay	4	South America
UZB	Uzbekistan	2	Asia
VUT	Vanuatu	2	Oceania
VEN	Venezuela	3	South America
VNM	Vietnam	2	Asia
YEM	Yemen	2	Asia
ZMB	Zambia	2	Africa
ZWE	Zimbabwe	1	Africa

Tbl. S3. Consumption price elasticities per income level and sector category. Values are based on GTAP.

	Income level			
Sector category	1	2	3	4
vital	-0.15	-0.2	-0.3	-0.45
relevant	-0.2	-0.3	-0.4	-0.65
other	-0.3	-0.4	-0.5	-0.75

Appendix of article B

Wave-like global economic ripple response to Hurricane Sandy

Authors

Robin Middelanis, Sven N Willner, Christian Otto, Kilian Kuhla, Lennart Quante and Anders Levermann

Status

Published in *Enviromental Research Letters* in December 2021,
doi: 10.1088/1748-9326/ac39c0.

Wave-like global economic ripple response to Hurricane Sandy

Appendix A: Methods

Business interruption recovery

We assume the business interruption (BI) to be very strong but short, representing the short-term disruptions after the storm that can be quickly recovered from to an extent that most business processes are again functional, e.g. interruptions due to power outages, flooding, transportation disruption, and disturbance in communication. We set the initial intensity of this BI for NY and NJ to the GDP share of the respective state that is physically exposed to the hurricane. As damage from Sandy was primarily due to precipitation and flooding, we focus on this physical factor. For that, we calculate GDP exposure on a county level. We consider those counties as exposed for which the U.S. Geological Survey (USGS) reported at least one high water mark[1].

We then assume exponential recovery from the BI as is commonly done with disaster recovery[2;3], assuming a rather efficient recovery of the local economy[4] which we esteem realistic for the economically strong regions of NY and NJ. The intuitive reason for using exponential recovery in this case is that most effective measures of recovery can be believed to take place first. Subsequent measures may be less effective in comparison to their effort, resulting in an exponential path of recovery. As an example, power supply was restored exponentially after Hurricane Sandy[5]. We can also observe exponential recovery after Hurricane Katrina as measured by the Louisiana Coincident Economic Activity Index[6] (the index is based on non-farm payroll employment, the unemployment rate, average hours worked in manufacturing, and wages and salaries). However, this is a long-term recovery over about one year and therefore presumably cannot be explained by BI alone but potentially also reflects losses due to reconstruction efforts and capital stock losses. To estimate a time scale for the exponential decay of the BI shock, we similarly use unemployment as a proxy. The Federal Reserve Bank of New York found unemployment claims in NY and NJ to rise due to Sandy with the number of initial claims showing a roughly exponential decay (see Fig. 1 in Abel et al. (2013)[7]) after an initial peak. According to this report, “both states saw employment rebound to above October (pre-Sandy) levels

by the end of the year" 2012. We therefore fit our BI recovery to end after 60 days (see Appendix A: Methods for details). This time scale is also in accordance with a Downtown Alliance report[8] which finds that over 95% of Manhattan office space was available again after Sandy by the end of the year 2012.

Note that our notion of recovery does not include any concept of growth, i.e. we consider recovery as completed once output quantities equal those before the disaster. Generally, disasters can have long-term or even permanent effects[9] and it has been shown that tropical cyclones have long-term impacts on economic growth[10] with effects lasting as long as 20 years[11]. Unlike for fluvial floods, countries with higher development are not well prepared against the impact of tropical cyclones and their associated long-term growth losses[12]. Since we focus here on the short-term impacts, we do not model growth and assume a constant baseline economy, resulting in much shorter recovery times.

We assume an initial production capacity reduction factor λ_0 in the direct aftermath of the disaster as the share of state GDP that is exposed to the disaster. We use reported high water marks associated with the disaster to determine how severely individual states are affected. We retrieve high water marks from the USGS Flood Event Viewer[1]. We consider each county within a state as affected by the disaster if it has at least one reported high water mark. We then calculate the relative GDP exposure, i.e. the initial production capacity reduction λ_0, of the entire state from

$$\lambda_0 = \frac{\sum_{c \in C} GDP_c}{GDP_s} \tag{1}$$

where GDP_c is the GDP of an affected county from the set of all affected counties C and GDP_s is the overall state's GDP.

While this approach to determine the initial production capacity reduction of a directly affected state is a rather simple one, we believe that it is still sufficiently good to achieve a realistic scenario of direct economic losses. Given that this initial reduction of production capacity level only prevails for a very short time and then is gradually relieved by the exponential recovery curve, we esteem variations in this value as less crucial for the outcome of the simulations than the direct economic loss which determines how long the production capacity reduction persists. For NY and NJ, we obtain initial production shock of $\sim$ 80.2% and $\sim$ 69.3%, respectively. This matches observations rather well. According to the Empire State Manufacturing Survey[13] by the Federal Reserve Bank of New York,

more than 90% of all businesses in the New York City area were shut down for at least one day due to Hurricane Sandy. For example, the New York stock exchange was shut down for two days after the hurricane[1]. The New York-Newark-Jersey City Metropolitan Statistical Area (NYMSA) accounts for a 2012 GDP of about $1.4bn and counts mostly to the GDP of New York and New Jersey (and a negligible fraction for Pennsylvania with only one county). NY and NJ have a combined 2012 GDP of about $1.8bn. Using GDP as a proxy for economic activity, we thus may assume that a 90% one-day shut down in the NYMSA is equivalent to a 68.4% one-day shutdown for both states combined. However, this number does not include businesses that were only partly disrupted and must hence be considered a lower bound for economic disruption. Our estimates for New York and New Jersey with 80.2% and 69.3% therefore seem reasonable for the day immediately following the hurricane.

After the disaster, we assume exponential recovery of the economy back to 100% from the initial production shock given by eq. (1). Reduction in productive capacity is then given by

$$f(t) := 1 - \lambda_0 e^{-t/\tau} \tag{2}$$

with initial shock λ_0 and characteristic time scale τ. We assume that full recovery is given at time t_r once the shock has decayed to 0.1% or less, i.e. $f_r = f(t_r) \geq 0.999$. With a prescribed recovery time t_r, we thus can derive τ:

$$\begin{aligned} f(t_r) = f_r &= 1 - \lambda_0 e^{-t_r/\tau} \\ \Rightarrow \tau &= -\frac{t_r}{ln(\frac{1-f_r}{\lambda_0})} \end{aligned} \tag{3}$$

The fully parametrised curve for the reduction of production capacity is then given by

$$f_{\lambda_0, f_r}(t) := \begin{cases} 1 - \lambda_0 e^{-t/\tau_{\lambda_0, f_r, t_r}} & \text{for } t \leq t_r \\ 1 & \text{for } t > t_r. \end{cases} \tag{4}$$

For the US states NY and NJ with recovery time $t_r = 60$, this yields the production capacity reduction curves shown in Supplementary Fig. 1. The initial production capacity reduction values λ_0 are listed in Supplementary Tbl. 1.

[1] https://www.theguardian.com/world/2012/oct/31/new-york-stock-exchange-opens-sandy

Indirect and consumption losses

To simulate indirect and consumption losses, we use the dynamic agent-based model *Acclimate*[14]. This model has been presented in different versions previously[15;16;14] and was used in studies regarding the higher-order economic losses from extreme weather events[17;18;19]. We here use the latest model presented in Otto et al. (2017)[14]. In this model, regional economic sectors are represented by individual agents that are interconnected through trade flows. The resolution of these regions is on a state-level in case of the United States, province-level in case of China and national level for all other regions of the world, resulting in a total of 268 individual regions. The economy is split into 27 sectors, including the final consumer as one sector without production output. All sectors of a region that is directly affected by the hurricane are subjected to the same production reduction curves as per eq. (4). Trade flows between the resulting total of 7,263 agents are taken from a disaggregated[20] version of the EORA multi-regional input-output dataset[21]. This data set contains annual monetary flows between the agents from the year 2012. We break this down to a monetary daily baseline flow by distributing equally over 365 days which we refer to as baseline equilibrium flow. This is the state around which *Acclimate* simulates deviations resulting from an externally enforced reduction of production capacity. This production shock results in perturbations of demand, supply and prices within the model, globally. The dynamics is a result from the profit maximisation that each individual agent performs by optimising production levels, demand distribution to suppliers and upstream demand to other agents. In this, increased demand from other agents can be addressed by activation of idle production capacities, resulting in elevated production prices. A comprehensive description of the model can be found in the original publication by Otto et al. (2017)[14].

For the present study, we look into the output variables of production, final consumption, and communicated demands along the supply chains as well as associated prices. Using the 2012 EORA dataset, the baseline flows must be considered influenced by the economic shock of Hurricane Sandy. However, this influence is small compared to the total volume of trade flows such that the introduced bias is negligible. For example, the impact of Hurricane Sandy on GDP in remote regions cannot be found in historic data.

While included in the simulations, for all calculations and analyses in this study, we exclude the EORA regions of Belarus, Moldova, Sudan, and South Sudan since the data quality for these regions is not reliable, especially with regards to final consumption.

Aggregate relative consumption changes $\Delta\bar{C}_r$ in each simulated region r for the direct aftermath of the hurricane are calculated from the simulated consumption levels as follows:

$$\Delta\bar{C}_r = -1 + \frac{1}{(T - t_0)c_r^*} \sum_{t=t_0}^{T} c_r^{(t)} \tag{5}$$

where $c_r^{(t)}$ is the final consumption in region r at time step t, c_r^* is the baseline consumption and $(T - t_0)$ is the time of aggregation after the disaster.

Consumption prices

Consumers in the model, like other agents, purchase at a price which they propose to producers together with their demand request. This reservation price is oriented towards offer prices that producers advertise to their trade partners. The entirety of reservation prices and the production quantity resulting from a producer's optimization process determine the final production price. The latter in turn influences the offer price that producers advertise. Therefore, in case of rising production prices, consumers also need to pay higher prices to ensure that their demand will be fulfilled. Production prices and consumer purchasing prices are therefore related. However, the measured consumption price is buffered by storage inventories that fill up and thus smooth production prices. Hence, the consumption price is an average of the goods' prices currently in storage and therefore averages production prices over a certain amount of time.

Capacity utilisation and demand exceedance

Capacity utilization that is defined as the ratio of actual output to the output that would minimise production costs[22]. In the *Acclimate* model, the production output that would minimise production costs is given by the baseline production level. Beyond this production level, production costs increase super-linearly. However, for the directly affected regions of NY and NJ, the production capacity is diminished due to the hurricane. We therefore need to adjust the capacity utilization to the applied production capacity reduction. We calculate

the change in capacity utilization u for region r at time step t from the applied production shock (i.e., the reduction in production capacity) f, the production level X and the baseline production level X^* as

$$u_r^{(t)} = \frac{X_r^{(t)}}{f_r^{(t)} X_r^*} - 1. \tag{6}$$

Hence, this measure quantifies if and by how much a region is in a state of overproduction, relative to the actual production capacity. In this, we need to adjust the baseline production level X^* with the production capacity reduction factor f_r in case of directly affected regions. A positive value means that the region is in a state of overproduction, causing production costs to increase super-linearly with the production quantity. Negative values indicate proportionality between production quantities and production prices.

Similarly, we define the demand exceedance e for region r at time step t as

$$e_r^{(t)} = \frac{d_r^{(t)}}{f_r^{(t)} X_r^*} - 1, \tag{7}$$

using the incoming demand d that the agent receives. Demand exceedance indicates if fulfilling the entire incoming demand at a given time step would drive the agent into overproduction (for positive values) or not (zero and negative values).

Sectorial and regional aggregation

Sectors in regions are represented by individual agents in the *Acclimate* model. Thus we obtain simulated time series for each sector in every simulated region, individually. A time series of quantity variable q_{ir} of agent ir is classified by its pair of sector i and region r. However, to present comprehensive results, we aggregate time series for variables of interest over sectors or regions. For this we aggregate the quantity variables over the agents ensemble $\{ir\}$:

$$q_{\{ir\}} = \sum_{ir \in \{ir\}} q_{ir} \tag{8}$$

to obtain the sum of quantity values $q_{\{ir\}}$. Quantity variables are, for example, demand quantities or production quantities.

Aggregated price variables $\langle p_{\{ir\}} \rangle$, on the other hand, are calculated as the weighted average over all prices p_{ir} of the individual agents ir:

$$\langle p_{\{ir\}} \rangle = \frac{\sum_{ir \in \{ir\}} p_{ir} q_{ir}}{\sum_{ir \in \{ir\}} q_{ir}}. \tag{9}$$

We note that this aggregation can lead to apparent contradictions when considering, for example, demand exceedance and capacity utilization of aggregated agents. For example, in Fig. 5 the pooled region USA-OTH shows positive demand exceedance and simultaneous low capacity utilization during the first days after the disaster. This is simply a result of the aggregation that we perform over the US regions and their individual sectors. Some agents receive less demand due to the upstream network effect and others experience higher demand to compensate for NY and NJ production outages. While production levels react proportionally to demand changes if the demand exceedance is below zero, they are bound by supply or costs and potential revenue if the demand exceedance is positive. Therefore, the average production for all non-affected US regions is below baseline despite a positive average demand exceedance. However, the longer the scarcity situation prevails, the more agents in the non-affected US receive elevated demand and switch to overproduction, eventually resulting in an increased capacity utilization of USA-OTH as well.

Consumer flexibility to price changes

Consumers with different income tend to have a diverse flexibility if prices change for different commodities and services. This flexibility is integrated into our model by the regionally and sectorally dependent parameter of consumption price elasticity. We divide the regions used in our simulation into four income level groups: low, lower-middle, upper-middle, high income level (Supplementary Tbl. 2). The classification of the income level groups is based on the gross national income (GNI) per capita (GNIpc) of each country. We use the annual, inflation-adjusted definition and classification of income level groups of the World Bank for the year 2012[23]. For this calibration, we only focus on average consumer income and do not consider other socio-economic structures (education, regional wealth distribution, etc.).

To obtain empirical parameters, we use the target income elasticities of demand for 140 regions and 10 commodity classes[24] of the Global Trade Analysis Project (GTAP)[25]. The regional resolutions of EORA and GTAP are not identical. To address this, we set the consumption price elasticities for non-GTAP-countries to the respective income level group parameter. Similarly, the sectoral resolutions of EORA and GTAP are not identical either. To handle this, we map EORA's economic sectors to the GTAP commodity classes and group them into three categories: vital, relevant and other (Supplementary Tbl. 3). Using these two classification parameters — income level groups of regions and economic relevance categories of sectors — we assign a specific consumption price elasticity from the GTAP data sets[26] for any tuple of income level and sector category (Supplementary Tbl. 4).

With these price elasticities, flexibility to price changes increases with rising income. Therefore, wealthier countries are more resilient against price fluctuations. At the same time, consumers adapt less flexibly to price changes of more life essential goods and services. Since there is little or no substitutability for EORA's large and clearly distinguished sectors (Supplementary Tbl. 3), we do not consider cross-sector elasticities.

Appendix B: Supplementary figures and tables

Table of contents

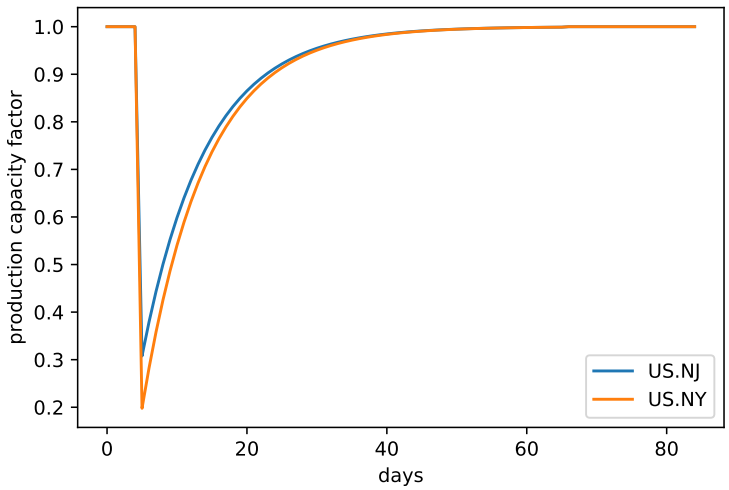

Supplementary Figure 1: Production capacity reduction for Hurricane Sandy. Time-dependent factor with which the prduction capacity is multiplied, representing the economic shock that results from the hurricane.

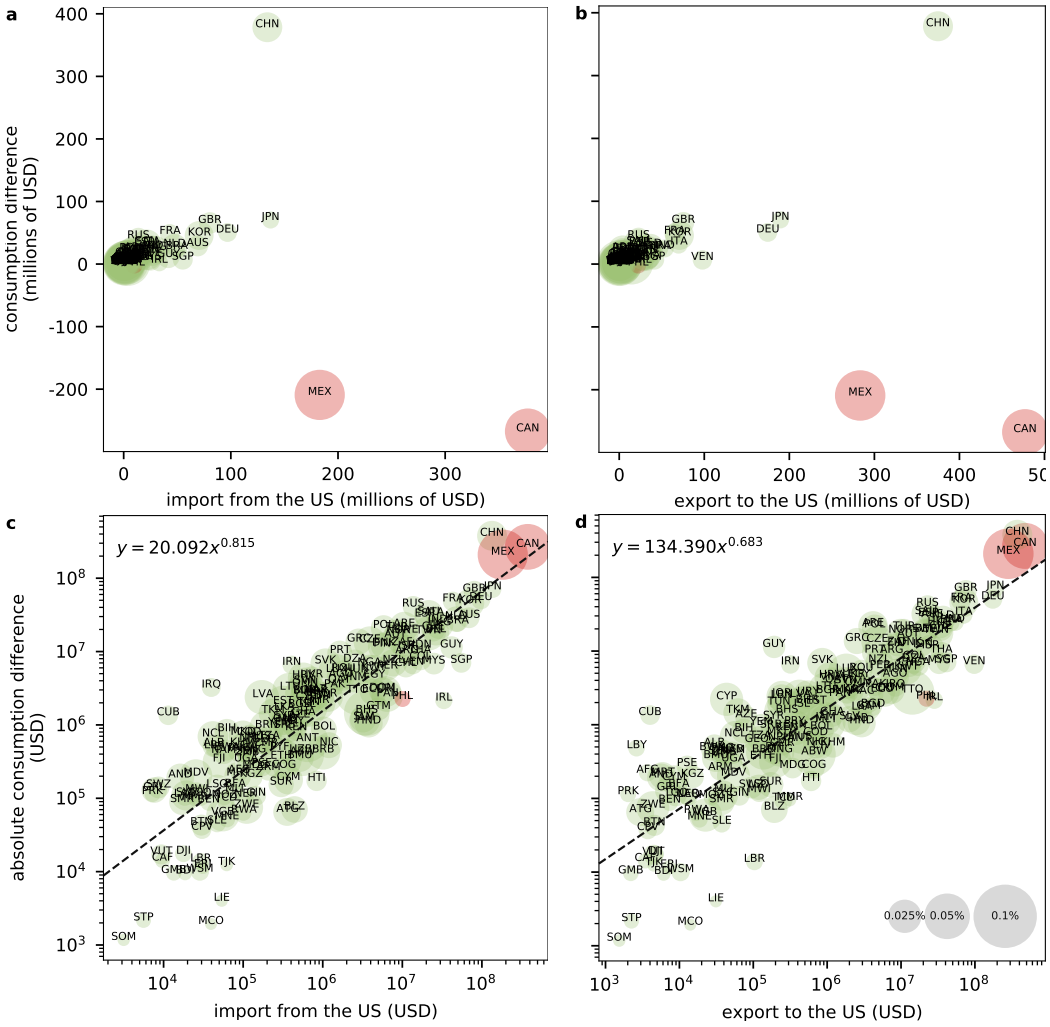

Supplementary Figure 2: Consumption change for all simulated regions over their import and export volume with the US. Consumption changes are cumulated for the first 100 days after the hurricane. Size of the scatters indicates the consumption change relative to what regions would consume under baseline conditions during this time. Green and red colors indicate consumption gains and losses, respectively. **a** consumption change over import volume from the US. **b** like panel a for export volume to the US. **c** absolute consumption change over import volume from the US on a log-log scale. Dashed line is the linear fit in the log-log space. **d** like panel c for export volume to the US.

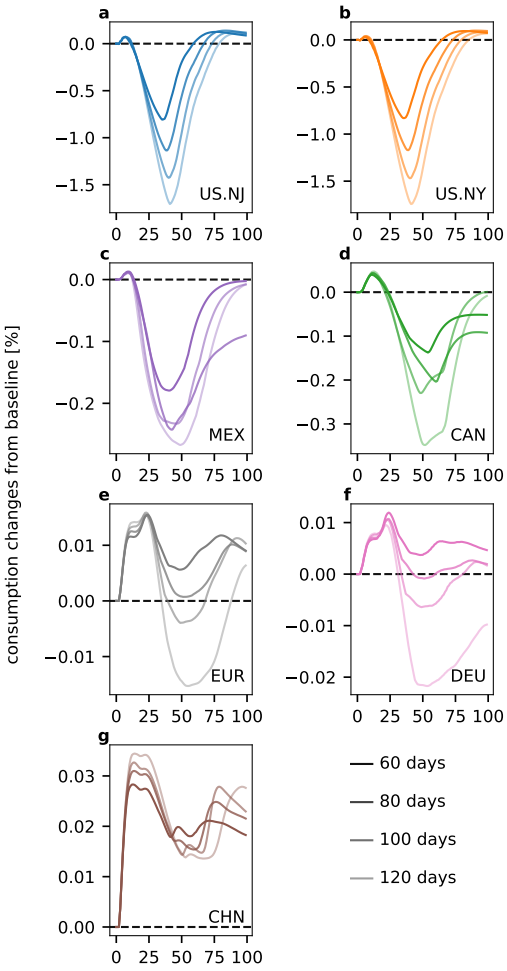

Supplementary Figure 3: Changes of consumption relative to baseline values with recovery time variation. Same as Fig. 3 with longer recovery durations.

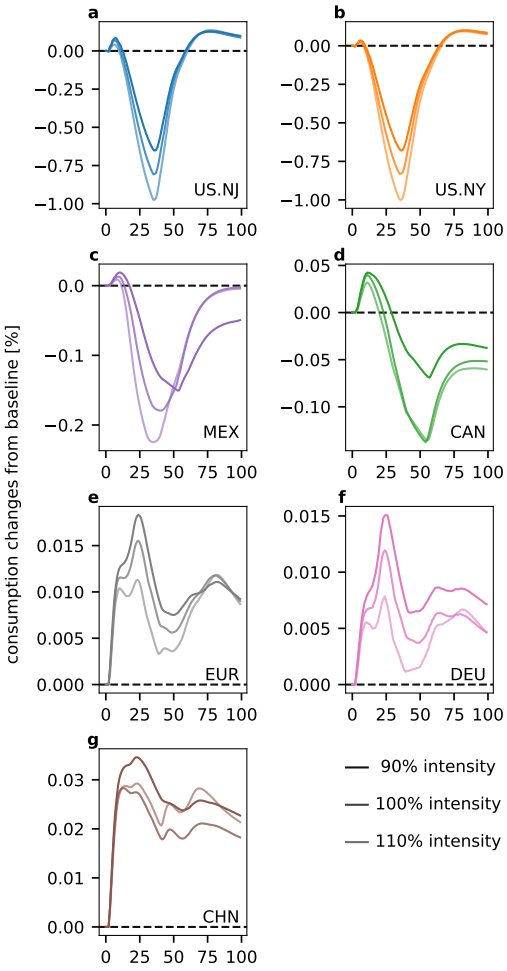

Supplementary Figure 4: Changes of consumption relative to baseline values with initial shock intensity variation. Same as Fig. 3 with slightly weaker and stronger initial shock intensity.

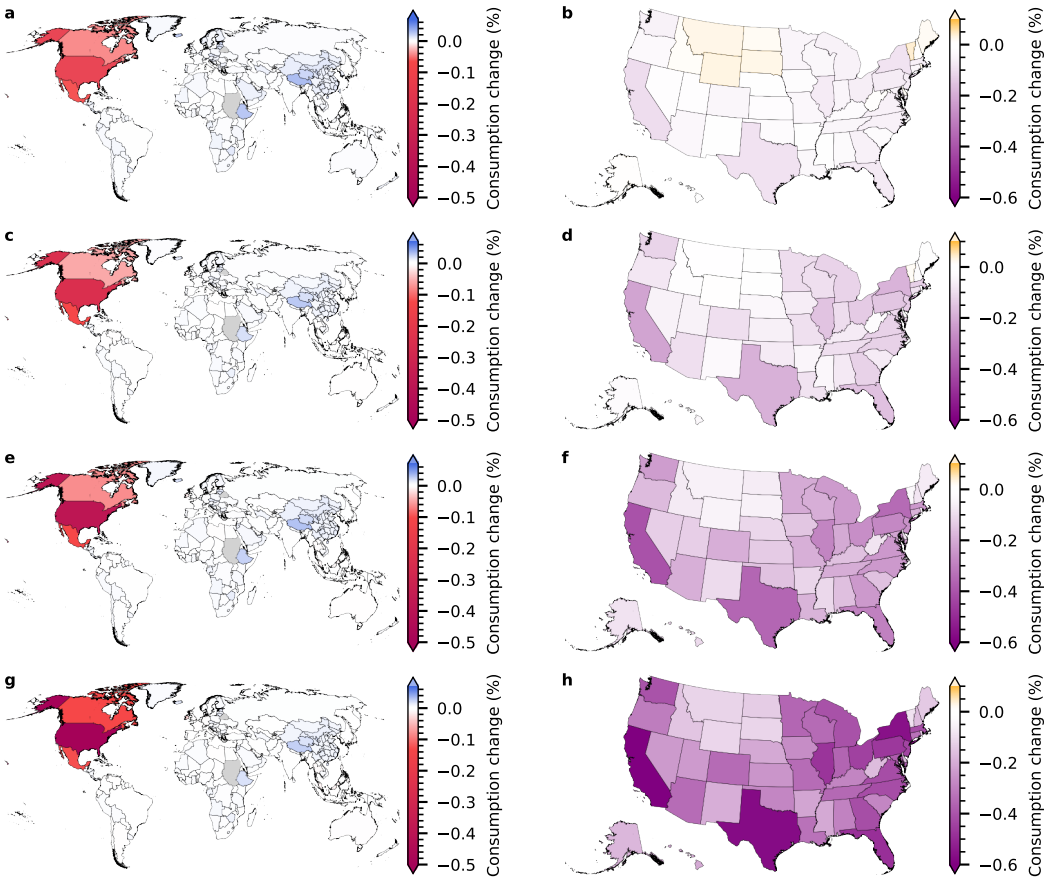

Supplementary Figure 5: Global consumption changes after the hurricane with different shock durations. Like Fig. 2 with longer BI recovery times. **left column** Global map. **right column** Detailed zoom on the United States. **a, b** 60 days, **c, d** 80 days, **e, f** 100 days, **g, h** 120 days. Region shapefiles retrieved from GADM[27].

Supplementary Table 1: Recovery curve parameters.

State	λ_0	t_r
New York	0.802032	60
New Jersey	0.693088	60

Supplementary Table 2: Regions used in the simulations. Income level corresponds to Gross National Income per capita (GNIpc) of 2012[23].

Income level 1: GNIpc $< \$\,1,305$

Income level 2: $\$\,1,036 <$ GNIpc $< \$\,4,085$

Income level 3: $\$\,4,086 <$ GNIpc $< \$\,12,615$

Income level 4: $\$\,12,616 <$ GNIpc

ISO code	Name	Income level	Geographic region	Consumption change [%]
AFG	Afghanistan	1	Asia	0.004
ALB	Albania	3	Europe	0.010
DZA	Algeria	3	Africa	0.013
AND	Andorra	4	Europe	0.017
AGO	Angola	3	Africa	0.018
ATG	Antigua and Barbuda	4	North America	0.017
ARG	Argentina	3	South America	0.008
ARM	Armenia	2	Asia	0.009
ABW	Aruba	4	South America	0.047
AUS	Australia	4	Oceania	0.008
AUT	Austria	4	Europe	0.014
AZE	Azerbaijan	3	Asia	0.010
BHS	Bahamas	4	North America	0.053
BHR	Bahrain	4	Asia	0.029
BGD	Bangladesh	1	Asia	0.005
BRB	Barbados	4	North America	0.028
BLR	Belarus	3	Europe	0.115
BEL	Belgium	4	Europe	0.015
BLZ	Belize	3	North America	0.016
BEN	Benin	1	Africa	0.004
BMU	Bermuda	4	North America	0.017
BTN	Bhutan	2	Asia	0.008
BOL	Bolivia	2	South America	0.015
BIH	Bosnia and Herzegovina	3	Europe	0.013
BWA	Botswana	3	Africa	0.008
BRA	Brazil	3	South America	0.004
VGB	British Virgin Islands	4	South America	0.026

ISO code	Name	Income level	Geographic region	Consumption change [%]
BRN	Brunei Darussalam	4	Asia	0.029
BGR	Bulgaria	3	Europe	0.017
BFA	Burkina Faso	1	Africa	0.005
BDI	Burundi	1	Africa	0.001
KHM	Cambodia	1	Asia	0.013
CMR	Cameroon	2	Africa	0.006
CAN	Canada	4	North America	−0.053
CPV	Cabo Verde	2	Africa	0.005
CYM	Cayman Islands	4	South America	0.019
CAF	Central African Republic	1	Africa	0.002
TCD	Chad	1	Africa	0.005
CHL	Chile	4	South America	0.010
CN.AH	Anhui	3	China, Asia	0.019
CN.BJ	Beijing	3	China, Asia	0.025
CN.CQ	Chongqing	3	China, Asia	0.021
CN.FJ	Fujian	3	China, Asia	0.024
CN.GS	Gansu	3	China, Asia	0.025
CN.GD	Guangdong	3	China, Asia	0.019
CN.GX	Guangxi	3	China, Asia	0.020
CN.GZ	Guizhou	3	China, Asia	0.024
CN.HA	Hainan	3	China, Asia	0.031
CN.HB	Hebei	3	China, Asia	0.017
CN.HL	Heilongjiang	3	China, Asia	0.019
CN.HE	Henan	3	China, Asia	0.017
CN.HU	Hubei	3	China, Asia	0.018
CN.HN	Hunan	3	China, Asia	0.018
CN.JS	Jiangsu	3	China, Asia	0.020
CN.JX	Jiangxi	3	China, Asia	0.020
CN.JL	Jilin	3	China, Asia	0.020
CN.LN	Liaoning	3	China, Asia	0.023
CN.NM	Nei Mongol	3	China, Asia	0.025
CN.NX	Ningxia Hui	3	China, Asia	0.034
CN.QH	Qinghai	3	China, Asia	0.036
CN.SA	Shaanxi	3	China, Asia	0.020
CN.SD	Shandong	3	China, Asia	0.020

ISO code	Name	Income level	Geographic region	Consumption change [%]
CN.SH	Shanghai	3	China, Asia	0.024
CN.SX	Shanxi	3	China, Asia	0.020
CN.SC	Sichuan	3	China, Asia	0.017
CN.TJ	Tianjin	3	China, Asia	0.027
CN.XJ	Xinjiang Uygur	3	China, Asia	0.023
CN.XZ	Xizang	3	China, Asia	0.046
CN.YN	Yunnan	3	China, Asia	0.021
CN.ZJ	Zhejiang	3	China, Asia	0.021
COL	Colombia	3	South America	0.009
COG	Republic Congo	2	Africa	0.009
CRI	Costa Rica	3	North America	0.022
HRV	Croatia	4	Europe	0.023
CUB	Cuba	3	North America	0.007
CYP	Cyprus	4	Europe	0.026
CZE	Czech Republic	4	Europe	0.024
CIV	Côte d'Ivoire	2	Africa	0.008
PRK	North Korea	1	Asia	0.003
COD	Democratic Republic Congo	1	Africa	0.008
DNK	Denmark	4	Europe	0.014
DJI	Djibouti	2	Africa	0.004
DOM	Dominican Republic	3	North America	0.016
ECU	Ecuador	3	South America	0.016
EGY	Egypt	2	Africa	0.005
SLV	El Salvador	2	North America	0.015
ERI	Eritrea	1	Africa	0.002
EST	Estonia	4	Europe	0.032
ETH	Ethiopia	1	Africa	0.042
FJI	Fiji	3	Oceania	0.025
FIN	Finland	4	Europe	0.018
FRA	France	4	Europe	0.007
PYF	French Polynesia	4	Oceania	0.019
GAB	Gabon	3	Africa	0.017
GMB	Gambia	1	Africa	0.003
GEO	Georgia	2	Asia	0.012
DEU	Germany	4	Europe	0.006

ISO code	Name	Income level	Geographic region	Consumption change [%]
GHA	Ghana	2	Africa	0.012
GRC	Greece	4	Europe	0.015
GRL	Greenland	4	North America	0.014
GTM	Guatemala	2	North America	0.011
GIN	Guinea	1	Africa	0.007
GUY	Guyana	2	South America	0.010
HTI	Haiti	1	North America	0.007
HND	Honduras	2	North America	0.017
HKG	Hong Kong	4	Asia	0.017
HUN	Hungary	3	Europe	0.015
ISL	Iceland	4	Europe	0.039
IND	India	2	Asia	0.005
IDN	Indonesia	2	Asia	0.005
IRN	Iran	3	Asia	0.005
IRQ	Iraq	3	Asia	0.006
IRL	Ireland	4	Europe	0.004
ISR	Israel	4	Asia	0.016
ITA	Italy	4	Europe	0.005
JAM	Jamaica	3	North America	0.022
JPN	Japan	4	Asia	0.004
JOR	Jordan	3	Asia	0.022
KAZ	Kazakhstan	3	Asia	0.006
KEN	Kenya	1	Africa	0.008
KWT	Kuwait	4	Asia	0.021
KGZ	Kyrgyz Republic	1	Asia	0.010
LAO	Lao PDR	2	Asia	0.005
LVA	Latvia	4	Europe	0.029
LBN	Lebanon	3	Asia	0.016
LSO	Lesotho	2	Africa	0.014
LBR	Liberia	1	Africa	0.004
LBY	Libya	3	Africa	0.004
LIE	Liechtenstein	4	Europe	0.000
LTU	Lithuania	4	Europe	0.027
LUX	Luxembourg	4	Europe	0.031
MAC	Macao	4	Asia	0.045

ISO code	Name	Income level	Geographic region	Consumption change [%]
MDG	Madagascar	1	Africa	0.008
MWI	Malawi	1	Africa	0.007
MYS	Malaysia	3	Asia	0.009
MDV	Maldives	3	Asia	0.025
MLI	Mali	1	Africa	0.004
MLT	Malta	4	Europe	0.040
MRT	Mauritania	2	Africa	0.016
MUS	Mauritius	3	Africa	0.018
MEX	Mexico	3	North America	−0.065
MCO	Monaco	4	Europe	0.000
MNG	Mongolia	2	Asia	0.019
MNE	Montenegro	3	Europe	0.003
MAR	Morocco	2	Africa	0.009
MOZ	Mozambique	1	Africa	0.002
MMR	Myanmar	1	Asia	0.001
NAM	Namibia	3	Africa	0.010
NPL	Nepal	1	Asia	0.010
NLD	Netherlands	4	Europe	0.014
ANT	Netherlands Antilles	4	Sout America	0.044
NCL	New Caledonia	4	Oceania	0.022
NZL	New Zealand	4	Oceania	0.017
NIC	Nicaragua	2	North America	0.015
NER	Niger	1	Africa	0.004
NGA	Nigeria	2	Africa	0.009
NOR	Norway	4	Europe	0.017
PSE	West Bank and Gaza	2	Asia	0.008
OMN	Oman	4	Asia	0.019
PAK	Pakistan	2	Asia	0.005
PAN	Panama	3	South America	0.023
PNG	Papua New Guinea	2	Asia	0.010
PRY	Paraguay	2	South America	0.012
PER	Peru	3	South America	0.012
PHL	Philippines	2	Asia	−0.003
POL	Poland	4	Europe	0.014
PRT	Portugal	4	Europe	0.013

ISO code	Name	Income level	Geographic region	Consumption change [%]
QAT	Qatar	4	Asia	0.011
KOR	South Korea	4	Asia	0.019
MDA	Moldova	2	Europe	0.083
ROU	Romania	3	Europe	0.009
RUS	Russian Federation	4	Asia	0.008
RWA	Rwanda	1	Africa	0.003
WSM	Samoa	2	Oceania	0.005
SMR	San Marino	4	Europe	0.015
STP	São Tomé and Principe	2	Africa	0.002
SAU	Saudi Arabia	4	Asia	0.020
SEN	Senegal	2	Africa	0.006
SRB	Serbia	3	Europe	0.007
SYC	Seychelles	3	Africa	0.021
SLE	Sierra Leone	1	Africa	0.005
SGP	Singapore	4	Asia	0.007
SVK	Slovak Republic	4	Europe	0.021
SVN	Slovenia	4	Europe	0.024
SOM	Somalia	1	Africa	0.000
ZAF	South Africa	3	Africa	0.011
SDS	South Sudan	1	Africa	0.000
ESP	Spain	4	Europe	0.007
LKA	Sri Lanka	2	Asia	0.008
SDN	Sudan	2	Africa	0.000
SUR	Suriname	3	South America	0.014
SWZ	Swaziland	2	Africa	0.009
SWE	Sweden	4	Europe	0.013
CHE	Switzerland	4	Europe	0.012
SYR	Syrian Arab Republic	2	Asia	0.007
TWN	Taiwan	4	Asia	0.028
TJK	Tajikistan	1	Asia	0.001
THA	Thailand	3	Asia	0.008
MKD	Macedonia	3	Europe	0.018
TGO	Togo	1	Africa	0.008
TTO	Trinidad and Tobago	4	South America	0.049
TUN	Tunisia	3	Africa	0.011

ISO code	Name	Income level	Geographic region	Consumption change [%]
TUR	Turkey	3	Asia	0.008
TKM	Turkmenistan	3	Asia	0.019
UGA	Uganda	1	Africa	0.005
UKR	Ukraine	2	Europe	0.009
ARE	United Arab Emirates	4	Asia	0.020
GBR	United Kingdom	4	Europe	0.009
TZA	Tanzania	1	Africa	0.014
US.AL	Alabama	4	USA, North America	−0.078
US.AK	Alaska	4	USA, North America	0.017
US.AZ	Arizona	4	USA, North America	−0.106
US.AR	Arkansas	4	USA, North America	−0.028
US.CA	California	4	USA, North America	−0.219
US.CO	Colorado	4	USA, North America	−0.108
US.CT	Connecticut	4	USA, North America	−0.099
US.DE	Delaware	4	USA, North America	0.032
US.DC	District of Columbia	4	USA, North America	−0.031
US.FL	Florida	4	USA, North America	−0.172
US.GA	Georgia	4	USA, North America	−0.139
US.HI	Hawaii	4	USA, North America	−0.007
US.ID	Idaho	4	USA, North America	0.035
US.IL	Illinois	4	USA, North America	−0.166
US.IN	Indiana	4	USA, North America	−0.115
US.IA	Iowa	4	USA, North America	−0.062
US.KS	Kansas	4	USA, North America	−0.054
US.KY	Kentucky	4	USA, North America	−0.074
US.LA	Louisiana	4	USA, North America	−0.097
US.ME	Maine	4	USA, North America	0.047
US.MD	Maryland	4	USA, North America	−0.121
US.MA	Massachusetts	4	USA, North America	−0.139
US.MI	Michigan	4	USA, North America	−0.135
US.MN	Minnesota	4	USA, North America	−0.112
US.MS	Mississippi	4	USA, North America	−0.021
US.MO	Missouri	4	USA, North America	−0.105
US.MT	Montana	4	USA, North America	0.073
US.NE	Nebraska	4	USA, North America	−0.022

ISO code	Name	Income level	Geographic region	Consumption change [%]
US.NV	Nevada	4	USA, North America	−0.045
US.NH	New Hampshire	4	USA, North America	0.021
US.NJ	New Jersey	4	USA, North America	−0.150
US.NM	New Mexico	4	USA, North America	−0.010
US.NY	New York	4	USA, North America	−0.196
US.NC	North Carolina	4	USA, North America	−0.139
US.ND	North Dakota	4	USA, North America	0.050
US.OH	Ohio	4	USA, North America	−0.154
US.OK	Oklahoma	4	USA, North America	−0.071
US.OR	Oregon	4	USA, North America	−0.085
US.PA	Pennsylvania	4	USA, North America	−0.162
US.RI	Rhode Island	4	USA, North America	0.051
US.SC	South Carolina	4	USA, North America	−0.073
US.SD	South Dakota	4	USA, North America	0.073
US.TN	Tennessee	4	USA, North America	−0.108
US.TX	Texas	4	USA, North America	−0.200
US.UT	Utah	4	USA, North America	−0.046
US.VT	Vermont	4	USA, North America	0.120
US.VA	Virginia	4	USA, North America	−0.140
US.WA	Washington	4	USA, North America	−0.133
US.WV	West Virginia	4	USA, North America	0.016
US.WI	Wisconsin	4	USA, North America	−0.107
US.WY	Wyoming	4	USA, North America	0.080
URY	Uruguay	4	South America	0.018
UZB	Uzbekistan	2	Asia	0.003
VUT	Vanuatu	2	Oceania	0.007
VEN	Venezuela	3	South America	0.006
VNM	Vietnam	2	Asia	0.013
YEM	Yemen	2	Asia	0.010
ZMB	Zambia	2	Africa	0.007
ZWE	Zimbabwe	1	Africa	0.026

Supplementary Table 3: Sectors used in the simulations.

Code	Name	Category
AGRI	Agriculture	vital
FISH	Fishing	vital
MINQ	Mining and quarrying	other
GAST	Hotels and restaurants	other
WHOT	Wholesale trade	relevant
OTHE	Others	other
REPA	Maintenance and repair	other
RETT	Retail trade	relevant
FOOD	Food and beverages	vital
TEXL	Textiles and wearing apparel	relevant
TRAN	Transport	relevant
WOOD	Wood and paper	relevant
OILC	Petroleum, chemical & non-metallic mineral products	relevant
FINC	Financial intermediation and business activities	other
METL	Metal products	relevant
MACH	Electrical and machinery	relevant
TREQ	Transport equipment	relevant
MANU	Other manufacturing	relevant
REXI	Re-export and re-import	other
CONS	Construction	relevant
ADMI	Public administration	other
EDHE	Education, health and other services	vital
HOUS	Private households	other
COMM	Post and telecommunications	relevant
RECY	Recycling	other
ELWA	Electricity, gas and water	vital
FCON	Final consumption	relevant

Supplementary Table 4: Consumption price elasticities per income level and sector category. Values are based on GTAP[26].

	Income level			
Sector category	1	2	3	4
vital	-0.15	-0.2	-0.3	-0.45
relevant	-0.2	-0.3	-0.4	-0.65
other	-0.3	-0.4	-0.5	-0.75

References

[1] USGS. USGS flood event viewer (FEV). URL https://stn.wim.usgs.gov/fev/. Accessed 10 Jun 2020.

[2] Hallegatte, S. *The indirect cost of natural disasters and an economic definition of macroeconomic resilience* (World Bank, 2015).

[3] Baghersad, M. & Zobel, C. W. Economic impact of production bottlenecks caused by disasters impacting interdependent industry sectors. *International Journal of Production Economics* **168**, 71–80 (2015).

[4] Koks, E. E. *et al.* Regional disaster impact analysis: comparing input–output and computable general equilibrium models. *Natural Hazards and Earth System Sciences* **16** (2016).

[5] Kunz, M. *et al.* Investigation of superstorm sandy 2012 in a multi-disciplinary approach. *Natural Hazards and Earth System Sciences* **13**, 2579–2598 (2013).

[6] Federal Reserve Bank of Philadelphia. Coincident economic activity index for louisiana. URL https://fred.stlouisfed.org/series/LAPHCI. Retrieved from FRED, Federal Reserve Bank of St. Louis, Accessed: 27 Apr 2021.

[7] Abel, J. R., Bram, J., Deitz, R. & Orr, J. A. The region's job rebound from superstorm sandy. URL https://libertystreeteconomics.newyorkfed.org/2013/03/the-regions-job-rebound-from-superstorm-sandy.html. Accessed 31 May 2021.

[8] Downtown Alliance. Back to business: The state oflower manhattan four months after hurricane sandy (2015). URL https://downtownny.com/research/back-to-business-the-state-of-lower-manhattan-four-months-after-hurricane-sandy. Accessed 31 May 2021.

[9] Hallegatte, S. & Przyluski, V. The economics of natural disasters: concepts and methods. *Policy Research working paper; no. WPS 5507* (2010).

[10] Strobl, E. The economic growth impact of hurricanes: Evidence from us coastal counties. *Review of Economics and Statistics* **93**, 575–589 (2011).

[11] Hsiang, S. M. & Jina, A. S. The causal effect of environmental catastrophe on long-run economic growth: Evidence from 6,700 cyclones. Tech. Rep., National Bureau of Economic Research (2014).

[12] Krichene, H. *et al.* Long-term impacts of tropical cyclones and fluvial floods on economic growth – empirical evidence on transmission channels at different levels of development. *World Development* **144**, 105475 (2021). 10.1016/j.worlddev.2021.105475.

[13] Federal Reserve Bank of New York. Empire state manufacturing survey supplemental report: Downstate manufacturers report severe disruptions from sandy (2012). URL https://www.newyorkfed.org/medialibrary/media/survey/empire/empire2012/2012_11Supplemental.pdf. Accessed 14 May 2021.

[14] Otto, C., Willner, S. N., Wenz, L., Frieler, K. & Levermann, A. Modeling loss-propagation in the global supply network: The dynamic agent-based model acclimate. *Journal of Economic Dynamics and Control* **83**, 232–269 (2017).

[15] Bierkandt, R., Wenz, L., Willner, S. N. & Levermann, A. Acclimate—a model for economic damage propagation. part 1: Basic formulation of damage transfer within a global supply network and damage conserving dynamics. *Environment Systems and Decisions* **34**, 507–524 (2014).

[16] Wenz, L., Willner, S. N., Bierkandt, R. & Levermann, A. Acclimate—a model for economic damage propagation. part ii: a dynamic formulation of the backward effects of disaster-induced production failures in the global supply network. *Environment Systems and Decisions* **34**, 525–539 (2014).

[17] Willner, S. N., Otto, C. & Levermann, A. Global economic response to river floods. *Nature Climate Change* **8**, 594–598 (2018).

[18] Kuhla, K., Willner, S. N., Otto, C., Wenz, L. & Levermann, A. Future heat stress to reduce people's purchasing power. *PloS one* **16**, e0251210 (2021).

[19] Kuhla, K., Willner, S. N., Otto, C., Geiger, T. & Levermann, A. Ripple resonance amplifies economic welfare loss from weather extremes. *Environmental Research Letters* (2021). In press.

[20] Wenz, L. *et al.* Regional and sectoral disaggregation of multi-regional input–output tables–a flexible algorithm. *Economic Systems Research* **27**, 194–212 (2015).

[21] Lenzen, M., Kanemoto, K., Moran, D. & Geschke, A. Mapping the structure of the world economy. *Environmental science & technology* **46**, 8374–8381 (2012).

[22] Berndt, E. R. & Morrison, C. J. Capacity utilization measures: underlying economic theory and an alternative approach. *The American Economic Review* **71**, 48–52 (1981).

[23] Khokhar, T. Chart: Global wealth grew 66% between 1995 and 2014. http://datatopics.worldbank.org/world-development-indicators/stories/the-classification-of-countries-by-income.html. Accessed 23 Mar 2020.

[24] Reimer, J. & Hertel, T. W. International cross section estimates of demand for use in the gtap model. *GTAP Technical paper* **23** (2004).

[25] Ianchovichina, E. & McDougall, R. Theoretical structure of dynamic gtap. GTAP Technical Paper 17, Global Trade Analysis Project (GTAP) (2000). URL https://www.gtap.agecon.purdue.edu/resources/res_display.asp?RecordID=480.

[26] Hertel, T. W. & van der Mensbrugghe, D. Behavioral parameters. https://www.gtap.agecon.purdue.edu/resources/download/8247.pdf. Accessed 23 May 2020.

[27] Global Administrative Areas. GADM database of global administrative areas, version 3.6 (2018). URL http://www.gadm.org. Accessed 16 Dec 2020.

Appendix of article C

Ripple resonance amplifies economic welfare loss from weather extremes

Authors

Kilian Kuhla, Sven N Willner, Christian Otto, Tobias Geiger and Anders Levermann

Status

Published in *Enviromental Research Letters* in October 2021,
doi: 10.1088/1748-9326/ac2932.

Ripple resonance amplifies economic welfare loss from weather extremes

Appendix A.

The loss-propagation model Acclimate has also been used and described in previous studies [1, 2, 3].

Appendix A.1. Population data for distribution of production

The population data to the corresponding disaster category heat stress, river floods and tropical cyclones bases on the Population Count v4.11 of the GPW data [4] for the year 2015 and are aggregated to the resolution $1800'' \times 1800''$, $150'' \times 150''$ and $360'' \times 360''$, respectively. These population data are used as proxies for the gridded production distribution of a region. That means that the population share of a cell within a region equals to the production share of these cell for this region. Thus, a disaster over a more dense populated site results in a higher direct production losses than over a less dense populated area. We use GADM data [5] to rasterize the same resolutions advanced in coastal areas to deal with inaccuracies at shape boundaries.

Appendix A.2. Global climate models and representative concentration pathways

For projected climate scenarios we use data from four global climate models (GCMs) from the CMIP5 [6] ensemble (HadGEM2-ES [7], IPSL-CM5A-LR [8], MIROC5 [9], GFDL-ESM2M [10]), which are driven by the representative concentration pathways (RCPs) 2.6 and 6.0. The results of the GCMs have been bias-corrected within ISIMIP (project phase 2b) [11] using an observation-based data set basing on a trend-preserving method [12]. As a result, extreme weather events are taken more into account in the time series, which otherwise tends to be averaged out by GCMs. Thus, the daily weather data are represented in the statistics over the ensemble, despite the fact, that there are not historical values. For the next decades, the temporal evolution of the RCPs are mainly determined due to the inertia of the climate system. We use two emissions pathways in order to obtain a larger simulation ensemble.

Appendix A.3. Direct output losses due to heat stress

We use the empirical relationship of daily mean temperature and production derived by Hsiang[13] to build a regional and sectoral production reduction function based on heat stress. This enables us to generate direct output production losses within a regional

sector from daily local mean temperatures. The productivity $p_{s,r}(t)$ of a grid cell r and sector s exhibits a linear reduction α_s (per °C) if the daily mean temperature $T_r(t)$ at day t surpasses 27° C. The affected sectors $\{s\}$ are

- hotels and restaurants (−6.1 p.p./°C),
- wholesale trade (−6.1 p.p./°C),
- mining and quarrying (−4.2 p.p./°C),
- and others (−2.2 p.p./°C).

The unit p.p./°C of the linear reduction α_s is percent points per additional degree Celsius. The empirical relations found [13] are only statistically significant for these sectors. The perturbed productivity per cell and sector states as

$$p_{s,r}(t) = 1 - \alpha_s(T_r(t) - 27\ ^\circ\mathrm{C}) \quad \text{for} \quad T_r(t) \geq 27\ ^\circ\mathrm{C}.$$

The perturbed productivity $p_{s,R}(t)$ per sector s of a region R is derived by aggregating perturbed productivity of every cell r in this region R weighted by the corresponding population distribution of P_r:

$$p_{s,R}(t) = \frac{\sum_{r \in R} p_{s,r}(t) P_r}{\sum_{r \in R} P_r}.$$

We calculate the absolute output losses per region by multiplying the perturbed productivity with the baseline production of the corresponding region.

Appendix A.4. Direct output losses due to river floods

For flood projections, we follow the method of Willner et al 2018 [14] for five hydrological models, CLM45 [15], H08 [16], LPJmL [17], PCR-GLOBWB [18], and WaterGAP2 [19], each of which is driven by the four GCMs for both RCPs (see above) resulting in an ensemble of 40 model/RCP combinations. Their total daily runoff (on a 0.5° resolution) is then further distributed along the river networks by the *CaMa-Flood* river routing model (v3.4.4) [20] with a spatial resolution of 0.005°. This improves the accuracy of peak river discharge compared to the direct use of the output from the hydrological models [21]. To correct for regional biases in the models, we fit a Generalized Extreme Value distribution to the time series of annual maximum discharge for the available historic period (1971–2004) using L-moment estimators. This yields the return period (in historic terms) for each event allowing to incorporate current, regionally distributed flood protection level data given in that spatial unit. Here, we rasterize the "Merged Layer" of the FLOPROS database [22], which incorporates physical infrastructure, policy requirements, and model results to derive protection level data on a sub-national scale. This threshold procedure implies that, when the protection level is exceeded, the flood happens as if there was no protection in the first place, e.g. dams break. We then lookup the return level, i.e. flood depth, corresponding to the return period in a MATSIRO [23] model run driven by observed climate forcing [24]. Cells with a mean daily discharge

of less than 0.1mm/d in 1971–2004 are excluded. After downscaling flood depth and flooded area fraction to a 0.005° resolution, we re-aggregate to a 2.5′ resolution.

In order to derive local production outages from direct flood events (e.g. flooded manufacture), we assume that production capacity is locally reduced by the same extend as the corresponding cell is flooded, regardless of flood depth — the latter, of course, has an effect on a flood's destructive potential. To consider this, we assume that after a flood event the direct production in the affected cells is exponentially (80% per day) recovered if the flood depth was at least 0.5 m, i. e. after roughly 21 days 99% of baseline production capacity of the cell is regained. Flooded regions with lower flood depth are assumed to return to pre-flood production capacity immediately. As a proxy for the distribution of production, we use the distribution of population. Accordingly, the flood fraction of each cell times the population count on the same resolution [4] (constant at 2015 population count) yields daily time series of flood-affected people. For mapping grid cells to regions, we use the GADM database [5] rasterized to 2.5′ and advanced on coastal cells to incorporate coastal population. We use these numbers relative to the total population per region as the production capacity reduction for a non-service sector subset of all sectors given by the input-output data (17 out of 26 economic sectors, given in Tbl. S1). All of these sectors are affected in equal measure with an 80% per day recovery of the production.

Appendix A.5. Direct output losses due to tropical cyclones

Tropical cyclones impacts are based on a probabilistic tool to access regionally-calibrated, high-resolution tropical cyclones landfall activity and associated societal risks as a function of global warming [25]. It is based on novel tropical cyclone simulations using an established dynamical downscaling method [26] in combination with a wind field model [27] and conducted under the protocol of the latest round of the Intersectoral Impact Model Intercomparison Project (ISIMIP2b) [11]. The dynamical downscaling method is driven by CMIP5 climate input data based on four different GCMs (HadGEM2-ES, MIROC5, IPSL-CM5A-LR, GFDL-ESM2M) and two RCPs (RCP2.6 and RCP6.0). For each simulated year and GCM a total of 300 tropical cyclone tracks have been produced. The number of simulated years varies depending on the GCM due to available climate variables in the CMIP5 archive and constraints of the ISIMIP simulation protocol (HadGEM2-ES: 1950-2100 (RCP2.6 & RCP6.0), MIROC5: 1861-2299 (RCP2.6), 1861-2100 (RCP6.0), IPSL-CM5A-LR: 1861-2299 (RCP2.6), 1861-2100 (RCP6.0), GFDL-ESM2M: 1861-2100 (RCP2.6 & RCP6.0)), where the corresponding RCP scenarios extend the historical scenario after 2005, jointly referred to as warming scenarios below. Note that ISIMIP provides access to the tropical cyclone simulations for research purposes only and upon a reasonable request.

Raw tropical cyclone track data (historical observations based on the International Best Track Archive for Climate Stewardship (IBTrACS v03r10) [28] and simulations) are processed with a wind field model in order to equip tropical cyclone tracks with

realistic size and intensity distribution according to the methodology used to produce the Tropical Cyclone Exposure Database (TCE-DAT) [29, 30] on a global spatial grid with $360'' \times 360''$ resolution. This allows for a globally and historically consistent comparison of tropical cyclone exposure across observations and simulations. Next, the full sample of observed and simulated tropical cyclone wind field data is reduced to contain landfalling events only, where we define landfall by exposure, i.e. if a given tropical cyclone produces a minimum wind speed of above 33 knots above land. For each of the considered eight world regions (East Pacific (EP), North Atlantic (NP), North Indian (NI), South Indian East (SIE), South Indian West (SIW), West Pacific North (WPN), West Pacific South (WPS), South Pacific (SP)) we then produce annual landfall time series for tropical cyclone frequency (i.e. annual number of landfalls) and intensity (i.e. mean annual maximum wind speed at landfall). For the southern hemisphere, where tropical cyclone seasons range across two years, effective annual time series are created by shifting the time stamp to cover a complete season, and dropping incomplete seasons from the analysis. For calibration purposes of the probabilistic tool, a tropical cyclone landfall is only counted once per region, i.e. multiple landfalls in different countries within a region are accounted for, but are only recorded where the neglected, and recorded where wind speed at landfall is maximum. The observational landfall time series are used to calibrate simulated landfall time series as the provided tropical cyclone simulations are not calibrated for this purpose. To do so, the total number of simulated landfalls as well as the mean annual wind speed at landfall per region between 1950 and 2015 (1980-2015 for NI, SIE, SIW, SP due to limited reliability of observations prior to the satellite era) are matched with observations. This provides a long-term average calibration of the hazard in physical terms (not in terms of exposure) that conserves fluctuations around the long-term mean caused by natural variability and stochasticity of landfall occurrence. Let us iterate again, that the assumption of counting only single landfalls is only used for calibration purposes and to avoid double-counting. The underlying simulated tropical cyclone tracks are accounted for their full extend and may observe landfalls in different countries.

To deduce how frequency and intensity of the simulated regional GCM- and RCP-specific tropical cyclone landfall time series vary with global mean temperature (GMT) change and large scale patterns of internal variability such as the El Nino Southern Oscillation (ENSO), we regress the respective time series with time series for GMT and ENSO, that are extracted from the respective variables ('tas' and 'psl') from the underlying GCMs. Correlation between GMT and ENSO time series are avoided by using a 21-year (3-month) running mean for GMT (ENSO) to capture long-term trends (seasonal/annual variability). Frequency is regressed using Poisson regression; intensity is regressed using ordinary least squares (OLS). We use a hierarchy of regressions to eliminate insignificant contributions, whose presence might alter the significance of the remaining climate indices. Depending on the region-GCM combination a substantial fraction of landfall variability can be explained by GMT and ENSO, in particular for landfall frequency. However, for some region-GCM combinations no or very little

explained variance is associated with GMT and ENSO, in particular for landfall intensity. This residual (or unexplained) variance is explicitly taken into account by the probabilistic tropical cyclone tool in the following step, as the stochasticity of landfall remains an essential characteristic of tropical cyclone activity.

Based on the functional dependence of simulated tropical cyclone landfall time series and GMT and ENSO retrieved above, the probabilistic tool allows to draw an arbitrary number of random tropical cyclone samples that mimic the number of tropical cyclone landfalls and mean landfall intensity in a given region and year (with given GMT and ENSO state). These samples are drawn from all available simulated tropical cyclones with landfall for a given GCM and warming scenario in two steps: First, a random sample without replacement of tropical cyclones by region is drawn according to a Poisson distribution with expected number of landfalls prescribed by the functional GMT and ENSO dependence. Second, the mean landfall intensity of this random sample is compared to the expected mean landfall intensity, which is rooted in the tropical cyclone track data analysis and the GMT and ENSO dependency considered above. If the mean landfall intensity does not fall into the interval given by the expected mean landfall intensity and the residual variation obtained from the intensity regression mentioned above, the random sample is rejected and a new sample is drawn in step 1. If repeatedly no representative sample can be drawn, the set of all landfalling tropical cyclones is iteratively and randomly reduced by an increasing fraction of events with landfall speed above (below) the expected mean landfall speed until the desired number of random tropical cyclone samples for a given year, i.e. a given GMT and ENSO state, are obtained. For the present work, we generated five tropical cyclone realizations for each year, basin, GCM, and warming scenario.

Using the diagonal extension of the individual static temporally fixed tropical cyclones wind footprints and assuming that the average translational speed of a tropical storm is 15 km/h, we assigned each storm a landfall life span in days (usually between 3-5 days) to obtain a time resolved tropical cyclone evolution. Afterwards, these time-resolved tropical cyclones are distributed randomly along the basin specific duration of the tropical cyclone season within the season usual for the basin . Finally, all basins with associated tropical cyclones are mapped onto a unified grid, resulting in daily global wind maps of tropical cyclones on an $360'' \times 360''$ resolved grid for 20 years.

Using this gridded tropical cyclones time series we calculated the regional and sectoral production outage. A wind speed higher than 64 kn results in a total production outage of non-service sectors for the production within this cell (see above). We assume that the direct production of a tropical cyclone affected cell recovers exponentially (80% per day) if the maximum wind speed exceeds 96 kn (major tropical cyclones). Thus, those affected production sites need about 21 days to recover 99% of their production capacity. Cells impacted by tropical cyclones with a lower wind speed are assumed to return to pre-disaster production capacity immediately. All non-service sectors are affected equally, whereas we do not make additional assumptions about the service sectors, which fulfill a broad and complex spectrum of operations, and leave them unaffected during the disaster.

The total production reduction of a firm is proportional to the failed cells in a region weighted by their total production share. Regional direct output losses are generated from the absolute production reduction with respect to the baseline production.

Appendix A.6. Simulation ensemble

In our study we use four global climate models, two representative concentration pathways, five hydrological models and five tropical cyclones realizations for our direct output loss time series and subsequent comprehensive economic damage via Acclimate. Tbl. A1 shows which models are used for which disaster scenario and how many simulation runs resulted.

Table A1. Simulation ensemble Table of disaster scenario with its corresponding physical models and resulting ensemble number.

	Scenarios of			
	Heat stress	River floods	Tropical cyclones	Consecutive disasters
Global climate models	×	×	×	×
Representative concentration pathways	×	×	×	×
Hydrological models		×		×
Tropical cyclones realizations			×	×
Resulting ensemble number	8	40	40	200

Each simulation run consists of 20 years (2020–2039). The accumulated absolute direct output losses of single disaster scenarios can exceed the direct output losses of consecutive disaster scenarios. This is due to the fact that production losses are capped at the lower end: a firm cannot produce less than 0% of its baseline production. But it may happen that the sum of the single production reductions of each disaster category yield to a negative production. In consecutive disaster scenarios, such production remains at 0% with respect to baseline. In the single disaster scenarios, the individual production does not fall below this value, but rather accumulate to negative production after the analysis. As a result, the sum of the single direct output losses and the direct losses of consecutive disasters may differ. To ensure that the quantities of the simulated years are as comparable as possible, we define a tolerance range (1.8%) within which the deviation of annual direct losses must fall and exclude those that do not pass this threshold. For this threshold none of the 4000 simulated years have to be excluded. A sensitivity analysis depicts that economic ripple effects do not significantly change for different thresholds of the tolerance range or rather fewer included simulated years (Fig. S6). It is important to note that the direct losses of consecutive disaster events may be rather smaller than those of aggregated single disaster scenarios. Nevertheless, we see the ripple resonance effects, loss offset and amplification, for the former compared to the latter.

Appendix A.7. Indirect production losses

With the agent-based loss-propagation model Acclimate [1] we calculate the dynamics of the global trade and overall production and consumption changes due to extreme events. The economic baseline network is thereby given by multi-regional input-output data (see below). Acclimate calculates the behavior of regional sectors and consumers if the baseline network is perturbed by direct production losses, which cause demand, supply, or price shocks. Each regional sector – an economic agent at a node of the network – tries to maximize its profit by choosing the optimal production level, distribution of demand among its suppliers and upstream demand to others. Within the network, storage inventories and transport delays may buffer supply shocks. If a regional sectors faces higher demand, it can activate idle capacities in acceptance of additional production costs, thus shifting prices. Important to note is that local prices change endogenously, and mismatches of supply and demand resolve explicitly over time. In the disaster aftermath, supply, demand, and production relax back to the unperturbed baseline. The relaxation time is thereby determined by the market dynamics. The computed production and consumption losses arise from price effects, demand surge as well as supply shortages. A comprehensive model description of Acclimate is provided in Otto et al 2017 [1].

Appendix A.8. Consumer price elasticity

The reactions of consumers to price shifts depend on the corresponding commodity or service and on the economic background network. Thus, we implement a regional and sectoral resolved consumer price elasticity in our model. We group the regions into four income levels – low, lower-middle, upper-middle, high income level – depending on their gross national income (GNI) per capita (GNIpc) (Tbl. S2). The flexibility to price rises increases with increasing income. Therefore ,countries with a higher GNIpc are able to react more resiliently to price changes. In this study we use the inflation-adjusted income level classification provided by World Bank [31] for the year 2012.

The Global Trade Analysis Project (GTAP) [32] provides income elasticities of demand for 140 regions and 10 commodity classes [33]. We map the economic sectors used in Acclimate to the GTAP commodity classes in GTAP and group them into three categories: vital, relevant, and other (see Tbl. S1). The consumer is less flexible to price fluctuations for more life essential commodities than for luxury goods or services. Using GTAP data set, we assign a specific consumer price elasticity to every pair of income level and sector category (Tbl. A2). We assume low to no substitutability between the large sector classes (Tbl. S1), thus we can neglect cross-sector elasticity.

Table A2. Consumption price elasticities per income level and sector category. Values are based on GTAP [34] for income levels low (1), lower-middle (2), upper-middle (3), and high (4) income level.

	Income level			
Sector category	1	2	3	4
vital	-0.15	-0.2	-0.3	-0.45
relevant	-0.2	-0.3	-0.4	-0.65
other	-0.3	-0.4	-0.5	-0.75

Appendix A.9. Economic network

We use the multi-regional input-output (MRIO) tables of the EORA simplified data set of the year 2015 (v199.82) [35] as baseline trading network. Flows of commodities or services between regional sectors are given as monetary flows in USD per year. We remove flows smaller than 1 million USD/year and regional sectors with negative value added from the network as well. We neglect a few regions (Belarus, Sudan, Moldova, Zimbabwe) in our analyses, since the inaccurate data basis for this regions causes partially unrealistic time series. Further, we disaggregate the United States of America and China into 51 states and 32 provinces, respectively, due to their immense economic power. For this we use the gross regional product data and a disaggregation algorithm [36]. In this study, we refer to a nation, US state or Chinese province as a "region". Every economic sector in a region or "regional sector" constitutes an individual economic agent, a representative firm, in the loss-propagation model Acclimate. We use the EORA MRIO table to calculate the baseline production of each regional sector. Overall, this baseline economic network consists of 27 sectors (including one consumer sector) and 268 regions, which results in $7,236$ agents (see Tbls. S1 and S2).

Appendix B.

Appendix B.1. Table of contents

Appendix B.2. Supplement figures

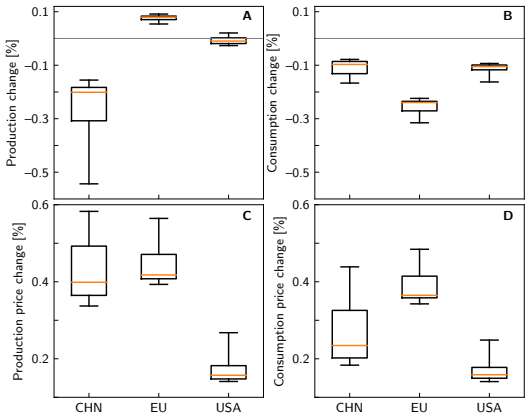

Fig. S1. Ensemble ranges of production and consumption changes for China, the EU, and the USA. The EU which is less exposed increases production to compensate for supply shortages which causes prices for consumers to rise. Orange lines, boxes and whiskers indicate median changes estimates, the 25–75 and 5–95 percentile ranges, respectively. Data sets rely on consecutive disaster scenarios.
(**A**): Annual production change relative to baseline production for China, the EU, and the USA. Changes are caused by direct output losses due to extreme events and by indirect market effects, such as shifted demand. The EU is able to increase production, while China has to reduce production.
(**B**): Annual consumption change relative to baseline consumption for China, the EU, and the USA.
(**C**): Annual production price change for China, the EU, and the USA. Due to increased demand the EU's production price rise. China's production price increases because of strong production outages due to extreme events.
(**D**): Annual consumption price change relative to initial condition for China, the EU, and the USA. Shifted demand leads to local price fluctuations. The loss of consumption goods due to local production failure caused by weather extremes lead to supply shortages and therefore price increases. The EU's increased production, caused by additional demand, further intensifies the price pressure on EU consumers.

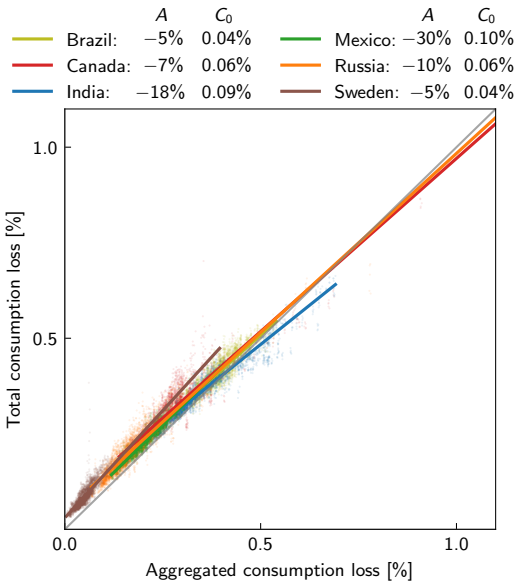

Fig. S2. Annual consumption losses for the total impact over those for the (aggregated) sum of independent impacts for countries with negative resonance amplification factor. Values for different countries are given in different colors; Brazil (yellow), Canada (red), India (blue), Mexico (green), Russia (orange), and Sweden (brown). Each data point represents the one year within ensemble. Losses are relative to the (unperturbed) baseline consumption.

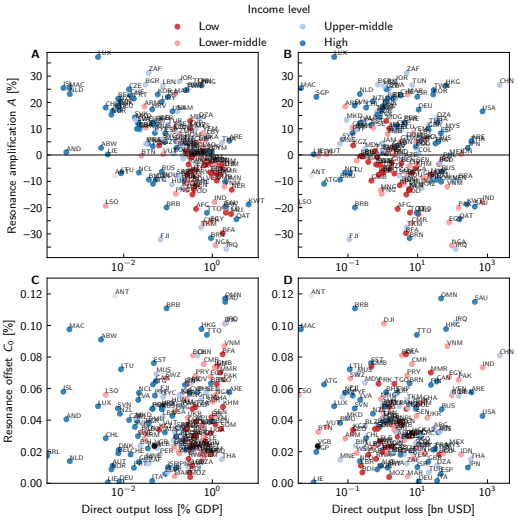

Fig. S3. Resonance amplification factors tend to fall with increasing direct output losses relative to baseline production output. Resonance amplification factor (upper panels – (**A**), (**B**)) and offset (lower panels – (**C**), (**D**)) per relative (left panels – (**A**), (**C**)) and absolute (right panels – (**B**), (**D**)) direct production loss per national share of world production. Colors depict the national income level.

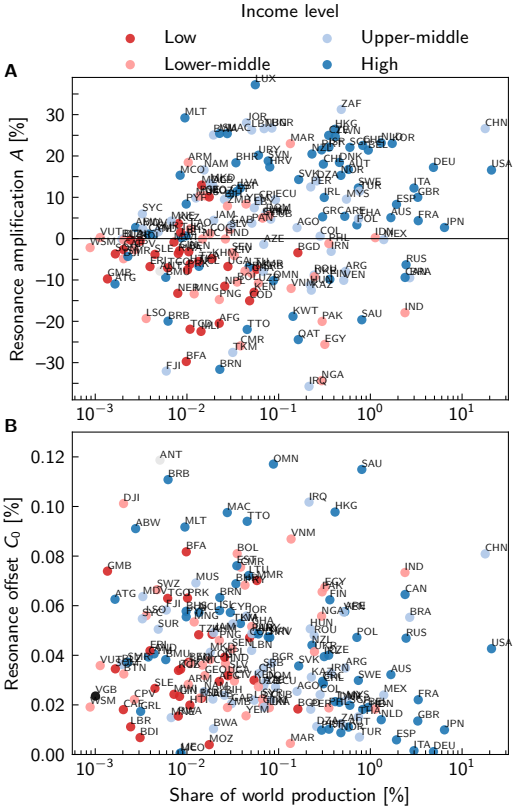

Fig. S4. Countries with higher income tend to have positive resonance amplification factors, whereas lower income countries tend to have a negative one. Resonance amplification factor (upper panel – (**A**)) and offset (lower panel – (**B**)) per national share of world production. Colors depict the national income level.

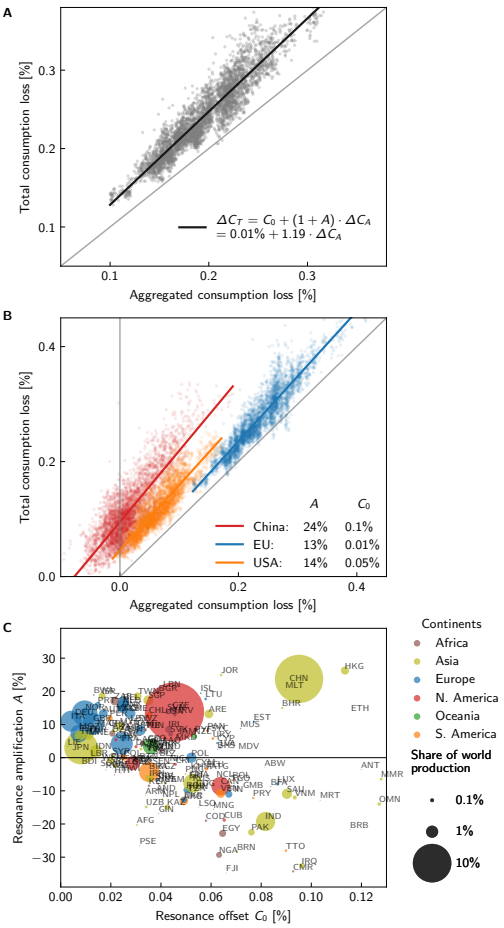

Fig. S5. Economic ripple resonance for economic network of 2012 — consumption losses of consecutive disasters are increased in comparison to losses of aggregated single disasters. (**A**), (**B**): Annual consumption losses for the *total* impact over those for the (*aggregated*) sum of independent impacts, globally (**A**), grey dots) as well as for China, EU, and the USA (**B**), coloured dots). Each data point represents one year within the ensemble. Losses are relative to the (unperturbed) baseline consumption. The solid lines depict the resonance analysis with *resonance amplification factor* A and *resonance offset* C_0. (**C**): Resonance amplification factor and offset per country. The area of each circle represents the country's share of the world production, its color depicts the geographic region. A few extreme outliers (of economically small countries) are not in the visual range.

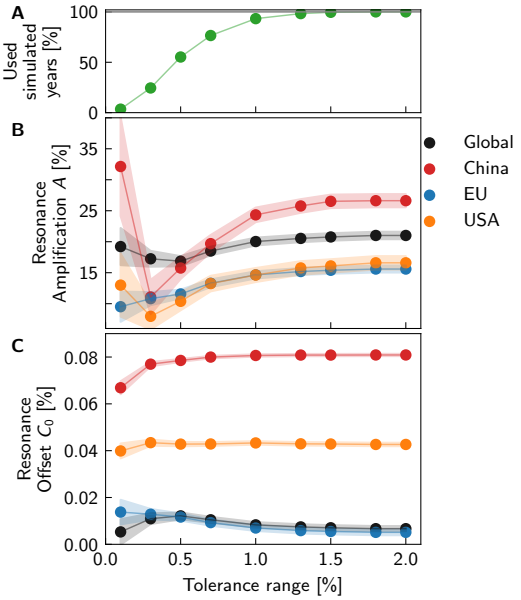

Fig. S6. Lowering the direct output loss tolerance range decreases the number of used simulation years but does not change the amplification factor and loss offset significantly. Annual total direct output losses have to lay in the tolerance range of corresponding aggregated direct output losses, if they are to be used in the consecutive analysis (cf. methods).
(**A**): Used data points to compare total and aggregated economic losses. Decreasing tolerance range leads to fewer suitable annual data pairs. Maximum possible number of annual data points is 4000 ($\equiv$ 100%). The exclusion of data pairs starts below a tolerance range of 1.8%.
(**B**): Amplification factor due to economic ripple resonance of global economy (black), China (red), the EU (blue) and the USA (orange) for fixed tolerance ranges of direct output losses. Shadow area corresponds to the likely range (16.7 to 83.3 percentiles).
(**C**): Loss offset due to economic ripple resonance of global economy (black), China (red), the EU (blue) and the USA (orange) for fixed tolerance ranges of direct production losses. Shadow area corresponds to the likely range (16.7 to 83.3 percentiles).

Appendix B.3. Supplement table

Table S1. Sectors used in the simulations.

Code	Name	Category	Affected by Heat stress	Affected by River floods	Affected by Trop. cycl.
AGRI	Agriculture	vital		×	×
FISH	Fishing	vital		×	×
MINQ	Mining and quarrying	other	×	×	×
GAST	Hotels and restaurants	other	×		
WHOT	Wholesale trade	relevant	×	×	×
OTHE	Others	other	×		
REPA	Maintenance and Repair	other		×	×
RETT	Retail Trade	relevant		×	×
FOOD	Food and Beverages	vital		×	×
TEXL	Textiles and Wearing Apparel	relevant		×	×
TRAN	Transport	relevant		×	×
WOOD	Wood and Paper	relevant		×	×
OILC	Petroleum, Chemical & Non-Metallic Mineral Products	relevant		×	×
FINC	Financial Intermediation & Business Activities	other			
METL	Metal Products	relevant		×	×
MACH	Electrical and Machinery	relevant		×	×
TREQ	Transport Equipment	relevant		×	×
MANU	Other Manufacturing	relevant		×	×
REXI	Re-export and Re-import	other			
CONS	Construction	relevant		×	×
ADMI	Public Administration	other			
EDHE	Education, Health and Other Services	vital			
HOUS	Private Households	other			
COMM	Post and Telecommunications	relevant			
RECY	Recycling	other			
ELWA	Electricity, Gas and Water	vital		×	×
FCON	Final consumption	relevant			

Table S2. Regions used in the simulations. Income level corresponds to Gross National Income per capita (GNIpc) of 2012.
Income level 1 ("low income"): GNIpc $< 1,305$ USD
Income level 2 ("lower-middle income"): $1,036$ USD $<$ GNIpc $< 4,085$ USD
Income level 3 ("upper-middle income"): $4,086$ USD $<$ GNIpc $< 12,615$ USD
Income level 4 ("high income"): $12,616$ USD $<$ GNIpc
Ripple resonance is expressed by resonance offset C_0 and resonance amplification factor A.

ISO3 code	Name of region	Income level	Continent	Amplification factor A	Resonance offset C_0
AFG	Afghanistan	1	Asia	−20.5 (±0.2)%	0.029 (±0.001)%
ALB	Albania	3	Europe	12.8 (±0.6)%	0.022 (±0.001)%
DZA	Algeria	3	Africa	14.0 (±0.8)%	0.011 (±0.001)%
AND	Andorra	4	Europe	1.1 (±1.4)%	0.041 (±0.001)%
AGO	Angola	3	Africa	2.7 (±0.6)%	0.025 (±0.001)%
ATG	Antigua and Barbuda	4	N. America	−11.0 (±0.8)%	0.063 (±0.001)%
ARG	Argentina	3	S. America	−7.9 (±0.3)%	0.035 (±0.001)%
ARM	Armenia	2	Asia	18.4 (±0.9)%	0.028 (±0.001)%
ABW	Aruba	4	S. America	2.7 (±1.4)%	0.091 (±0.001)%
AUS	Australia	4	Oceania	5.1 (±1.0)%	0.032 (±0.002)%
AUT	Austria	4	Europe	16.7 (±0.7)%	0.011 (±0.001)%
AZE	Azerbaijan	3	Asia	−1.4 (±0.5)%	0.028 (±0.001)%
BHS	Bahamas	4	N. America	0.7 (±0.5)%	0.058 (±0.001)%
BHR	Bahrain	4	Asia	18.4 (±1.3)%	0.069 (±0.001)%
BGD	Bangladesh	1	Asia	−3.4 (±0.3)%	0.018 (±0.001)%
BRB	Barbados	4	N. America	−20.0 (±1.0)%	0.111 (±0.001)%
BLR	Belarus	3	Europe	—-	—-
BEL	Belgium	4	Europe	21.4 (±0.8)%	0.019 (±0.001)%
BLZ	Belize	3	N. America	−0.1 (±0.2)%	0.036 (±0.001)%
BEN	Benin	1	Africa	−3.2 (±0.4)%	0.037 (±0.002)%
BMU	Bermuda	4	N. America	−9.4 (±1.4)%	0.038 (±0.001)%
BTN	Bhutan	2	Asia	−0.3 (±0.8)%	0.032 (±0.001)%
BOL	Bolivia	2	S. America	−10.5 (±0.7)%	0.081 (±0.003)%
BIH	Bosnia and Herzegovina	3	Europe	9.5 (±0.9)%	0.024 (±0.001)%
BWA	Botswana	3	Africa	25.1 (±1.1)%	0.010 (±0.001)%
BRA	Brazil	3	S. America	−9.5 (±0.7)%	0.055 (±0.003)%
VGB	British Virgin Islands	0	S. America	−77.6 (±0.6)%	0.024 (±0.001)%
BRN	Brunei Darussalam	4	Asia	−31.6 (±1.3)%	0.063 (±0.001)%
BGR	Bulgaria	3	Europe	26.7 (±1.2)%	0.037 (±0.001)%
BFA	Burkina Faso	1	Africa	−29.7 (±0.5)%	0.082 (±0.001)%
BDI	Burundi	1	Africa	−0.6 (±0.1)%	0.007 (±0.001)%
KHM	Cambodia	1	Asia	−4.8 (±0.3)%	0.048 (±0.001)%
CMR	Cameroon	2	Africa	−25.9 (±0.4)%	0.076 (±0.001)%
CAN	Canada	4	N. America	−9.4 (±0.6)%	0.065 (±0.002)%
CPV	Cabo Verde	2	Africa	−2.7 (±1.0)%	0.022 (±0.001)%
CYM	Cayman Islands	4	S. America	1.1 (±0.4)%	0.039 (±0.001)%
CAF	Central African Republic	1	Africa	−2.6 (±0.1)%	0.018 (±0.001)%
TCD	Chad	1	Africa	−21.9 (±0.6)%	0.266 (±0.009)%

ISO3 code	Name of region	Income level	Continent	Amplification factor A	Resonance offset C_0
CHL	Chile	4	S. America	18.0 (±0.8)%	0.029 (±0.001)%
CN.AH	Anhui	3	China	27.5 (±1.2)%	0.073 (±0.001)%
CN.BJ	Beijing	3	China	28.3 (±1.2)%	0.100 (±0.001)%
CN.CQ	Chongqing	3	China	28.2 (±1.4)%	0.083 (±0.001)%
CN.FJ	Fujian	3	China	27.5 (±1.1)%	0.096 (±0.001)%
CN.GS	Gansu	3	China	13.1 (±2.1)%	0.106 (±0.001)%
CN.GD	Guangdong	3	China	21.3 (±0.8)%	0.074 (±0.001)%
CN.GX	Guangxi	3	China	28.2 (±1.3)%	0.081 (±0.001)%
CN.GZ	Guizhou	3	China	24.9 (±1.7)%	0.096 (±0.001)%
CN.HA	Hainan	3	China	−17.8 (±2.4)%	0.094 (±0.003)%
CN.HB	Hebei	3	China	25.8 (±1.0)%	0.066 (±0.001)%
CN.HL	Heilongjiang	3	China	28.1 (±1.4)%	0.084 (±0.001)%
CN.HE	Henan	3	China	24.4 (±1.0)%	0.062 (±0.001)%
CN.HU	Hubei	3	China	25.9 (±1.0)%	0.067 (±0.001)%
CN.HN	Hunan	3	China	26.0 (±1.1)%	0.067 (±0.001)%
CN.JS	Jiangsu	3	China	21.4 (±0.8)%	0.075 (±0.001)%
CN.JX	Jiangxi	3	China	28.2 (±1.3)%	0.081 (±0.001)%
CN.JL	Jilin	3	China	27.9 (±1.5)%	0.087 (±0.001)%
CN.LN	Liaoning	3	China	27.0 (±1.1)%	0.093 (±0.001)%
CN.NM	Nei Mongol	3	China	29.3 (±1.3)%	0.109 (±0.001)%
CN.NX	Ningxia Hui	3	China	−31.4 (±2.4)%	0.079 (±0.004)%
CN.QH	Qinghai	3	China	−40.7 (±2.4)%	0.066 (±0.004)%
CN.SA	Shaanxi	3	China	28.1 (±1.3)%	0.079 (±0.001)%
CN.SD	Shandong	3	China	22.0 (±0.8)%	0.076 (±0.001)%
CN.SH	Shanghai	3	China	27.7 (±1.1)%	0.097 (±0.001)%
CN.SX	Shanxi	3	China	27.2 (±1.5)%	0.090 (±0.001)%
CN.SC	Sichuan	3	China	25.7 (±1.0)%	0.066 (±0.001)%
CN.TJ	Tianjin	3	China	29.4 (±1.4)%	0.113 (±0.001)%
CN.XJ	Xinjiang Uygur	3	China	22.3 (±1.8)%	0.099 (±0.001)%
CN.XZ	Xizang	3	China	−68.7 (±2.2)%	−0.004 (±0.006)%
CN.YN	Yunnan	3	China	27.7 (±1.5)%	0.088 (±0.001)%
CN.ZJ	Zhejiang	3	China	24.2 (±0.9)%	0.083 (±0.001)%
COL	Colombia	3	S. America	0.6 (±0.3)%	0.024 (±0.001)%
COG	Republic Congo	2	Africa	1.2 (±0.6)%	0.038 (±0.001)%
CRI	Costa Rica	3	N. America	9.1 (±0.6)%	0.033 (±0.001)%
HRV	Croatia	4	Europe	17.3 (±1.1)%	0.047 (±0.001)%
CUB	Cuba	3	N. America	4.7 (±0.4)%	0.022 (±0.001)%
CYP	Cyprus	4	Europe	10.8 (±0.9)%	0.057 (±0.001)%
CZE	Czech Republic	4	Europe	25.0 (±1.1)%	0.040 (±0.001)%
CIV	Côte d'Ivoire	2	Africa	−4.1 (±0.5)%	0.030 (±0.001)%
PRK	North Korea	1	Asia	−7.6 (±1.2)%	0.063 (±0.001)%
COD	Democratic Republic Congo	1	Africa	−15.0 (±0.5)%	0.047 (±0.001)%
DNK	Denmark	4	Europe	18.4 (±0.8)%	0.021 (±0.001)%
DJI	Djibouti	2	Africa	−4.9 (±0.8)%	0.101 (±0.010)%
DOM	Dominican Republic	3	N. America	6.0 (±0.4)%	0.029 (±0.001)%
ECU	Ecuador	3	S. America	9.4 (±0.5)%	0.027 (±0.001)%
EGY	Egypt	2	Africa	−25.6 (±0.4)%	0.067 (±0.001)%

ISO3 code	Name of region	Income level	Continent	Amplification factor A	Resonance offset C_0
SLV	El Salvador	2	N. America	2.2 (±0.3)%	0.034 (±0.001)%
ERI	Eritrea	1	Africa	−6.8 (±0.5)%	0.042 (±0.003)%
EST	Estonia	4	Europe	11.4 (±0.4)%	0.076 (±0.001)%
ETH	Ethiopia	1	Africa	42.2 (±3.5)%	0.158 (±0.005)%
FJI	Fiji	3	Oceania	−32.0 (±1.4)%	0.058 (±0.001)%
FIN	Finland	4	Europe	−9.8 (±0.1)%	0.062 (±0.001)%
FRA	France	4	Europe	4.3 (±0.4)%	0.022 (±0.001)%
PYF	French Polynesia	4	Oceania	8.4 (±1.2)%	0.056 (±0.001)%
GAB	Gabon	3	Africa	3.2 (±0.3)%	0.020 (±0.001)%
GMB	Gambia	1	Africa	−9.7 (±0.3)%	0.074 (±0.003)%
GEO	Georgia	2	Asia	10.4 (±1.0)%	0.032 (±0.001)%
DEU	Germany	4	Europe	17.2 (±0.6)%	0.001 (±0.001)%
GHA	Ghana	2	Africa	−8.4 (±0.4)%	0.052 (±0.001)%
GRC	Greece	4	Europe	5.3 (±0.4)%	0.030 (±0.001)%
GRL	Greenland	4	N. America	−42.1 (±1.2)%	0.017 (±0.001)%
GTM	Guatemala	2	N. America	5.0 (±0.4)%	0.020 (±0.001)%
GIN	Guinea	1	Africa	−2.9 (±0.2)%	0.023 (±0.001)%
GUY	Guyana	2	S. America	−1.8 (±0.4)%	0.033 (±0.001)%
HTI	Haiti	1	N. America	−6.2 (±0.2)%	0.020 (±0.001)%
HND	Honduras	2	N. America	−0.1 (±0.3)%	0.037 (±0.001)%
HKG	Hong Kong	4	Asia	26.5 (±0.9)%	0.098 (±0.001)%
HUN	Hungary	3	Europe	−11.3 (±0.3)%	0.051 (±0.001)%
ISL	Iceland	4	Europe	25.5 (±1.6)%	0.058 (±0.001)%
IND	India	2	Asia	−17.9 (±0.4)%	0.073 (±0.001)%
IDN	Indonesia	2	Asia	0.2 (±0.5)%	0.018 (±0.001)%
IRN	Iran	3	Asia	−3.1 (±0.5)%	0.033 (±0.001)%
IRQ	Iraq	3	Asia	−35.7 (±0.5)%	0.102 (±0.001)%
IRL	Ireland	4	Europe	10.0 (±0.6)%	0.039 (±0.001)%
ISR	Israel	4	Asia	22.1 (±0.9)%	0.010 (±0.001)%
ITA	Italy	4	Europe	12.2 (±0.5)%	0.002 (±0.001)%
JAM	Jamaica	3	N. America	4.4 (±0.8)%	0.049 (±0.001)%
JPN	Japan	4	Asia	2.7 (±0.3)%	0.010 (±0.001)%
JOR	Jordan	3	Asia	28.0 (±1.0)%	0.056 (±0.001)%
KAZ	Kazakhstan	3	Asia	−12.5 (±0.3)%	0.031 (±0.001)%
KEN	Kenya	1	Africa	−13.0 (±0.2)%	0.030 (±0.001)%
KWT	Kuwait	4	Asia	−18.8 (±1.1)%	0.264 (±0.010)%
KGZ	Kyrgyz Republic	1	Asia	3.7 (±0.9)%	0.034 (±0.001)%
LAO	Lao PDR	2	Asia	2.4 (±0.3)%	0.037 (±0.001)%
LVA	Latvia	4	Europe	12.2 (±0.5)%	0.053 (±0.001)%
LBN	Lebanon	3	Asia	26.3 (±1.2)%	0.042 (±0.001)%
LSO	Lesotho	2	Africa	−19.3 (±2.1)%	0.056 (±0.001)%
LBR	Liberia	1	Africa	−0.4 (±0.2)%	0.011 (±0.001)%
LBY	Libya	3	Africa	7.5 (±0.6)%	0.022 (±0.001)%
LIE	Liechtenstein	4	Europe	0.2 (±0.1)%	0.001 (±0.001)%
LTU	Lithuania	4	Europe	−6.9 (±1.3)%	0.072 (±0.001)%
LUX	Luxembourg	4	Europe	37.2 (±1.5)%	0.049 (±0.001)%
MAC	Macao	4	Asia	25.4 (±1.8)%	0.098 (±0.001)%

ISO3 code	Name of region	Income level	Continent	Amplification factor A	Resonance offset C_0
MDG	Madagascar	1	Africa	12.9 (±0.4)%	0.023 (±0.001)%
MWI	Malawi	1	Africa	−0.8 (±0.3)%	0.024 (±0.001)%
MYS	Malaysia	3	Asia	9.5 (±0.5)%	0.022 (±0.002)%
MDV	Maldives	3	Asia	2.3 (±0.5)%	0.064 (±0.001)%
MLI	Mali	1	Africa	−22.4 (±0.5)%	0.244 (±0.006)%
MLT	Malta	4	Europe	29.2 (±1.9)%	0.092 (±0.001)%
MRT	Mauritania	2	Africa	−100.1 (±0.4)%	0.713 (±0.010)%
MUS	Mauritius	3	Africa	9.8 (±1.1)%	0.069 (±0.001)%
MEX	Mexico	3	N. America	−0.2 (±0.5)%	0.024 (±0.001)%
MCO	Monaco	4	Europe	15.3 (±0.6)%	0.000 (±0.001)%
MNG	Mongolia	2	Asia	−13.4 (±0.7)%	0.053 (±0.001)%
MNE	Montenegro	3	Europe	4.2 (±0.4)%	0.015 (±0.001)%
MAR	Morocco	2	Africa	23.0 (±0.8)%	0.004 (±0.001)%
MOZ	Mozambique	1	Africa	10.1 (±0.3)%	0.004 (±0.001)%
MMR	Myanmar	1	Asia	−7.4 (±0.1)%	0.070 (±0.002)%
NAM	Namibia	3	Africa	16.6 (±1.1)%	0.025 (±0.001)%
NPL	Nepal	1	Asia	−11.5 (±0.9)%	0.039 (±0.001)%
NLD	Netherlands	4	Europe	23.2 (±0.8)%	0.014 (±0.001)%
ANT	Netherlands Antilles	0	Europe	−7.9 (±2.0)%	0.119 (±0.004)%
NCL	New Caledonia	4	Oceania	−6.7 (±1.2)%	0.057 (±0.001)%
NZL	New Zealand	4	Oceania	20.5 (±1.2)%	0.044 (±0.001)%
NIC	Nicaragua	2	N. America	−0.1 (±0.2)%	0.036 (±0.001)%
NER	Niger	1	Africa	−13.2 (±0.9)%	0.185 (±0.013)%
NGA	Nigeria	2	Africa	−34.4 (±0.4)%	0.056 (±0.001)%
NOR	Norway	4	Europe	15.3 (±0.7)%	0.009 (±0.002)%
PSE	West Bank and Gaza	2	Asia	10.3 (±0.6)%	0.023 (±0.001)%
OMN	Oman	4	Asia	−10.2 (±1.0)%	0.117 (±0.004)%
PAK	Pakistan	2	Asia	−20.0 (±0.3)%	0.066 (±0.001)%
PAN	Panama	3	S. America	3.7 (±0.5)%	0.049 (±0.001)%
PNG	Papua New Guinea	2	Asia	−14.7 (±1.0)%	0.046 (±0.001)%
PRY	Paraguay	2	S. America	−7.9 (±0.5)%	0.068 (±0.002)%
PER	Peru	3	S. America	12.5 (±0.6)%	0.018 (±0.001)%
PHL	Philippines	2	Asia	−1.2 (±0.3)%	0.019 (±0.001)%
POL	Poland	4	Europe	3.3 (±0.6)%	0.047 (±0.001)%
PRT	Portugal	4	Europe	21.5 (±0.9)%	0.010 (±0.001)%
QAT	Qatar	4	Asia	−24.4 (±1.1)%	0.294 (±0.011)%
KOR	South Korea	4	Asia	23.0 (±0.6)%	−0.016 (±0.002)%
MDA	Moldova	2	Europe	—	—
ROU	Romania	3	Europe	−8.8 (±0.4)%	0.048 (±0.001)%
RUS	Russian Federation	4	Asia	−6.3 (±0.5)%	0.047 (±0.001)%
RWA	Rwanda	1	Africa	−3.6 (±0.1)%	0.015 (±0.001)%
WSM	Samoa	2	Oceania	−2.2 (±0.4)%	0.019 (±0.001)%
SMR	San Marino	4	Europe	−4.3 (±0.8)%	0.037 (±0.001)%
STP	São Tomé and Principe	2	Africa	10.4 (±0.6)%	0.010 (±0.001)%
SAU	Saudi Arabia	4	Asia	−19.6 (±1.2)%	0.115 (±0.004)%
SEN	Senegal	2	Africa	−3.4 (±0.3)%	0.043 (±0.002)%
SRB	Serbia	3	Europe	−7.9 (±0.2)%	0.035 (±0.001)%

ISO3 code	Name of region	Income level	Continent	Amplification factor A	Resonance offset C_0
SYC	Seychelles	3	Africa	6.0 (±0.6)%	0.055 (±0.001)%
SLE	Sierra Leone	1	Africa	−3.8 (±0.2)%	0.027 (±0.001)%
SGP	Singapore	4	Asia	22.1 (±0.7)%	0.020 (±0.002)%
SVK	Slovak Republic	4	Europe	14.3 (±0.8)%	0.036 (±0.002)%
SVN	Slovenia	4	Europe	18.8 (±1.0)%	0.047 (±0.001)%
SOM	Somalia	1	Africa	−3.7 (±0.3)%	0.035 (±0.005)%
ZAF	South Africa	3	Africa	31.3 (±1.1)%	0.012 (±0.001)%
SSD	South Sudan	1	Africa	−0.4 (±0.1)%	0.009 (±0.001)%
ESP	Spain	4	Europe	8.3 (±0.4)%	0.006 (±0.002)%
LKA	Sri Lanka	2	Asia	5.7 (±0.5)%	0.019 (±0.001)%
SDN	Sudan	2	Africa	—-	—-
SUR	Suriname	3	S. America	1.6 (±0.1)%	0.051 (±0.001)%
SWZ	Swaziland	2	Africa	−88.5 (±1.0)%	0.066 (±0.001)%
SWE	Sweden	4	Europe	12.3 (±0.7)%	0.030 (±0.001)%
CHE	Switzerland	4	Europe	22.6 (±0.9)%	0.018 (±0.001)%
SYR	Syrian Arab Republic	2	Asia	5.0 (±0.6)%	0.022 (±0.001)%
TWN	Taiwan	4	Asia	24.7 (±0.9)%	0.021 (±0.001)%
TJK	Tajikistan	1	Asia	1.5 (±0.9)%	0.034 (±0.001)%
THA	Thailand	3	Asia	4.8 (±0.4)%	0.015 (±0.002)%
MKD	Macedonia	3	Europe	13.3 (±0.8)%	0.041 (±0.001)%
TGO	Togo	1	Africa	−7.1 (±0.3)%	0.063 (±0.002)%
TTO	Trinidad and Tobago	4	S. America	−22.0 (±1.5)%	0.094 (±0.001)%
TUN	Tunisia	3	Africa	26.6 (±1.0)%	0.019 (±0.001)%
TUR	Turkey	3	Asia	11.5 (±0.6)%	0.007 (±0.001)%
TKM	Turkmenistan	3	Asia	−27.5 (±0.5)%	0.053 (±0.001)%
UGA	Uganda	1	Africa	−6.7 (±0.1)%	0.032 (±0.001)%
UKR	Ukraine	2	Europe	−9.2 (±0.2)%	0.041 (±0.001)%
ARE	United Arab Emirates	4	Asia	5.4 (±0.9)%	0.058 (±0.003)%
GBR	United Kingdom	4	Europe	10.0 (±0.5)%	0.014 (±0.001)%
TZA	Tanzania	1	Africa	−5.5 (±0.3)%	0.048 (±0.001)%
US.AL	Alabama	4	USA	16.2 (±1.3)%	0.056 (±0.001)%
US.AK	Alaska	4	USA	−12.6 (±1.5)%	0.063 (±0.001)%
US.AZ	Arizona	4	USA	17.5 (±1.2)%	0.050 (±0.001)%
US.AR	Arkansas	4	USA	10.7 (±1.4)%	0.066 (±0.001)%
US.CA	California	4	USA	14.2 (±0.9)%	0.030 (±0.001)%
US.CO	Colorado	4	USA	17.7 (±1.2)%	0.048 (±0.001)%
US.CT	Connecticut	4	USA	17.3 (±1.3)%	0.052 (±0.001)%
US.DE	Delaware	4	USA	−3.0 (±1.5)%	0.068 (±0.001)%
US.DC	District of Columbia	4	USA	11.0 (±1.4)%	0.065 (±0.001)%
US.FL	Florida	4	USA	16.5 (±1.0)%	0.036 (±0.001)%
US.GA	Georgia	4	USA	17.6 (±1.1)%	0.042 (±0.001)%
US.HI	Hawaii	4	USA	2.2 (±1.5)%	0.069 (±0.001)%
US.ID	Idaho	4	USA	−4.7 (±1.5)%	0.068 (±0.001)%
US.IL	Illinois	4	USA	16.8 (±1.0)%	0.037 (±0.001)%
US.IN	Indiana	4	USA	17.8 (±1.2)%	0.047 (±0.001)%
US.IA	Iowa	4	USA	15.4 (±1.3)%	0.059 (±0.001)%
US.KS	Kansas	4	USA	13.9 (±1.4)%	0.062 (±0.001)%

ISO3 code	Name of region	Income level	Continent	Amplification factor A	Resonance offset C_0
US.KY	Kentucky	4	USA	15.9 (±1.3)%	0.057 (±0.001)%
US.LA	Louisiana	4	USA	17.1 (±1.3)%	0.053 (±0.001)%
US.ME	Maine	4	USA	−9.9 (±1.5)%	0.065 (±0.001)%
US.MD	Maryland	4	USA	17.8 (±1.2)%	0.046 (±0.001)%
US.MA	Massachusetts	4	USA	17.6 (±1.1)%	0.042 (±0.001)%
US.MI	Michigan	4	USA	17.6 (±1.1)%	0.042 (±0.001)%
US.MN	Minnesota	4	USA	17.7 (±1.2)%	0.048 (±0.001)%
US.MS	Mississippi	4	USA	8.6 (±1.5)%	0.067 (±0.001)%
US.MO	Missouri	4	USA	17.6 (±1.2)%	0.049 (±0.001)%
US.MT	Montana	4	USA	−19.8 (±1.5)%	0.057 (±0.001)%
US.NE	Nebraska	4	USA	9.9 (±1.4)%	0.066 (±0.001)%
US.NV	Nevada	4	USA	13.2 (±1.4)%	0.063 (±0.001)%
US.NH	New Hampshire	4	USA	−0.5 (±1.5)%	0.069 (±0.001)%
US.NJ	New Jersey	4	USA	17.4 (±1.1)%	0.040 (±0.001)%
US.NM	New Mexico	4	USA	5.8 (±1.5)%	0.069 (±0.001)%
US.NY	New York	4	USA	15.3 (±0.9)%	0.033 (±0.001)%
US.NC	North Carolina	4	USA	17.5 (±1.1)%	0.042 (±0.001)%
US.ND	North Dakota	4	USA	−11.0 (±1.5)%	0.065 (±0.001)%
US.OH	Ohio	4	USA	17.3 (±1.1)%	0.039 (±0.001)%
US.OK	Oklahoma	4	USA	15.8 (±1.3)%	0.058 (±0.001)%
US.OR	Oregon	4	USA	16.6 (±1.3)%	0.055 (±0.001)%
US.PA	Pennsylvania	4	USA	17.0 (±1.0)%	0.038 (±0.001)%
US.RI	Rhode Island	4	USA	−11.1 (±1.5)%	0.064 (±0.001)%
US.SC	South Carolina	4	USA	16.2 (±1.3)%	0.056 (±0.001)%
US.SD	South Dakota	4	USA	−18.5 (±1.5)%	0.058 (±0.001)%
US.TN	Tennessee	4	USA	17.7 (±1.2)%	0.048 (±0.001)%
US.TX	Texas	4	USA	15.0 (±0.9)%	0.032 (±0.001)%
US.UT	Utah	4	USA	13.8 (±1.4)%	0.062 (±0.001)%
US.VT	Vermont	4	USA	−40.2 (±1.4)%	0.029 (±0.002)%
US.VA	Virginia	4	USA	17.6 (±1.1)%	0.042 (±0.001)%
US.WA	Washington	4	USA	17.7 (±1.1)%	0.043 (±0.001)%
US.WV	West Virginia	4	USA	−0.9 (±1.5)%	0.069 (±0.001)%
US.WI	Wisconsin	4	USA	17.6 (±1.2)%	0.049 (±0.001)%
US.WY	Wyoming	4	USA	−27.0 (±1.5)%	0.049 (±0.002)%
URY	Uruguay	4	S. America	20.2 (±0.6)%	0.049 (±0.001)%
UZB	Uzbekistan	2	Asia	−10.7 (±0.3)%	0.027 (±0.001)%
VUT	Vanuatu	2	Oceania	0.3 (±0.5)%	0.036 (±0.001)%
VEN	Venezuela	3	S. America	−10.1 (±0.3)%	0.057 (±0.001)%
VNM	Vietnam	2	Asia	−12.0 (±0.2)%	0.087 (±0.001)%
YEM	Yemen	2	Asia	8.4 (±0.6)%	0.016 (±0.001)%
ZMB	Zambia	2	Africa	7.9 (±0.5)%	0.019 (±0.001)%
ZWE	Zimbabwe	1	Africa	—-	—-

Table S3. Resonance amplification factor and offset for regions of FUND.

Region code	Amplification factor A	Resonance offset C_0
WEU	15.4 (±0.5)%	0.004 (±0.001)%
JPK	6.1 (±0.3)%	0.002 (±0.001)%
ANZ	8.5 (±1.0)%	0.028 (±0.002)%
CEE	7.2 (±0.7)%	0.042 (±0.001)%
FSU	−2.8 (±0.5)%	0.039 (±0.001)%
MDE	7.7 (±0.8)%	0.021 (±0.002)%
CAM	1.2 (±0.5)%	0.023 (±0.001)%
SAM	0.9 (±0.5)%	0.021 (±0.001)%
SAS	−16.1 (±0.4)%	0.062 (±0.001)%
SEA	9.1 (±0.4)%	0.008 (±0.001)%
CHI	27.9 (±1.0)%	0.081 (±0.001)%
NAF	−20.6 (±0.5)%	0.049 (±0.001)%
SSA	−4.6 (±0.6)%	0.029 (±0.001)%
SIS	10.8 (±0.6)%	0.038 (±0.001)%

Table S4. Resonance amplification factor and offset for regions of GCAM.

Region code	Amplification factor A	Resonance offset C_0
Africa_Eastern	−6.5 (±0.2)%	0.034 (±0.001)%
Africa_Northern	−20.6 (±0.5)%	0.049 (±0.001)%
Africa_Southern	8.9 (±0.6)%	0.021 (±0.001)%
Africa_Western	−23.2 (±0.6)%	0.069 (±0.002)%
Australia_NZ	8.5 (±1.0)%	0.028 (±0.002)%
Central_America_and_the_Caribbean	9.7 (±0.4)%	0.032 (±0.001)%
Central_Asia	−6.8 (±0.4)%	0.029 (±0.001)%
EU-12	8.9 (±0.7)%	0.042 (±0.001)%
EU-15	14.9 (±0.5)%	0.004 (±0.001)%
Europe_Eastern	−9.2 (±0.2)%	0.042 (±0.001)%
European_Free_Trade_Association	20.5 (±0.8)%	0.012 (±0.001)%
Europe_Non_EU	13.3 (±0.6)%	0.010 (±0.001)%
Middle_East	4.9 (±0.8)%	0.032 (±0.003)%
South_America_Northern	−7.2 (±0.3)%	0.043 (±0.001)%
South_America_Southern	18.9 (±0.7)%	0.018 (±0.001)%
South_Asia	2.5 (±0.4)%	0.018 (±0.001)%
Southeast_Asia	14.2 (±0.5)%	−0.001 (±0.002)%

Table S5. Resonance amplification factor and offset for regions of IMAGE.

Region code	Amplification factor A	Resonance offset C_0
CAM	9.0 (±0.4)%	0.036 (±0.001)%
RSAM	2.6 (±0.3)%	0.026 (±0.001)%
NAF	−20.6 (±0.5)%	0.049 (±0.001)%
WAF	−23.2 (±0.6)%	0.069 (±0.002)%
EAF	−6.5 (±0.2)%	0.035 (±0.001)%
WEU	15.4 (±0.5)%	0.004 (±0.001)%
CEU	8.7 (±0.7)%	0.042 (±0.001)%
UKR	−9.2 (±0.2)%	0.042 (±0.001)%
CAS	−9.7 (±0.3)%	0.030 (±0.001)%
RUR	−5.8 (±0.5)%	0.045 (±0.001)%
MDE	4.8 (±0.8)%	0.032 (±0.003)%
KOR	23.0 (±0.6)%	−0.015 (±0.002)%
CHI	28.4 (±1.0)%	0.080 (±0.001)%
SEA	7.8 (±0.4)%	0.016 (±0.002)%
IDR	0.4 (±0.5)%	0.018 (±0.001)%
OCE	8.9 (±1.0)%	0.028 (±0.002)%
RSAS	−15.3 (±0.3)%	0.043 (±0.001)%
RSAF	8.9 (±0.6)%	0.021 (±0.001)%

Table S6. Resonance amplification factor and offset for regions of REMIND.

Region code	Amplification factor A	Resonance offset C_0
LAM	3.3 (±0.4)%	0.017 (±0.001)%
OAS	13.0 (±0.4)%	0.001 (±0.001)%
AFR	−12.2 (±0.5)%	0.041 (±0.001)%
EUR	15.5 (±0.6)%	0.005 (±0.001)%
ROW	9.0 (±0.7)%	0.023 (±0.001)%
MEA	4.1 (±0.7)%	0.028 (±0.002)%
CHN	27.9 (±1.0)%	0.082 (±0.001)%

Table S7. Resonance amplification factor and offset for regions of RICE.

Region code	Amplification factor A	Resonance offset C_0
AFR	−8.3 (±0.5)%	0.034 (±0.001)%
OTHASIA	5.1 (±0.3)%	0.010 (±0.001)%
EURASIA	3.3 (±0.5)%	0.033 (±0.001)%
LATAM	3.3 (±0.4)%	0.017 (±0.001)%
OHI	14.9 (±0.7)%	0.021 (±0.002)%
MIDEAST	5.1 (±0.8)%	0.032 (±0.003)%
FSU	−0.4 (±0.4)%	0.031 (±0.001)%

Table S8. Resonance amplification factor and offset for regions of WITCH.

Region code	Amplification factor A	Resonance offset C_0
CAJAZ	5.8 (±0.4)%	0.006 (±0.001)%
CHINA	27.2 (±1.1)%	0.079 (±0.001)%
EASIA	6.5 (±0.4)%	0.019 (±0.001)%
KOSAU	21.6 (±0.8)%	−0.002 (±0.002)%
LACA	3.3 (±0.4)%	0.017 (±0.001)%
NEWEURO	14.9 (±0.5)%	0.004 (±0.001)%
OLDEURO	15.7 (±0.8)%	0.027 (±0.001)%
SASIA	−15.9 (±0.3)%	0.044 (±0.001)%
MENA	0.4 (±0.7)%	0.041 (±0.002)%
SSA	−4.7 (±0.6)%	0.030 (±0.001)%
TE	−7.1 (±0.3)%	0.037 (±0.001)%

References

[1] C. Otto, S. Willner, L. Wenz, K. Frieler, A. Levermann, Modeling loss-propagation in the global supply network: The dynamic agent-based model acclimate. *J. Econ. Dyn. Control* **83**, 232–269 (2017).

[2] S. N. Willner, C. Otto, A. Levermann, Global economic response to river floods. *Nat. Clim. Chang.* **8**, 594–598 (2018).

[3] K. Kuhla, S. N. Willner, C. Otto, L. Wenz, A. Levermann, Future heat stress to reduce people's purchasing power. *PLoS One* **16**, e0251210 (2021).

[4] Center for International Earth Science Information Network – CIESIN – Columbia University, Gridded population of the world, version 4 (GPWv4): Population count (2016). URL `http://dx.doi.org/10.7927/H4X63JVC` Accessed: 2019-3-19.

[5] Global Administrative Areas, GADM database of global administrative areas, version 3.6 (2019). URL `http://www.gadm.org`. Accessed: 2019-12-19.

[6] K. E. Taylor, R. J. Stouffer, G. A. Meehl, An overview of CMIP5 and the experiment design. *Bull. Amer. Meteor. Soc.* **93**, 485–498 (2012).

[7] C. Jones, J. Hughes, N. Bellouin, S. Hardiman, G. Jones, J. Knight, S. Liddicoat, F. O'Connor, R. Andres, C. Bell, K.-O. Boo, A. Bozzo, N. Butchart, P. Cadule, K. Corbin, M. Doutriaux-Boucher, P. Friedlingstein, J. Gornall, L. Gray, P. Halloran, G. Hurtt, W. Ingram, J.-F. Lamarque, R. Law, M. Meinshausen, S. Osprey, E. Palin, L. Parsons Chini, T. Raddatz, M. Sanderson, A. Sellar, A. Schurer, P. Valdes, N. Wood, S. Woodward, M. Yoshioka, M. Zerroukat, The HadGEM2-ES implementation of CMIP5 centennial simulations. *Geosci. Model Dev.* **4**, 543–570 (2011).

[8] J.-L. Dufresne, M.-A. Foujols, S. Denvil, A. Caubel, O. Marti, O. Aumont, Y. Balkanski, S. Bekki, H. Bellenger, R. Benshila, S. Bony, L. Bopp, P. Braconnot, P. Brockmann, P. Cadule, F. Cheruy, F. Codron, A. Cozic, D. Cugnet, N. de Noblet, J.-P. Duvel, C. Ethé, L. Fairhead, T. Fichefet, S. Flavoni, P. Friedlingstein, J.-Y. Grandpeix, L. Guez, E. Guilyardi, D. Hauglustaine, F. Hourdin, A. Idelkadi, J. Ghattas, S. Joussaume, M. Kageyama, G. Krinner, S. Labetoulle, A. Lahellec, M.-P. Lefebvre, F. Lefevre, C. Levy, Z. Li, J. Lloyd, F. Lott, G. Madec, M. Mancip, M. Marchand, S. Masson, Y. Meurdesoif, J. Mignot, I. Musat, S. Parouty, J. Polcher, C. Rio, M. Schulz, D. Swingedouw, S. Szopa, C. Talandier, P. Terray, N. Viovy, N. Vuichard, Climate change projections using the IPSL-CM5 earth system model: From CMIP3 to CMIP5. *Clim. Dyn.* **40**, 2123–2165 (2013).

[9] M. Watanabe, T. Suzuki, R. O'ishi, Y. Komuro, S. Watanabe, S. Emori, T. Takemura, M. Chikira, T. Ogura, M. Sekiguchi, K. Takata, D. Yamazaki, T. Yokohata, T. Nozawa, H. Hasumi, H. Tatebe, M. Kimoto, Improved climate simulation by MIROC5: Mean states, variability, and climate sensitivity. *J. Climate* **23**, 6312–6335 (2010).

[10] J. P. Dunne, J. G. John, A. J. Adcroft, S. M. Griffies, R. W. Hallberg, E. Shevliakova, R. J. Stouffer, W. Cooke, K. A. Dunne, M. J. Harrison, J. P. Krasting, S. L. Malyshev, P. Milly, P. J. Phillipps, L. T. Sentman, B. L. Samuels, M. J. Spelman, M. Winton, A. T. Wittenberg, N. Zadeh, GFDL's ESM2 global coupled Climate–Carbon earth system models. Part I: Physical formulation and baseline simulation characteristics. *J. Clim.* **25**, 6646–6665 (2012).

[11] K. Frieler, S. Lange, F. Piontek, C. P. Reyer, J. Schewe, L. Warszawski, F. Zhao, L. Chini, S. Denvil, K. Emanuel, T. Geiger, K. Halladay, G. Hurtt, M. Mengel, D. Murakami, S. Ostberg, A. Popp, R. Riva, M. Stevanovic, T. Suzuki, J. Volkholz, E. Burke, P. Ciais, K. Ebi, T. D. Eddy, J. Elliott, E. Galbraith, S. N. Gosling, F. Hattermann, T. Hickler, J. Hinkel, C. Hof, V. Huber, J. Jägermeyr, V. Krysanova, R. Marcé, H. Müller Schmied, I. Mouratiadou, D. Pierson, D. P. Tittensor, R. Vautard, M. van Vliet, M. F. Biber, R. A. Betts, B. L. Bodirsky, D. Deryng, S. Frolking, C. D. Jones, H. K. Lotze, H. Lotze-Campen, R. Sahajpal, K. Thonicke, H. Tian, Y. Yamagata, Assessing the impacts of 1.5 °C global warming – simulation protocol of the inter-sectoral impact model intercomparison project (ISIMIP2b). *Geosci. Model Dev.* **10**, 4321–4345 (2017).

[12] S. Hempel, K. Frieler, L. Warszawski, J. Schewe, F. Piontek, A trend-preserving bias correction –

the ISI-MIP approach. *Earth Syst. Dynam.* **4**, 219–236 (2013).

[13] S. Hsiang, Temperatures and cyclones strongly associated with economic production in the Caribbean and central America. *Proc. Nat. Acad. Sci. USA* **107**, 15367–15372 (2010).

[14] S. N. Willner, A. Levermann, F. Zhao, K. Frieler, Adaptation required to preserve future high-end river flood risk at present levels. *Sci. Adv.* **4**, eaao1914 (2018).

[15] G. Leng, M. Huang, Q. Tang, L. R. Leung, A modeling study of irrigation effects on global surface water and groundwater resources under a changing climate. *J. Adv. Model. Earth Syst.* **7**, 1285–1304 (2015).

[16] N. Hanasaki, S. Yoshikawa, Y. Pokhrel, S. Kanae, A global hydrological simulation to specify the sources of water used by humans. *Hydrol. Earth Syst. Sci.* **22**, 789–817 (2018).

[17] S. Sitch, B. Smith, I. Prentice, A. Arneth, A. Bondeau, W. Cramer, J. Kaplan, S. Levis, W. Lucht, M. Sykes, K. Thonicke, S. Venevsky, Evaluation of ecosystem dynamics, plant geography and terrestrial carbon cycling in the LPJ dynamic global vegetation model. *Glob. Chang. Biol.* **9**, 161–185 (2003).

[18] Y. Wada, D. Wisser, M. Bierkens, Global modeling of withdrawal, allocation and consumptive use of surface water and groundwater resources. *Earth Syst. Dynam.* **5**, 15–40 (2014).

[19] H. Müller Schmied, L. Adam, S. Eisner, G. Fink, M. Flörke, H. Kim, T. Oki, F. T. Portmann, R. Reinecke, C. Riedel, Q. Song, J. Zhang, P. Döll, Variations of global and continental water balance components as impacted by climate forcing uncertainty and human water use. *Hydrol. Earth Syst. Sci.* **20**, 2877–2898 (2016).

[20] D. Yamazaki, S. Kanae, H. Kim, T. Oki, A physically based description of floodplain inundation dynamics in a global river routing model. *Water Resour. Res.* **47** (2011).

[21] F. Zhao, T. I. E. Veldkamp, K. Frieler, J. Schewe, S. Ostberg, S. Willner, B. Schauberger, S. N. Gosling, H. M. Schmied, F. T. Portmann, G. Leng, M. Huang, X. Liu, Q. Tang, N. Hanasaki, H. Biemans, D. Gerten, Y. Satoh, Y. Pokhrel, T. Stacke, P. Ciais, J. Chang, A. Ducharne, M. Guimberteau, Y. Wada, H. Kim, D. Yamazaki, The critical role of the routing scheme in simulating peak river discharge in global hydrological models. *Environ. Res. Lett.* **12**, 075003 (2017).

[22] P. Scussolini, J. Aerts, B. Jongman, L. Bouwer, H. Winsemius, H. de Moel, P. Ward, FLOPROS: An evolving global database of flood protection standards. *Nat. Hazards Earth Syst. Sci.* **3**, 7275–7309 (2015).

[23] K. Takata, S. Emori, T. Watanabe, Development of the minimal advanced treatments of surface interaction and runoff. *Glob. Planet Change* **38**, 209–222 (2003).

[24] H. Kim, P. J.-F. Yeh, T. Oki, S. Kanae, Role of rivers in the seasonal variations of terrestrial water storage over global basins. *Geophys. Res. Lett.* **36** (2009).

[25] M. Bertrand, P. Pfleiderer, M. Kretschmer, T. Geiger, C.-F. Schleussner, Using discovery algorithms to forecast seasonal tropical cyclone genesis in the Atlantic. In *Geophysical Research Abstracts*, vol. 21 (2019).

[26] K. Emanuel, Downscaling CMIP5 climate models shows increased tropical cyclone activity over the 21st century. *Proc. Nat. Acad. Sci. USA* **110**, 12219–12224 (2013).

[27] G. Holland, A revised hurricane Pressure–Wind model. *Mon. Weather Rev.* **136**, 3432–3445 (2008).

[28] K. R. Knapp, M. C. Kruk, D. H. Levinson, H. J. Diamond, C. J. Neumann, The international best track archive for climate stewardship (IBTrACS). *Bull. Amer. Meteor. Soc.* **91**, 363–376 (2010).

[29] T. Geiger, K. Frieler, D. N. Bresch, A global historical data set of tropical cyclone exposure (TCE-DAT). *Earth Syst. Sci. Data* **10**, 185–194 (2018).

[30] T. Geiger, J. Gütschow, D. N. Bresch, K. Emanuel, K. Frieler, Double benefit of limiting global warming for tropical cyclone exposure. *Nat. Clim. Chang.* **in press**, (2021).

[31] T. Khokhar, Chart: Global wealth grew 66% between 1995 and 2014. URL `http://datatopics.worldbank.org/world-development-indicators/stories/the-classification-of-countries-by-income.html`. Accessed: 2020-3-23.

[32] E. Ianchovichina, R. McDougall, Theoretical structure of dynamic GTAP. GTAP Technical Paper 17, Global Trade Analysis Project (GTAP) (2000). URL `https://www.gtap.agecon.purdue.edu/resources/res_display.asp?RecordID=480`.

[33] J. Reimer, T. Hertel, International Cross Section Estimates of Demand for Use in the GTAP Model. *GTAP Technical paper* **23** (2004).

[34] T. W. Hertel, D. van der Mensbrugghe, Behavioral parameters. URL `https://www.gtap.agecon.purdue.edu/resources/download/8247.pdf`. Accessed: 2020-3-23.

[35] M. Lenzen, K. Kanemoto,D. Moran, A. Geschke, Mapping the structure of the world economy. *Environ. Sci. Technol.* **46**, 8374–381 (2012).

[36] L. Wenz, S. N. Willner, A. Radebach, R. Bierkandt, J. C. Steckel, A. Levermann, Regional and sectoral disaggregation of multi-regional Input–Output tables – a flexible algorithm. *Econ. Syst. Res.* **27**, 194–212 (2014).

Appendix of article D

Non-linear amplification of economic growth losses from US hurricanes under global warming

Authors

Christian Otto[†], Kilian Kuhla[†], Tobias Geiger, Jacob Schewe, Katja Frieler
[†] with equal contributions

Status

Submitted to *Nature Communications*,
preprint doi: 10.21203/rs.3.rs-654258/v2.

B Supplementary information

B.1 Supplementary tables and figures for the US

Tbl. S1. Historical hurricanes that made landfall in the US between 1980 and 2014. 1st through 4th columns list names and years of landfall of the storms as reported by the IBTRaCS database[66], storm severity (category 4-5 hurricanes according to Saffir-Simpsons scale[8]), and storm surge index according to ref.[64], respectively. The 5th column reports categorized asset losses based on reported asset losses by Munich Re's NatCatSERVICE database[1]: small ($> 10^{-4}$%), moderate ($> 10^{-3}$%), strong ($> 10^{-2}$%), severe ($> 10^{-1}$%). The asset losses are measured relative to the growth domestic product of the US (according to World Banks' and OECD's National Accounts database[5]) in the year of landfall.

Name	Year	Cat. 4-5 hurricane	Surge index	Asset losses category
Alberto	1994		9.2	strong
Alicia	1983		52.7	strong
Allen	1980	x	36.4	strong
Allison	1989		20.8	moderate
Allison	2001		24.1	strong
Andrew	1992	x	23.4	severe
Arlene	1993		11.5	small
Barry	2001		9.8	small
Bertha	1996		16.4	moderate
Beryl	1994		4.6	moderate
Bill	2003		9.4	small
Bob	1985		6.8	small
Bob	1991		3.4	strong
Bonnie	1986		14.6	small
Bonnie	1998		22.7	strong
Bonnie	2004		5.8	small
Bret	1999	x	4.7	moderate
Chantal	1989		11.9	moderate
Charley	2004	x	3.2	severe
Charley	1986		7.8	small
Charley	1998		12.7	moderate
Cindy	2005		1.9	moderate
Claudette	2003		55.1	moderate

Name	Year	Cat. 4-5 hurricane	Surge index	Asset losses category
Danielle	1980		2.6	small
Danny	1985		14.5	moderate
Danny	1997		19.1	moderate
Debby	2012		8.1	moderate
Dennis	2005	x	108.1	strong
Dennis	1981		5.6	small
Dennis	1999		5.3	moderate
Diana	1984	x	9.6	moderate
Dolly	2008		7.9	moderate
Earl	1998		22.7	small
Edouard	1996	x	2.6	small
Elena	1985		33	strong
Emily	1993		7.3	small
Erin	1995		30.3	moderate
Erin	2007		7.9	small
Ernesto	2006		7.2	moderate
Fay	2008		6.9	moderate
Florence	1988		9.2	small
Floyd	1999	x	17.6	strong
Fran	1996		4.4	strong
Frances	2004	x	9.4	strong
Frances	1998		25.8	moderate
Gabrielle	2001		5.4	moderate
Gaston	2004		5	small
Georges	1998	x	85.4	strong
Gilbert	1988	x	9.5	moderate
Gloria	1985		15.7	strong
Gordon	1994		6.1	moderate
Gordon	2000		7	small
Gustav	2008	x	71	strong
Hanna	2008		2.3	small
Hermine	2010		8.5	moderate
Hugo	1989	x	25.9	severe
Humberto	2007		7.9	small

Name	Year	Cat. 4-5 hurricane	Surge index	Asset losses category
Ida	2009		16.3	moderate
Ike	2008	x	105.1	severe
Iniki	1992		3.9	strong
Irene	1999		10.8	moderate
Irene	2011		55.6	strong
Isaac	2012		80.3	strong
Isabel	2003	x	8.1	strong
Iselle	2014		3.5	small
Isidore	1984		5.5	small
Isidore	2002		47.4	moderate
Ivan	2004	x	53	severe
Iwa	1982		2.5	moderate
Jeanne	2004		14	strong
Jerry	1989		6.8	small
Josephine	1996		10.1	moderate
Juan	1985		34.1	strong
Kate	1985		8.4	moderate
Katrina	2005	x	114.4	severe
Keith	1988		9.4	small
Lee	2011		14.9	strong
Lili	2002	x	5.6	strong
Marco	1990		6.7	small
Mitch	1998	x	5.1	moderate
Opal	1995	x	59.3	strong
Ophelia	2005		6.1	small
Paul	2006		13.7	small
Rita	2005	x	35.6	severe
Sandy	2012		15.7	severe
Tammy	2005		5.6	small
Wilma	2005	x	55.1	severe
?	1987		–	small

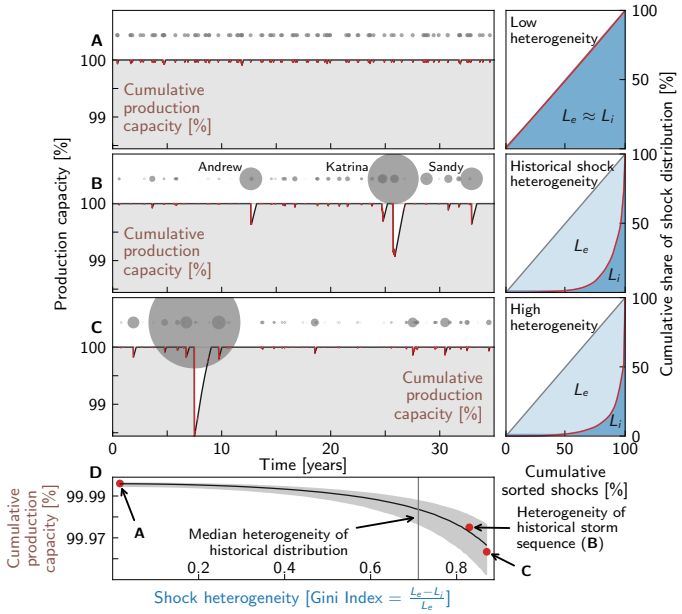

Fig. S1. Recovery dynamics of production capacity in dependence of shock heterogeneity for 1% reconstruction investment limit. Same as Fig. 2 but for a 1% reconstruction investment cap.

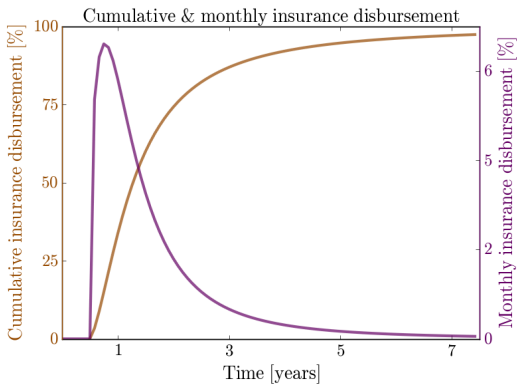

Fig. S2. Insurance payout dynamics. Cumulative (brown) and monthly (violet) insurance payouts in the aftermath of an individual shock to the physical capital stock. The sigmoidal function for the cumulative payouts is calibrated such that 60% (90%) of the insured values are reimbursed within one (three) year(s) according to insurance data of the Reinsurance Association of America[31]. The monthly payouts are then obtained by deriving this function with respect to time.

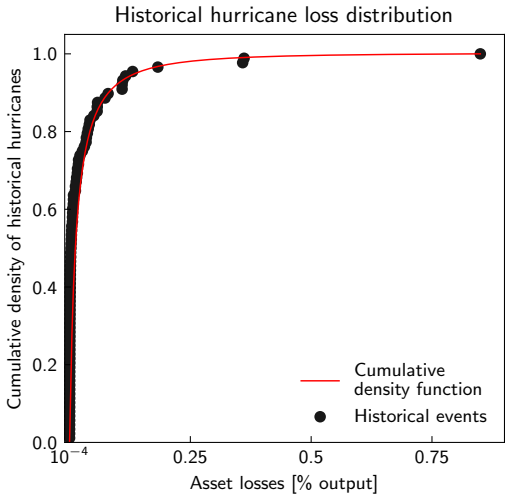

Fig. S3. Distribution of the historical asset losses of hurricanes that made landfall in the US in the period 1980–2014.
Black dots depict the asset losses as reported by the NatCatSERVICE database[1] in the period 1980–2014 relative to the US growth domestic product of the years in which the hurricanes made landfall. The red line depicts a fit with a log-normal cumulative density function.

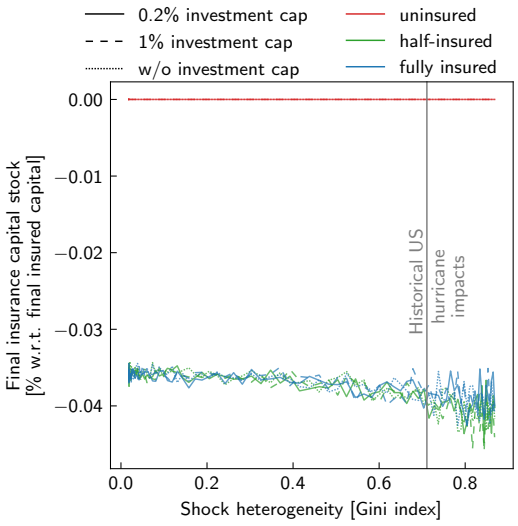

Fig. S4. Insurance is non-profit. Median insurance capital stock in terms of the insured potential capital stock after $\mathcal{T} = 35$ years. Same scenarios and colour code as in Fig. 1.

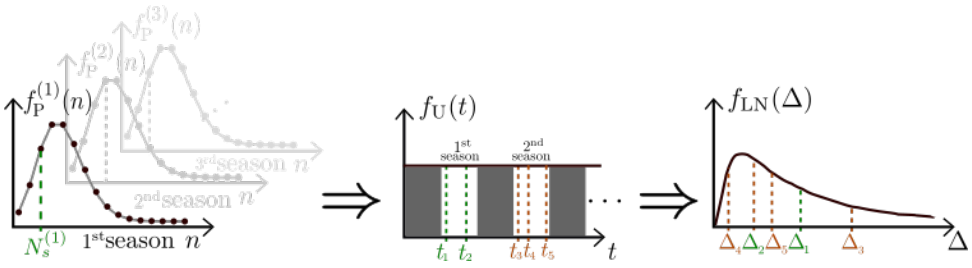

Fig. S5. Sketch of construction of synthetic asset loss time series caused by hurricanes with landfall. Synthetic time series of asset losses are generated in three steps: First, the number of hurricane shocks in each US hurricane season (June–November) is drawn from a Poisson distribution f_P. Second, the times of landfalls are determines assuming the same probability of landfall within each season, excluding the possibility of two landfalls on the same day. Third, the relative asset loss of each landfall is drawn from the log-normal distribution of Fig. S3.

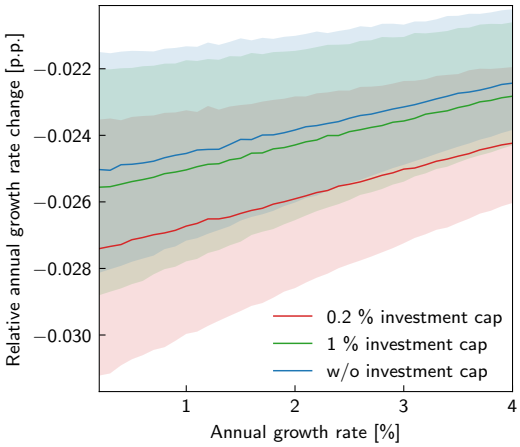

Fig. S6. Robustness of relative growth losses with regard to choice of baseline growth rate. Dependence of relative annual growth losses upon the growth rate of corresponding unperturbed baseline scenario for an insurance coverage of 50% without reconstruction investment limit (blue) as well as for for reconstruction investment caps of 0.2% (red) and 1% (green) of weekly output. Lines indicate median growth rate reductions and shaded areas the corresponding 16.7–88.3 percentile confidence intervals.

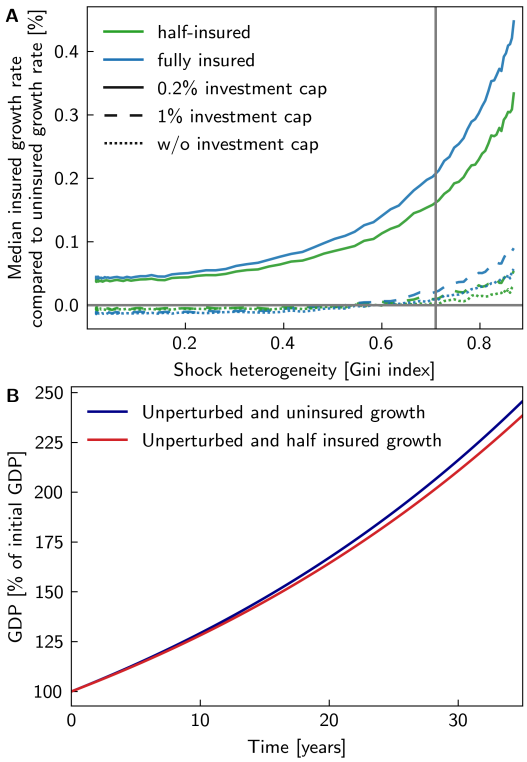

Fig. S7. Impact of insurance coverage on economic growth.
A: Change of median growth rate for half (green lines) and fully (blue lines) insured economies with regard to an economy without insurance in dependence of shock heterogeneity for reconstruction investments capped to 0.2% (solid), 1% (dashed) of weekly output and without investment cap (dotted). The vertical gray solid line denotes the median Gini index of the historical shock distribution. Parameters as in Tbl. 1.
B: GDP time series for an unperturbed and uninsured economy (blue solid line) and an unperturbed but half insured economy (red solid line) for the historical period of 35 years. Parameters as in Tbl. 1.

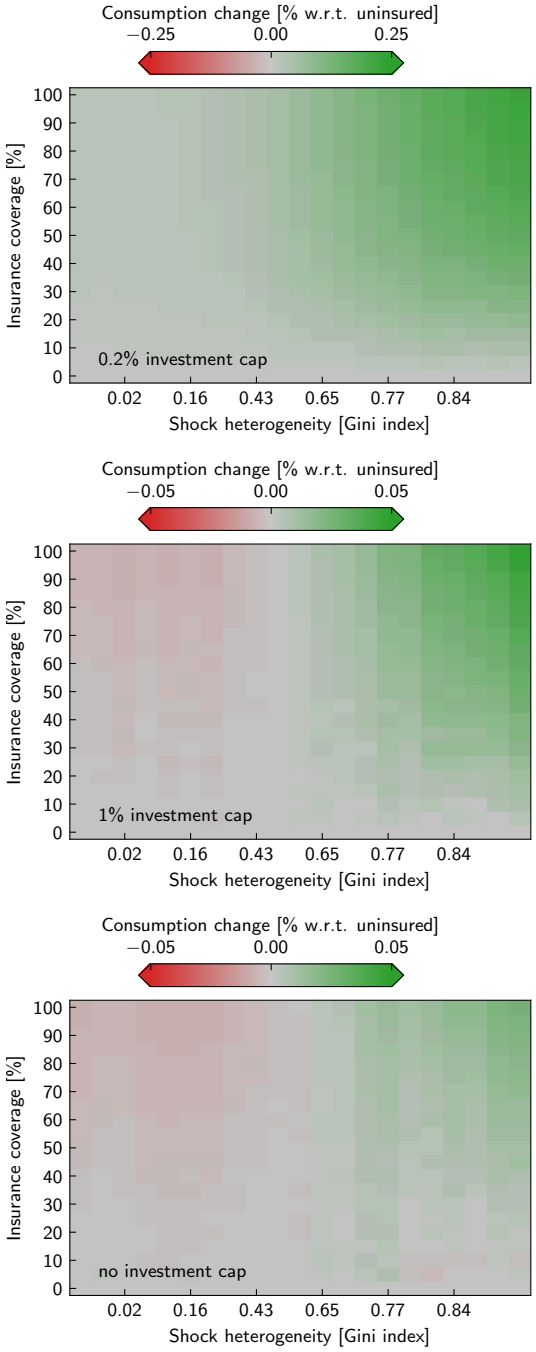

Fig. S8. Consumption change in dependence of shock heterogeneity and insurance coverage. Parameters as in Tbl. 1.

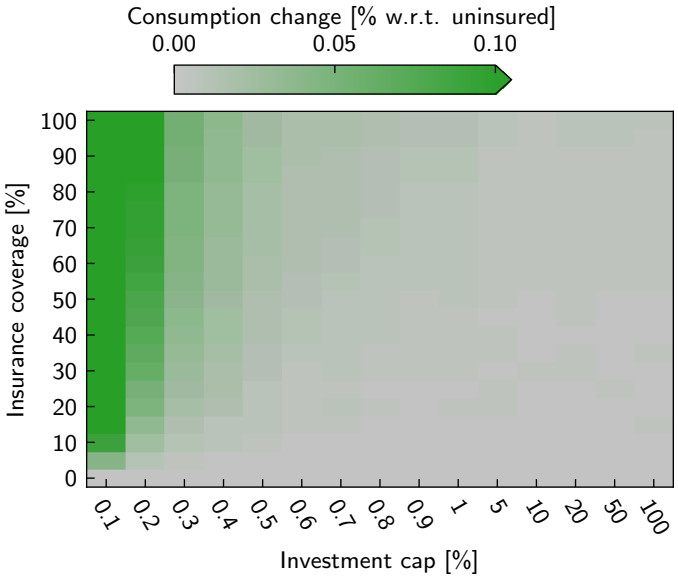

Fig. S9. Consumption change in dependence of insurance coverage and investment cap. Parameters as in Tbl. 1.

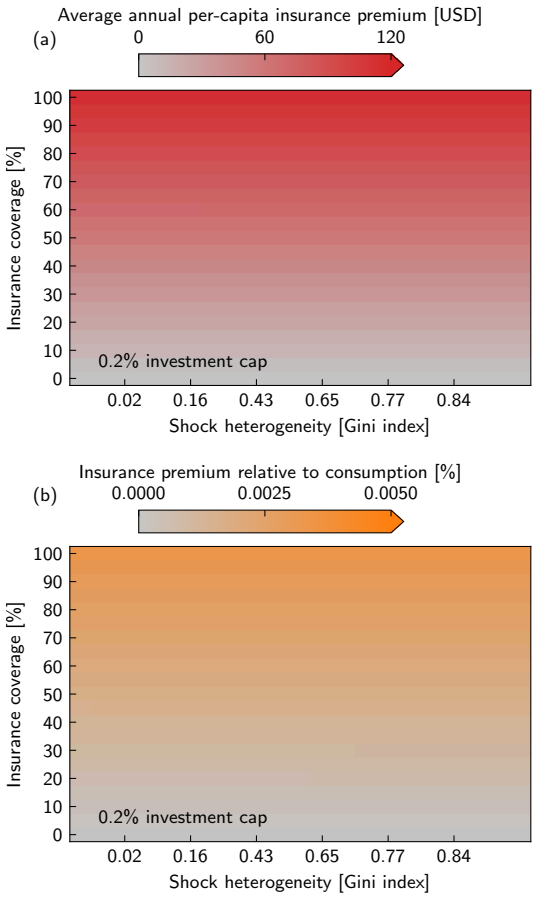

Fig. S10. Average annual insurance premium in dependence of shock heterogeneity and insurance coverage. **A**: Absolute per-capita insurance premium in US$. **B**: Insurance premium relative to average consumption. Parameters: investment cap: 0.2% of weekly output; other parameters as in Tbl. 1.

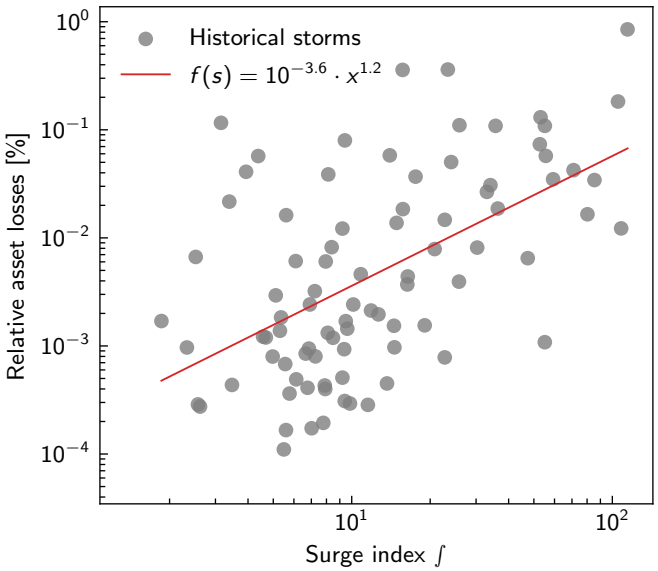

Fig. S11. Dependence of asset losses on surge index. Log-log plot of asset losses (grey dots) of the 88 historical hurricane that made landfall in the US between 1980 and 2014 according to NatCatSERVICE database[1] relative to the growth domestic output the year of landfall (according to the World Banks' and OECD's National Accounts database[a]) as function of their surge index[64]. The red line denotes a non-linear fit of the data (damage function $f(\int)$). The Pearson's chi-squared criteria for the goodness-of-fit is $\chi^2 = 0.59$).

[a] https://data.worldbank.org/indicator/NY.GDP.PCAP.CD

B.2 The case of the Small Island Developing State of Haiti

In this section, we repeat the modeling exercise described in the main text to the tropical cyclone prone Small Island Developing State of Haiti. According to MunichRe's NatCat-SERVICE[1] database, Haiti experienced 18 tropical cyclones with landfalls in the study period 1980–2014 (Tbl. S3). The direct asset losses (relative to the growth domestic product of the years the hurricanes made landfall) accumulate to 11.86%. After fitting them with a log-normal distribution, we obtain a median Gini index of 0.58. Driving the model with the parameters of Tbls. 1 and S2, we find that, as for the US, growth losses increase non-linearly with shock heterogeneity but decrease with insurance coverage (cf. Fig. 3 with Fig. S12. Noteworthy, according to NatCatSERVICE none of the tropical cyclone damages were insured in the historical study period, compared to 50% in the US. Further, we assume the same insurance payout dynamics as for the US since there are no data available for Haiti.

B.2.1 Future projections of damages

Due to the lack of better data and to use the same method, we assume for the storm surge-based estimate that the scaling of the return frequencies of tropical cyclone induces storm surges with global warming is the same as in the US. Further, assuming that the number of events remains unchanged compared to the historical study period, we find an increase of cumulative relative asset losses of 13.89% and 17.60% for the +2°C and +2.7°C degree scenarios, respectively. Growth losses more than double and tripple for the +2°C and +2.7°C degree scenarios, respectively (appendix B.2.1). According to the wind-speed based estimate, the total number of events declines to 14 landfalls for both, the +2°C and +2.7°C degree scenarios which results in moderate decreases of cumulative relative asset losses to 11.82% and 11.76%, respectively. In consequence, median growth losses also slightly decrease compared to the historical period (appendix B.2.1. As for the US, increasing insurance coverage allows mitigating the additional climate change induced growth losses arising for the storm surge-based estimate. However, it is important to note that already in the historical period Haiti suffered growth losses which may be unsustainably high.

Quantity	Symbol	Value	Unit
Initial GDP per capita	y^0	1402.1	US$
GDP growth rate	g	1.95%	year^{-1}
Cumulative relative historical asset losses	$\Delta_{\mathcal{T}}$	11.86	%
Number of historical landfalling hurricanes	N_s	18	
Standard deviation of historical log-normal asset loss distribution	σ_0	1.3909	

Tbl. S2. Exogenous parameters used in the numerical simulations for Haiti that differ from the parameters used for the US in Tbl. 1

Tbl. S3. Historical tropical cyclones that made landfall in Haiti between 1980 and 2014. 1st through 4th columns list names and years of landfall of the storms as reported by the IBTRaCS database[66], storm severity (category 4-5 hurricanes according to Saffir-Simpsons scale[8]), and storm surge index according to ref.[64], respectively. The 5th column reports categorized asset losses based on reported asset losses by Munich Re's NatCat-SERVICE database[1]: small ($> 10^{-4}$%), moderate ($> 10^{-3}$%), strong ($> 10^{-2}$%), severe ($> 10^{-1}$%), devastating (> 1%). The asset losses are measured relative to the growth domestic product of the US (according to World Banks' and OECD's National Accounts database[6]) in the year of landfall.

Name	Year	Cat. 4-5 hurricane	Surge index	Asset losses category
Allen	1980	x	36.4	devastating
Alpha	2005		-	moderate
Dean	2007	x	-	moderate
Dennis	2005	x	108.1	severe
Ernesto	2006		7.2	moderate
Georges	1998	x	6.9	devastating
Gilbert	1988	x	85.4	moderate
Gordon	1994		9.5	severe
Gustav	2008	x	6.1	moderate
Hanna	2008		71.0	moderate
Ike	2008		2.3	moderate
Irene	2011		105.1	moderate
Isaac	2012		55.6	strong
Jeanne	2004		80.3	severe
Noel	2007		14.0	strong

Name	Year	Cat. 4-5 hurricane	Surge index	Asset losses category
Olga	2007		-	moderate
Sandy	2012		15.7	devastating
Sandy	2008		-	small

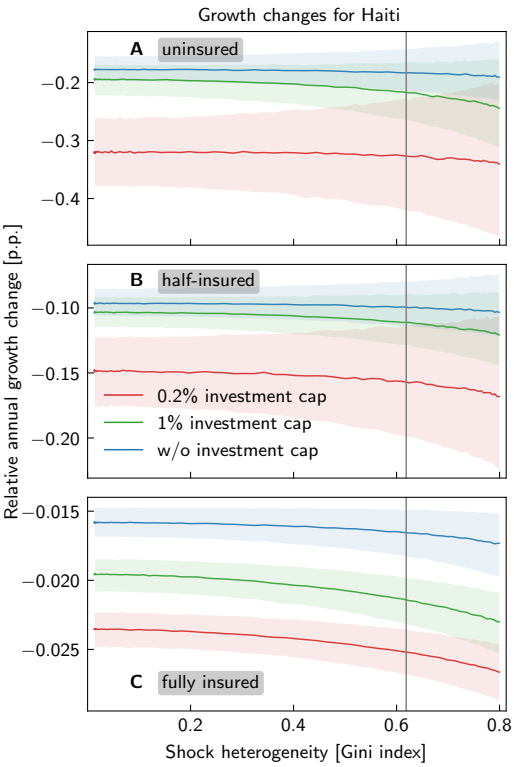

Fig. S12. Impact of hurricane shock heterogeneity on annual output growth rate of Haiti. Median annual growth rate change of the Haitian economy under hurricane shocks relative to the growth rate of the corresponding unperturbed economy, as a function of shock heterogeneity – measured by the Gini index – for no (**A**), half (**B**), and full (**C**) insurance coverage. Blue, green, and red lines depict median growth rate changes for scenarios where reconstruction investment is not limited, limited to 0.2%, and 1% of weekly output, respectively; shaded areas mark the corresponding 16.7-83.3 percentile confidence intervals. The grey vertical line indicates the median Gini index of the historical distribution of relative direct asset losses. In each simulation run, the Haitian GDP per capita (1402.1 USD) grows initially with 1.95% per year and is threatened by 18 landfalling hurricane within 33 years, which add up to 11.86% capital damage.

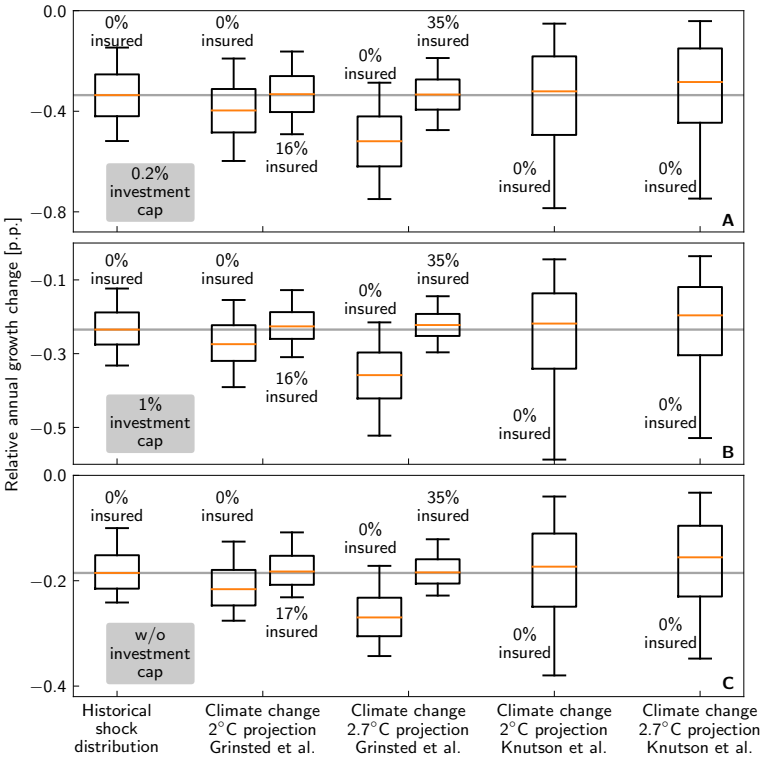

Fig. S13. Projected impacts of hurricanes on economic growth in 2°C and 2.7°C worlds and the effectiveness of insurance as coping strategy for Haiti. Annual growth losses (relative to the corresponding unperturbed economies evolving on the balanced growth paths) as obtained for the historical shock distribution (0% insurance coverage, period 1980-2012; 1st column), for Paris-compatible +2°C warming above pre-industrial levels (2nd , 3rd , 6th and 7th column) and +2.7°C (4th , 5th , 8th and 9th column) warming in compliance with current policies for reconstruction investment caps of 0.2% (**A**, standard scenario), 1% (**B**) and without reconstruction investment cap (**C**). Climate change projections of growth losses are derived from two different methods to estimate climate change-induced changes in the return frequencies of hurricanes by Grinsted et al.[6] and Knutson et al.[7] (0% insurance coverage, 2nd and 4th column, respectively). Additionally, for both estimates and warming levels the insurance coverages that would be necessary to reduce growth losses to the historical level are shown (3rd , 5th , 7th and 9th column). Orange lines, boxes, and whiskers indicate median loss estimates as well as the 25th-75th and 5th-95th percentile ranges, respectively.

Appendix of article E

Post-Brexit no-trade-deal scenario: Short-term consumer benefit at the expense of long-term economic development

Authors

Leonie Wenz, Anders Levermann, Sven N Willner, Christian Otto, Kilian Kuhla

Status

Published in *PLOS ONE* in September 2020,
doi: 10.1371/journal.pone.0237500.

Supplementary Information

Brexit no-trade-deal scenario: short-term consumer benefit at the expense of long-term economic development

This document provides supplementary tables and figures to Wenz, Levermann, Willner, Otto & Kuhla (2020).

Supplementary Tables

S1 Table: **Countries and administrative units included in simulations.** Superscripts indicate that region belongs to the United Kingdom (UK), the European Union (EU), the United States of America (USA), China (CHN) or the Commonwealth of Nations (COMM). They also denote whether a country has a trade agreement with the EU thereby distinguishing between different types of agreement: Stabilisation and Association Agreement (SAA), Association Agreement (AA), Customs Union (CU), Partnership and Cooperation Agreement (PCA), Economic Partnership Agreement (EPA), Economic Area Agreement (EAA), Global Agreement (GA), Free Trade Agreement (FTA), Agreement (TA), Interim Association Agreement (IAA), Cooperation Agreement (COA) and Cooperation and Partnership Agreement (CPA). Source: European Commission (https://ec.europa.eu/trade/policy/countries-and-regions/negotiations-and-agreements/).

Afghanistan	France^{EU}	Slovakia^{EU}
Albania^{SAA}	French Polynesia	Slovenia^{EU}
Algeria^{AA}	Gabon	Somalia
Andorra^{CU}	Gambia^{COMM}	South Africa$^{EPA,\ COMM}$
Angola	Georgia^{AA}	South Sudan
Antigua and Barbuda^{COMM}	Germany^{EU}	Spain^{EU}
Argentina	Ghana^{COMM}	Sri Lanka$^{CPA,\ COMM}$
Armenia^{PCA}	Greece^{EU}	Sudan
Aruba	Greenland	Suriname
Australia^{COMM}	Guatemala	Swaziland^{COMM}
Austria^{EU}	Guinea	Sweden^{EU}
Azerbaijan	Guyana^{COMM}	Switzerland^{TA}
Bahamas^{COMM}	Haiti	Syria^{COA}
Bahrain	Honduras	Taiwan
Bangladesh^{COMM}	Hong Kong	Tajikistan
Barbados^{COMM}	Hungary^{EU}	Thailand
Belarus	Iceland^{EAA}	Macedonia^{SAA}
Belgium^{EU}	India^{COMM}	Togo
Belize^{COMM}	Indonesia	Trinidad and Tobago^{COMM}
Benin	Iran	Tunisia^{AA}
Bermuda	Iraq	Turkey^{CU}
Bhutan	Ireland^{EU}	Turkmenistan
Bolivia	Israel^{AA}	Uganda^{COMM}
Bosnia and Herzegovina^{SAA}	Italy^{EU}	Ukraine
Botswana$^{EPA,\ COMM}$	Jamaica^{COMM}	United Arab Emirates
Brazil	Japan^{EPA}	England^{UK}
British Virgin Islands	Jordan^{AA}	Northern Ireland^{UK}
Brunei^{COMM}	Kazakhstan	Scotland^{UK}
Bulgaria^{EU}	Kenya^{COMM}	Wales^{UK}
Burkina Faso	Kuwait	Tanzania^{COMM}
Burundi	Kyrgyzstan	Alabama^{USA}
Cambodia	Laos	Alaska^{USA}
Cameroon^{COMM}	Latvia^{EU}	Arizona^{USA}
Canada^{COMM}	Lebanon^{AA}	Arkansas^{USA}
Cape Verde	Lesotho$^{EPA,\ COMM}$	California^{USA}
Cayman Islands	Liberia	Colorado^{USA}
Central African Republic	Libya	Connecticut^{USA}
Chad	Liechtenstein^{EAA}	Delaware^{USA}
Chile^{AA}	Lithuania^{EU}	District of Columbia^{USA}
Anhui^{CHN}	Luxembourg^{EU}	Florida^{USA}

Beijing
Chongqing[CHN]
Fujian[CHN]
Gansu[CHN]
Guangdong[CHN]
Guangxi[CHN]
Guizhou[CHN]
Hainan[CHN]
Hebei[CHN]
Heilongjiang[CHN]
Henan[CHN]
Hubei[CHN]
Hunan[CHN]
Jiangsu
Jiangxi
Jilin
Liaoning
Nei Mongol
Ningxia Hui
Qinghai
Shaanxi
Shandong
Shanghai
Shanxi
Sichuan
Tianjin
Xinjiang Uygur
Xizang
Yunnan
Zhejiang
Colombia
Republic of Congo
Costa Rica
Croatia[EU]
Cuba
Cyprus[EU]
Czech Republic[EU]
Côte d'Ivoire
North Korea
Democratic Republic of the Congo
Denmark[EU]
Djibouti
Dominican Republic
Ecuador
Egypt[AA]
El Salvador
Eritrea
Estonia[EU]
Ethiopia
Fiji[COMM]
Finland[EU]
Macao
Madagascar
Malawi[COMM]
Malaysia[COMM]
Maldives
Mali
Malta[EU, COMM]
Mauritania
Mauritius[COMM]
Mexico[GA]
Monaco
Mongolia
Montenegro[SAA]
Morocco[AA]
Mozambique[EPA, COMM]
Myanmar
Namibia[EPA, COMM]
Nepal
Netherlands[EU]
Netherlands Antilles
New Caledonia
New Zealand[COMM]
Nicaragua
Niger
Nigeria[COMM]
Norway[EAA]
Palestina[IAA]
Oman
Pakistan[COMM]
Panama
Papua New Guinea[COMM]
Paraguay
Peru
Philippines
Poland[EU]
Portugal[EU]
Qatar
South Korea[FTA]
Moldova[AA]
Romania[EU]
Russia
Rwanda[COMM]
Samoa[COMM]
San Marino[CU]
São Tomé and Príncipe
Saudi Arabia
Senegal
Serbia[SAA]
Seychelles[COMM]
Sierra Leone[COMM]
Singapore[COMM]
Georgia[USA]
Hawaii[USA]
Idaho[USA]
Illinois[USA]
Indiana[USA]
Iowa[USA]
Kansas[USA]
Kentucky[USA]
Louisiana[USA]
Maine[USA]
Maryland[USA]
Massachusetts[USA]
Michigan[USA]
Minnesota[USA]
Mississippi[USA]
Missouri[USA]
Montana[USA]
Nebraska[USA]
Nevada[USA]
New Hampshire[USA]
New Jersey[USA]
New Mexico[USA]
New York[USA]
North Carolina[USA]
North Dakota[USA]
Ohio[USA]
Oklahoma[USA]
Oregon[USA]
Pennsylvania[USA]
Rhode Island[USA]
South Carolina[USA]
South Dakota[USA]
Tennessee[USA]
Texas[USA]
Utah[USA]
Vermont[USA]
Virginia[USA]
Washington[USA]
West Virginia[USA]
Wisconsin[USA]
Wyoming[USA]
Uruguay
Uzbekistan
Vanuatu[COMM]
Venezuela
Vietnam
Yemen
Zambia[COMM]
Zimbabwe

S2 Table: **Sectors included in the simulation.** In the main modeling specification, we assume that commodity and service sectors are both affected by a no-trade-deal event between the EU and the UK. In a further model variant, service sectors are assumed to be unaffected by reduced permeability of the UK-EU border. Abbreviations for sectors as used in Fig. 3 are given in brackets.

Commodity sectors	Service sectors
Agriculture (AGRI)	Public Administration (ADMI)
Construction (CONS)	Post & Telecommunications (COMM)
Financial Intermediation & Business Activities (FINC)	Education, Health & Other Services (EDHE)
Fishing (FISH)	Electricity, Gas & Water (ELWA)
Food & Beverages (FOOD)	Hotels & Restaurants (GAST)
Electrical & Machinery (MACH)	Private Households (HOUS)
Other Manufacturing (MANU)	Others (OTHE)
Metal Products (METL)	Recycling (RECY)
Mining & Quarrying (MINQ)	
Petroleum, Chemical & Non-Metallic Mineral Products (OILC)	
Maintenance & Repair (REPA)	
Retail Trade (RETT)	
Re-export & Re-import (REXI)	
Textiles & Wearing Apparel (TEXL)	
Transport (TRAN)	
Transport Equipment (TREQ)	
Wholesale Trade (WHOT)	
Wood & Paper (WOOD)	

Supplementary Figures

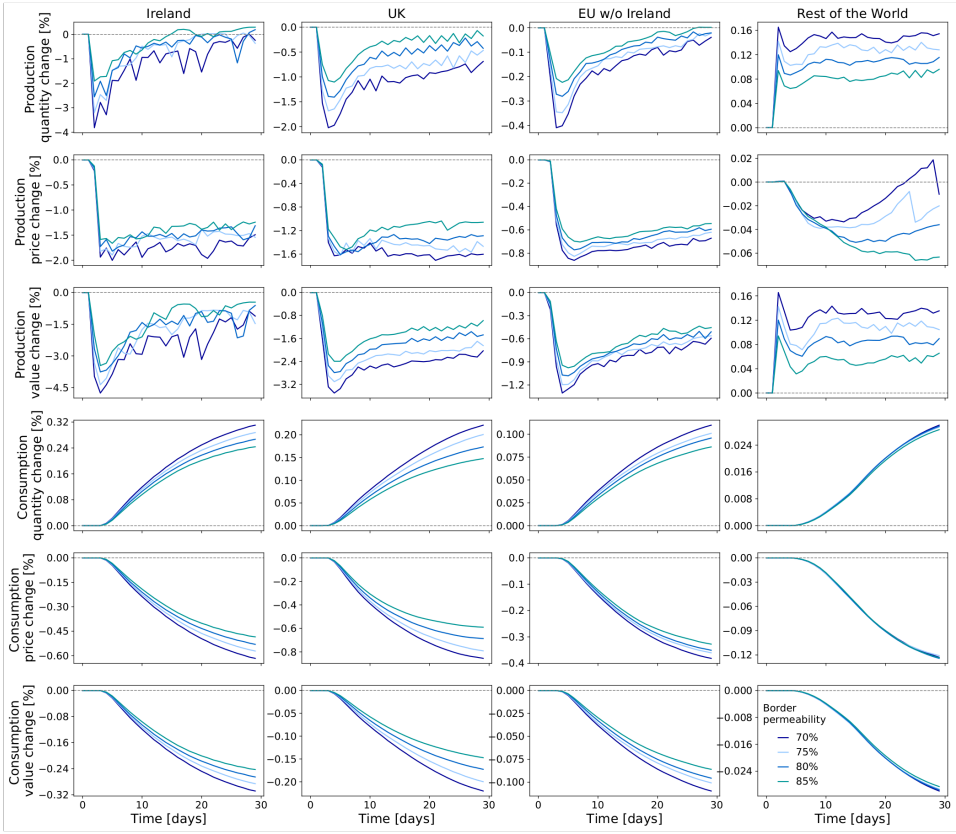

S1 Fig: **Changes in production and consumption quantities, prices and values in Ireland, the UK, the remaining EU and the rest of the world during the 30 days following a no-trade-deal event (main modeling specification).** Different scenarios of border permeability show similar dynamics. Reduced border permeability is assumed throughout the simulation period. In response to drops in production quantities in the UK and the EU, production prices and consumer prices fall. Even though lower prices stimulate demand for products slightly, production and consumption values remain below baseline levels throughout the simulation period. In the rest of the world, production slightly increases as customers request more from their suppliers that are not affected by the trade restriction. All changes are depicted as relative deviation from the respective baseline levels.

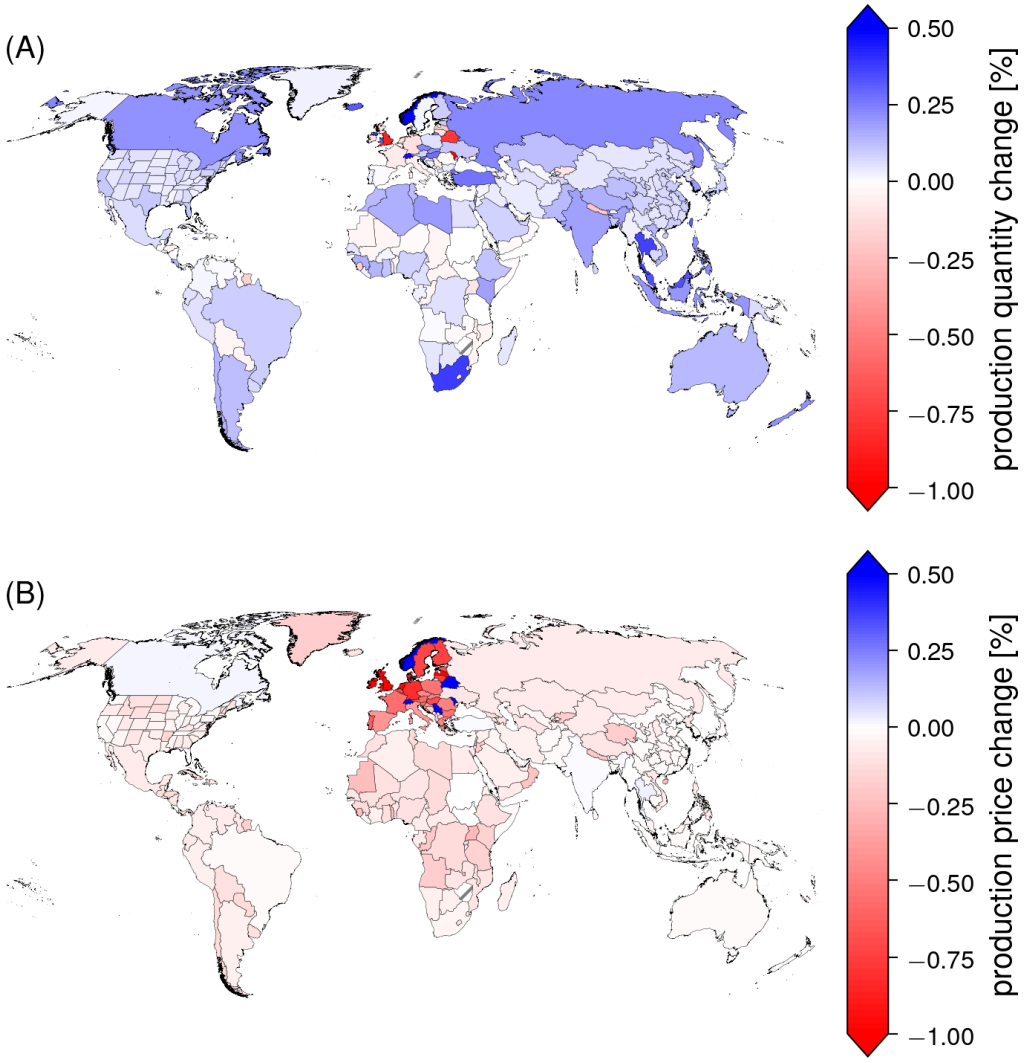

S2 Fig: **World map of production quantity and price changes after 30 days of a no-trade-deal event (main modeling specification).** Shading of colors is according to production quantity and production price changes after 30 days of reduced border permeability. Underlying scenario assumes 70% border permeability. Changes in production value are shown in Fig. 1 in main manuscript.

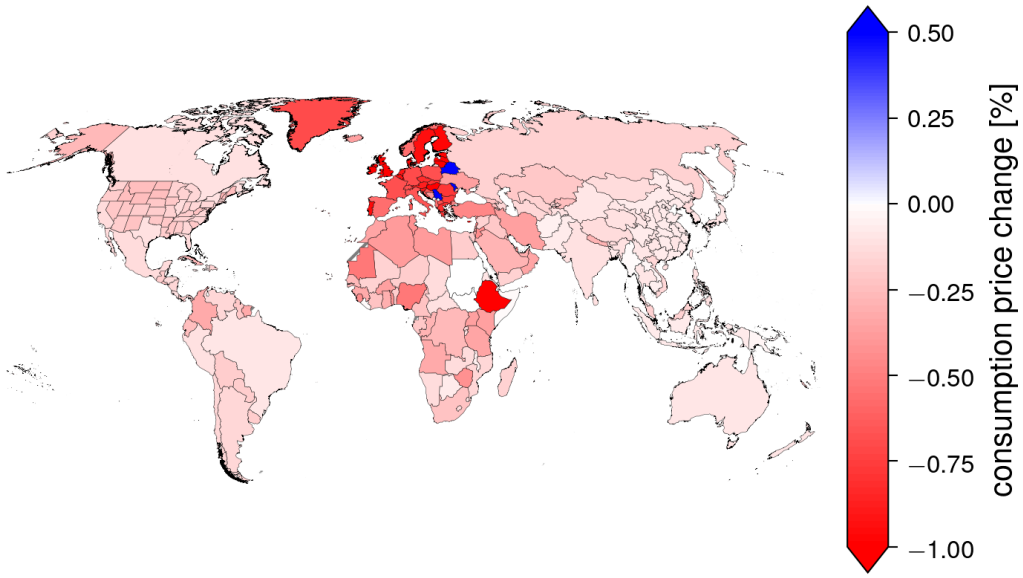

S3 Fig: **World map of consumption price changes after 30 days of a no-trade-deal event (main modeling specification).** Shading of colors is according to consumption price changes after 30 days of reduced border permeability. Underlying scenario assumes 70% border permeability. Changes in consumption quantity and consumption value are shown in Fig. 5 in main manuscript.

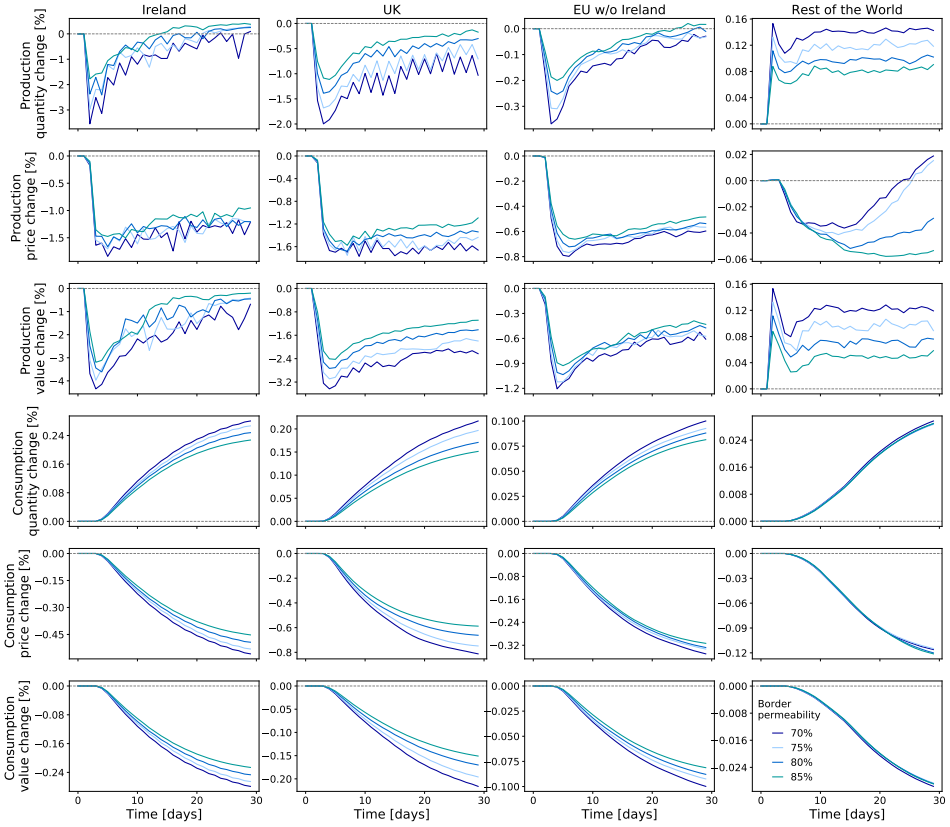

S4 Fig: **Changes in production and consumption quantities, prices and values in Ireland, the UK, the remaining EU and the rest of the world during the 30 days following a no-trade-deal event (alternative modeling specification #1).** Simulation results for alternative modeling specification where only commodity sectors but not service sectors are affected by the trade restriction between the UK and the EU. Overall dynamics are very similar to those of the main modeling specification. Most notably, the negative effect on Ireland is stronger than in the main modeling specification. All changes are depicted as relative deviation from the respective baseline levels.

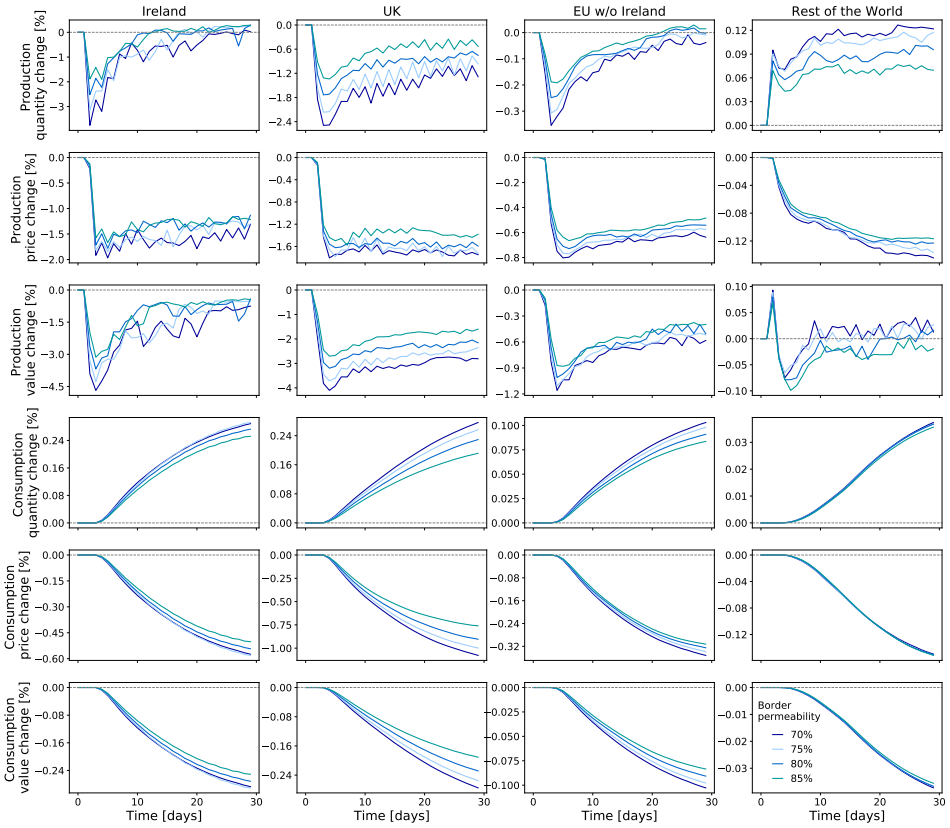

S5 Fig: **Changes in production and consumption quantities, prices and values in Ireland, the UK, the remaining EU and the rest of the world during the 30 days following a no-trade-deal event (alternative modeling specification #2).** Simulation results for alternative modeling specification where trade between the UK and countries with which the EU has trade agreements is also restricted. Overall dynamics are very similar to those of the main modeling specification. Most notably, the negative impact on the UK is stronger whereas the positive effects in the rest of the world are less pronounced. All changes are depicted as relative deviation from the respective baseline levels.

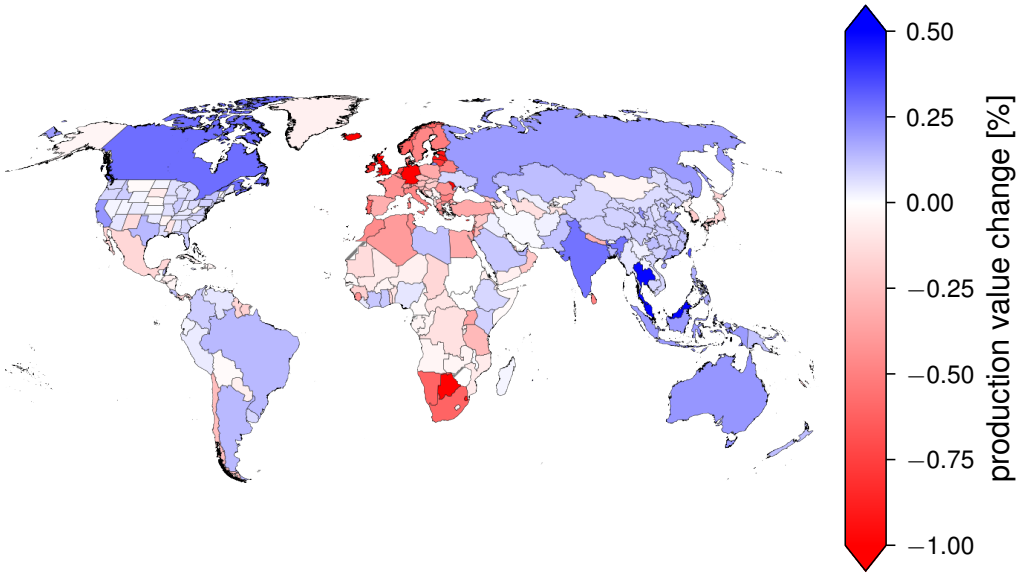

S6 Fig: **World map of production value changes after 30 days of a no-trade-deal event (alternative modeling specification #2).** Production value changes in many of the EU trading partner countries are reversed (from positive in the main modeling specification to negative here). Shading of colors is according to consumption price changes after 30 days of reduced border permeability. Underlying scenario assumes 70% border permeability.

Appendix of article F

Resilience of international trade to typhoon-related supply disruptions

Authors

Kilian Kuhla, Sven N Willner, Christian Otto, Anders Levermann

Status

Submitted to *Journal of Economic Dynamics and Control*,
preprint: https://ssrn.com/abstract=4014484.

Supplementary information

Table of contents

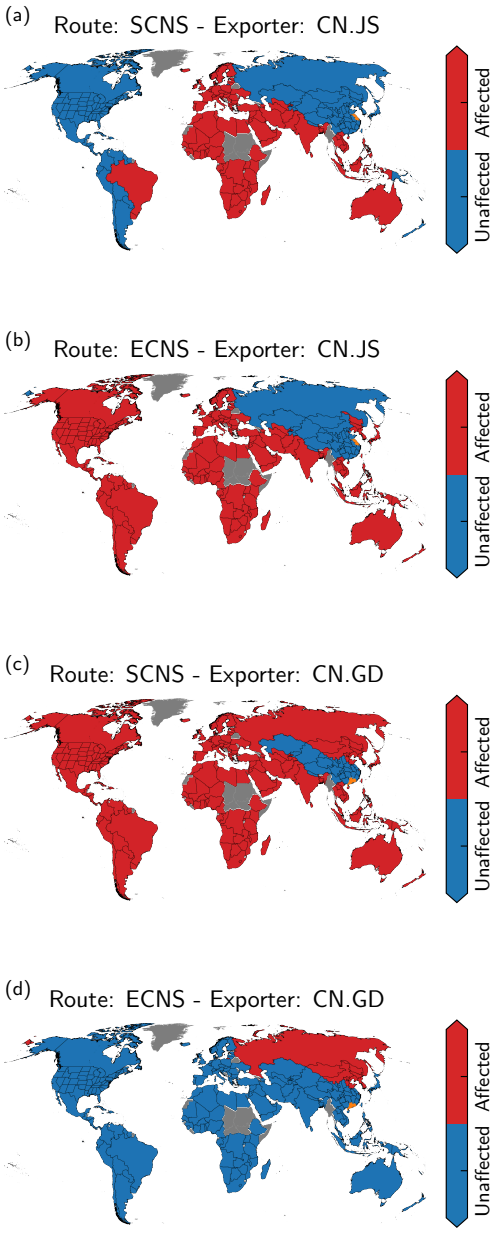

Figure S1: **Chinese exports to NAFTA are split into two spheres: Depending on South China Sea or Depending on East China Sea**

(a) Affected exports for Jiangsu – CN.JS ("Northern" China) if South China Sea – SCNS is perturbed.

(b) Affected exports for Jiangsu – CN.JS ("Northern" China) if East China Sea – ECNS is perturbed.

(c) Affected exports for Guandong – CN.GD ("Southern" China) if South China Sea – SCNS is perturbed.

(d) Affected exports for Guandong – CN.GD ("Southern" China) if East China Sea – ECNS is perturbed.

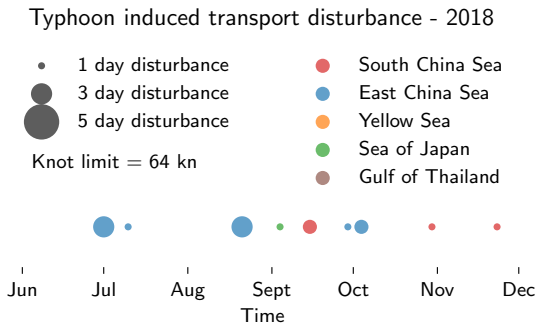

Figure S2: **Larger disturbance threshold causes less disruption days.**
Same as Fig. 1d with an disturbance threshold of 64 kn.

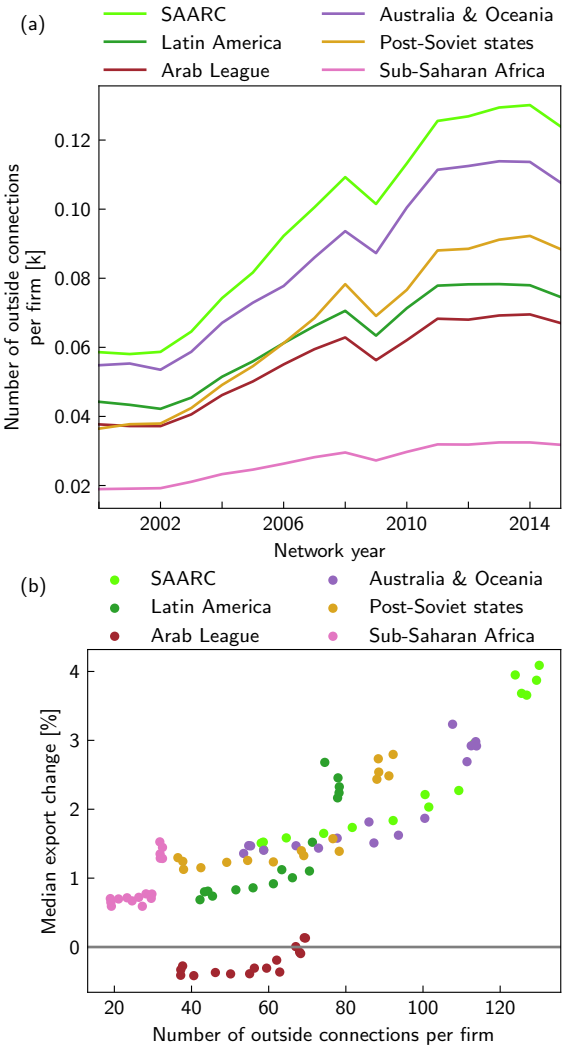

Figure S3: **Trade-interconnectivity increases except for economic blocs and builds resilience towards transport disruptions.**
(a) Number of foreign connections per firm within the economic bloc connections.
(b) Median annual export change in quantity per region over number of foreign connections per firm. Export resilience tends to increase with more foreign connections.

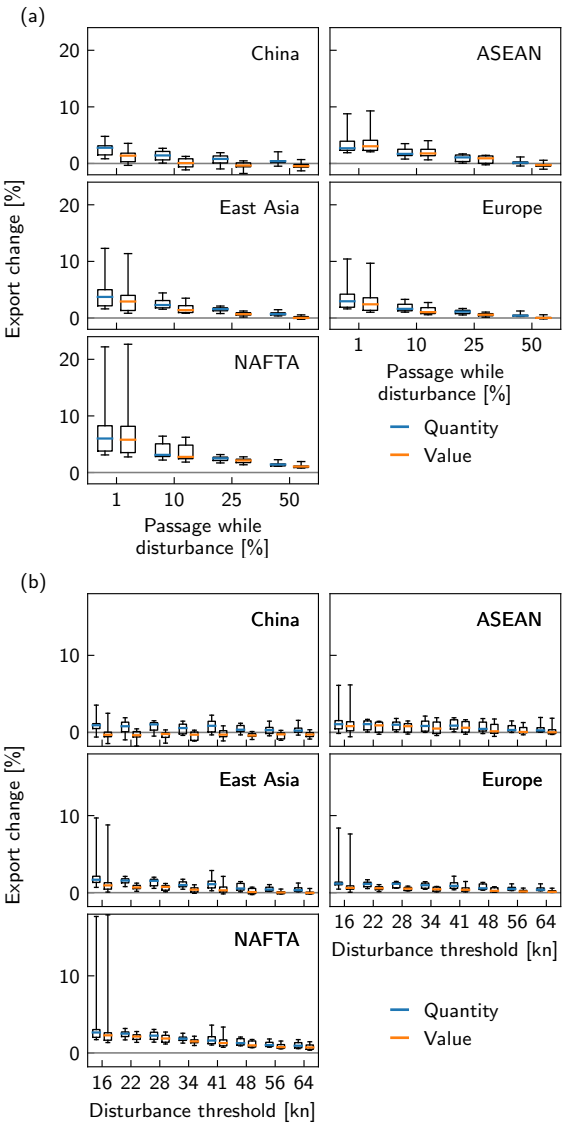

Figure S4: **Trends in result are robust against changes of disturbance modeling.**
Same results and description as 8 but entire 5–95 percentile ranges is shown.

Table S1: **Sectors used in the simulations.** Non-service sectors are affected by typhoon-induced transport perturbation, whereas service sectors are not.

Code	Name	Affected by typhoon-induced transport perturbation
AGRI	Agriculture	×
FISH	Fishing	×
MINQ	Mining and quarrying	×
GAST	Hotels and restaurants	×
WHOT	Wholesale trade	×
OTHE	Others	×
REPA	Maintenance and Repair	×
RETT	Retail Trade	×
FOOD	Food and Beverages	×
TEXL	Textiles and Wearing Apparel	×
TRAN	Transport	×
WOOD	Wood and Paper	×
OILC	Petroleum, Chemical & Non-Metallic Mineral Products	×
METL	Metal Products	×
MACH	Electrical and Machinery	×
TREQ	Transport Equipment	×
MANU	Other Manufacturing	×
REXI	Re-export and Re-import	×
CONS	Construction	×
RECY	Recycling	×
ELWA	Electricity, Gas & Water	×
ADMI	Public Administration	
EDHE	Education, Health & Other Services	
HOUS	Private Households	
COMM	Post and Telecommunications	
FINC	Financial Intermediation & Business Activities	
FCON	Final consumption	

Table S2: **Regions used in the simulations.**

ISO3 code and corresponding economic bloc of used simulations.

ISO3 code	Name of region	Economic bloc
AFG	Afghanistan	SAARC
ALB	Albania	Europe
DZA	Algeria	Arab League
AND	Andorra	Europe
AGO	Angola	Sub-Saharan Africa
ATG	Antigua and Barbuda	Latin America
ARG	Argentina	Latin America
ARM	Armenia	Post-Soviet states
ABW	Aruba	Latin America
AUS	Australia	Australia & Oceania
AUT	Austria	Europe
AZE	Azerbaijan	Post-Soviet states
BHS	Bahamas	Latin America
BHR	Bahrain	Arab League
BGD	Bangladesh	SAARC
BRB	Barbados	Latin America
BLR	Belarus	Europe
BEL	Belgium	Europe
BLZ	Belize	Latin America
BEN	Benin	Sub-Saharan Africa
BMU	Bermuda	Rest of World
BTN	Bhutan	SAARC
BOL	Bolivia	Latin America
BIH	Bosnia and Herzegovina	Europe
BWA	Botswana	Sub-Saharan Africa
BRA	Brazil	Latin America
VGB	British Virgin Islands	Latin America
BRN	Brunei Darussalam	ASEAN
BGR	Bulgaria	Europe
BFA	Burkina Faso	Sub-Saharan Africa
BDI	Burundi	Sub-Saharan Africa
KHM	Cambodia	ASEAN

ISO3 code	Name of region	Economic bloc
CMR	Cameroon	Sub-Saharan Africa
CAN	Canada	NAFTA
CPV	Cabo Verde	Sub-Saharan Africa
CYM	Cayman Islands	Latin America
CAF	Central African Republic	Sub-Saharan Africa
TCD	Chad	Sub-Saharan Africa
CHL	Chile	Latin America
CN.AH	Anhui	China
CN.BJ	Beijing	China
CN.CQ	Chongqing	China
CN.FJ	Fujian	China
CN.GS	Gansu	China
CN.GD	Guangdong	China
CN.GX	Guangxi	China
CN.GZ	Guizhou	China
CN.HA	Hainan	China
CN.HB	Hebei	China
CN.HL	Heilongjiang	China
CN.HE	Henan	China
CN.HU	Hubei	China
CN.HN	Hunan	China
CN.JS	Jiangsu	China
CN.JX	Jiangxi	China
CN.JL	Jilin	China
CN.LN	Liaoning	China
CN.NM	Nei Mongol	China
CN.NX	Ningxia Hui	China
CN.QH	Qinghai	China
CN.SA	Shaanxi	China
CN.SD	Shandong	China
CN.SH	Shanghai	China
CN.SX	Shanxi	China
CN.SC	Sichuan	China
CN.TJ	Tianjin	China
CN.XJ	Xinjiang Uygur	China

ISO3 code	Name of region	Economic bloc
CN.XZ	Xizang	China
CN.YN	Yunnan	China
CN.ZJ	Zhejiang	China
COL	Colombia	Latin America
COG	Republic Congo	Sub-Saharan Africa
CRI	Costa Rica	Latin America
HRV	Croatia	Europe
CUB	Cuba	Latin America
CYP	Cyprus	Europe
CZE	Czech Republic	Europe
CIV	Côte d'Ivoire	Sub-Saharan Africa
PRK	North Korea	East Asia
COD	Democratic Republic Congo	Sub-Saharan Africa
DNK	Denmark	Europe
DJI	Djibouti	Sub-Saharan Africa
DOM	Dominican Republic	Latin America
ECU	Ecuador	Latin America
EGY	Egypt	Arab League
SLV	El Salvador	Latin America
ERI	Eritrea	Sub-Saharan Africa
EST	Estonia	Europe
ETH	Ethiopia	Sub-Saharan Africa
FJI	Fiji	Australia & Oceania
FIN	Finland	Europe
FRA	France	Europe
PYF	French Polynesia	Australia & Oceania
GAB	Gabon	Sub-Saharan Africa
GMB	Gambia	Sub-Saharan Africa
GEO	Georgia	Post-Soviet states
DEU	Germany	Europe
GHA	Ghana	Sub-Saharan Africa
GRC	Greece	Europe
GRL	Greenland	Rest of World
GTM	Guatemala	Latin America
GIN	Guinea	Sub-Saharan Africa

ISO3 code	Name of region	Economic bloc
GUY	Guyana	Latin America
HTI	Haiti	Latin America
HND	Honduras	Latin America
HKG	Hong Kong	Rest of World
HUN	Hungary	Europe
ISL	Iceland	Europe
IND	India	SAARC
IDN	Indonesia	ASEAN
IRN	Iran	Rest of World
IRQ	Iraq	Arab League
IRL	Ireland	Europe
ISR	Israel	Rest of World
ITA	Italy	Europe
JAM	Jamaica	Latin America
JPN	Japan	East Asia
JOR	Jordan	Arab League
KAZ	Kazakhstan	Post-Soviet states
KEN	Kenya	Sub-Saharan Africa
KWT	Kuwait	Arab League
KGZ	Kyrgyz Republic	Post-Soviet states
LAO	Lao PDR	ASEAN
LVA	Latvia	Europe
LBN	Lebanon	Arab League
LSO	Lesotho	Sub-Saharan Africa
LBR	Liberia	Sub-Saharan Africa
LBY	Libya	Arab League
LIE	Liechtenstein	Europe
LTU	Lithuania	Europe
LUX	Luxembourg	Europe
MAC	Macao	Rest of World
MDG	Madagascar	Sub-Saharan Africa
MWI	Malawi	Sub-Saharan Africa
MYS	Malaysia	ASEAN
MDV	Maldives	SAARC
MLI	Mali	Sub-Saharan Africa

ISO3 code	Name of region	Economic bloc
MLT	Malta	Europe
MRT	Mauritania	Arab League
MUS	Mauritius	Sub-Saharan Africa
MEX	Mexico	NAFTA
MCO	Monaco	Europe
MNG	Mongolia	Post-Soviet states
MNE	Montenegro	Europe
MAR	Morocco	Arab League
MOZ	Mozambique	Sub-Saharan Africa
MMR	Myanmar	ASEAN
NAM	Namibia	Sub-Saharan Africa
NPL	Nepal	SAARC
NLD	Netherlands	Europe
ANT	Netherlands Antilles	Europe
NCL	New Caledonia	Australia & Oceania
NZL	New Zealand	Australia & Oceania
NIC	Nicaragua	Latin America
NER	Niger	Sub-Saharan Africa
NGA	Nigeria	Sub-Saharan Africa
NOR	Norway	Europe
PSE	West Bank and Gaza	Rest of World
OMN	Oman	Arab League
PAK	Pakistan	SAARC
PAN	Panama	Latin America
PNG	Papua New Guinea	Australia & Oceania
PRY	Paraguay	Latin America
PER	Peru	Latin America
PHL	Philippines	ASEAN
POL	Poland	Europe
PRT	Portugal	Europe
QAT	Qatar	Arab League
KOR	South Korea	East Asia
MDA	Moldova	Europe
ROU	Romania	Europe
RUS	Russian Federation	Post-Soviet states

ISO3 code	Name of region	Economic bloc
RWA	Rwanda	Sub-Saharan Africa
WSM	Samoa	Australia & Oceania
SMR	San Marino	Europe
STP	São Tomé and Principe	Sub-Saharan Africa
SAU	Saudi Arabia	Arab League
SEN	Senegal	Sub-Saharan Africa
SRB	Serbia	Europe
SYC	Seychelles	Sub-Saharan Africa
SLE	Sierra Leone	Sub-Saharan Africa
SGP	Singapore	ASEAN
SVK	Slovak Republic	Europe
SVN	Slovenia	Europe
SOM	Somalia	Sub-Saharan Africa
ZAF	South Africa	Sub-Saharan Africa
SSD	South Sudan	Sub-Saharan Africa
ESP	Spain	Europe
LKA	Sri Lanka	SAARC
SDN	Sudan	Arab League
SUR	Suriname	Latin America
SWZ	Swaziland	Sub-Saharan Africa
SWE	Sweden	Europe
CHE	Switzerland	Europe
SYR	Syrian Arab Republic	Arab League
TWN	Taiwan	East Asia
TJK	Tajikistan	Post-Soviet states
THA	Thailand	ASEAN
MKD	Macedonia	Europe
TGO	Togo	Sub-Saharan Africa
TTO	Trinidad and Tobago	Latin America
TUN	Tunisia	Arab League
TUR	Turkey	Rest of World
TKM	Turkmenistan	Post-Soviet states
UGA	Uganda	Sub-Saharan Africa
UKR	Ukraine	Europe
ARE	United Arab Emirates	Arab League

ISO3 code	Name of region	Economic bloc
GBR	United Kingdom	Europe
TZA	Tanzania	Sub-Saharan Africa
US.AL	Alabama	NAFTA
US.AK	Alaska	NAFTA
US.AZ	Arizona	NAFTA
US.AR	Arkansas	NAFTA
US.CA	California	NAFTA
US.CO	Colorado	NAFTA
US.CT	Connecticut	NAFTA
US.DE	Delaware	NAFTA
US.DC	District of Columbia	NAFTA
US.FL	Florida	NAFTA
US.GA	Georgia	NAFTA
US.HI	Hawaii	NAFTA
US.ID	Idaho	NAFTA
US.IL	Illinois	NAFTA
US.IN	Indiana	NAFTA
US.IA	Iowa	NAFTA
US.KS	Kansas	NAFTA
US.KY	Kentucky	NAFTA
US.LA	Louisiana	NAFTA
US.ME	Maine	NAFTA
US.MD	Maryland	NAFTA
US.MA	Massachusetts	NAFTA
US.MI	Michigan	NAFTA
US.MN	Minnesota	NAFTA
US.MS	Mississippi	NAFTA
US.MO	Missouri	NAFTA
US.MT	Montana	NAFTA
US.NE	Nebraska	NAFTA
US.NV	Nevada	NAFTA
US.NH	New Hampshire	NAFTA
US.NJ	New Jersey	NAFTA
US.NM	New Mexico	NAFTA
US.NY	New York	NAFTA

ISO3 code	Name of region	Economic bloc
US.NC	North Carolina	NAFTA
US.ND	North Dakota	NAFTA
US.OH	Ohio	NAFTA
US.OK	Oklahoma	NAFTA
US.OR	Oregon	NAFTA
US.PA	Pennsylvania	NAFTA
US.RI	Rhode Island	NAFTA
US.SC	South Carolina	NAFTA
US.SD	South Dakota	NAFTA
US.TN	Tennessee	NAFTA
US.TX	Texas	NAFTA
US.UT	Utah	NAFTA
US.VT	Vermont	NAFTA
US.VA	Virginia	NAFTA
US.WA	Washington	NAFTA
US.WV	West Virginia	NAFTA
US.WI	Wisconsin	NAFTA
US.WY	Wyoming	NAFTA
URY	Uruguay	Latin America
UZB	Uzbekistan	Post-Soviet states
VUT	Vanuatu	Australia & Oceania
VEN	Venezuela	Latin America
VNM	Vietnam	ASEAN
YEM	Yemen	Arab League
ZMB	Zambia	Sub-Saharan Africa
ZWE	Zimbabwe	Sub-Saharan Africa

Table S3: **Ports implemented in loss-propagation model Acclimate.**
Name and code corresponding latitude and longitude coordinates of implemented ports. The usage of ports depend on economic baseline and spatial resolution.

Name	code	Latitude [°]	Longitude [°]
Abidjan	CIABJ	5.299	-4.026
Adelaide	AUADL	-34.802	138.498
Algeciras	ESALG	36.137	-5.437

Name	code	Latitude [°]	Longitude [°]
Ambarli	TRAMR	40.967	28.690
Antwerp	BEANR	51.298	4.307
Auckland	NZAKL	-36.837	174.772
Balboa	PABLB	8.980	-79.581
Bandar Abbas	IRBND	27.102	56.077
Beira	MZBEW	-19.813	34.832
Bergen	NOBGO	60.386	5.237
Bordeaux	FRBOD	44.899	-0.538
Bremerhaven	DEBRV	53.551	8.562
Brisbane	AUBNE	-27.374	153.172
Buenaventura	COBUN	3.892	-77.072
Buenos Aires	ARBUE	-34.613	-58.362
Busan	KRPUS	35.105	129.071
Callao	PECLL	-12.045	-77.148
Cartagena	COCTG	10.351	-75.516
Caucdeo	DOCAU	18.434	-69.628
Charleston	USCHS	32.809	-79.891
Chennai	INMAA	13.099	80.302
Chittagong	BDCGP	22.448	91.725
Colombo	LKCMB	6.951	79.850
Colon	PAONX	9.357	-79.909
Constanta	ROCND	44.152	28.662
Cork	IEORK	51.900	-8.440
Dalian	CNDLC	38.967	121.751
Darwin	AUDRW	-12.519	130.861
Djibouti	DJJIB	11.601	43.117
Durban	ZADUR	-29.890	31.030
Felixstowe	GBFXT	51.960	1.345
Freeport	BSFPO	26.529	-78.763
Gdansk	PLGDN	54.382	18.695
Genova	ITGOA	44.408	8.857
Gioia Tauro	ITGIT	38.457	15.907
Gothenburg	SEGOT	57.698	11.895
Guayaquil	ECGYE	-2.262	-79.926
Hamburg	DEHAM	53.519	9.939

Name	code	Latitude [°]	Longitude [°]
Havanna	CUHAV	23.130	-82.340
Ho Chi Minh	VNSGN	10.713	106.769
Hobart	AUHBA	-42.880	147.336
Honolulu	USHNL	21.317	-157.893
Houston	USHOU	29.636	-95.071
Jebel Ali	AEJEA	25.018	55.010
Jeddah	SAJED	21.488	39.157
Kaohsiung	TWKHH	22.574	120.307
Karachi	PKKHI	24.826	66.980
Kingston	JMKIN	17.967	-76.797
Laem Chabang	THLCH	13.111	100.900
Lagos	NGLOS	6.445	3.358
Lazaro Cardenas	MXLZC	17.959	-102.211
Le Havre	FRLEH	49.450	0.318
Limassol	CYLMS	34.680	33.040
Limon-Moin	CRMOB	10.007	-83.077
Long Beach	USLGB	33.755	-118.214
Los Angeles	USLAX	33.745	-118.198
Luanda	AOLAD	-8.789	13.265
Manila	PHMNL	14.606	120.965
Manzanillo	MXZLO	19.069	-104.303
Marseille	FRMRS	43.332	5.340
Miami	USMIA	25.770	-80.204
Mombasa	KEMBA	-4.059	39.644
Montevideo	UYMVD	-34.892	-56.224
Montreal	CAMTR	45.426	-73.769
Moresby	PGPOM	-9.447	147.119
New York & New Jersey	USNYC	40.664	-74.090
Nhava Sheva	INNSA	18.953	72.945
Norfolk	USORF	36.895	-76.216
Novorossiysk	RUNVS	44.721	37.810
Oakland	USOAK	37.798	-122.286
Osaka	JPOSA	34.582	135.427
Paranagua	BRPNG	-25.502	-48.469
Perth	AUFRE	-32.056	115.744

Name	code	Latitude [°]	Longitude [°]
Piraeus	GRPIR	37.937	23.654
Port Klang	MYPKG	2.978	101.337
Port Said	EGPSD	31.233	32.335
Primorsk	RUPRI	60.346	28.665
Qingdao	CNTAO	36.053	120.273
Reykjavik	ISREY	64.150	-21.870
Richards Bay	ZARCB	-28.812	32.062
Rotterdam	NLRTM	51.888	4.386
Saldanha	ZASDB	-33.018	17.980
San Antonio	CLSAI	-33.589	-71.619
San Juan	PRSJU	18.444	-66.093
Santos	BRSSZ	-23.925	-46.337
Savannah	USSAV	31.997	-80.959
Seattle	USSEA	47.670	-122.567
Shangai	CNSHA	31.321	121.434
Shenzhen	CNSZX	22.494	113.936
Sines	PTSIE	37.938	-8.847
Sinpapore	SGSIN	1.310	103.710
Southampton	GBSOU	50.898	-1.424
Suzhou	CNSZH	31.225	120.468
Sydney	AUSYD	-33.912	151.183
Tanger-Med	MAPTM	35.894	-5.496
Tanjung Priok	IDJKT	-6.099	106.895
Teluk Bayur	IDPDG	-1.001	100.375
Tianjin	CNTXG	38.991	117.715
Tokyo	JPTYO	35.618	139.916
Valencia	ESVLC	39.440	-0.318
Valparaiso	CLVAP	-33.035	-71.618
Vancouver	CAVAN	49.194	-122.982
Veracruz	MXVER	19.207	-96.137
Walvis Bay	NAWVB	-22.970	14.487
Wellington	NZWLG	-41.277	174.786
Xiamen	CNXMN	24.486	118.030
Åland	ALA	60.221	19.974
American Samoa	ASM	-14.300	-170.718

Name	code	Latitude [°]	Longitude [°]
Anguilla	AIA	18.215	-63.054
Antarctica	ATA	-80.562	20.814
Antigua & Barbuda	ATG	17.077	-61.798
Aruba	ABW	12.509	-69.970
Barbados	BRB	13.172	-59.556
Bermuda	BMU	32.298	-64.782
Bonaire	BES	12.185	-68.290
Bouvet Island	BVT	-54.428	3.382
British Indian Ocean Territory	IOT	-7.340	72.434
British Virgin Islands	VGB	18.424	-64.620
Cape Verde	CPV	15.084	-23.625
Cayman Islands	CYM	19.318	-81.244
Christmas Island	CXR	-10.485	105.637
Clipperton Island	XCL	10.303	-109.217
Cocos Islands	CCK	-12.168	96.909
Comoros	COM	-11.663	43.354
Cook Islands	COK	-21.235	-159.778
Cuba	CUB	21.617	-78.936
Curaçao	CUW	12.194	-68.973
Cyprus	CYP	34.850	32.700
Dominica	DMA	15.435	-61.350
Dominican Republic	DOM	18.490	-69.940
Falkland Islands	FLK	-51.740	-58.753
Faroe Islands	FRO	62.169	-6.953
Fiji	FJI	-17.836	177.965
French Polynesia	PYF	-17.730	-149.410
French Southern Territories	ATF	-49.315	69.487
Grenada	GRD	12.114	-61.684
Guadeloupe	GLP	16.228	-61.576
Guam	GUM	13.444	144.777
Guernsey	GGY	49.456	-2.579
Haiti	HTI	18.570	-72.310
Heard Island & McDonald Islands	HMD	-53.093	73.517
Iceland	ISL	64.983	-18.579
Isle of Man	IMN	54.228	-4.538

Name	code	Latitude [°]	Longitude [°]
Jamaica	JAM	18.157	-77.310
Jersey	JEY	49.214	-2.133
Madagascar	MDG	-19.382	46.697
Maldives	MDV	1.906	73.538
Malta	MLT	35.888	14.440
Marshall Islands	MHL	7.096	171.222
Martinique	MTQ	14.653	-61.018
Mauritius	MUS	-20.284	57.572
Mayotte	MYT	-12.824	45.144
Micronesia	FSM	6.880	158.227
Montserrat	MSR	16.739	-62.190
Nauru	NRU	-0.528	166.934
Netherlands Antilles	ANT	17.640	-63.230
New Caledonia	NCL	-21.326	165.489
Niue	NIU	-19.052	-169.859
Norfolk Island	NFK	-29.033	167.952
Northern Mariana Islands	MNP	15.189	145.754
Palau	PLW	7.499	134.565
Paracel Islands	PIS	16.067	112.545
Pitcairn Islands	PCN	-24.377	-128.323
Puerto Rico	PRI	18.224	-66.480
Reunion	REU	-21.133	55.533
Saint-Barthélemy	BLM	17.902	-62.830
Saint Helena	SHN	-15.965	-5.707
Saint Kitts & Nevis	KNA	17.339	-62.765
Saint Lucia	LCA	13.898	-60.967
Saint Pierre & Miquelon	SPM	46.951	-56.322
Saint Vincent & the Grenadines	VCT	13.251	-61.189
Samoa	WSM	-13.621	-172.447
Sao Tome & Principe	STP	0.239	6.602
Seychelles	SYC	-4.677	55.468
Solomon Islands	SLB	-9.623	160.160
South Georgia & the South Sandwich Islands	SGS	-54.375	-36.688
Spratly islands	SP-	11.053	114.284
Svalbard & Jan Mayen	SJM	78.608	15.828

Name	code	Latitude [°]	Longitude [°]
Taiwan	TWN	23.751	120.974
Tokelau	TKL	-9.178	-171.779
Tonga	TON	-21.174	-175.192
Trinidad & Tobago	TTO	10.424	-61.296
Turks & Caicos Islands	TCA	21.775	-71.758
Tuvalu	TUV	-7.480	178.680
United States Minor Outlying Islands	UMI	19.289	166.636
Vanuatu	VUT	-15.241	166.873
Virgin Islands	VIR	17.733	-64.768
Wallis and Futuna	WLF	-13.285	-176.205

	China	Europe	NAFTA	ASEAN	Latin America	SAARC	East Asia	Arab League	Post-Soviet states	Australia & Oceania	Sub-Saharan Africa	Rest of World
China	-0.25	-4.37	-1.32	0.26	-5.31	-1.84	8.78	-7.14	-2.82	1.77	-7.6	4.48
	(-0.3,0.01)	(-4.85,-2.83)	(-1.86,-0.94)	(-0.22,1.0)	(-5.83,-4.23)	(-2.12,-0.2)	(8.33,11.73)	(-7.46,-5.58)	(-3.24,-1.18)	(-2.38,3.18)	(-8.14,-5.91)	(4.06,6.3)
Europe	-0.96	-0.02	1.09	4.57	1.47	3.17	-2.42	2.26	2.72	6.54	2.1	0.05
	(-2.01,0.26)	(-0.05,0.08)	(0.98,1.38)	(3.9,5.98)	(1.27,1.6)	(2.83,3.87)	(-2.9,-1.78)	(1.95,2.71)	(2.33,3.45)	(3.72,7.71)	(1.6,2.56)	(-0.11,0.17)
NAFTA	2.52	2.51	0.07	-0.75	1.16	0.71	6.24	0.68	0.57	4.23	2.71	-2.43
	(1.51,3.84)	(1.98,2.95)	(0.05,0.07)	(-0.85,-0.29)	(1.06,1.27)	(0.56,1.15)	(5.46,8.22)	(0.57,0.75)	(0.28,1.33)	(1.79,5.15)	(1.93,2.96)	(-3.05,-1.74)
ASEAN	4.83	4.65	-1.83	-0.52	0.63	7.19	-2.47	2.77	-9.65	3.03	2.32	-3.24
	(0.58,5.86)	(3.84,5.79)	(-2.38,-1.32)	(-0.56,-0.26)	(0.39,1.09)	(5.89,8.04)	(-3.07,-2.12)	(2.49,3.31)	(-11.24,-7.49)	(2.39,3.55)	(1.78,2.82)	(-4.77,-2.59)
Latin	8.02	3.51	0.93	3.67	-0.09	3.91	4.89	2.66	4.05	23.19	3.68	-0.05
America	(-0.35,10.02)	(2.98,4.32)	(0.87,1.06)	(3.28,4.66)	(-0.11,0.0)	(3.01,4.67)	(4.28,5.9)	(2.31,3.35)	(3.46,5.3)	(5.47,31.47)	(2.66,4.19)	(-0.55,0.55)
SAARC	10.77	4.43	0.17	12.71	2.18	-0.22	-3.34	2.33	4.58	15.25	1.87	0.03
	(2.04,16.76)	(3.99,5.71)	(-0.05,0.42)	(10.07,14.18)	(1.95,2.5)	(-0.32,-0.1)	(-3.63,-2.48)	(2.14,2.79)	(3.04,6.94)	(5.77,21.62)	(1.52,2.21)	(-0.01,0.4)
East	6.34	-1.12	3.14	-2.74	3.6	-4.95	-0.42	-4.57	5.14	1.76	1.5	-5.73
Asia	(5.53,8.75)	(-1.69,-0.52)	(2.88,4.11)	(-3.19,-2.1)	(2.96,4.07)	(-5.64,-4.42)	(-0.46,-0.31)	(-5.21,-3.53)	(4.23,5.79)	(1.32,2.53)	(1.0,1.95)	(-6.54,-4.48)
Arab	4.42	1.58	2.46	3.0	3.76	3.88	-6.26	-0.12	1.55	8.76	2.73	1.81
League	(0.51,6.39)	(1.41,1.91)	(1.89,2.97)	(2.58,3.71)	(3.37,4.36)	(3.32,4.6)	(-7.0,-5.39)	(-0.15,-0.07)	(1.39,1.82)	(7.02,10.88)	(2.25,3.25)	(1.7,2.15)
Post-Soviet	9.77	1.34	0.49	-4.98	2.13	2.82	4.86	3.25	-0.16	0.07	3.2	0.0
states	(5.73,16.92)	(1.12,1.53)	(0.34,0.6)	(-5.72,-3.76)	(1.71,2.6)	(2.43,3.58)	(4.48,6.01)	(2.71,3.53)	(-0.27,-0.05)	(-3.94,28.36)	(1.19,3.55)	(-0.1,0.06)
Australia	2.67	6.89	3.29	4.35	3.44	6.85	1.94	4.77	-5.65	-0.68	7.18	-3.96
& Oceania	(-0.03,4.01)	(5.2,8.15)	(2.57,3.86)	(3.24,4.91)	(2.77,4.2)	(5.54,7.79)	(1.34,2.36)	(3.79,6.07)	(-7.49,-3.85)	(-0.76,-0.2)	(5.24,8.59)	(-4.34,-2.98)
Sub-Saharan	-1.98	1.99	1.57	3.82	3.5	5.26	-0.87	2.9	-3.58	7.39	-0.21	-0.61
Africa	(-4.68,-0.39)	(1.78,2.45)	(1.36,2.19)	(3.34,4.04)	(3.02,3.99)	(4.38,5.99)	(-1.03,-0.68)	(2.26,3.43)	(-4.12,-2.84)	(4.9,8.22)	(-0.24,-0.05)	(-1.08,-0.29)
Rest of	6.23	1.53	-2.69	-0.35	-3.06	0.6	-2.29	1.13	1.96	9.17	-0.17	-0.39
World	(3.49,7.83)	(0.78,1.72)	(-3.01,-1.87)	(-0.94,0.21)	(-4.02,-1.93)	(0.31,1.19)	(-2.98,-1.8)	(0.9,1.26)	(1.65,2.27)	(0.62,14.76)	(-1.12,0.79)	(-0.47,-0.16)

Table S4: **Annual trade change in quantity.** Annual median quantity supply change per supplier (row) and purchaser (column). Digits in parentheses represent the 25-75 percentile.

	China	Europe	NAFTA	ASEAN	Latin America	SAARC	East Asia	Arab League	Post-Soviet states	Australia & Oceania	Sub-Saharan Africa	Rest of World
China	-1.34	-5.5	-2.41	-0.85	-6.5	-2.9	7.83	-7.98	-3.92	0.5	-8.66	3.6
	(-1.48,-0.72)	(-5.87,-4.21)	(-2.94,-2.16)	(-1.2,-0.39)	(-6.78,-5.58)	(-3.35,-1.63)	(6.89,10.27)	(-8.66,-6.89)	(-4.17,-2.33)	(-3.13,1.84)	(-9.25,-6.67)	(3.17,5.12)
Europe	-1.53	-0.12	0.54	3.88	0.89	2.72	-2.8	1.78	2.23	6.2	1.55	-0.38
	(-2.42,-0.32)	(-0.14,-0.02)	(0.4,0.81)	(3.36,5.28)	(0.66,1.0)	(2.38,3.38)	(-3.35,-2.18)	(1.44,2.04)	(1.96,2.94)	(3.36,7.35)	(1.14,1.89)	(-0.54,-0.3)
NAFTA	1.89	2.13	-0.07	-1.08	0.7	0.27	5.83	0.21	0.13	4.09	2.25	-2.78
	(1.03,3.69)	(1.62,2.54)	(-0.08,-0.05)	(-1.34,-0.77)	(0.58,0.92)	(0.0,0.66)	(5.11,7.83)	(0.16,0.32)	(-0.15,0.79)	(1.57,4.97)	(1.46,2.51)	(-3.57,-2.23)
ASEAN	5.43	4.48	-2.1	-0.31	-0.06	6.53	-2.68	2.13	-9.95	2.65	1.62	-3.69
	(0.34,6.92)	(3.5,5.79)	(-2.79,-1.78)	(-0.41,-0.23)	(-0.16,0.34)	(5.4,7.39)	(-3.3,-2.39)	(1.71,2.88)	(-11.61,-7.74)	(2.06,3.19)	(1.25,2.17)	(-5.28,-3.05)
Latin	10.48	3.23	0.74	3.13	-0.01	3.42	4.54	2.03	3.71	25.23	3.19	-0.43
America	(-0.61,12.66)	(2.69,4.14)	(0.63,0.83)	(2.8,4.05)	(-0.02,0.01)	(2.51,4.27)	(3.98,5.64)	(1.9,2.7)	(3.12,4.91)	(5.12,36.48)	(2.3,3.73)	(-0.86,0.01)
SAARC	11.68	4.14	-0.27	12.3	1.59	-0.08	-3.67	2.02	3.86	15.25	1.4	-0.33
	(1.63,18.87)	(3.62,5.34)	(-0.57,-0.13)	(9.5,13.61)	(1.42,1.85)	(-0.12,0.01)	(-3.96,-2.7)	(1.7,2.37)	(2.64,6.36)	(5.38,23.8)	(1.13,1.72)	(-0.56,-0.07)
East	5.48	-1.7	2.23	-3.47	2.68	-5.43	-0.4	-5.15	4.08	1.1	0.56	-6.18
Asia	(4.59,7.69)	(-2.27,-1.18)	(1.95,3.07)	(-3.7,-2.84)	(1.89,3.12)	(-6.41,-5.13)	(-0.47,-0.31)	(-5.78,-4.45)	(3.31,4.58)	(0.75,1.78)	(0.2,0.9)	(-7.12,-4.89)
ARAB	3.93	1.32	1.92	2.49	3.38	3.15	-6.44	-0.2	1.03	8.26	2.12	1.35
	(0.19,5.89)	(1.22,1.64)	(1.39,2.54)	(2.03,3.09)	(3.04,3.95)	(2.85,3.85)	(-7.23,-5.43)	(-0.24,-0.18)	(0.9,1.24)	(6.33,10.31)	(1.7,2.52)	(1.22,1.62)
Post-Soviet	9.73	1.12	-0.24	-5.69	1.36	2.38	4.68	2.48	-0.07	-0.63	2.39	-0.2
states	(5.23,18.04)	(0.94,1.3)	(-0.43,0.05)	(-6.47,-4.5)	(1.06,1.94)	(2.08,3.05)	(4.32,5.72)	(2.13,2.85)	(-0.09,-0.05)	(-4.45,28.29)	(0.6,2.73)	(-0.31,-0.16)
Australia	1.87	6.55	2.54	3.57	3.12	6.23	1.36	3.91	-6.17	-0.91	6.25	-4.31
& Oceania	(-0.43,3.12)	(4.92,7.4)	(1.88,3.06)	(2.73,4.1)	(2.33,3.48)	(5.02,6.83)	(1.01,1.92)	(3.07,5.15)	(-7.77,-4.62)	(-1.0,-0.3)	(4.65,7.49)	(-4.86,-3.39)
Sub-Saharan	-1.7	1.76	1.11	3.06	3.12	4.74	-1.22	2.13	-3.87	6.58	-0.23	-1.01
Africa	(-5.14,0.55)	(1.47,1.98)	(0.83,1.53)	(2.73,3.54)	(2.4,3.56)	(3.9,5.33)	(-1.38,-1.02)	(1.57,2.56)	(-4.59,-3.31)	(4.58,7.26)	(-0.28,-0.15)	(-1.76,-0.75)
Rest of	5.35	1.16	-3.12	-0.98	-3.65	0.05	-2.7	0.56	1.54	9.57	-0.85	-0.24
World	(2.69,7.41)	(0.46,1.34)	(-3.66,-2.42)	(-1.56,-0.22)	(-4.5,-2.54)	(-0.32,0.71)	(-3.5,-2.06)	(0.4,0.65)	(1.18,1.85)	(0.09,15.72)	(-1.53,0.23)	(-0.29,-0.2)

Table S5: **Annual trade change in value.** Annual median value supply change per supplier (row) and purchaser (column). Digits in parentheses represent the 25-75 percentile.

Danksagung

Im Laufe meines Lebens haben mir unzählige Menschen auf verschiedene Weise geholfen, so dass ich nun in der Lage bin, diese Dissertation zu schreiben. Da ich all diese Menschen wahrscheinlich nicht zusammen bekommen werde, sollen meine folgenden Dankesworte nicht als vollständige Liste angesehen werden. Um eine Art Rangliste zu vermeiden, möchte ich mich bei den Menschen bedanken in der Reihenfolge ihres Erscheinens.
Ich danke meinen Eltern, die mich in all den Jahren gefördert und unterstützt haben. Ich wusste, dass ich bei ihnen immer ein Sicherheitsnetz habe und konnte dadurch meinen Weg mit einer gewissen Zuversicht bestreiten. Als große Schwester und quasi erste Lehrerin hat mich Karo früh geprägt, wofür ich sehr dankbar bin. Ich bin froh, dass wir uns trotz manch großer physischer Entfernung nicht aus den Augen verloren haben.
Großer Dank geht an meine Freundinnen und Freunde vom Budapester Bumsorchester. Bei und mit euch konnte ich die vielen stressigen Momente im Studium und während meiner Promotion mal hinter mir lassen. Das gleiche gilt für Anika, mit der ich das Experiment In-Berlin-leben vor mittlerweile elfeinhalb Jahren begonnen habe. Bevor ich mein Promotionsprojekt begonnen habe, hatte ich fünfeinhalb lehrreiche Jahre an der TU Berlin. Bei Nie-enden-wollenden Praktikumsversuchen, fast täglichen PC-Pool-Arbeiten und intensiven Lernsessions wurde nicht nur mein wissenschaftliches Verständnis sondern auch wunderbare Freundschaften gefestigt. Auch wenn die meisten meiner alten Kommiliton*innen mittlerweile über die Stadt- und Landesgrenze verstreut sind, bin ich sehr dankbar und froh über jede einzelne Begegnung.
Am Ende meines Masterstudiums habe ich nach einer neuen wissenschaftlichen Richtung gesucht und hatte das große Glück Anders Levermann kennen zu lernen. Er hat mir die Chance gegeben mich am PIK zu bewähren und lehrte mich viel über Modellierung und die wissenschaftlichen Praxis. Auch wenn die Arbeit im interdisziplinären Bereich oft mühsam und steinig ist, hatte er als Doktorvater stets eine unerschütterliche Zuversicht, die mir geholfen hat Projektrückschläge durchzuhalten.
Am PIK hatte ich das Glück mit Christian und Sven zusammen arbeiten zu können. Neben ihrer Forschungserfahrung, die sie reichlich mit mir teilten, bin ich vor allem für ihre immense Geduld beim langwierigen Paperschreiben unglaublich dankbar. Ich bedanke mich bei Anja dafür, dass sie stets den organisatorischen und finanziellen Überblick während meiner Promotion behielt. Die gemeinsame Zeit mit meiner Büronachbarin

Anne, hat mir viel Heiterkeit und Lebensfreude an manch frustrierenden Arbeitstagen bereitet. Dafür bin ich sehr dankbar, sowie dass bei Fragen und Nöten, ich stets wusste, dass ich mich auf die gesamte Arbeitsgruppe verlassen kann. Ich bedanke mich bei der Studienstiftung des deutschen Volkes für die finanzielle Unterstützung.
In den letzten Jahren wurden gemeinsame Mittagessen und Kaffeepausen durch Zoom-Konferenzen und Mattermost-Gespräche abgelöst. Ich bin dankbar, dass trotz dieser Distanz die Zusammenarbeit mit meinen Doktorbrüdern Robin und Lennart wissenschaftlich fruchtbar war. Ein weiter Dank geht an meine Doktorbrüder und -schwestern, die zum letzten Drittel meiner Promotion in die Arbeitsgruppe kamen. Ich hätte mir gewünscht, dass unsere gemeinsame Zeit am PIK länger hätte sein können.
Die Pandemie war, wie für alle, auch für mich eine neue Herausforderung. Ich bin unglaublich dankbar, dass in dieser Zeit Anna und Michi an meiner Seite waren, um diese Zeiten besser durchzustehen.
Am Ende breche ich nun doch mit meiner Regel der Rangliste. Ich bedanke mich vom ganzen Herzen bei meiner Frau Janina. Ich bin froh und dankbar, für unseren gemeinsamen Weg und dass sie vor und während meiner Promotion immer für mich da war, um mich aufzufangen.

Selbstständigkeitserklärung

Hiermit versichere ich an Eides statt, dass ich die vorliegende Dissertation selbst verfasst und keine anderen als die angegebenen Hilfsmittel benutzt habe. Desweiteren versichere ich, dass diese Dissertation nicht in einem früheren Promotionsverfahren verwendet oder an einer anderen Hochschule eingereicht wurde.

Januar 2022, Berlin